Selectivity and Mechanisms of Human Cytochrome P450 Inhibition by Chlormethiazole

Robert D. Pelletier

A dissertation

submitted in partial fulfillment of the

requirements for the degree of

Doctor of Philosophy

University of Washington

2019

Reading Committee:

Kent L. Kunze, Chair

Allan E. Rettie

Rheem A. Totah

Program Authorized to Offer Degree:

Medicinal Chemistry

University of Washington

Abstract

Selectivity and Mechanisms of Human Cytochrome P450 Inhibition by Chlormethiazole

Robert. D Pelletier

Chair of the Supervisory Committee:

Professor Emeritus Kent L. Kunze

Medicinal Chemistry

The cytochrome P450 (CYP) superfamily of enzymes are heme containing enzymes that primarily perform oxidative reactions to a variety of substrates, including small molecule drugs and other xenobiotics. Formation of polar metabolites by metabolism of small molecule drugs by CYP enzymes is often a major determinant of the clearance of those drugs, and changes in the activity of the enzymes involved in the metabolism of a particular xenobiotic can lead to alteration of pharmacokinetics for that xenobiotic. The most frequent cause for change in CYP activity is enzyme inhibition, which can result in accumulations of a xenobiotic, and those accumulations have the potential to result in overdose toxicity. However, CYP inhibition can be beneficial if the formation of toxic metabolites can be blocked, or a desired increase in drug exposure is desirable. CYP mediated drug-drug interactions have been the focus of intensive research since they are common and potentially harmful, and can have dramatic implications for drug development.

This dissertation explores the selectivity of CYP inhibition by the $GABA_A$ agonist chlormethiazole (CMZ) and the mechanisms of inhibition of cytochrome P450 2E1 (CYP2E1), 2B6 (CYP2B6), and 3A4/5 (CYP3A4/5) by CMZ. CMZ elicits a clinically significant drug-drug interaction (DDI) with chlorzoxazone due to potent CYP2E1 inhibition in vivo. It has been reported that chlormethiazole is a time-dependent inhibitor of CYP2E1 and CYP2B6, but the mechanisms

were not investigated. Herein, we identified CYP3A4/5 as being susceptible to time-dependent inhibition by CMZ, and we were able to identify a potential role for an N-oxide metabolite in the mechanisms of time-dependent inhibition of CYP2E1 and CYP3A4/5. We also determined that time- dependent inhibition of CYP2B6, 2E1, and CYP3A4/5 by CMZ was NADPH-dependent and irreversible by dialysis.

The formation of CMZ N-oxide by CYP2E1 and CYP3A4/5 appears to play a major role in the inactivation of these enzymes. Thiazole N-oxides are quasi-stable carbenes, which should be capable of forming metabolic intermediate (MI) complexes and possibly N-alkylated porphyrins, as other carbenes do. We found that CYP3A4 makes a MI complex when incubated with CMZ, and that the addition of dithionite and CMZ N-oxide to purified CYP3A4 replicates the observed complex. In the case of CYP2E1, we were able to identify an unstable alkylated porphyrin species that consisted of a mono-oxygenated CMZ metabolite attached to protoporphyrin IX, and we were able to generate a MI complex with the addition of CMZ N-oxide and dithionite to purified CYP2E1. Therefore, we propose that both enzymes generate MI complexes with CMZ N-oxide, but the MI complex of CYP2E1 can rearrange to an unstable N-alkylated porphyrin species.

CYP2B6 mechanistic data was inconclusive, but does not refute the idea that the N-oxide metabolite is playing a role in the time-dependent inhibition. No distinct spectral changes or adducts were detected in recombinant CYP2B6 incubations. However, CMZ N-oxide is produced by CYP2B6, so it is possible that the same unstable alkylated porphyrin found for CYP2E1 could be formed by CYP2B6 at a rate that is too low to be detected.

In summary, we have investigated the selectivity of inhibition for the major liver CYP isoforms by CMZ and the mechanisms of time-dependent inhibition for CYP2E1, CYP2B6, and CYP3A4 by CMZ. The N-oxide metabolite of CMZ appears to play a major role in the time-dependent inhibition of CYP2E1 and CYP3A4, and that effect is likely mediated by the formation

of its carbene tautomer. The mechanism of time-dependent inhibition of CYP2B6 by CMZ is not clear since we do not have direct evidence of the molecular target of inhibition.

Table of Contents

List of Figures

List of Appendices

List of Supplementary Figures

Acknowledgements

Thank you to:

Kent Kunze for allowing an old dog to learn some new tricks and to unlearn being Pavlov's dog. I hope that this project was a fitting ending to a long career.

Allan Rettie and Rheem Totah. Thank you for helping me get through getting this process of preparing this thesis and my defense. I hope you never have to deal with a chapter like Chapter 2 ever again.

Bill Atkins, thank you for serving on my committee and putting up with my East coast barbs.

Terrence Kavanagh, thank you for serving on my committee. Hopefully, we can work together in the future.

Brian Werth and Stanley McKnight. Thank you for being a part of my committee. I hope that being my GSR was as painless as possible.

Wendel Nelson for putting up with my questions about synthesis and giving me the sass I deserve. I am still wondering why you would want to deal with me as a TA… twice.

Members of the Kunze Lab: Cristina Fernandez and Mariko Nakano. Our time together was not long, but I am so glad to have had you for lab mates.

My intern: Danillo dos Santos Oliveira. I hope your enthusiasm for science remains boundless.

Ryan Seguin, thank you for being the last holdout other than me. I appreciated our nerdy science chats and completely random conversations.

Michelle Redhair, my classmate and friend. Thanks for understanding the methods to my madness in the lab and being a friend through this whole thing.

James Williams, my classmate and purveyor of fun stories. I know you've always got the Rock's back.

Mass spectrometry: Dale Whittington and Scott Edgar. Thanks for keeping things running and teaching me about protein mass spec.

David Baggett, for Friendsmas, Friendsgiving, and driving me to the airport when it mattered most.

Eric Evangelista, John Kowalski, and Ben Maldonato for being good friends.

Medicinal Chemistry staff: We'd all be lost without you.

Thank you to my family and friends from back home. I wouldn't have made it here without you.

Dedication

To my dad

For teaching me,

Change only one thing at a time

Chapter 1: Introduction

1.1 Dissertation Purpose and Organization

The primary purpose of this dissertation is two-fold; (i) to determine the inhibition selectivity of the major liver drug metabolizing cytochrome P450 (CYP) isoforms and (ii) to elucidate the mechanism of inhibition of CYP2E1, CYP2B6, and CYP3A4 by the thiamine analog and $GABA_A$ analog chlormethiazole (CMZ). In this investigation, we hope to provide insight into thiazole bioactivation and inactivation of CYP isoforms that could be useful for future drug discovery and development. Furthermore, it has been suggested that CMZ could be beneficial as a treatment for acetaminophen overdose, and the data contained in this dissertation may serve to evaluate CMZ's potential use in that regard.(1)

In Chapter One, we provide background information regarding multiple facets of this dissertation. It begins with background on cytochrome P450 xenobiotic metabolism with a focus on CYP2E1 and on CMZ including relevant in vivo drug-drug interactions and published in vitro interaction data. That is followed by a summary of thiazole chemistry that is pertinent to CMZ metabolism and bioactivation.

In Chapter 2, an overview of the in vitro interactions and metabolism of CMZ by human liver microsomes and various types of recombinant CYPs is presented. The majority of the interaction studies were performed with pooled human liver microsomes (HLM), which is the standard enzyme source for performing in vitro drug-drug interaction (DDI) studies since it is the simplest system that generally predicts CYP inhibition-related DDI with relative accuracy. In order to more precisely isolate the metabolic events of individual isoforms, Supersomes™ (Corning Gentest), which are full length CYP enzymes expressed in the Sf9 insect cell line, were used in several

experiments. The combination of these two systems allows for a thorough analysis of mechanistic aspects and potential in vivo relevance.

In Chapter 3, the development and validation of a new and simplified procedure for extraction and detection of heme adducts and a new LC/High Resolution Mass Spectrometry (HRMS) heme quantification method are described. Previous methods for isolating heme adducts for LC/MS analysis required either harsh conditions for heme extraction from the protein source followed by derivatization or use of unique LC gel columns to separate the heme from the protein.(2-4) Both isolation methods potentially involve salts that cause ion suppression during analysis so further sample cleanup is often required. We sought to simplify and increase the speed of heme isolation while avoiding the ion suppressing salts. By employing mass defect filtering with HRMS, a technique commonly employed in metabolite identification, we are able to more easily identify potential heme adducts.(5-7) UV absorbance based assays have long been the standard for quantifying heme, so we sought to establish a more contemporary LC/MS based method with increased sensitivity and selectivity.(8-10)

In Chapter 4, a detailed analysis of the mechanism of inhibition for all of the CYP isoforms that we have identified as undergoing time-dependent inhibition (TDI) by CMZ is summarized. Using Silverman's criteria as a guide, we investigated whether CMZ acted as mechanism-based inhibitor (MBI) for any of the isoforms that undergo TDI.(11) UV spectroscopy, protein mass spectrometry, and the heme adduct methods described in Chapter 3 were used to identify the molecular target of chlormethiazole for any irreversible inhibition observed.

1.2 Cytochrome P450 Enzymes in Drug-Drug Interactions

The cytochrome P450 family of enzymes are important in precipitating drug-drug interactions (DDI) and the bioactivation of protoxins.(12) CYP isoforms metabolize 70-80% of small molecule drugs that are cleared by oxidation and are responsible for 52.5% of the major

metabolites of small molecule drugs.(13,14) As a result, alterations in the activity of those enzymes can have large effects upon the clearance of drugs and their systemic exposure. Since CYP enzymes are powerful oxidizing enzymes, they have the ability to generate numerous types of reactive species.(15,16) The generation of those reactive species can result in the covalent modification of biomolecules and also deplete the cellular stores of antioxidants.(17-19) Formation of reactive species and the depletion of antioxidants together often result in cellular toxicity. Therefore, understanding how CYP activity can be affected and the types of reactive species that can be formed from drug entities are critical to human health.

DDIs can have both deleterious and beneficial effects. Out of the 2 million adverse drug reactions that result in approximately 100,000 deaths, which are estimated by the FDA to occur each year, DDIs constitute 26% of that total. (20) By this estimate, adverse drug reactions are the fourth leading cause of death in the United States and cost the healthcare system approximately $136 billion annually. While it is obvious that DDIs inflict a large toll upon human health and money spent in healthcare, there are some instances of beneficial DDIs. In the case of highly active antiretroviral therapy (HAART) for the treatment of HIV infection, there are some regimens that employ cobicistat or ritonavir as a boosting agent for other drugs in the cocktail.(21) Cobicistat and ritonavir are inactivators of CYP3A4/5, and several HIV drugs are rapidly metabolized by CYP3A4/5, such as atazanavir and darunavir. By co-administering cobicistat or ritonavir with atazanavir or darunavir, the rapid clearance of atazanavir and darunavir is decreased, which leads to greater exposure and less frequent dosing. As a result, substantial research has been performed in the study of DDIs with a strong focus on xenobiotic metabolizing CYPs.

Even though there are 57 human isozymes from the cytochrome P450 family, only about 10 play a substantial role in drug and xenobiotic metabolism.(22) The most important cytochrome P450 isoforms in drug and xenobiotic metabolism are CYP1A2, CYP2C9, CYP2C19, CYP2D6,

and especially CYP3A4/5, whereas CYP2A6, CYP2B6, CYP2C8, CYP2E1, and CYP2J2 play more minor roles.(14,23,24) While there are some apparent preferences for substrate types, there is overlap between the isoforms due to the nature of the large and flexible active sites of xenobiotic-metabolizing CYPs. However, the majority metabolism of a drug or xenobiotic is accomplished by a small number of CYPs.(12,25) Consequently, the limited number of CYP isoforms involved in the metabolism of most drugs during polytherapy, leads to potential DDIs when the activity of those isoforms are altered in vivo.

Xenobiotic metabolizing CYP isoforms can exhibit complex behavior that deviates from the assumptions of the Michaelis-Menten model of enzyme kinetics.(26,27) Equation 1 shows the kinetic process of an enzyme with a single binding site. The Michaelis-Menten model assumes that the rate of association of a substrate and the rate of dissociation of the product are much faster than the rate of product formation and that there is only one binding site. While CYP isoforms can violate the rate assumptions of the Michaelis-Menten model, the more commonly observed violation is multiple binding events that are likely a result of the large, flexible binding pockets in xenobiotic metabolizing CYPs. CYP3A4, which possesses one of the largest volumes in its active site, according to X-ray crystallography data, has been documented to exhibit allosteric interactions due to multiple binding sites in several instances.(28-30) A prime example is the probe substrate midazolam whose metabolism results in 1'-hydroxy- and 4-hydroxy-metabolites that have different K_m values and the formation of 1'-hydroxymidazolam that displays substrate inhibition kinetics.(28,31,32) Additional examples include progesterone and α-naphthoflavone which can act as allosteric modulators in a substrate-dependent manner.(33) However, allosterism is not limited to CYP3A4 and large CYP active sites. CYP2E1, which is a major focus of this work and has a substantially smaller active site than CYP3A4, shows allosteric behavior in the metabolism of styrene.(34,35) CYP2E1 also demonstrates unusual kinetics in the metabolism of ethanol where it appears to favor a non-dissociative kinetic profile in the conversion

of ethanol to acetic acid with very little release of the intermediary product acetaldehyde.(36,37) These deviations from simple kinetic models complicate predictions of DDIs from in vitro data so any potential interaction needs to be investigated thoroughly so as to describe the enzyme kinetics as accurately as possible.

Equation 1: $S + E \leftrightharpoons SE \rightarrow SP \leftrightharpoons S + P$

1.3 Cytochrome P450 Enzymes in the Bioactivation of Xenobiotics

CYP enzymes perform various powerful, versatile oxidative chemistry and some reductions, and, as a result, numerous types of chemical reactions result from their enzymatic activity.(12,15,38-40) These reactions produce a wide diversity of metabolic products, some of which react with other endogenous proteins. The majority of reactive products of CYP metabolism are the results of oxidation and, therefore, have the chemical properties of electrophiles. The reactivity of these reactive products can be rationalized using Pearson Hard and Soft Acid and Bases Theory (HSAB) so the targets of these reactive products are dependent upon the type of reactive species formed.(41,42) Even though HSAB has been supplanted in the chemistry community by the more complex Marcus Theory, which takes into account kinetic vs. thermodynamic control of the reaction products, HSAB is sufficiently useful as a starting point to explain the reactivity that will be discussed here.(43)

According to HSAB, soft electrophiles, such as quinones, have larger molecular orbitals, are polarizable, but do not have a charge.(42) Additionally, they tend to react with soft nucleophiles such as thiols that are present mostly in proteins and glutathione.(44-48) Harder electrophiles, such as nitrenium and iminium ions, tend to be charged with smaller orbitals. The harder nucleophiles, like amines, which are present in nucleic acids and proteins, react with harder electrophiles. The generation of electrophiles result in biological consequences through the modification of the biomolecules that electrophiles modify.

CYP enzymes can produce radicals via both normal catalysis and through uncoupling of their catalytic cycle. These radicals have the ability to react with many types of molecules and further propagate radical formation.(12,19,49,50) Carbenes can also be produced. These may perform carbon-carbon bond insertions, metal chelation including iron, and other reactions due to their dual nature as an electrophile or nucleophile.(51-54) As a consequence of the rather nonspecific nature of the reactivity of radicals and carbenes, their molecular targets are generally more difficult to predict. However, the biomolecules they modify may precipitate dramatic outcomes.

One of the most well-known and best understood examples of bioactivation is the conversion of acetaminophen (APAP) into the proximate hepatotoxicant N-acetyl-p-benzoquinone imine (NAPQI).(55-60) NAPQI is a soft electrophile and tends to react with thiol groups that are typically present in proteins and the cellular protectant molecule, glutathione. Detoxification by glutathione conjugation occurs under therapeutic conditions, but acetaminophen overdose results in overproduction of NAPQI that overwhelms the glutathione pool, which leads sequentially to cellular damage, hepatic failure and possibly death.(61-66) Not only have glutathione adducts of NAPQI and downstream metabolites of that adduct have been found from in vivo samples, protein targets of NAPQI have been identified that are consistent with the expected reactivity of NAPQI.

CYP2E1 is considered to be one major CYP isoforms involved in the production of NAPQI, and modulation of CYP2E1 activity has pharmacological implications.(67-72) Use of recombinant enzymes without modern scaling techniques, such as intersystem extrapolation factors (ISEF), and older non-selective chemical inhibitors were used in identifying the importance of CYP2E1 in APAP bioactivation, but other data also supports the importance of CYP2E1 in NAPQI-mediated liver toxicity.(73) Induction of CYP2E1 by ethanol consumption can lead to increases in NAPQI formation and toxicity, and ethanol consumption has been

associated with greater risk in APAP overdose. It has been suggested that use of selective inhibitors for CYP2E1 would be of benefit in treating APAP overdose, and CMZ, the focus of this thesis project, has been proposed as a potential candidate for this therapeutic application.(1)

The production of reactive metabolites by CYP also has implications for DDIs. The reactive species generated by metabolism of a substrate can lead to TDI and possibly MBI with either the heme or apo-protein as the target. Since the enzyme is covalently modified and there is no repair mechanism, a replacement enzyme must be synthesized in order to restore activity to previous levels. This leads to long lasting reductions of CYP activity and potentially serious DDIs.

1.4 Mechanisms of Time Dependent Inhibition (TDI) of CYP Enzymes

TDI results in a situation in which the expected CYP inhibition resulting solely from reversible inhibition by the parent drug or xenobiotic under predicts the actual inhibition in the system being tested.(74-79) During TDI, the effect of inhibition grows over time and will be longer lived than predicted simply by the concentration of the parent compound. CYP enzymes can be inhibited reversibly or irreversibly, and either reversible inhibition or irreversible inhibition can manifest in TDI in vivo and in vitro.(80) Each of these potential types of inhibition has various characteristics that can lead to complications in prediction and assessment of in vivo effects. Therefore, in order to properly model the potential inhibitory effects in vivo, the mechanism of inhibition must be delineated and appropriate kinetics of any process involved should be determined.

If a metabolite is generated that is a more potent reversible inhibitor than the parent or accumulates in a drug metabolizing organ, the metabolite may cause reversible TDI. As a potent inhibitory metabolite accumulates, the apparent inhibition could increase over time. Additionally, the duration of inhibition will be longer than predicted by the concentration of the parent

compound. Since most metabolites are more polar and more readily excreted as compared to the parent, reversible TDI is not very common, but there are examples in the literature. Fluoxetine inhibition of CYP2D6 is probably the best documented example of this kind of apparent TDI where the in vitro enzyme kinetics and in vivo disposition described the mechanism of CYP2D6 accurately.(81) S-Norfluoxetine is a more potent inhibitor of CYP2D6 than S-fluoxetine and R-fluoxetine, and is a metabolite of S-fluoxetine. It was estimated by Sager et al, that S-norfluoxetine contributed 50% of the apparent CYP2D6 in vivo inhibition through a reversible mechanism.(81) In vitro, this type of inhibition can be readily distinguished from irreversible and quasi-irreversible inhibition by the use of dialysis and the testing of various metabolites for CYP inhibition.

Another possible type of TDI is quasi-irreversible inhibition.(82) This type of inhibition is the result of metabolic intermediate complexes (MI) with the heme, and these complexes require the heme iron to be in a ferrous state (+2).(54,74,79,83-89) These complexes can be disrupted by oxidation of the heme iron which can occur in vivo, but the process of oxidation is considered to proceed at a rate that is too slow to have a significant impact upon the potency of inhibition. In vitro, ferricyanide is used to oxidize these complexes to quickly differentiate them from true covalent modification of heme or apo protein. These complexes typically form from nitroso and carbene metabolites, such as those generated from the metabolism of macrolide antibiotics or methylenedioxyphenyl compounds, respectively.(15,16) The DDI between erythromycin/terfenadine is one of the most important clinical examples of this type. The combination had potential lethal outcomes through the induction of torsades de pointes as a result of the dramatic increases in terfenadine concentrations through the inhibition of CYP3A.(90-93)

TDI of CYP enzymes that is irreversible occurs through modification of the apo-protein or of the prosthetic heme.(16,76,77,82,85,94-99) Covalent modifications of the protein or heme can be generated through reactive metabolites or by reactive oxygen species resulting from uncoupling of the CYP catalytic cycle. The covalent modification of the enzymes by these reactive

species usually results in the total inactivation of the enzyme, however, it possible that the inhibition can vary from substrate to substrate depending upon the location of the modification. There are multiple types of processes that could lead to irreversible inhibition of CYP enzymes. Each type has its own considerations when trying to properly describe all of the relevant variables that could influence the inhibition process. Therefore, it is useful to further explore the mechanism of these inhibitory events so that the most appropriate models to predict the outcome of these TDIs in vivo can be chosen. One useful set of criteria that can be used as a guide to investigate the mechanisms of irreversible inhibition are Silverman's criteria for a MBI.(11)

The purpose of Silverman's criteria for a MBI is to establish that the irreversible inhibition of the enzyme is the result of an enzyme-catalyzed formation of a reactive species that immediately adducts a portion of the enzyme active site leading to inactivation of the enzyme that generated the reactive species.(11) If the TDI meets the criteria of a MBI, the kinetic process of the TDI can be expressed in a very similar manner to a fairly typical enzyme catalytic event, however, any deviation from these criteria can result in a vastly more complicated situation. Silverman's criteria for a mechanism based inhibitor (MBI) are the following:

1. Time-dependent loss of enzyme activity.
2. The rate of enzyme inactivation is saturable at high concentrations of inactivator (i.e. The rate of the reaction follows enzyme kinetics).
3. Inactivation is slowed in the presence of an alternative substrate (i.e. The inhibition can be competitively inhibited).
4. Dialysis does not restore enzyme activity (i.e. The inactivation is irreversible).
5. A 1:1 stoichiometry of inhibitor bound to enzyme is observed.
6. A catalytic step by the enzyme is required for inactivation to occur.
7. Inactivation occurs before reactive species release (Inactivation occurs in the active site.)

There are numerous instances of (apo)protein being the target of CYP inactivation by TDI, but the levels of certainty vary greatly from case to case. There are some discrete instances that have been noted in the literature, including ritonavir adducting lysine 258 of CYP3A4 and raloxifene adducting tyrosine 75 and cysteine 239 of CYP3A4, but frequently, the amino acid site is not identified due to the technical difficulties that complicate identification of the specific adduct.(4,100,101) In particular, the adduct must survive the process of protease digestion of the protein, which usually involves a reducing agent to prevent the formation of disulfide bonds, and it must not fall apart during the LC/MS analysis. In lieu of directly identifying the site of adduction, whole protein LC/MS, such as the case of diethyldithiocarbamate with CYP2E1, or use of radioactively labeled compounds can confirm the covalent modification of the protein.(102) In many cases, however, there are no data available to confirm the actual amino acid target so analysis of changes in the heme structure and the trapping of reactive metabolites are used to infer whether the protein was the true target of the inactivation.

There are several documented cases of the modification of the heme prosthetic group by time-dependent inhibitors, and the resulting complexes have been characterized using UV spectroscopy, NMR spectroscopy, and mass spectrometry.(3,52,54,85,103-109) One of the first well documented modifications of a P450 heme that led to enzyme inhibition is the formation of carbene based MI complexes from methylenedioxyphenyl compounds.(54,83) The generation of metabolites from these compounds in rat liver microsomal incubations produced 430 and 455 nm maximum absorbance peaks in the Soret spectrum that required the heme to be reduced because complete consumption of NADPH resulted in dissociation of the detected complexes. Additionally, there are examples of more stable complexes after catalysis that usually result in the ejection of iron from the heme leading to a final protoporphyrin IX adduct.(84-86,110,111) These stable complexes exhibit substantial changes in the Soret spectrum when compared to heme or PPIX.

Many reactive products, including ketenes, epoxides, and carbenes, have been shown to make stable adducts to CYPs, but one of the most well-characterized examples is benzyne, which is produced by metabolism of 1-aminobenzotriazole (ABT). Stable adducts from ABT metabolism were isolated from the livers of rats dosed with the compound, and characterized by UV, NMR and mass spectrometry (49,104,105,107,111-118). The benzyne group can form a bridge between the heme iron and a neighboring pyrrole nitrogen or a bridge between two pyrrole nitrogens. The N-alkylated products isolated from these processes tend to lose iron easily, but it is occasionally possible to identify adducts with the iron still present in the porphyrin. In Chapter 3, ABT adducts and several others will be discussed as they are used as examples to validate the heme adduct detection system that we developed.

In the context of predicting DDIs, the effects of TDI are typically estimated using physiologically based pharmacokinetic (PBPK) models, but this computational approach still has issues with accuracy when compared to clinical data.(87,119-121) PBPK models employ known physiological parameters and compound specific in vitro parameters, such as protein binding, permeability, and drug-metabolizing enzyme kinetics, to predict the disposition and potential interactions of a xenobiotic. The net loss of enzyme activity is a function of the inactivation rate and the synthesis rate of the enzyme being affected. In order to accurately predict the rate of inactivation at any time point, the effective drug concentration in the target tissue has to be measured or accurately predicted. However, the effective drug concentration in the target tissue is a function of many compound-dependent variables, including protein binding, permeability, transport, and enzymatic turnover. It is often difficult to adequately investigate all of the potential variables in sufficient depth and to scale vitro data correctly. The rates of degradation and synthesis for CYP isoforms are complicated to model due to the multitude of variables involved in both processes.(79) CYP expression can be regulated at multiple levels with transcription, siRNA, and protein stability playing roles in the amount of functional enzyme present.(14) Even though

some in vivo data on basal degradation and synthesis rates for major CYP isoforms exist, often times the amount and quality of data are lacking, which can introduce uncertainty into the prediction of DDI.

The data regarding degradation and synthesis rates of human CYP isoforms tends to be limited in both the cases of in vivo and in vitro assessments).(75,78,79,122) In vivo assessment often reflects a limited number of patients and almost never the result of a direct measurement of the enzyme itself. In a case example for CYP2E1, the formation ratio of 6-hydroxychlorzoxazone:chlorzoxazone, in plasma from only 11 patients, was used as surrogate for more direct measurement of functional CYP2E1 in studies with disulfiram.(123) Additionally, chlorzoxazone is not a truly selective substrate for CYP2E1 as CYP3A4/5 and CYP1A2 also contribute to the formation of 6-hydroxychlorzoxazone, so the duration of inhibition of CYP2E1 by disulfiram is likely to be underestimated. These studies provide an estimate of the rate of synthesis for CYP2E1 but, due to low number of patients and non-specificity of the substrate, the accuracy of that estimate is suspect. Additionally, the limited data set does not provide sufficient information on ranges and frequency distribution of the CYP2E1 synthesis rate. In vitro systems have been used to attempt to estimate the degradation and synthesis rates of CYP isoforms as well, but they lack the autocrine, endocrine, and exocrine signaling components that comprise the complete regulatory system of the isoforms in question.(124) Overall, this lack of high quality data for intrinsic degradation and synthesis rates of CYPs can introduce substantial error into any model attempting to predict changes in activity due to TDI.(79,119,125-129)

1.5 Therapeutic History and Drug-Drug Interactions of Chlormethiazole (CMZ)

CMZ is an allosteric $GABA_A$ agonist developed in the 1930's by Hoffman-LaRoche that is currently used in Europe for the treatment of acute alcohol withdrawal, restlessness, epilepsy, Parkinson's disease, and stroke.(130-147) Since CMZ has been in clinical use for several

decades, there is substantial pharmacokinetic data available at several doses and population groups. CMZ is usually given orally at doses ranging between 191 mg to 2.4 grams per day but is also available for use in intravenous administration. CMZ has an oral bioavailability of approximately 15%, and very little of CMZ is excreted unchanged. Several metabolites of CMZ have been reported, but no information exists on metabolic pathways and enzymes responsible for CMZ metabolism. Recently, a paper addressing in vitro selectivity of the inhibition of human CYP isoforms was published, but no other in vitro metabolism information has been published.(148)

CMZ is a known inhibitor of CYP2E1 metabolism in mice, rat, and human, but selectivity of inhibition has only been investigated in human in vitro systems.(149-152) Little is known about the mechanism of inhibition in any of those other species. In vivo and in vitro, CMZ can dramatically inhibit chlorzoxazone (CHZ) 6-hydroxylation, which is considered a probe reaction for CYP2E1 activity in humans. Inhibition of CYP2E1 by CMZ has a time delay to reach maximum effect and a prolonged inhibitory effect in vivo. The first in vitro characterization of CYP2E1 inhibition by CMZ was a co-incubation of experiment of CMZ with CHZ in HLM incubations. That co-incubation experiment indicated that CMZ inhibition of CHZ 6-hydroxylation had a Ki of 12 μM and was non-competitive.(152) Pharmacokinetic data from other sources indicate that circulating concentrations of CMZ of approximately 1 μM are present at the time of maximum inhibition for a 384 mg dose (~5.5 mg/kg).(137) These circulating concentrations are not able to explain the magnitude of inhibition seen with CMZ if the inhibition was reversible. Additionally, doses above 384 mg did not yield lower 6-OH CHZ/CHZ ratios, which suggests that CYP2E1 had been completely inhibited with the lower doses.(152) No further experiments have been performed to show dose dependence of inhibition by CMZ in humans or other species. Prolonged inhibition, delay in inhibitory effect, and under-prediction from reversible inhibition and pharmacokinetic data are hallmarks of TDI.(75,79) More recent in vitro data clearly shows CMZ as a time dependent

inhibitor of CYP2E1 with rapid kinetics and of CYP2B6 to a lesser extent.(148) In vitro inhibition data from Stresser et al. are consistent with the in vivo data, but we believe that the kinetic model used for TDI of CYP2E1 by these authors was not appropriate. Additionally, we determined the kinetics of TDI for CYP2B6 and CYP3A4/5. In Chapter 2, we will present a comprehensive examination of in vitro inhibition by CMZ of these major liver drug metabolizing CYP isoforms.

Even though chlormethiazole is a relatively small drug with few functional groups, there are multiple pathways of bioactivation that could occur. Thiazole moieties are known to be bioactivated as in the cases of sudoxicam and meloxicam.(15,153,154) Other known time dependent CYP inhibitors, such as cobicistat and ritonavir, also contain thiazoles, so other bioactivation routes may exist that have not been described previously.(155) Additionally, radical reactions involving the 5-ethyl chlorine also have potential to generate reactive species as seen with other alkyl halides, such as halothane.(156-161)

1.6 Chemical Reactivity of Thiazoles in the Context of Bioactivation

Thiazoles are 5-membered aromatic rings containing a sulfur atom and a nitrogen atom that are present in some biologically active molecules including abafungin, meloxicam, pramipexole, ritonavir, sudoxicam, sulfathiazole, and thiamine.(162-164) The presence of the sulfur atom leads to an asymmetric π electron density resulting in differing reactivities of the carbon atoms in the ring. C-5 has the greatest π electron density and so has higher nucleophilic character while C-2 has the least π electron density, which leads to its greater electrophilic character. Alkylation of nitrogen provides an ylide tautomer that can serve as a catalyst for the formation of carbon-carbon bonds, as seen with transketolase enzymes containing thiamine.(165,166) N-alkylated thiazoles have also been shown to form MI complexes (MIC?) with CYP3A4.(167) Oxidation at the C-3/C-4 double bond, the nitrogen, and the sulfur are likely the most important in the context of CYP bioactivation because each of these can lead to reactive products.(15,153)

When an oxidizing agent, such as mCPBA, reacts with a thiazole, the nitrogen is more readily oxidized than the sulfur, but the resulting N-oxide and S-oxide are both of interest due to their distinct reactivities.(168-170) Thiazole N-oxides without substitutions at C-2 can be in equilibrium with the corresponding carbene tautomer, which has been shown to undergo facile arylations, but also has the potential to chelate transition metals.(53,168,169,171) N-alkylated thiazoles have been shown be useful chelators of metals and function as catalysts via the ylide tautomer.(165,172,173) Other types of carbenes have been shown to form a MIC or to adduct heme so it is likely that N-oxide thiazole carbenes are capable of similar heme interactions.(52,83,85,167) Thiazole S-oxides and fused aryl thiazole S-oxides are electrophilic and will react with thiols and other nucleophiles.(174,175) CMZ has a C-4 methyl and a C-5 chloroethyl substituent, so it is not clear if the C-2 position will be reactive with electrophiles after S-oxidation. A scheme of S-oxide reactivity from Kalgutkar et al is presented in Figure 1.1.

Meloxicam and sudoxicam and MTEP (3-[2-methyl-1,3-thiazol-4-yl)ethynyl]pyridine), serve as examples for CMZ oxidation at C-4 and C-5 resulting in ring cleavages.(154) These three compounds are proposed to undergo an epoxidation across the C-4/C-5 double bond, but the authors suggest different subsequent steps for ring opening. For meloxicam and sudoxicam, Obach et al suggest that the epoxide rearranges to open the thiazole ring, and the ring opening is followed by hydrolysis to eliminate part of the ring. A scheme for this type of thiazole ring opening and scission is presented in Figure 1.2. Yang et al. propose that S-oxidation occurs before epoxidation and subsequent hydrolysis of the epoxide.(176,177) After the hydrolysis of the epoxide, they propose a series of rearrangements including a transfer of the oxygen from the S-oxide to portion of the ring that remains attached to the rest of the molecule. The mechanism for thiazole ring opening and scission proposed by Yang is presented in Figure 1.3. CMZ is substituted at C-4 and C-5 so these proposed ring scission reactions are unlikely to occur. However, ring scission cannot ruled out completely without appropriate data. We will examine

the metabolites generated in incubations containing human liver microsomes and recombinant CYPs in Chapter 2, and we will examine the mechanisms of CMZ TDI in Chapter 4.

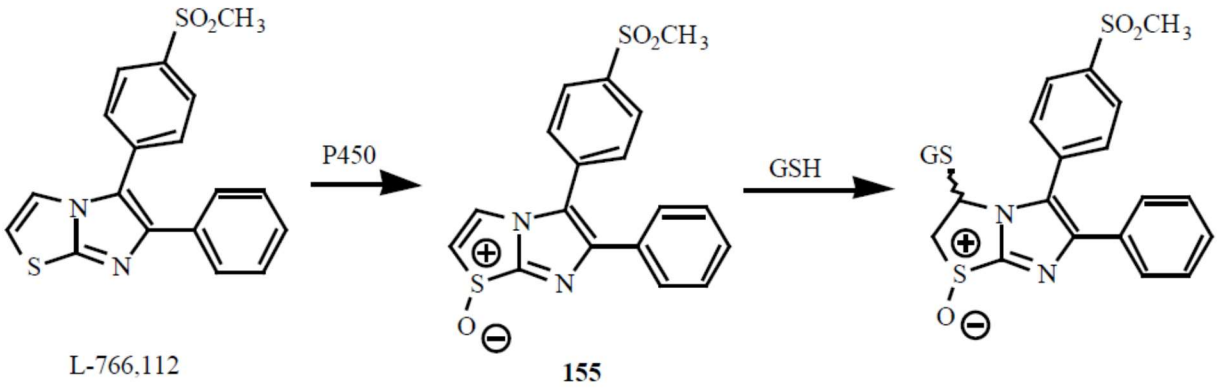

Figure 1.1 Bioactivation of Benzthiazole System via S-Oxidation
Scheme is from Kalgutkar, et al. (15)

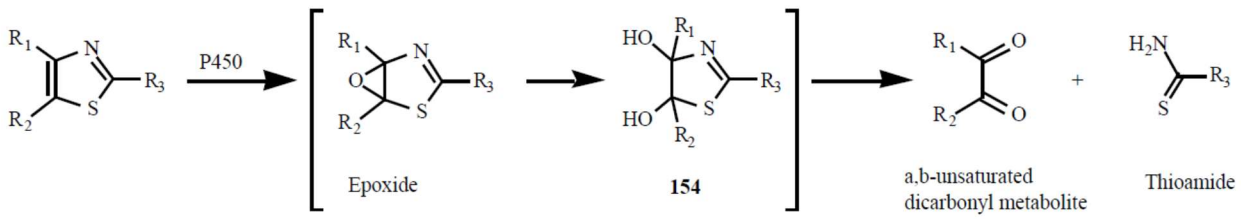

Figure 1.2 Thiazole Ring Opening and Cleavage via Epoxidation and Hydrolysis
Scheme is from Kalgutkar, et al. (15)

.

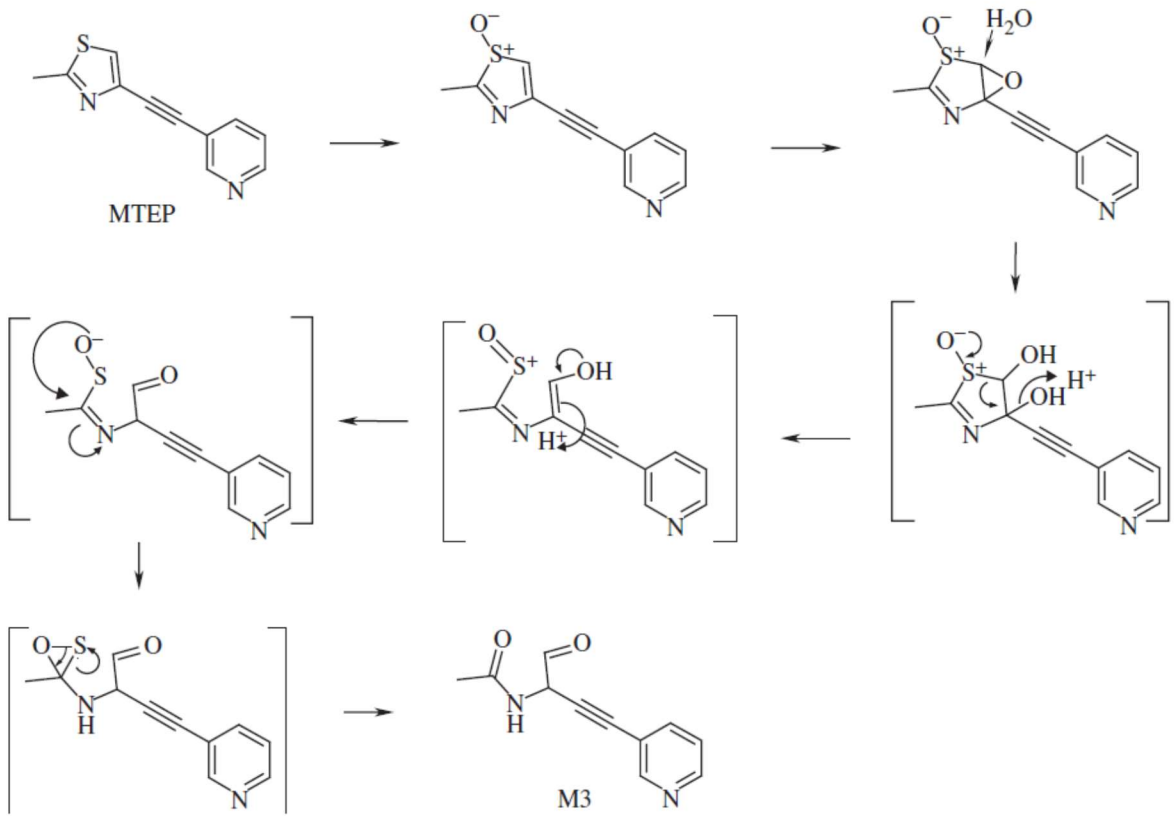

Figure 1.3 Thiazole Ring Opening via S-Oxidation, Epoxidation, and Hydrolysis
Scheme is from Yang, et al.(176)

Chapter 2: Interactions of CMZ with Major Drug Metabolizing CYP Isoforms

2.1 Introduction

Chlormethiazole (CMZ) has been used extensively over the past 40 years, especially in Europe, for the treatment of alcohol withdrawal states, and its structure is presented in Figure 2.1. (131-134,136,138,140,144,145,178,179) Studies on the interaction between CMZ and cytochrome P450s date back to the 1970s when it was reported that CMZ is not an inducer of hepatic microsomal drug metabolizing enzymes.(180) Conversely, CMZ was found to inhibit the O-de-ethylation of 7-ethoxycoumarin in human liver microsomes (HLMs) prepared from alcoholic subjects treated with CMZ, compared to HLMs from alcoholic subjects alone.(181) As discussed in Hu et al.,(149), because the major catalyst of ethoxycoumarin O-deethylation in HLMs is CYP2E1, this finding may, in retrospect, be the first data to show that CMZ has important interactions with human CYP2E1.(182)

The mechanism of inhibition of CYP2E1 by CMZ was examined in rat liver by Ingelman-Sundberg and co-workers.(149) Interestingly, this group found that CMZ did not affect CYP2E1 catalysis in rat liver microsomes, but instead reduced enzyme activity by inhibiting *CYP2E1* gene transcription. In contrast, several other studies that have been conducted both in vivo and in vitro concluded that CMZ inhibits human CYP2E1. In vivo experiments used chlorzoxazone as a catalytic probe for CYP2E1 with the consistent finding that CMZ reduced chlorzoxazone clearance.(152,183) Additionally, kinetic studies were conducted with HLMs that indicated CMZ was a non-competitive inhibitor of CYP2E1.(152) More recently, Stresser et al have reported that CMZ is a time dependent inhibitor of CYP2E1 and CYP2B6 in vitro.(148) Additionally, CYP2A6 was reversibly inhibited by CMZ, although K_i was not determined. This group's in vitro data and resulting conclusions are primarily the result of several IC_{50} shift assays using a single reporter

substrate concentration with a range of 1 to 300 μM CMZ. In vivo, doses of CMZ are as high as 2.4 grams per day, so first pass concentrations are likely to be in excess of 1 mM, assuming that dilution in the GI tract is a major driver during absorption.(183,184) In order to accurately predict an in vivo interaction, either substrate concentrations must be sufficient to derive the relevant kinetic and affinity constants or they must cover the range likely to be seen in vivo. Another gap from this earlier study is that it did not determine TDI kinetics of other relevant P450s, such as CYP2B6 and 3A4/5.

We have taken the commonly used approach of applying selective probe substrates, selective chemical inhibitors, and HLMs to comprehensively determine the inhibition potential of CMZ.(75-78,122,185-188) For the major drug metabolizing CYP isoforms, there is at least one sufficiently selective substrate/metabolite pair for CYP1A1/2, 2A6, 2B6, 2C8, 2C9, 2C19, 2D6, 2E1, and 3A4/5 to use as a marker activity that is well accepted by the FDA, industrial, and academic researchers.(185,189-191) There are known selective inhibitors for most of the same isoforms, but for CYP2E1, no thoroughly characterized, selective inhibitor is known.(192)

The primary aims of this chapter are to fully characterize the interactions of CMZ with major drug metabolizing CYPs in order to assess its potential as a selective inhibitor of CYP2E1 and to clarify the mechanism(s) of inhibition. Substrate concentrations near K_M were chosen to initially determine IC_{50} values for CMZ with the 8 major liver drug metabolizing CYP members. The isoforms with the lowest IC_{50} were then chosen to undergo screening for TDI using a dilution assay at concentrations relevant to the determined IC_{50}. Any isoform that exhibited detectable TDI by CMZ was then further characterized with regard to a full kinetic determination of K_{inact} and K_I. Much of this work was performed with HLMs, since it is the simplest system that maintains the ability to produce relatively accurate data in regards to CYP-mediated liver metabolism.(20) Also included are kinetic data for the inhibition of CYP2E1 in human hepatocytes since human hepatocytes represent a more complete system of liver metabolism. Finally, we assessed

included kinetic data for mouse liver microsomes and mouse hepatocytes since CMZ is frequently used in these animal models to assess the effect of CYP2E1 activity in human disease states.

We also examined the metabolic disposition of CMZ. While there is information regarding in vivo metabolites of CMZ, there is no published information on the metabolites formed in vitro. Therefore, metabolite identification experiments with trapping agents were performed using HLM and Supersomes™ for 10 major CYP isoforms as the enzyme sources. These metabolite identification experiments were done with the purpose of determining not only the enzymatic source of particular metabolites in vivo, but also to identify possible reactive species that could cause the apparent TDI effects seen in the kinetic experiments.

2.2 Experimental

2.2.1 Materials.

All chemicals from commercial sources were of analytical grade or better where possible. Optima LC-MS grade acetonitrile, formic acid, and methanol, ACS Plus grade isopropyl alcohol, para-nitrophenol were purchased from Thermo Fisher Scientific (Waltham, MA). All water was distilled, deionized using a house distilled water followed by a Barnstead NANOpure UV system (Thermo Fisher Scientific). Human liver microsomes were prepared from liver samples taken from the University of Washington Liver Bank. Mouse liver microsomes (MLM) and Human CYP1A2, CYP2A6, CYP2B6, CYP2C8, CYP2C9, CYP2C19, CYP2D6, CYP2E1, CYP3A4, and CYP3A5 Supersomes were obtained from Corning Gentest (Corning, New York). Human hepatocytes, mouse hepatocytes, recovery media, and plating media were obtained from Triangle Research Labs (Lonza, Walkersville, MD). Acetaminophen, acetaminophen, amodiaquine, chlorzoxazone, coumarin, hydroxycoumarin, p-nitrocatechol, midazolam, 1'-hydroxymidazolam, 1'-hydroxymidazolam-D_4, potassium cyanide, potassium phosphate monobasic, potassium phosphate dibasic, reduced glutathione, tolbutamide, testosterone, 6β-hydroxytestosterone, 6β-

hydroxytestosterone-D_3, were purchased from Sigma-Aldrich (St. Louis, MO). Catechol-$^{13}C_6$, chlormethiazole, bupropion, hydroxybupropion, hydroxybupropion-D_6, desethylamodiaquine, desethylamodiaquine-D_5, hydrodroxytolbutamide, hydroxytolbutamide-D_9, mephenytoin, hydroxymephenytoin, hydroxymephenytoin-D_3, dextromethorphan, dextorphan, dextorphan-D_3, 6-hydroxychlorazoxazone, 6-hydroxychlorzoxazone-$^{13}C_6$, 4-hydroxymidazolam, nifedipine, dehydronifedipine, and dehydronifedipine-D_6 were purchased from Toronto Research Chemicals (Toronto, ON, Canada). The internal standard, methyl-labeled acetaminophen-d_3, was purchased from TLC PharmaChem (Vaughan, ON, Canada). NADPH was obtained from OYC Americas (Vista, CA). Protease inhibitor cocktail for the preparation of subcellular fractions were obtained from Promega (Madison, WI). Para-Nitrocatechol-$^{13}C_6$ and chlormethiazole N-oxide were synthesized in house and their identities were confirmed by high resolution mass spectrometry.(169,193) The identity of chlormethiazole N-oxide was further confirmed by NMR by Dr. Michele Scian. All other chemicals were from Sigma-Aldrich unless specified.

2.2.2 NMR Spectroscopy

Analysis of synthetic products was performed on an Agilent DD2 500 MHz spectrometer equipped with 5 mm triple-resonance $^1H(^{13}C/^{15}N)$, z-axis pulsed-field gradient probe or 500-MHz PFG AutoXDB probe for ^{13}C scans by Dr. Michele Scian using 1-D and 2-D NMR techniques including ^1H-^{15}N-CIGAR HMBC which was required for the assignment of oxygen for the N-oxide.(194) Deuterated solvents were purchased from Cambridge Isotopes (Andover, MA, USA).

2.2.3 Organic Synthesis.

Preparation of Chlormethiazole N-Oxide:

To a round-bottom flask with a stir bar was added 500 mg (3.07 mmol) of chlormethiazole (Sigma) and 100 mL of dichloromethane. With stirring at room temperature, 1 g (5.7 mmol) of mCPBA was slowly added in one portion. The flask was sealed then stirred for 4 hours with

continued stirring. The reaction mixture was partially evaporated under reduced pressure then loaded onto a 5 g silica column. The CMZ N-oxide was eluted with 90% ethyl acetate/10% methanol after 5 column volumes with CMZ N-oxide continuing to elute at up to 25 column volumes. Unreacted CMZ, mCPBA, and mCBA were eluted in the first 2 column volumes. The synthetic N-oxide NMR spectra were compared to commercial CMZ to aid in the assignment of all spectra. All NMR experiments are presented in Figures 1.S1-1.S9. Exact mass was confirmed using a Thermo LTQ Orbitrap by direct infusion. Found exact mass [MH+]: 178.0088 (C_6H_8ClNOS, requires 177.0015).

Preparation of para-Nitrocatechol-$^{13}C_6$:

Nitration of Catechol-$^{13}C_6$: 3.28 mg of catechol-$^{13}C_6$ (28.25 µmoles) and 2.4 mg of sodium nitrite (34 µmol) were weighed. Catechol-$^{13}C_6$ was added to a round bottom flask with 14 mL of water and 15.3 µL of sulfuric acid and stirred in an ice bath. Sodium nitrite was slowly added, and the solution became orange yellow in a few minutes. The reaction mixture was washed three times with 30 mL of methylene chloride. The methylene chloride solution was then partially dried using reduced pressure before transferring the final 4 mL to a tared vial for final drying and weighing. A total of 3.4 mg of material was recovered. LC/MS indicated that the material was a mixture of approximately 15% doubly nitrated catechol, 35% unreacted catechol, and 50% of the desired product. Since this sample is only required as an internal standard and these species would not cause interference with quantification, no further purification was warranted. Exact mass was confirmed using a Thermo LTQ Orbitrap by direct infusion. Found exact mass [M-H]: 160.0347 ($^{13}C_6H_5NO_4$, requires 161.0420).

2.2.4 Preparation of Pooled Human Liver Microsomes and Other Subcellular Fractions.

Two lots of pooled human microsomes were made from liver samples from the University of Washington Liver Bank using previously described protocols.(195) The first lot contained a 20 donor pool with tissue from 10 male and 10 female donors (HL-150-169). The second lot

contained 4 lots of liver samples that were chosen due to the genotype of CYP3A5*3/CYP3A5*3 (HL-155, HL-160, HL-161, and HL-169). Approximately 1 gram of tissue was used from each donor, and each tissue sample was homogenized separately before being combined for centrifugation. Tissue samples were homogenized in 10 mM KPi, 10 mM EDTA, 150 mM KCl, protease inhibitor cocktail, 1 mM DTT at pH 7.4 with a Potter-Elvehjem homogenizer on ice. Samples were then transferred to 50 mL conical tubes then spun at 800 g for 15 minutes.

Supernatants were transferred from the 50 mL conical tubes to ultracentrifuge tubes. For the 20 donor lot, the supernatant was centrifuged at 6000 g for 15 minutes to yield the heavy mitochondrial fraction as the pellet then the remaining supernatant was centrifuged at 10,000 g for 30 minutes to yield the light mitochondrial fraction as the pellet and S9 as the supernatant. The 4 donor lot was centrifuged at 10,000 g for 30 minutes to yield S9. Both lots of S9 were then spun at 100,000 g for 1 hour. Microsomal and mitochondrial pellets were reconstituted with 10 mM potassium phosphate and 250 mM sucrose at pH 7.4. Cytosol and S9 were diluted with 50 mM Tris, 2 mM EDTA, and 150 mM KCl at pH 7.4 to reach 10 mg/mL and 20 mg/mL, respectively. Protein concentrations were determined using a Pierce™ BCA assay kit from Fisher Scientific.

2.2.5 Co-incubation Experiments of CMZ to Estimate IC_{50} Values with Selective Probe Substrates and HLM.

Incubations were performed in a total volume 100 µL containing 0.1 M potassium phosphate buffer with 0.1 mg/mL pooled human liver microsomes, 2 mg/mL NADPH, CMZ solvated in water, and a selective substrate for the CYP isoform solvated in acetonitrile or methanol with the final concentration of organic solvent in the incubation being 1% or less. The concentration of those substrates were the following: 25 µM phenacetin (CYP1A), 0.5 µM coumarin (CYP2A6), 80 µM bupropion (CYP2B6), 200 µM tolbutamide (CYP2C9), 200 µM S-mephenytoin (CYP2C19), 5 µM dextromethorphan, 3 µM midazolam, 40 µM testosterone, and 20 µM nifedipine. The concentrations of CMZ used in the assays were 0, 0.1, 0.3, 1, 3, 10, 30, 100, 300, and 1000 µM.

The samples were preincubated for 5 minutes using a 37° C water bath in a 96 well PCR plate then the incubation was started by the addition of NADPH. The samples were incubated in the linear range of product formation with incubation times ranging between 2-10 minutes at 37º C. Incubations were terminated with 100 µL of methanol/acetonitrile containing the internal standard (IS). A standard curve was prepared by using serial dilution of the metabolite in 0.1 M potassium phosphate buffer at pH 7.4 followed by addition of the appropriate of IS which are indicated in Appendices 1-12. The samples were analyzed with the LC/MS/MS appropriate method from Appendices 1-12. Data were fit with GraphPad Prism 8 (San Diego, CA) using the IC_{50} model with variable slope and variable response or fixed slope with normalized response. The choice of model was dependent upon the extent of coverage for the inhibition by the concentrations in the assay.

2.2.6 CMZ K_i Determinations for CYP2A6, 2B6, 2C19, and 2E1.

Incubations were performed a near identical manner as the co-incubation IC_{50} experiments except 3 substrate concentrations were used with each of inhibitor concentrations. 0.5, 1, and 2 µM coumarin were used for CYP2A6, and 40, 80, and 160 µM bupropion were used for CYP2B6. 25, 50, and 150 µM S-mephenytoin were used for CYP2C19, and 25, 75, 225 µM chlorzoxazone were used for CYP2E1. For CYP2A6, 2B6, and 2E1, the same inhibitor concentrations as the IC_{50} experiment were used. The samples were preincubated for 5 minutes using a 37° C water bath in a 96 well PCR plate then the incubation was started by the addition of NADPH. The samples were incubated in the linear range of product formation with incubation times ranging between 2-10 minutes at 37º C.

Data were fit using GraphPad Prism 8 using the mixed inhibition model which is the following set of equations:(27,196)

$$V_{max,apparent} = \frac{V_{max}}{\left(1 + \frac{[Inhibitor]}{alpha \times K_i}\right)}$$

$$K_{m,apparent} = \frac{K_m \times \left(1 + \frac{[Inhibitor]}{K_i}\right)}{\left(1 + \frac{[Inhibitor]}{alpha \times K_i}\right)}$$

$$Y = \frac{V_{max,apparent} \times [Substrate]}{K_{m,apparent} + [Substrate]}$$

2.2.7 Co-incubation Allosteric and Inhibitory Interactions of CMZ with Midazolam in HLM and Recombinant CYP3A4

Incubations were performed in a total volume 100 µL containing 0.1 M potassium phosphate buffer with 0.1 mg/mL pooled human liver microsomes or 20 pM CYP3A4 + OR + b_5 Supersomes™, 2 mg/mL NADPH, CMZ solvated in water, and midazolam solvated in methanol with a final concentration of methanol being 0.4%. Midazolam was used at 1, 3, 10, and 30 µM. The samples were preincubated for 5 minutes using a 37° C water bath in a 96 well PCR plate then the incubation was started by the addition of NADPH. The samples were incubated in the linear range of product formation with incubation times ranging between or 90 seconds for HLM incubation or 2 minutes for recombinant incubations at 37º C. CMZ concentrations used in the assays were: 0, 10, 25, 50, 125, 250, 500, 750, 1000, 2000, 4000, and 8000 µM. All of these samples were analyzed by LC/MS/MS method described in Appendix 10. Data were fit using GraphPad Prism 8 using the following equation set that is a nested set of equations for allosteric activation and a mixed model of inhibition with a Hill coefficient for the inhibitory and allosteric sites:(27)

$$V_{apparent,allo\ unbound} = \frac{V_{max,unbound}}{\left(1 + \frac{[CMZ]^{Hill}}{Alpha\ \times {K_i}^{Hill}}\right)} \times \left\{1 - \left(\frac{[CMZ]^{Hill}}{{K_{allo}}^{Hill} + [CMZ]^{Hill}}\right)\right\}$$

$$V_{apparent,allo\ bound} = \frac{A \times V_{max,unbound}}{\left(1 + \frac{[CMZ]^{Hill}}{Alpha\ \times K_i{}^{Hill}}\right)} \times \left(\frac{[CMT]^{Hill}}{K_{allo}{}^{Hill} + [CMZ]^{Hill}}\right)$$

$$K_{m,apparent,allo\ unbound} = \frac{K_m \times \left(1 + \frac{[CMZ]^{Hill}}{K_i{}^{Hill}}\right)}{(1 + [CMZ]^{Hill})}$$

$$K_{m,apparent,allo\ bound} = \frac{B \times K_m \times \left(1 + \frac{[CMZ]^{Hill}}{K_i{}^{Hill}}\right)}{(1 + [CMZ]^{Hill})}$$

$$Y = \left(\frac{V_{apparent,allo\ unbound} \times [Midazolam]}{K_{m,apparent,allo\ unbound} + [Midazolam]}\right) + \left(\frac{V_{apparent,allo\ bound} \times [Midazolam]}{K_{m,apparent,allo\ bound} + [Midazolam]}\right)$$

$$X = [Midazolam]$$

2.2.8 TDI Screening of CYP2A6, 2B6, 2C19, 2E1, 3A4/5 in HLM Incubations

TDI screening was performed at 37º C in a water bath using a dilution assay at 1/10th dilution from the pre-incubation to the secondary incubation which used to determine the remaining activity.(75,76,78,187) 3 non-zero concentrations were chosen with at least one concentration being above the IC_{50} or K_i, and a no compound control was used to normalize the λ values against gain or less of enzyme activity due to pre-incubation NADPH. Pre-incubations consisted of total volume 100 µL containing 0.1 M potassium phosphate buffer with 0.5 mg/mL pooled human liver microsomes, 2 mg/mL NADPH, and CMZ solvated in water. Pre-incubations were pre-incubated for 5 minutes before the addition of NADPH in a 37º C water bath. Pre-incubation samples were mixed for 15 seconds before transfer into the secondary.

10 µL of pre-incubation sample was transferred and added to 90 µL of secondary incubation containing 0.1 M potassium phosphate at pH 7.4, 2 mg/mL NADPH, and the appropriate substrate at 10/9ths of the final concentration. We used 20 µM coumarin, 500 µM bupropion, 400 µM chlorzoxazone, 200 µM S-mephenytoin, and 200 µM testosterone as the

substrates for these screening assays. The secondary incubation was terminated using 100 µL of acetonitrile/methanol containing the appropriate IS. Standard curves were prepared in the same manner as the co-incubation assays, and samples were analyzed used methods in Appendices 2, 3, 6, 8, and 10.

Data were analyzed using GraphPad Prism 8.2. Remaining activity was natural log transformed and plotted versus time, and linear regression was performed to determine the rate of loss of CYP activity (λ). K_I/k_{inact} values were estimated using the method described by Albaugh et al (Drug Metabolism Letters 2009) for design of subsequent experiments.

2.2.9 Time-Dependent Inhibition Kinetics for CYP2B6 and CYP3A4/5.

Assays were carried out in similar manner as the screening assays with limited changes. The pre-incubation times for CYP2B6 and CYP3A4/5 assays were 30 seconds, 5 minutes, 15 minutes, and 30 minutes. The concentrations of CMZ used for CYP2B6 were: 0, 3, 10, 30, 100, 300, 1000, and 3000 µM, and the CMZ concentrations used for CYP3A4/5 were 0, 78.125, 156.25, 312.5, 1250, 2500, 5000, and 10000 µM. 40 µM Midazolam was substituted for testosterone as the CYP3A4/5 substrate while bupropion was still used for CYP2B6. All other conditions were retained in reference to the screening conditions.

Data were analyzed using GraphPad Prism 8.2. Remaining activity was natural log transformed and plotted versus time, and linear regression was performed to determine the rate of loss of CYP activity (λ). The resulting λ values were then used to generate Michaelis-Menten fits to estimate K_I and k_{inact}.(75,76,78,122,187)

2.2.10 Time-Dependent Inhibition Kinetics for CYP2E1 in HLM and MLM.

Due to the rapid inactivation of CYP2E1 by CMZ, a modified version of the dilution assay was used involving direct addition of the secondary incubation to the primary incubation. Approximately 120 holes were drilled into a 1 mL deep well plate to allow air to escape from the

structure of the deep well plate and to allow better circulation of water around the wells. The deep well plate was weighted down in the water bath by deep sea fishing weights tied to the plate by fishing line. Incubations still occurred in a 37º C water bath.

Pre-incubations consisted of total volume 80 µL containing 0.1 M potassium phosphate buffer with 0.5 mg/mL pooled human liver microsomes or pooled male CD-1 mouse liver microsomes, 2 mg/mL NADPH, and CMZ solvated in water. CMZ concentrations for HLM pre-incubations were 0, 10, 30, 100, 300, 1000, 3000, and 10000 µM, and CMZ concentrations for MLM were 0, 3, 10, 30, 100, 300, 1000, and 3000 µM. Secondary incubation solutions contained 0.1 M potassium phosphate at pH 7.4, 2 mg/mL NADPH, and the appropriate substrate at 10/9ths of the final concentration of CHZ (400 µM final).

Pre-incubation times were 1, 15, 30, and 60 seconds for HLM incubations and 1, 30, 60, and 120 seconds for MLM incubations. 720 µL of the secondary incubation was directly added to the primary incubation to start the secondary reaction. After a 5 minute secondary incubation. the entire volume was transferred to a kill plate with 800 µL of acetonitrile/methanol containing IS to stop the reaction. Standards were prepared in the same manner as all other assays and analyzed used the same method in Appendix 1.6 as other chlorzoxazone assays.

Data were analyzed using GraphPad Prism 8.2. Remaining activity was natural log transformed and plotted versus time, and linear regression was performed to determine the rate of loss of CYP activity (λ). The resulting λ values were then fit using the substrate inhibition model to estimate K_I and k_{inact}.(197)

2.2.11 Time-Dependent Inhibition Kinetics for CYP2E1 in Human and Mouse Hepatocyte Incubations.

Human hepatocytes were recovered from cryopreservation by thawing with lukewarm water and then gently resuspended in recovery media according to the manufacturer's specifications.

The cells were spun at 55 g for 10 minutes, and the recovery media was removed. Cells were resuspended in plating media at 750,000 cells/mL. Williams' E media containing 10% FBS and 1x pencillin/streptomycin/glutamine was added at 50 µL/well to a 96-well collagen I coated plate. 80 µL of hepatocytes (60,000/well) were added to each well, and cells were allowed to attach for 4 hours in a 5% CO_2 incubator at 37º C.

Mouse hepatocytes were received as a fresh suspension. The cells were spun at 55 g, and media was removed. The cells were resuspended at 750,000 cells/well in Williams' E media containing 10% FBS, 1x penicillin/streptomycin/glutamine, 1x insulin/transferrin/selenium solution, and 10 mM HEPES. 50 µL/well of the same media was added to each well before the addition of 80 µL of cells to a 96-well collagen I coated plate. Cells were allowed to attach for 4 hours in a 5% CO_2 incubator at 37º C.

CMZ, CHZ, and p-nitrophenol were solvated with Hanks' Balanced Salt Solution (HBSS) with 10 mM HEPES. CMZ concentrations in HBSS for human hepatocyte incubations were 0, 10, 30, 100, 300, 1000, 3000, and 10000 µM, and CMZ concentrations for mouse hepatocyte incubations, were 0, 3, 10, 30, 100, 300, 1000, and 3000 µM. The substrates, CHZ and p-nitrophenol, were at 400 µM.

The TDI kinetic experiments were performed in a 37º C water bath. The incubations were initiated by the addition of HBSS containing CMZ after aspiration of the plating media. CMZ containing media was aspirated at the end of the pre-incubation time (1 second, 30 seconds, 60 seconds, and 120 seconds), and CHZ or p-nitrophenol containing HBSS was added for the secondary incubation. 90 µL of secondary incubation media was transferred into a 96-well analysis plate after a 5 minutes. 90 µL of acetonitrile/methanol containing the appropriate IS was added to each samples. A standard curve was generated by serial dilution of the appropriate metabolite standard in HBSS with 10 mM HEPES. IS was added in the same manner as the

incubation samples to the standard curve samples. Samples were analyzed using the LC/MS/MS methods in Appendices 8 and 9.

Data were analyzed using GraphPad Prism 8.2. Remaining activity was natural log transformed and plotted versus time, and linear regression was performed to determine the rate of loss of CYP activity (λ). The resulting λ values were then fit using the substrate inhibition model to estimate K_I and k_{inact}.(197)

2.2.12 Metabolite Identification in HLM and Recombinant CYP Incubations.

Incubations were performed in a 96 well plate in 37º C water bath. All samples contained 0.5 mg/mL of HLM or 100 pM Supersomes™ recombinant CYP enzymes with containing 0.1 M potassium phosphate buffer at pH 7.4 with 100 µM CMZ. Most samples contained 2 mg/mL NADPH with 5 mM glutathione as the reactive species trapping agent, but 1 mM potassium cyanide and 1 mM methoxamine were also used as alternative trapping agents. Other samples containing 1 mM UDPGA/50 µg/mL alamethicin with 2 mg/mL NADPH were also performed with HLM. 1 mg/mL Human liver S9 was used with 1 mM 3'-phosphoadenosine 5'-phosphosulfate with 2 mg/mL NADPH. The incubations were terminated with an equal volume of acetonitrile/methanol and centrifuged. The supernatants were removed for LC/MS analysis, and those samples were analyzed using an AB Sciex 5600 TripleTOF™ system with the method described in Appendix 13. Data were also analyzed with the software described in Appendix 13. Synthetic standards for CMZ N-oxide and 5(1-hydroxyethyl) 4-methylthiazole were diluted to 10 µM in 0.1 M potassium phosphate at pH 7.4 and analyzed using the same analytical and data analysis methods as the incubated samples.

2.3 Results

Research Strategy

Results are presented in a sequence roughly following the workflow required to identify the CYP isoforms that serve as targets of inhibition for CMZ, the type of inhibition associated with each isoform, and potential metabolic routes that could result in time dependent inhibition (TDI). Initially, a set of co-incubation experiments was performed with CMZ to estimate IC_{50} values for all major drug metabolizing CYP isoforms so that isoforms of greatest interest could be selected for later experiments. If the IC_{50} for an isoform was substantially lower than 1 mM, additional co-incubation experiments were performed to determine the K_i and type of apparent reversible inhibition. Furthermore, those same isoforms with sub 1 mM IC_{50} values were tested for TDI using a limited set of concentrations and pre-incubation times in dilution experiments. If TDI was detected, a dilution experiment was performed using a wider range of CMZ concentrations and pre-incubation times to determine the TDI kinetic parameters. Finally, a series of metabolite identification experiments was performed for HLM and major liver drug metabolizing CYP isoforms to link any potential metabolite formation to TDI.

2.3.1 Selectivity of Chlormethiazole CYP Inhibition in Co-incubation Experiments.

As a first level of analysis of the selectivity of CYP inhibition, CMZ inhibition potency was tested in HLMs with selective CYP substrates to obtain IC_{50} values with substrate concentrations near K_m for enzymes other than CYP2E1, which was already selected to undergo detailed analysis. The results are summarized in Figure 2.2. CYP2A6 and CYP2B6 had the lowest IC_{50} values of all enzymes tested, and, overall these results were similar to those of Stresser et al.(148)

CMZ effects on CYP3A4/5 inhibition proved to be highly substrate dependent. Testosterone 6β-hydroxylation was inhibited by CMZ, but nifedipine dehydrogenation was clearly not inhibited and was even mildly enhanced. CMZ exerted positive allosteric modulation upon 1'-OH midazolam formation before inhibition occurred. Since 4-hydroxymidazolam formation was not analyzed in these experiments, no information was obtained regarding the effect of CMZ upon

this other major CYP3A4/5 metabolite of midazolam. In sum, the enzymes that were inhibited by CMZ with IC_{50} values lower than 1 mM were selected for further detailed analysis including K_i determinations and screens for TDI.

2.3.2 Co-incubation K_i Determinations for CYP2E1, 2A6, 2B6, and 2C19.

CYP2E1, 2A6, 2B6, and 2C19 were most potently inhibited by CMZ and so were chosen for co-incubation experiments to determine K_i and the apparent mechanism of reversible inhibition. The same probe substrates used during the IC_{50} screens were used to determine K_i and the mode of reversible inhibition using a mixed model of inhibition.

For CYP2E1, K_i was determined across 3 substrate concentrations (25, 75, 225 μM) and the data analyzed using a mixed model of inhibition (Figure 2.3). The kinetics of chlorzoxazone formation in HLMs (K_M of 33.9 μM and V_{max} of 1623 pmol/min/mg) were in line with much of the extant literature.(198-201) The apparent K_i is 18.0 μM, which is close to 12 μM, the first value ever reported for CMZ, although that study was reported for an apparent non-competitive mechanism.(152) In the mixed inhibition model, alpha is a variable that tries to account for inhibition types that are not competitive. When alpha is greater than 10, the data more closely fit a competitive inhibition scenario, which is what is seen for CYP2E1 with an alpha value of 180.

CMZ inhibition kinetics for CYP2A6, 2B6, and 2C19 have not been reported previously, so the model fits from experiments employing 3 substrate concentrations with several inhibitor concentrations are presented in Figures 2.4, 2.5, and 2.6, respectively. CMZ exhibited a K_i of 7.7 μM towards CYP2A6 which is slightly lower than for CYP2E1 and an alpha value that is consistent with competitive inhibition. CYP2B6 and CYP2C19 were more weakly inhibited by CMZ with K_i values of 169 and 178 μM, respectively. However, both sets of interactions exhibited alpha values that are indicative of non-competitive inhibition playing a greater role in the inhibition of those isoforms compared to CYP2E1 and CYP2A6.

2.3.3 Complex Interactions of CMZ, CYP3A4/5, and Midazolam.

The IC_{50} inhibition data for CYP3A4/5 substrates indicated substrate dependent effects of CMZ upon the metabolism of those common 3 substrates. 1'-Hydroxylation of midazolam appeared to be enhanced by CMZ co-incubation at lower CMZ concentrations, which indicates positive allosteric modulation in the initial IC_{50} screening experiments, but this activity appears to be reduced by some form of inhibition. 6β-Hydroxylation of testosterone alone is inhibited by CMZ, whereas nifedipine dehydrogenation may undergo mild positive allosteric modulation by CMZ without any apparent inhibition in the concentration range tested. Therefore, a set of experiments to further explore the complexity of interactions of CYP3A4/5 using multiple concentrations of midazolam and CMZ using HLM, HLM deficient in CYP3A5, and recombinant CYP3A4 were performed. In addition to monitoring 1'-hydroxymidazolam formation, 4-hydroxymidazolam was also monitored during these experiments to elucidate potential differences between the effects of CMZ on both metabolites.

In the first follow-up experiment, more midazolam concentrations and a wider range of CMZ concentrations were used in a co-incubation experiment with the goal of defining the unusual effects of CMZ upon 1'-hydroxymidazolam and 4-hydroxymidazolam formation. The pattern of positive allosteric modulation followed by inhibition with increasing concentrations of CMZ was recapitulated. Due to the importance of CYP3A4/5 in drug metabolism and the complex interaction of CMZ with midazolam, a more in-depth analysis of midazolam and CMZ interactions than we present here is warranted. This may require an analysis of CMZ metabolites since models, such as those developed by Shou et al, use kinetics of metabolites to characterize the binding sites for each compound in the interaction.(27,202). However, we do not have synthetic standards for all metabolites formed by CMZ in human liver microsomes, and the metabolite identification experiments describing all of the metabolites that were found in HLM containing incubations appear later in this chapter. Therefore, to model the behavior in the absence of

metabolite kinetics of CMZ, a set of equations were used under the assumption that the behavior of CYP3A4/5 could be described with CMZ binding at an allosteric site and/or an inhibitory site with the major underlying assumption that the behavior of the formation of 1'-hydroxymidazolam could be described with Michaelis-Menten kinetics. A Hill coefficient was included to apply to the allosteric binding site and inhibitory binding site to account for any possible cooperative or uncooperative binding between the binding sites. The rest of the underlying assumptions and implications for use of these equations (27) will be discussed later.

The data and fit for 1'-hydroxymidazolam activity in HLM are presented in Figure 2.7. For 1'-hydroxymidazolam activity in microsomes, the midazolam K_m of 2.9 μM and V_{max} of 1903 pmol/min/mg were in line with expectations for pooled HLM, and the fit of the set of equations using least squares resulted in a reasonable R^2 of 0.9864. The affinity for the allosteric binding site as indicated by K_{allo} is estimated to be 202 μM, and the inhibitory binding site (Ki) was estimated to be 1.34 mM. The shared Hill coefficient was approximately 1.6 indicating some cooperativity occurred. The alpha value for inhibition was 17.45 indicating a mixture between competitive inhibition and non-competitive inhibition. The apparent A value indicating changes in V_{max} caused by binding at the allosteric binding site was 1.23 suggestive of a mild increase. The apparent B value, which indicates changes in K_m, was 0.59 indicating a potential increase in affinity for the substrate. Overall, these values describe the apparent relationship between CMZ concentration and changes in 1'-hydroxymidazolam activity.

The same model was applied to 4-hydroxymidazolam activity in HLM incubations, and the data and fit are presented in Figure 2.8. The global fit was 0.9937 with a K_m of 22.2 μM and V_{max} of 2269 pmol/min/mg for 4-hydroxymidazolam formation. The apparent K_{allo} was similar to 1.6 mM, and K_i was approximately 324 μM. Both of these values are reasonably close to the values obtained for 1'-hydroxymidazolam. However, the Hill coefficient was estimated to be 0.70 which indicates negative cooperativity. The alpha value for inhibition was 0.0716 which is consistent

with uncompetitive inhibition. The A value was 19.52 suggesting an increase in V with binding of the allosteric site, but the B value was 12.51 suggesting a lowered affinity for the substrate with allosteric binding. The apparent effect of positive allosteric modulation appeared to be more muted than was seen for 1'-hydroxymidazolam activity.

Since midazolam can be metabolized by both CYP3A4 and CYP3A5, a pool of HLM possessing the null genotype CYP3A5*3/CYP3A5*3 was made to eliminate the contribution of CYP3A5 to the metabolism of midazolam. This preparation of HLM was used to produce the data presented in Figure 2.9 for 1'-hydroxymidazolam and Figure 2.10 for 4-hydroxymidazolam. The apparent rates of metabolite formation were lower than seen with the HLM used for previous experiments, and the overall 4-hydroxymidazolam kinetics appeared to be affected to a greater extent than 1'-hydroxymidazolam kinetics.

While the V_{max} for 1'-hydroxymidazolam in CYP3A5 deficient HLM was lower, much of the remainder of the kinetic parameters; K_m, inhibition alpha value, Hill coefficient for the allosteric and inhibitory sites, A parameter, and B parameter were similar to the HLMs prepared from the larger (CYP3A5-active) donor lot. The K_{allo} and K_i exhibited a similar pattern to that seen with the previous pool of HLM containing active CYP3A5, but were approximately 43% lower and 43% higher, respectively, when compared to the pool containing active CYP3A5.

Data for 4-hydroxymidazolam activity from the CYP3A5 deficient pool are presented in Figure 2.10. 4-Hydroxylation kinetics in this pool are substantially different as compared to the other HLM preparation, but the allosteric effect is muted as compared to 1'-hydroxymidazolam as seen with the 3A5-active pool. If a simple Michaelis-Menten analysis is performed, a good estimate of K_m is not captured since saturation does not appear to be occurring and the extracted K_m is more than 10 fold above the highest concentration tested. The fit is ambiguous in part due to lack of definition of the K_m and V_{max} and lack of the points defining the small region of positive

allosteric modulation. Therefore, the values from the curve fitting are not reliable and were not reported.

To further investigate the interactions between CMZ and CYP3A4, Supersomes™ with cytochrome P450 reductase and cytochrome b_5 were used in similar experiments to those conducted in HLM. The same range of concentrations were used as with the other experiments. The data was fit with the same set of equations as the HLM experiments for 1'-hydroxymidazolam formation and is presented in Figure 2.11. The positive allosteric modulation for 1'-hydroxymidazolam is muted with the recombinant system with an A value of 1 meaning no effect upon the maximum rate of the catalysis. However, the values for many of the parameters are similar to those from the HLM experiments including a mild apparent increased affinity for the substrate when the allosteric site is occupied, as signified by the B value of 0.81. The fit for 4-hydroxymidazolam activity, which is presented in Figure 2.12, was ambiguous since the K_m could not be determined with the concentration set that was used, and there was no apparent allosteric effect upon 4-hydroxymidazolam activity.

2.3.4 Screening of TDI for CYP2E1, CYP2B6, CYP2C19, CYP2E1 and CYP3A in HLM Incubations

A series of dilution time dependent experiments were performed using 0.5 mg/mL pooled HLM in the primary incubation with a 10x dilution to screen the potential of CYP2A6, CYP2B6, CYP2C19, CYP2E1, and CYP3A4/5 for TDI with limited concentrations and time points (30 seconds, 5 minutes, and 30 minutes) for the pre-incubation. The 3 concentrations were chosen for each CYP isoform with the goal of having one concentration below the IC_{50} or $K_{i,}$ one concentration being near the IC_{50} or K_i, and one concentration above IC_{50} or K_i. Each of these isoforms exhibited IC_{50} values that were below 500 µM which is why they were chosen. The data from these experiments, used to estimate K_I and k_{inact} with a derivation of a Kitz-Wilson plot, are presented in Figure 2.13.(203)

Since, in the presence of a source of reducing equivalents alone, CYP enzymes will inactivate themselves through the uncoupling process, a vehicle control was used to compare the inactivation rates (λ) of the enzyme in the presence of NADPH vs. NADPH with CMZ in order to determine the inactivation rate due to bioactivation of CMZ. CYP2A6-dependent 7-hydroxycoumarin activity decreased with time and with no appreciable difference between any of the treatment conditions. CYP2B6-dependent bupropion hydroxylation activity decreased at a similar rate to CYP2A6 activity with the NADPH control but exhibited substantial TDI at 200 and 2000 μM. CYP2C19-dependent 4-hydroxymephenytoin activity increased over time and was exacerbated by CMZ in a time dependent and concentration dependent manner. CYP2E1 underwent rapid time-dependent and concentration-dependent inhibition while whereas CYP3A4/5-dependent 1'-hydroxymidazolam activity was also concentration and time dependent, the rate of TDI was much slower as compared to CYP2E1. Since CYP2B6, CYP2E1, and CYP3A4/5 were each inhibited in a time and concentration dependent manner by CMZ, they were selected to undergo further experiments to determine the kinetic parameters, K_I and k_{inact}.

2.3.5 Determination of K_I and K_{inact} Parameters Incubations for Microsomal CYP2B6, CYP2E1, and CYP3A4/5.

A series of dilution experiments were performed to measure the kinetics of TDI by CMZ for CYP2B6, CYP2E1, and CYP3A4/5. Four time points and 7 non-zero concentrations were chosen for each isoform based upon the preliminary data generated in the preliminary screening experiment. The incubation conditions were otherwise similar to those in the screening experiment. Activity remaining was natural log transformed, and a linear regression was performed for each CMZ concentration to determine the apparent inactivation rate (λ). The control containing all reaction components except CMZ was used to normalize the data in order to eliminate the contribution of TDI from enzyme uncoupling.(75,76,78,187)

The TDI kinetic experiments for CYP2B6, CYP2E1, CYP3A4/5 are presented in Figures 2.14, 2.15, 2.16, respectively. While TDI of CYP2B6 and CYP3A4/5 appeared to follow Michaelis-Menten kinetics, TDI of CYP2E1 does not follow Michaelis-Menten kinetics, but fits a substrate inhibition model fairly well. CYP2E1 exhibited both the lowest K_I (49.4 μM) and highest k_{inact} (0.325/min), which is in line with the findings of Stresser, et al.(148) CYP2B6 exhibited a slightly higher K_I than CYP2E1, but the k_{inact} was far lower. The K_I for CYP3A4/5 was 5 mM, which was by far the highest of the three isoforms tested, but the k_{inact} was higher than for CYP2B6.

2.3.6 Kinetics of CYP2E1 Inhibition in Human and Mouse Hepatocytes and Mouse Liver Microsomes

CMZ is used as an inhibitor for CYP2E1 in human hepatocytes and animal toxicology models, but the inhibition kinetics in those systems are not defined.(1,151,204-207) There could be numerous potential reasons for differences in TDI rates in whole cell systems as compared to microsomes, such as permeability, transport, deactivation of reactive species, endogenous substrates, non-microsomal metabolism, and non-CYP metabolism. Not only does the determination of inhibition kinetics in these systems allow for proper use of CMZ to obtain the desired degree of inhibition, but may also indicate issues with scaling to in vivo from microsomes that should be investigated. It has been claimed that para-nitrophenol hydroxylation to the catechol is more selective for capturing CYP2E1 activity in mice than chlorzoxazone 6-hydroxylation, but there has been no systematic analysis to substantiate that claim, so both assays were performed in mouse hepatocytes.(208)

Results for all assays are presented in Figure 2.17. Each assay type displayed substrate inhibition kinetics as was seen with HLM. TDI kinetic values in plated human hepatocytes were very similar to those obtained with HLM, as shown in Figure 2.15 and 2.17. Mouse liver microsome and mouse hepatocyte kinetics also exhibited a substrate inhibition profile as seen in Figure 2.17, but there are issues with the fits for the mouse hepatocyte data as compared to

mouse microsomal data. Chlorzoxazone 6-hydroxylation in hepatocytes did not fit a standard substrate inhibition kinetic model, and the fit for p-nitrophenol catechol formation was significantly worse than the mouse liver microsome data, even though a substrate inhibition kinetic profile is clearly evident.

2.3.7 Metabolite Identification in HLM.

CMZ (100 μM) was incubated with HLM (0.5 mg/mL), reduced glutathione (5 mM), NADPH (2 mg/mL) for 1 hour, and reactions were terminated by addition of acetonitrile and methanol. The supernatant was removed after centrifugation for analysis. Samples were then analyzed using high pressure liquid chromatography and a 5600 Triple TOF mass spectrometer with an Information Dependent Acquisition (IDA) method that used mass defect filtering as the major triggering criteria for product ion scans. The test sample was compared to control samples that lacked CMZ or cofactors or had been terminated with organic solvent before the addition of cofactors.

A total of 5 CMZ metabolites (M1-M5) were identified. An overlay of all of the metabolites and parent compound is presented in Figure 2.18. An inset was necessary to clearly show M2 and M3 relative to M1, due to large disparities in signal intensity. M1 and M4 have similar responses and exhibit the largest signal intensities of any of the metabolites, which suggests they are likely the major metabolites of CMZ. A commercial standard for M1 was obtained, and only a standard for M3 – the N-oxide - could be synthesized easily. Therefore, we are only able to definitively confirm the structural assignment of M1 and M3 and possibly provide a quantitative assessment of M1 and M3 formation rates. The extracted ion current chromatograms for these standards are presented in Figure 2.19.

The fragmentation patterns acquired from the data dependent product ion spectra for CMZ, each of the metabolites, 5(1-hydroxyethyl) 4-methylthiazole standard, and N-oxide synthetic standard are shown in Figures 2.20 to 2.27. The interpretation of the fragmentation patterns is

also included in those figures as is a table of predicted and experimentally found fragment masses. Due to the low concentrations of the M3 N-oxide formed in the HLM incubations, the amount of detected fragments from the N-oxide was low compared to the N-oxide standard. However, major fragments from both aligned well with each other. We do not have standards for the other metabolites, so the fragmentation pattern was used to assign metabolite structures, which must be regarded as tentative. Notably, all mDa errors are for assigned fragments are less than 5 mDa which is within acceptable limits.

When considering the mass of the parent CMZ, dechlorination and a net insertion of hydroxide must have occurred to generate the m/z of M1. A loss of water occurs without a loss of any other portions of M1, which is consistent with the loss of water from an alcohol on an aliphatic group attached to the thiazole core. We were able to determine the position of the alcohol via the use of the synthetic standard since the fragmentation and retention time of 5(1-hydroxyethyl) 4-methylthiazole matched M1. If oxidative dechlorination occurred, further oxidation should result in an aldehyde at the original position of the halogen, which then would likely be reduced to the alcohol by a carbonyl reductase.(12,38,158,159,209) Reductive dehalogenation would result in a carbon centered radical at the position of the chlorine that could rearrange to the carbon alpha to the ring of the ethyl side chain.(12,156,157) To form the alcohol, a hydroxide radical would need to be generated that then recombined with the carbon radical. Since the aldehyde was not observed, it is likely that oxidative dechlorination did not occur, but it cannot be excluded.

M2 is the result of a net dehydrogenation and adduction by glutathione. The 194 m/z fragment indicates that the sulfur is retained while the rest of the glutathione moiety can be removed by fragmentation. This type of sulfur-containing fragment from a glutathione adduct is highly suggestive of the sulfur of glutathione adducting to the C-2 position, since the carbon-sulfur bond is stabilized by an aromatic ring.(6,210,211) When glutathione is adducted to an aromatic

carbon, the sulfur from the cysteine forms a fairly stable bond that interacts with the π system of the aromatic ring, which enables the sulfur to remain attached to the ring during fragmentation. In contrast, the linkage between cysteine and a non-aromatic position of a reactive species, such as an α,β-unsaturated ketone or methyl group attached to an aromatic, is far weaker and the glutathione moiety can be lost in its entirety. The majority of the other fragments are related to the fragmentation of glutathione. The step leading to the time-dependent reactivity is not indicated directly by any of the data obtained from fragmentation of this metabolite.

M3 is the N-oxide based on similarities in retention time and fragmentation of the synthetic N-oxide and HLM-generated metabolite. N-oxide thiazoles can exist as the tautomeric form, which is a hydroxylamine with a C-2 carbene center.(162,168,212) The 161 m/z fragment that is common to both is likely the loss of a hydroxyl radical that could occur from the carbene tautomer. Oxygen is retained in the 129 and 142 m/z fragments, which is consistent with a more stable bond between oxygen and the atom to which it is attached, or greater difficulty in the elimination of the oxygen as water as with other positions, such as aromatic methyl groups. The aforementioned fragments are consistent with the position of oxidation being the thiazole nitrogen.

M4 is likely the result of oxidation of C-2 of the thiazole ring. The unique 114 m/z fragment is the most important in assigning the site of oxidation. The cleavage to form the 114 m/z fragment is consistent with the elimination of the chloro-ethyl side chain, which would leave the sulfur, C-4 methyl, C-4/C-5 double bond, and C-2 as likely positions of oxidation. No fragment exists to definitively assign the oxidation to the C-2 carbon, but there are circumstances that make it more likely that it is C-2 oxidation. S-oxides of heterocyclic systems tend to be reactive with glutathione, so it seems unlikely that substantial amounts of the metabolite could be formed without large amounts of glutathione adduct being generated.(15,154,174,175) The facile loss of water during fragmentation is frequently a strong indicator of the hydroxylation of an aromatic methyl group, but that does not appear to occur with M4. Epoxidation of the C-4/C-5 double bond is sterically

hindered and would also likely be reactive since the aromaticity of the ring would be eliminated.(153) Therefore, oxidation at C-2 is the most likely candidate for the identity of M4.

M5 corresponds to hydroxylation of the C-4 methyl as indicated by multiple fragments. The 160 m/z fragment is a loss of water, which is consistent with oxidation of an alkyl position attached to an aromatic system. Therefore, it is expected that either the chloroethyl or methyl groups would be the potential sites of oxidation. The pair of 128/129 m/z fragments are associated with the elimination of the β-carbon of the chloroethyl side chain, but the oxygen is retained. An oxidation of the α-carbon of that side chain should result in dechlorination due to an increase in acidity of the neighboring protons leading to facile elimination of a chloride ion. The oxygen is likely stabilized in the 128 m/z fragment by the formation of a carbonyl double bond when the chloroethyl β-carbon is eliminated by heterolytic cleavage. The combination of these factors supports assignment of M5 as the C-4 methyl alcohol.

2.3.8 Metabolite Identification for Individual CYP Isoforms

Since the CMZ-dependent TDI is isoform dependent, a metabolite identification study using Supersomes™ was performed with all of the major liver drug metabolizing CYP isoforms in order to identify metabolites that may be related to the mechanism of TDI. The rationale here is that only CYPs exhibiting TDI would be expected to generate metabolites responsible for generating reactive intermediates. The incubations consisted of 100 pmol/mL recombinant CYP, 100 μM CMZ, 2 mg/mL NADPH, and 5 mM reduced glutathione, and those reactions were allowed to proceed for an hour before termination. The overlayed extracted ion current chromatographs are presented in Figures 2.28 to 2.37. While these figures show the distribution of metabolism in a qualitative manner, it is easier to visualize the differences between the various isoforms in a table of integrated areas for both absolute values and relative percent, as shown in Figure 2.38

If the relative ionization efficiency for each metabolite is assumed to be fairly similar, the amounts of metabolite formed can roughly be compared. M4 is the most prominent metabolite

for most isoforms, which is consistent with M4 being the major metabolite from HLM incubations. CYP2A6 produces the greatest total area of metabolites followed by CYP3A4. Due to CYP3A4 being the most highly expressed isoform in the liver, it is expected that CYP3A4 would be the major contributor to CYP-mediated liver metabolism of CMZ. Even though M1 has roughly the same area response in the HLM incubation, only CYP2B6-catalyzed metabolism of CMZ produced more area counts for M1 compared to M4. CYP2A6 produces a relatively large amount of M1 relative to M4, but most other isoforms do not generate a large quantity of M1. CYP2B6 appears to be the major enzyme for the formation of M5, with CYP2E1 likely being the other major contributor. Importantly, we identify M2 and M3 as the two metabolites that are generated by the isoforms that are most inhibited in a time dependent manner by CMZ.

2.4 Discussion

2.4.1 Chapter Overview and Hypothesis.

The inhibition of CYP2E1 by chlormethiazole was first identified by Gebhardt et al in vivo and in vitro.(152) These workers showed approximately an 80% decrease in the 6-hydroxychlorzoxazone/chlorzoxazone blood ratio in a control group of subjects when they were treated with 192 mg of chlormethiazole.(152) They also showed that the inhibition was prolonged, but only characterized the inhibition in vitro using a co-incubation assay with chlorzoxazone. Taking into account that the C_{max} for a higher dose of 384 mg was only 2.4-3.7 μM and that the noncompetitive K_i was 12 μM, the in vitro inhibition did not account for the in vivo inhibition.(137) While the studies described herein were underway, Stresser et al published on CMZ selectivity of CYP inhibition and performed TDI kinetics for CYP2E1.(148) These workers clearly showed that CMZ is a TDI of CYP2E1 and suggested that CMZ may also be a time-dependent inhibitor of CYP2B6. Stresser et al also performed a static prediction of CYP2E1 TDI by CMZ, which appears to mostly explain the in vivo effects on CYP2E1, as seen with chlorzoxazone as the victim drug.

The overall conclusion from the preceding work is that CMZ is a selective, potent TDI of CYP2E1. However, in order to the test this thoroughly, the CYP selectivity of inhibition must be fully established, and the mechanism of any TDI needs to be investigated in detail. Towards these ends, the inhibition by CMZ of all major liver drug metabolizing CYPs was assessed. These studies included an initial IC_{50} screen, co-incubation K_i determination, TDI screen for selected CYPs and full TDI kinetic experiments for the most affected enzymes. The kinetic data obtained in these experiments can also be used to build a physiologically based pharmacokinetic (PBPK) model to predict the drug-drug interaction potential of CMZ.(76,78) In addition, metabolite identification with reactive metabolite trapping was performed to identify any potential metabolites and trapped reactive species that could suggest potential chemical mechanisms for the TDI process.

While several in vivo metabolites have been identified by multiple investigators (Figure 2.38), no in vitro metabolism has been reported, and there is limited information on potential reactive species that could be related to the TDI.(135,213,214) While it is likely that the reported metabolites are mostly generated in the liver, it is not clear if that assumption is true or which enzymes produce each metabolite. The chloroethyl group is truncated in some of the reported metabolites. The truncation of chloroethyl group could be due to a β-oxidation or β-oxidation like process since there are also other reported metabolites that are consistent with multiple oxidation steps occurring to the chloroethyl chain.(215) There also appears to be missing intermediates in the formation of some metabolites. The dual N-oxide/S-oxide with truncation of the chloroethyl group has been reported, but no other N- or S-oxide-containing metabolites have been observed and identified. From these data, it is not evident at which point during catabolism the N- or S-oxidation may have occurred, and there is no explanation as to why there are no metabolites detected due to N- or S-oxidation alone. Therefore, we undertook the microsomal metabolism identification to help clarify how these metabolites are formed. While there is a report of an ethylene metabolite that could function as a Michael Acceptor, no downstream products of glutathione adduction have been reported, so it is not clear what other reactive species might explain the observed TDI. Finally, discovery of potential reactive metabolites is also a focus of this chapter, since they could be critical in understanding the mechanisms for TDI of CYPs due to CMZ.

2.4.2 Selectivity and Complexity of CMZ Inhibition of Major Liver Drug Metabolizing CYP Isoforms in Co-incubation Experiments.

To assess the inhibition selectivity of CMZ with major liver CYP isoforms, a series of co-incubation and dilution TDI experiments were performed using generally accepted selective CYP substrates.(185,189-191) These studies were also performed in line with standard practices for

evaluation of drug-drug interactions including the use of multiple substrates for CYP3A4/5 for the IC_{50} assessment.(75,122,185)

Since it is impractical to fully characterize every isoform completely, a workflow was created to funnel isoforms of interest based upon previous assays. The initial screen consisted of co-incubation experiments of CMZ with isoform-selective substrates in HLM incubations to obtain IC_{50} values as shown in Figure 2.2. Any isoform that was inhibited by CMZ with an IC_{50} significantly below 1 mM was then tested with CMZ to screen for TDI using a dilution assay with concentrations of CMZ below, near, and above the IC_{50} from the co-incubation assays. CYP2E1 plus any isoform providing a positive result in the screen was further tested to determine full kinetic parameters (K_I, K_{inact}) for the TDI.

The alpha values from all 4 isoforms that were examined indicated a diversity of inhibition modes in co-incubation experiments by CMZ upon CYP enzymes. Fits of the CYP2A6 and CYP2E1 inhibition yielded alpha values over 100 which are indicative of competitive inhibition. Inhibition of CYP2C19 by CMZ behaved in a manner more consistent with non-competitive inhibition since the alpha value was 2.83. The alpha value of the fit for CYP2B6 inhibition was 12.7 which is an intermediate value consistent with a mixed mode of inhibition. Since we used racemic bupropion and did not perform any separation of the enantiomers of hydroxybuproprion, we cannot hypothesize further on the mechanism of the mixed inhibition mode for CYP2B6 by CMZ.(216-220) It is possible that the same binding site could function both in a noncompetitive mode for one enantiomer of buproprion and in a competitive mode for the other enantiomer. It is also possible that CMZ is binding to an allosteric site that affects the activity of the enzyme, but CMZ has higher affinity for either the substrate bound state or substrate free state.

Interactions between CMZ and CYP3A4/5-mediated metabolism are very complex. CMZ interactions with midazolam, testosterone, and nifedipine exhibit substrate dependent effects and potencies, but substrate dependent effects are not entirely unique.(30,221-223) The FDA

recommends at least two substrates of different classes to address potential of drug-drug interactions because there are multiple examples of substrate dependent effects for drug interactions involving CYP3A4 substrates. One publication by Stresser et al used four distinct fluorogenic probes and compared the effects of a variety of other CYP3A4 substrates on the turnover of those fluorogenic probes then compares these effects to those seen with midazolam, testosterone, and nifedipine. When the effects of various substrates upon each other are compared, there are similarities in many cases, but there are also clear disparities including potency of inhibition (as indicated by the IC_{50}) and even changes in the type of effect.(223) CMZ interactions with the three substrates that were examined exhibit both of the aforementioned disparities.

Several models of varying complexity have been used to describe complex interactions of CYP enzymes with multiple substrates. The multiple conformer model proposed by Koley et al assumed that multiple conformers exist that have differing abilities to bind various substrates.(224) Ueng et al used an allosteric model that utilizes a Hill coefficient for the substrate and K_m to describe the interactions between α-naphthoflavone and multiple substrates.(29) Another variant is a two substrate model proposed by Korzekwa et al, which assumes two catalytically active binding sites with their own distinct V_{max} and K_m values.(26) One of the most complex models is that proposed by Shou et al, which requires metabolite formation for each of the two interacting substrates.(202) The Shou model was used to fit two of the metabolites of losartan and α-naphthoflavone, and by having metabolite formation data for both substrates, the authors were able to derive binding constants for the proposed binding states of CYP3A4. While this is one of the most rigorous examples of kinetic analysis of multi-substrate binding and catalysis, the requirement for sufficient information to employ this type of model can be prohibitive, especially when the appropriate metabolite standards are not all available.

The metabolite identification experiment using CYP3A4 Supersomes indicated at least 4 metabolites were formed by this isoform. While the synthesis and purification of the M3 N-oxide metabolite is relatively straightforward, the synthesis of the other metabolites, including M4 and M5, would require a vastly more complicated synthetic path. The synthesis of M4 and M5 were deemed outside of the immediate requirements of this study since it is not likely that they are reactive metabolites that could explain the TDI effects, which will be examined in more depth later in this thesis.

Due to the lack of metabolite standards with which to fully account for the kinetics of CMZ metabolism, we could not perform an analysis similar to the Shou model and had to employ a simpler model to fit the 1'-hydroxymidazolam and 4-hydroxymidazolam activity. The model we have employed to describe the interaction of CMZ with both 1'-hydroxymidazolam and 4-hydroxymidazolam is a form of a two-state model in which binding the allosteric site results in a distinct enzymatic species with changes in V_{max} and K_m. It employs a mixed model of inhibition in an attempt to capture the nature of the inhibition seen with 1'-hydroxymidazolam and 4-hydroxymidazolam formation with higher concentrations of CMZ. The two distinct species are described by A and B values that relate to V_{max} and K_m, respectively. The apparent constant for binding the allosteric site (K_{allo}) and binding of the inhibitory site (K_i) share a Hill coefficient that is incorporated to the apparent influence of those two binding sites exert upon one another.

When the Hill coefficient is either not used or applied to only the inhibitor or allosteric binding site, the goodness of fit was impaired as compared to when the Hill coefficient was applied to both binding sites. For example, the reported global fit R^2 value of 0.9864 for 1'-hydroxymidazolam activity with HLM when applying the Hill coefficient to both the allosteric and inhibitory binding sites, but, when the Hill coefficient is applied only to the inhibitory site, the R^2 value drops to 0.9493. With no Hill coefficient, the fit becomes ambiguous with every data set examined, and, as a result, we propose that there is cooperativity between the allosteric and

inhibitory binding sites. With all 1'-hydroxymidazolam activity measurements, the fitted Hill coefficients were all about 1.6 and, thereby, suggest positive cooperativity and consistent enzymatic behavior in the three systems that were tested. Due to the ambiguity of the two fits for 4-hydroxymidazolam activity using HLM without CYP3A5 and recombinant CYP3A4, we cannot make such an observation for this metabolite. The Hill coefficient that was derived from the 4-hydroxymidazolam activity data for HLM was 0.699 suggesting that CMZ interaction is exhibiting negative cooperativity with 4-hydroxymidazolam formation. The global fit R^2 for 4-hydroxymidazolam applying the Hill coefficient to both the inhibitory and allosteric binding sites is 0.9937. When a Hill coefficient is only applied to the inhibitory site, the fit is only slightly worse with a R^2 value of 0.9918, but, when the Hill coefficient is completely removed, the fit becomes ambiguous. Taking into account all of these fitting scenarios, it is highly likely that there is some interaction between the binding sites, and the Hill coefficient was necessary to describe these interactions with the current data sets.

The use of a mixed model of inhibition is necessary for describing at least the 1'-hydroxymidazolam data for all three systems, and probably necessary to describe the 4-hydroxymidazolam data in a more mechanistic way. If a competitive inhibition model with allosterism is used for the HLM 1'-hydroxymidazolam data set, the 1 and 3 μM midazolam data are very poorly described, and the overall fit is much worse in terms of R^2 value (0.9477 vs. 0.9864). A non-competitive inhibition model also fits the same data poorly, and those poor fits are consistent with the alpha values from the full model being 11.2 - 17.5 since that range of alpha values indicates a mixed mode of inhibition. The 4-hydroxymidazolam data for HLM is fit reasonably well (R^2 = 0.9867) with a strict non-competitive model that ignores the very subtle allosteric modulation of activity, and a mixed model of inhibition fit (R^2 = 0.9867) also resulted in an alpha of 1.34 that is indicative of non-competitive inhibition. Since there is a clear allosteric modulation from the 1'-hydroxymidazolam data and a mild allosteric modulation is evident at 10

and 30 μM for the 4-hydroxymidazolam data set, it is likely that using a model including allosteric modulation is more appropriate even though the quality of fit is only mildly improved with an R^2 of 0.9937. The quality of the fits for the 4-hydroxymidazolam data were limited by substrate concentrations that were picked to cover the K_m of the 1-hydroxymidazolam formation and not the 4-hydroxymidazolam formation. It is possible that a concentration range more appropriate for 4-hydroxymidazolam would allow a better assessment of models that could be used to fit 4-hydroxymidazolam formation data.

The constants that were derived from the fit of the 1'-hydroxymidazolam activity are fairly consistent from system to system with the exception of the A value. The K_i values range from 1.34 to 2 mM, and the K_{allo} values ranged from 101 to 202 μM. The alpha value for inhibition was similar for all three systems as mentioned previously, so the mechanism of inhibition in the co-incubation experiments are likely the same. In all three model systems for CYP3A4 activity, the B value, which is a modifier of K_m, was lower than 1 suggested that occupation of the allosteric site increases the affinity of the enzyme for the substrate. The A value, which is the V_{max} modifier for allosteric binding site occupation, was less consistent in all three systems. For the two HLM pools, the A value was greater than 1.2, but for recombinant CYP3A4, the A value was 1.00. It is not clear why there is a difference between the recombinant system and the two types of HLM tested, but there are possible explanations.

One explanation for the disparity in the A value between the HLM data and Supersome data is that the ratio of the reductase partners, cytochrome P450 reductase (CPR) and cytochrome b_5, to CYP3A4 is vastly different between HLM and recombinant systems. Recombinant systems are intentionally constructed to optimize turnover rates per unit of P450 so the ratio of reductase partners to P450 are significantly higher than the 1 CPR:5-20 CYP ratios that are typically referenced in the literature for HLMs.(225,226) The increase in reductase partners may mask enhanced coupling or electron transfer rates due to CMZ binding because

increased reductase binding could increase reaction rates at magnitudes in excess of effects due to CMZ allosteric binding.

Another explanation for the A value disparity between systems is the enzyme source of the recombinant Supersomes™ being the Sf9 insect cell line. Supersomes™ CYP preparations are membrane preparations from Sf9 cells which have low expression of endogenous xenobiotic metabolic enzymes. HLM contains numerous metabolic enzymes so there are possible interactions that are missing that could lead to differing enzyme behavior between the two systems.(227) It is also not clear if the lipid composition of Supersomes is similar to that in HLM, so this could also lead to changes in enzymatic behavior across enzyme sources.

CMZ appears to inhibit various CYP isoforms with not only differing affinities, but also different modes of inhibition. These varying modes and complex interactions, as exemplified by the midazolam co-incubation data, suggest modelling any potential interaction with a PBPK model would likely be an even more appropriate approach, since the static models typically only assume competitive inhibition. The [Inhibitor C_{max}]/K_i ratio and other related static models had been frequently used in the past with several assumptions including the inhibition being competitive, and numerous studies and reviews have shown this ratio to be very inaccurate in terms of predicting any DDI.(80,190) Therefore, it is a fair to expect that these and any other available data should be inputted into an appropriate PBPK model to minimize the assumptions and more accurately gauge any potential DDI. To complete the analysis of inhibition, TDI was assessed for CYP isoforms of interest.

2.4.3 Selectivity and Kinetics of TDI of CYP Isoforms by CMZ.

Dilution experiments with HLM show that CMZ is not a generic time dependent inhibitor for the major drug metabolizing CYP isoforms. Even though CYP2A6 has the lowest K_i (7.7 μM) of all isoforms examined in co-incubation experiments, no time-dependent and CMZ-dependent inhibition was detectable relative to the background TDI that was likely the result of uncoupled

catalytic cycles of CYP2A6. CYP2C19 was not inhibited in a time dependent manner by CMZ, but CYP2C19 appeared to undergo time and concentration dependent enhancement by incubation with CMZ. CYP2B6, 2E1, and 3A4/5 were clearly inhibited in a time dependent and concentration dependent manner by CMZ, but they exhibited different kinetics.

TDI of CYP2B6 and CYP3A4/5 exhibited relatively simple kinetics, since they were fit using a standard Michaelis-Menten equation, and those kinetics can be used to estimate the in vivo effects of CMZ upon those isoforms. The K_I value for CYP2B6 (68.3 μM) and the K_I for CYP3A4/5 (5.2 mM) are well above the circulating concentrations of CMZ after 384 mg/day dosing for 7 days, including the C_{max} of 3.7 μM. If the plasma free fraction of approximately 35% is taken into account, the estimated λ at C_{max} for CYP2B6 would be $3.4 * 10^{-4}$/min, and the estimated λ at C_{max} for CYP3A4/5 would be $9.2 * 10^{-6}$/min. In order to calculate the net effect of the inactivation the synthesis rate needs to be considered, but a wide range exists for all isoforms that have been examined.(75) It has been proposed that the half-life of most CYP isoforms is related to the turnover of hepatocytes with a typical times of about 24 hours, which equates to roughly a rate of $4.8 * 10^{-4}$/min. While the fraction enzyme inhibited per minute by CMZ for CYP2B6 is fairly small at circulating concentrations, the λ at circulating concentrations would eventually reduce the steady enzyme concentrations of CYP2B6 by 70% if the circulating concentrations of CMZ are maintained for a sufficient amount of time and the half-life of CYP2B6 synthesis is assumed to be 24 hours with no change in the CYP2B6 synthesis rate due to induction or other processes. The magnitude of CYP3A4/5 inhibition rates at circulating concentrations is far too low to have an effect upon steady state CYP3A4/5 concentrations. CMZ can be dosed orally at up to 2.4 grams/day so it is expected that first pass concentrations would be in the millimolar range. Moreover, it is expected that both CYP2B6 and CYP3A4/5 would undergo TDI in the intestine and liver during first pass. While these estimates can be used as an initial guess at assessing TDI

potency, a PBPK model should be employed to account for the entire inhibition profile during a dosing regimen.

In all systems tested, CMZ TDI of CYP2E1 is best described by a substrate inhibition kinetic model that has the lowest K_I and highest k_{inact} of the isoforms tested. Our kinetic parameters for human CYP2E1 are similar to those described by Stresser et al, but the authors of that manuscript did not go to higher concentrations so they did not encounter substrate inhibition. The kinetic constants for HLM incubations and human hepatocytes were fairly similar so it does not appear that any major confounding effects for the kinetics of TDI are present in human hepatocytes compared to HLM incubations. If the circulating concentrations of CMZ are used to estimate the rate of inactivation and the half-life of CYP2E1 synthesis is assumed to be approximately 24 hours with no compensatory upregulation of protein synthesis, the loss of CYP2E1 activity would be expected to be 94-96% depending upon which constants for HLM TDI or human hepatocyte TDI were used even without considering any first pass effects.(123) Interestingly, the TDI in mouse systems had an even lower K_I and even higher k_{inact}, which indicates that CMZ is even more potent at inhibiting mouse CYP2E1 than human CYP2E1 in vitro. The in vivo inhibition data for CYP2E1, as indicated by changes in the 6-hydroxychlorzoxazone/chlorzoxazone ratio, fall in line with these estimates since it appears that nearly all CYP2E1 activity has been inhibited by a single dose of CMZ, as evidenced by the 6-hydroxychlorzoxazone/chlorzoxazone ratios reaching the same lower level post CMZ administration for patients with elevated CYP2E1 activities due to alcoholism and for control patients.(152)

It should be noted that TDI may not result in apparent non-competitive inhibition in co-incubation experiments. After CYP2E1 is inactivated, the binding of substrate is irrelevant to the individual enzyme's catalytic activity so the V_{max} of the enzyme will decrease with increasing inhibitor concentration. That decrease in V_{max} could be consistent with noncompetitive inhibition

if the binding site for inactivation of the enzyme is not in competition with the site for catalysis of the substrate. However, if the time dependent inhibitor and the substrate are competing in the active site or if the substrate can block the binding of the reactive metabolite to its molecular target on the enzyme, it is possible that the inhibition mode could still resemble competitive inhibition. For CYP2E1, the K_i is similar but lower than K_I so it is likely that the competitive binding site for inhibition is the same as the catalytic site for TDI, but it is not certain.

While the pattern of inhibition in mouse enzyme sources is very similar to human, there may be slight differences in kinetics between mouse liver microsome (MLM) incubations and mouse hepatocytes. The inhibition of 6-hydroxychlorzoxazone activity in mouse hepatocytes could not be fit with the substrate inhibition model even though MLM data could fit those data. Also, the goodness of fit is poorer for mouse hepatocyte data with p-nitrophenol as the substrate, as evidenced by the R^2 value being 0.915, than the fit of MLM data with chlorzoxazone, which has a R^2 of .951. By taking a closer look at the lower concentrations of CMZ, there seems to be a delay in the increases of TDI rates before a sharper rise in the rate of TDI occurs when referenced to increasing concentrations of CMZ. It is likely that the rate of TDI is so high and the K_I is sufficiently low that permeability has become an issue in determining the rates of TDI in mouse hepatocytes for CMZ. In order to accurately describe the hepatocyte data, hepatocyte uptake experiments would need to be performed, and it is also likely that a PBPK model would, again, be the best choice to estimate any TDI effect in vivo since those models do take in account permeability.

These in vitro TDI data are consistent with the in vivo effects of CMZ upon CYP2E1 activity and suggest the possibility of drug-drug interactions with CYP2B6 and CYP3A4/5 to a far lesser extent, but these data also indicate the need for mechanistic analysis of the TDI for those isoforms. While it seems that the in vivo data for CYP2E1 is consistent with irreversible inhibition of CYP2E1, other situations that can explain the inhibition, such as potent reversible inhibitor with

prolonged residence time in the body, cannot be ruled without further analysis. This will be addressed later in this dissertation. The prediction of the potential DDI with CYP2B6 and CYP3A4/5 substrates require further analysis to construct the proper TDI model that will enable the design of appropriate studies to probe these potential issues. Therefore, we designed and carried out further experiments to elucidate the mechanisms of inhibition by CMZ for CYP2E1, 2B6, and 3A4/5. These studies included metabolite identification in HLM and recombinant systems to identify potential inhibitory metabolites and reactive species that could explain the mechanism of TDI.

2.4.4 Identification of Liver Metabolites and Their Potential Relationship to TDI.

As mentioned previously, many in vivo metabolites of CMZ have been identified, but there is no information regarding their tissue source. Therefore, to clarify this, we performed a series of experiments using HLM and recombinant CYP isoforms. While the primary focus of our study was NADPH dependent liver metabolism that would explain the TDI seen for CYP2B6, 2E1, and 3A4/5, we had performed an initial study with HLM, human liver cytosol, and human liver S9, along with NADPH and cofactors for glucuronidation (Uridine 5′-diphosphoglucuronic acid and alamethicin) and sulfonation (3'-phosphoadenosine-5'-phosphosulfate), to also explore whether these phase 2 biotransformations would take place.(228,229) No glucuronide or sulfate conjugates were identified so we continued the metabolite formation analysis with a focus upon NADPH-dependent metabolism and trapping reactive species generated from microsomal metabolism supported by NADPH.

For this we employed three common trapping agents in incubations with CMZ, HLM, and NADPH while using neutral loss scans in an attempt to identify possible reactive species. Trapping experiments utilizing cyanide, which typically traps imine/iminium species, and methoxylamine, which traps aldehydes and ketones, did not yield any trapped species.(47,48,230) Glutathione was able to trap one species (M2) that has the elemental

composition of CMZ – H_2 + glutathione. Glutathione appears to be reacting with a reactive species at the C-2 position because there is the presence of the major 194 m/z fragment, which contains the parent CMZ with a sulfhydryl group, and the lack of a fragment where the entire glutathione adduct is lost. While the position of glutathione adduct appears to be fairly certain, the identity of the trapped reactive species is not known so identification of the rest of the HLM metabolites was necessary to enable speculation on its nature.

The source of the M2 adduct still was not clear from the HLM metabolite identification data. The most likely candidates would be N-oxides, S-oxides, and hydroxylations that lose water to yield a methide metabolite. Synthetic N-oxide (100 μM) after purification was incubated with 5 mM glutathione in buffer and in a HLM incubation, but the incubation did not yield any M2. Interestingly, some M2 could be formed if the mCPBA/CMZ reaction that was performed to synthesize M3 was not purified. The reaction conditions greatly favor the synthesis of N-oxide, but other oxidation products, such as the S-oxide, are possible. Since we did not identify a S-oxide metabolite, it is possible that the S-oxide is highly reactive with glutathione and no free S-oxide remained. There are no procedures in the literature that allow selective synthesis and purification of the S-oxide thiazole, so a metabolite standard could not be made to assess whether this species was the source of M2. The other remaining candidates would involve mono-oxidation followed by loss of water. If M2 is related to either of the two remaining identified mono-oxidations, one would expect that there would be a constant ratio between the released products, M4 or M5:M2, that would remain constant. By performing a metabolite identification experiment with recombinant CYPs, we attempted to correlate other metabolites with M2 formation and identify any other metabolites that potentially correlate with TDI.

None of the identified metabolites appear to maintain a ratio with M2 so it is likely that M2 is not directly related to any of the other four metabolites. M2 and M3 appear to be the two metabolites that with the apparent TDI for CYP2B6, CYP2E1, and CYP3A4/5. The area counts

for these two metabolites are generally elevated in incubations with CYP2B6, CYP2E1, and CYP3A4 when compared to other CYP isoforms that do not undergo TDI. However, some isoforms do generate M2 and M3 at substantial amounts and yet are not subject to TDI, so formation of these metabolites does not completely account for all the factors involved in TDI. It is possible that both M2 and M3 could contribute to the apparent TDI seen with the three isoforms in question, but each of them would be expected to have different mechanisms of TDI since their metabolite profiles are different from one another.

N-oxides of thiazoles behave as quasi-stable carbenes and can react extensively at C-2 after deprotonation.(162,168,169,171,212) As noted by several authors, carbenes have the potential to form metabolic intermediate complexes (MICs) that are bonded to the iron of heme when it is in the ferrous state.(52,54) These MICs can be often characterized by UV spectra with maximum absorbances near 430 nm and 450 nm and can also result in a migration of the carbene to the pyrrole nitrogens as noted by Lange et al.(52) Therefore, one would expect that the N-oxide metabolite could have the possibility of forming MIC and heme adducts if it is the source of TDI.

If M2 is related to an S-oxide that is responsible for the apparent TDI of CYP2B6, 2E1, and/or CYP3A4/5, it would be expected that the molecular target of inhibition would be different from the N-oxide.(15,154,175) S-oxide thiazoles that are not substituted at C-4 will react with glutathione at this position.(174,175) In the case of CMZ, C-4 has a methyl substituent so it is not clear if and where glutathione or another cysteine containing biomolecule would adduct a C-4 substituted S-oxide thiazole-containing compound. Since C-5 is also substituted in CMZ, the most likely site for the nucleophilic attack by glutathione or another cysteine would be C-2, which is consistent with the fragmentation. S-oxide thiazoles have not been reported to form carbenes like N-oxides so it is more likely that S-oxides will adduct the apoprotein of the target CYP and not heme, but there are no data available that strongly support either conjecture.

2.5 Summary and Conclusions

In this chapter, we delineated the interactions of CMZ with major drug metabolizing liver CYP isoforms. The contents of this chapter can be divided into two types of interactions: the effects of CMZ upon the CYP isoforms and the reactions performed by those CYPs upon CMZ. The interactions of CMZ were examined by co-incubation experiments to assess time independent interactions and dilution experiments to assess TDI. The metabolite identification experiments were performed to examine how CYP enzymes metabolize CMZ.

The co-incubation experiments of CMZ with various selective probe CYP substrates and HLM stratified the relative binding affinities for inhibitory binding sites by CMZ and revealed that the modes of interaction that CMZ has with various CYP isoforms are varied and sometimes complex. Inhibition of CYP2A6 and CYP2E1 by CMZ have lowest K_i values out of all the isoforms tested in co-incubation experiments, but appear to behave in the simplest manner of all of the isoforms that were thoroughly examined since they appear to follow a mostly competitive mechanism. CYP2C19 inhibition followed the pattern of a noncompetitive inhibitor while CYP2B6 inhibition resembled a mixed mode of inhibition that was part competitive and noncompetitive. CMZ had widely disparate effects upon each of the three model substrates for CYP3A4/5 with the effects upon midazolam being the most complex. These data not only allowed us to unveil a multitude of modes of interactions for CMZ, but they also allowed us to narrow the number of CYP isoforms to examine for potential TDI in subsequent experiments by the use of the IC_{50} and K_i values determined in those experiments.

Dilution experiments performed to identify which isoforms underwent TDI by CMZ revealed that CYP2E1, 2B6, and 3A4/5 were inhibited in time dependent manner by CMZ. The rapid TDI kinetics for CYP2E1 with HLM and human hepatocytes were similar to those of Stresser et al, but we revealed the kinetics followed a substrate inhibition model. CYP2B6 was also suggested by Stresser et al to undergo TDI, and we were able to determine the kinetics for that phenomenon.

CYP3A4/5 also was inhibited in a time dependent manner by CMZ. Even though 1'-hydroxymidazolam activity is subject to a very complex interaction with CMZ during co-incubation experiments, the TDI kinetics followed a simple Michaelis-Menten model. The K_I for CYP3A4/5 was similar to the K_i suggests that the inhibitory binding site for reversible inhibition is likely the same as the TDI and at the catalytic site of the enzyme. With the isoforms undergoing TDI identified and the kinetics determined for each of the isoforms, the mechanisms of TDI for each of the isoforms can be examined.

By performing metabolite identification with HLM and recombinant enzymes, we are now able to describe how the liver metabolizes CMZ and to begin to formulate possible mechanisms of TDI. We were able to identify some metabolites that were previously found in vivo, but we also described new metabolites that were not seen previously. M1 and M5 are previously described metabolites in human samples and are likely not to be important in terms of the TDI mechanism. If our assignment of M4 is correct, M4 would be a novel metabolite since no C-2 oxidation has been described at all in the literature regarding CMZ metabolism, but it is unlikely that M4 would play a role in CMZ related TDI. We have unambiguously identified the M3 N-oxide, which may be a precursor to the dual N-oxide/S-oxide found in vivo, and this new metabolite suggests that heme adduction may be a possible mechanism for TDI. The newly discovered glutathione adduct, M2, suggests that adduction of apo protein could be a mechanism of TDI. Since we have uncovered metabolites that are suggestive of apoprotein and prosthetic heme modification, we must perform experiments with both of these possible targets in mind.

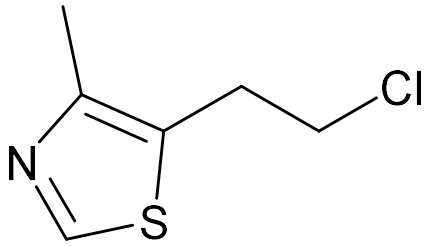

Chlormethiazole
Chemical Formula: C_6H_8ClNS
Exact Mass: 161.0066
Molecular Weight: 161.6470

Figure 2.1 Structure of Chlormethiazole (CMZ)

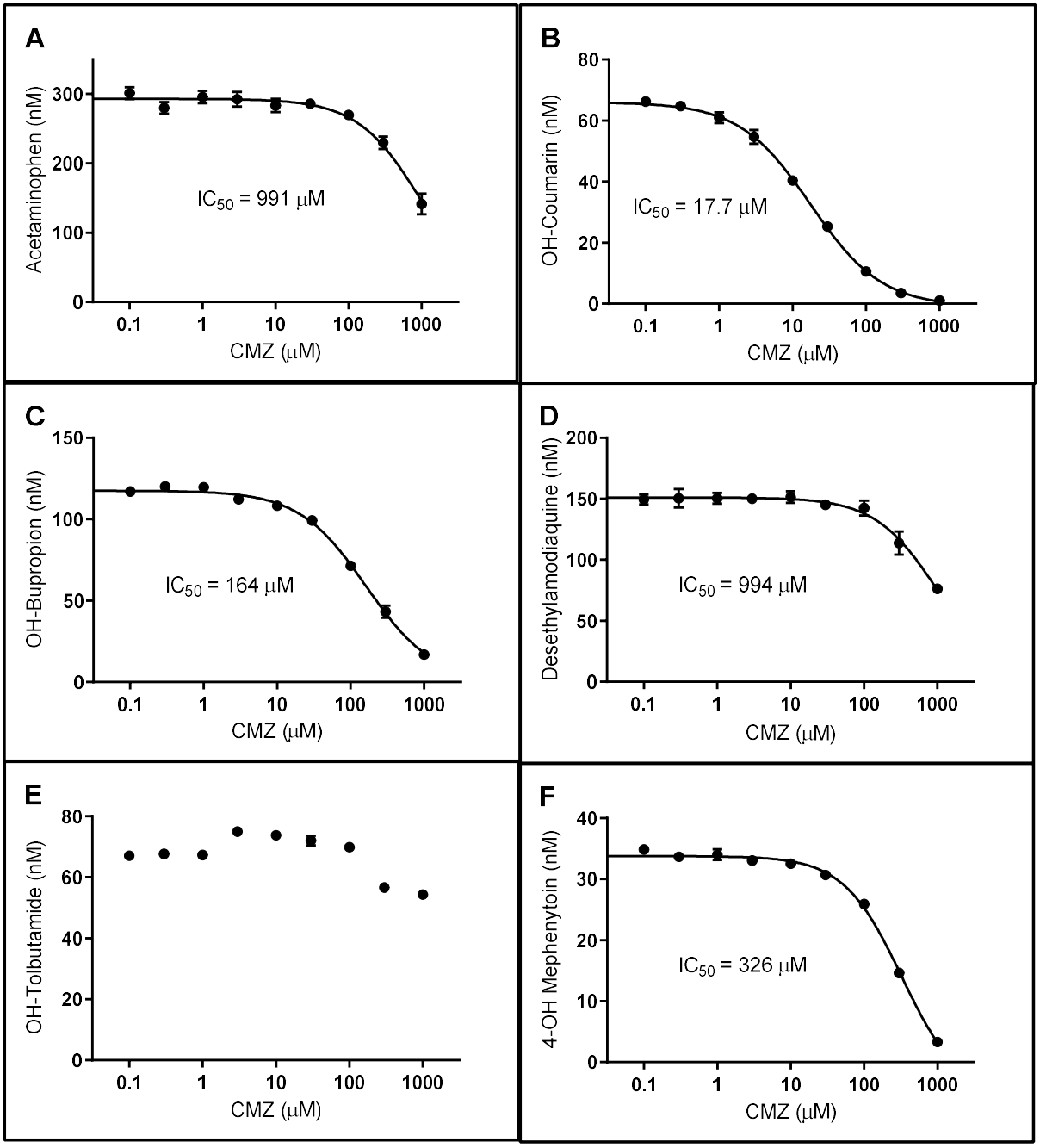

Figure 2.2 Part I – Selectivity of Time Independent Inhibition in HLM Incubations
IC_{50} Plots for CYP1A2-mediated phenacetin *O*-deethylation (A), CYP2A6-mediated coumarin 7-hydroxylation (B), CYP2B6-mediated bupropion hydroxylation (C), CYP2C8-mediated amodiaquine *N*-deethylation (D), CYP2C9-mediated tolbutamide 4-hydroxylation (E), CYP2C19-mediated mephenytoin 4-hydroxylation (F)

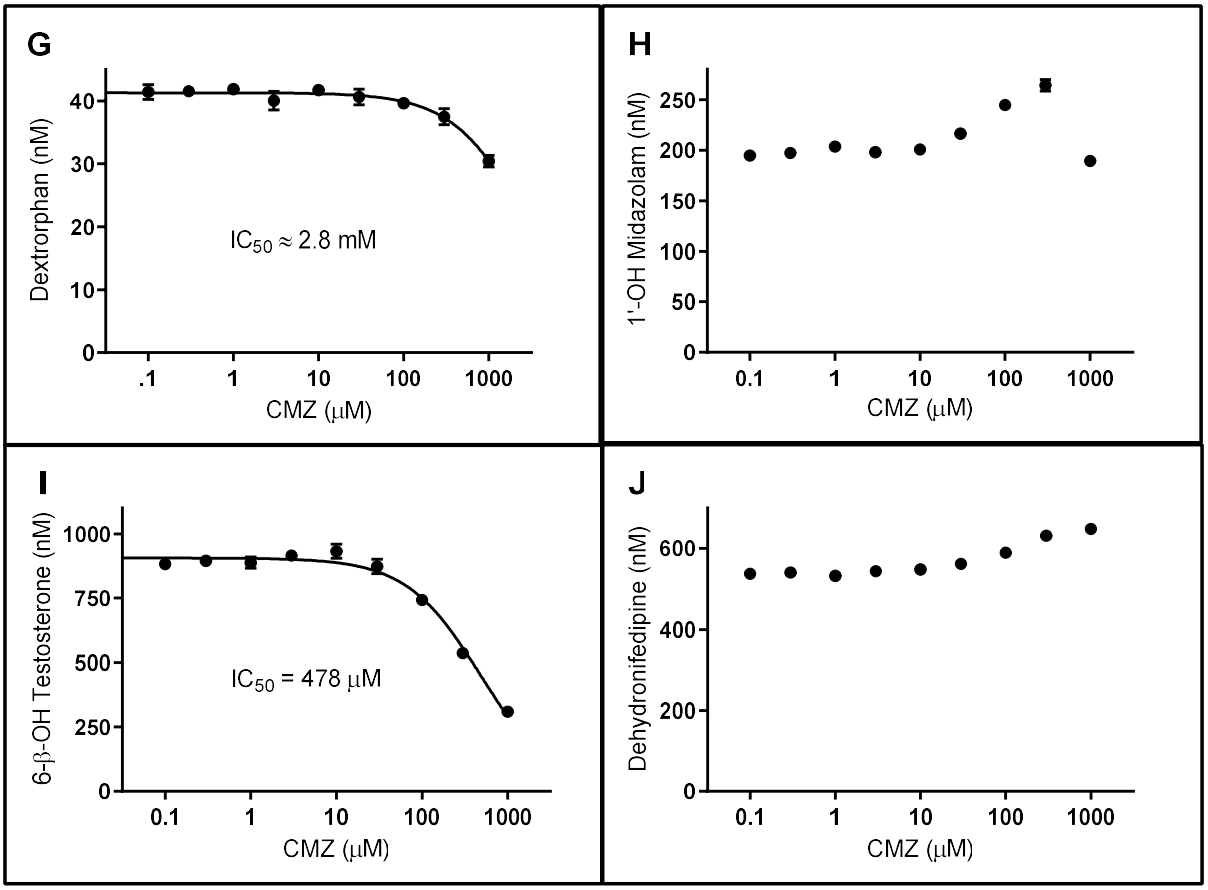

Figure 2.2 Part II – Selectivity of Time Independent Inhibition in HLM Incubations
IC_{50} Plots for CYP2D6-mediated dextromethorphan *O*-demethylation (G), CYP3A4/5-mediated midazolam 1'-hydroxylation (H), CYP3A4/5-mediated testosterone 6β-hydroxylation (I), CYP3A4/5-mediated nifedipine dehydrogenation (J)

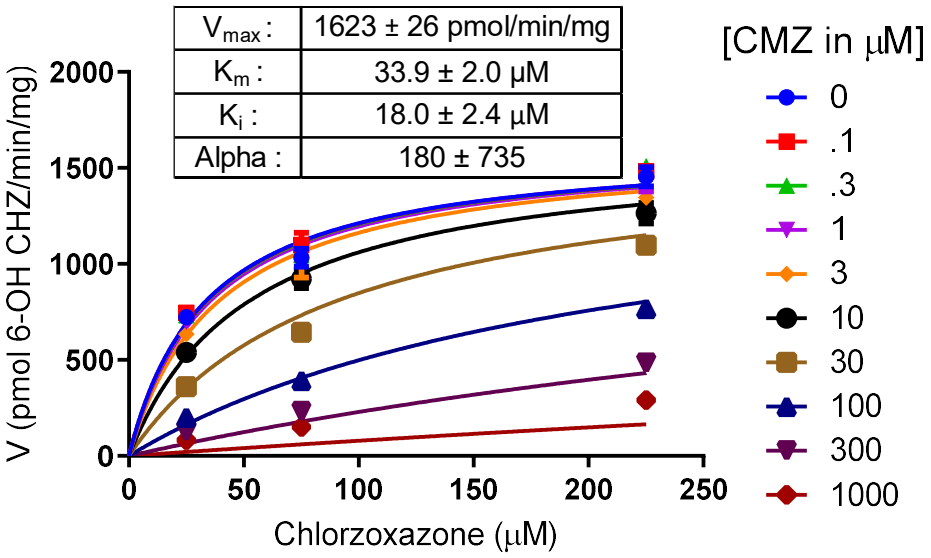

Figure 2.3 Fit of Mixed Inhibition Model to Determine Inhibition Mechanism and K_i of CMZ for Chlorzoxazone 6-Hydroxylation in a Co-incubation Experiment in Human Liver Microsome Incubations

Reported V_{max} and K_m values apply to chlorzoxazone 6-hydroxylation and are derived from the fitting of the model while K_i and Alpha values apply to inhibition by CMZ.

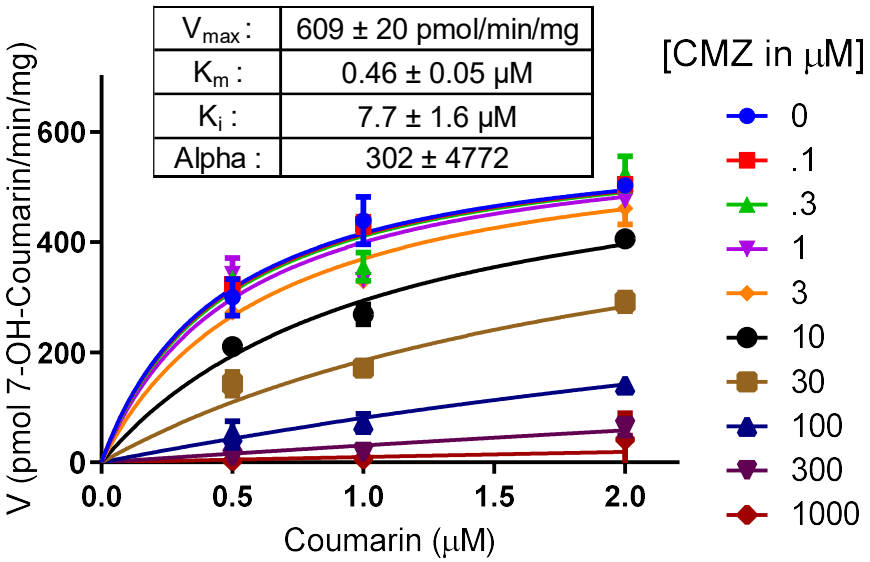

Figure 2.4 Fit of Mixed Inhibition Model to Determine Inhibition Mechanism and K_i of CMZ for Coumarin 7-Hydroxylation in a Co-incubation Experiment in Human Liver Microsome Incubations

Reported V_{max} and K_m values apply to coumarin 7-hydroxylation and are derived from the fitting of the model while K_i and Alpha values apply to inhibition by CMZ.

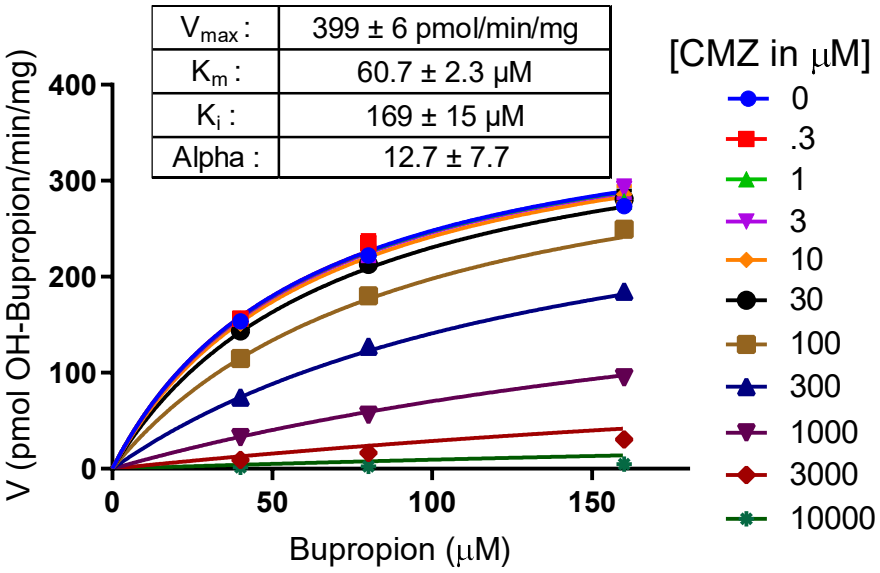

Figure 2.5 Fit of Mixed Inhibition Model to Determine Inhibition Mechanism and K_i of CMZ for Bupropion Hydroxylation in a Co-incubation Experiment in Human Liver Microsome Incubations

Reported V_{max} and K_m values apply to bupropion hydroxylation and are derived from the fitting of the model while K_i and Alpha values apply to inhibition by CMZ.

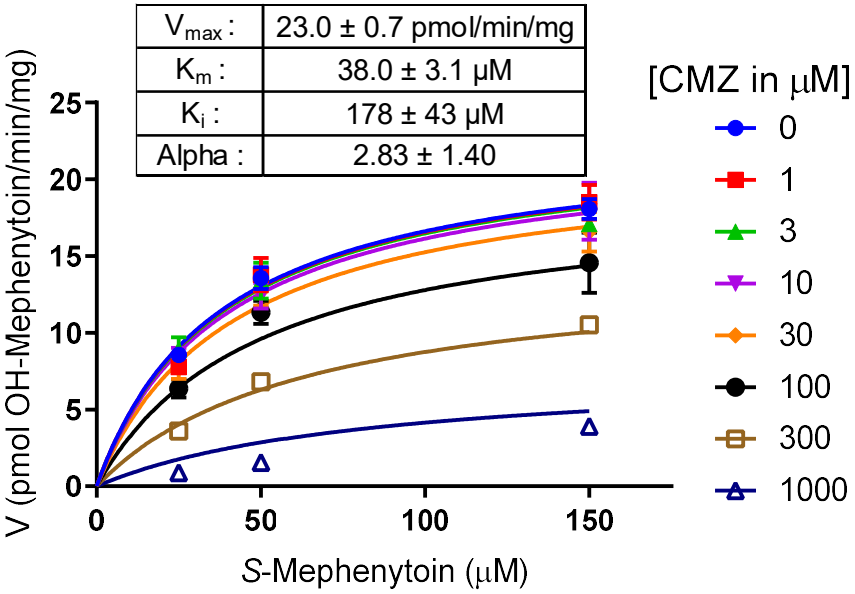

Figure 2.6 Fit of Mixed Inhibition Model to Determine Inhibition Mechanism and K_i of CMZ for Mephenytoin 4-Hydroxylation in a Co-incubation Experiment in Human Liver Microsome Incubations

Reported V_{max} and K_m values apply to mephenytoin 4-hydroxylation and are derived from the fitting of the model while K_i and Alpha values apply to inhibition by CMZ

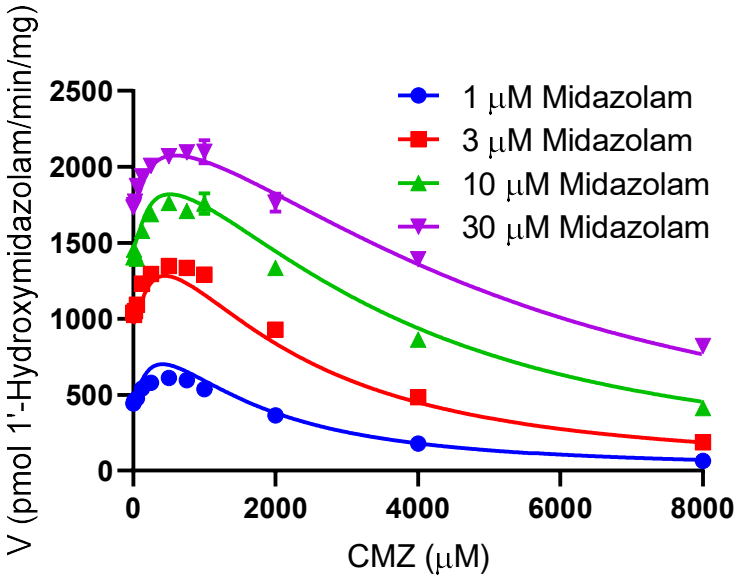

Fit Parameters	
V_{max} (pmol/min/mg)	1903
K_m (μM)	2.9
Hill Coefficient	1.596
K_i (μM)	1335
Alpha (Inhibition)	17.45
K_{allo} (μM)	202
A	1.227
B	0.5862

Figure 2.7 Effect of CMZ upon 1'-Hydroxymidazolam Formation in HLM Incubations
V_{max} and K_m apply to 1'-hydroxymidazolam formation. The Hill coefficient applies to the inhibition and allosteric binding of CMZ. Alpha is indicative of the mode of inhibition since this was fit with a modified mixed inhibition model. A is the modifier for V_{max} by the binding of the allosteric modulation site, and B is the modifier for K_m by the binding of the allosteric site.

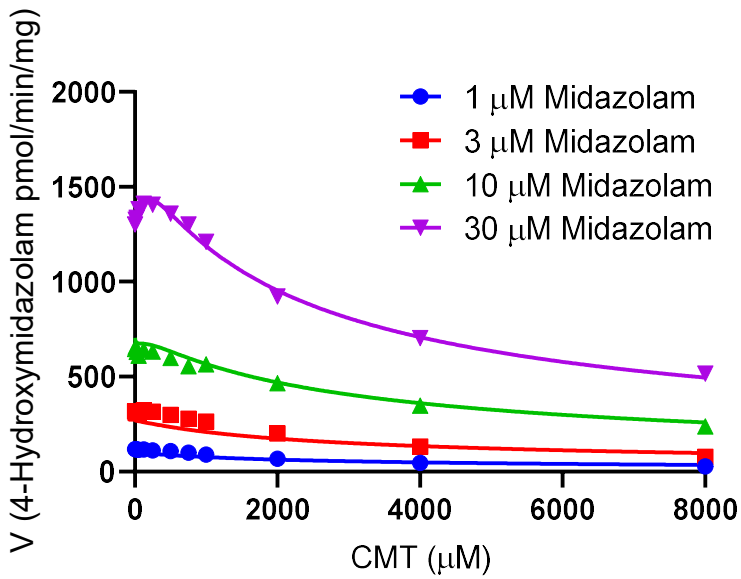

Fit Parameters	
V_{max} (pmol/min/mg)	2269
K_m (μM)	22.2
Hill Coefficient	0.699
K_i (μM)	1604
Alpha (Inhibition)	0.0716
K_{allo} (μM)	324
A	19.52
B	12.51

Figure 2.8 Effect of CMZ upon 4-Hydroxymidazolam Formation in HLM Incubations
V_{max} and K_m apply to 4-hydroxymidazolam formation. The Hill coefficient applies to the inhibition and allosteric binding of CMZ. Alpha is indicative of the mode of inhibition since this was fit with a modified mixed inhibition model. A is the modifier for V_{max} by the binding of the allosteric modulation site, and B is the modifier for K_m by the binding of the allosteric site.

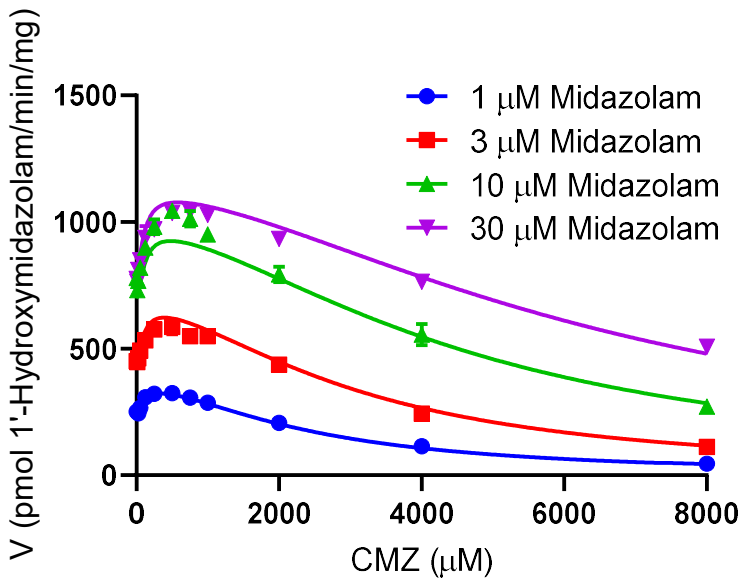

Fit Parameters	
V_{max} (pmol/min/mg)	884
K_m (μM)	2.6
Hill Coefficient	1.635
K_i (μM)	2002
Alpha (Inhibition)	14.79
K_{allo} (μM)	116
A	1.367
B	0.919

Figure 2.9 Effect of CMZ upon 1'-Hydroxymidazolam Formation in HLM Deficient in CYP3A5 Incubations

V_{max} and K_m apply to 1'-hydroxymidazolam formation. The Hill coefficient applies to the inhibition and allosteric binding of CMZ. Alpha is indicative of the mode of inhibition since this was fit with a modified mixed inhibition model. A is the modifier for V_{max} by the binding of the allosteric modulation site, and B is the modifier for K_m by the binding of the allosteric site.

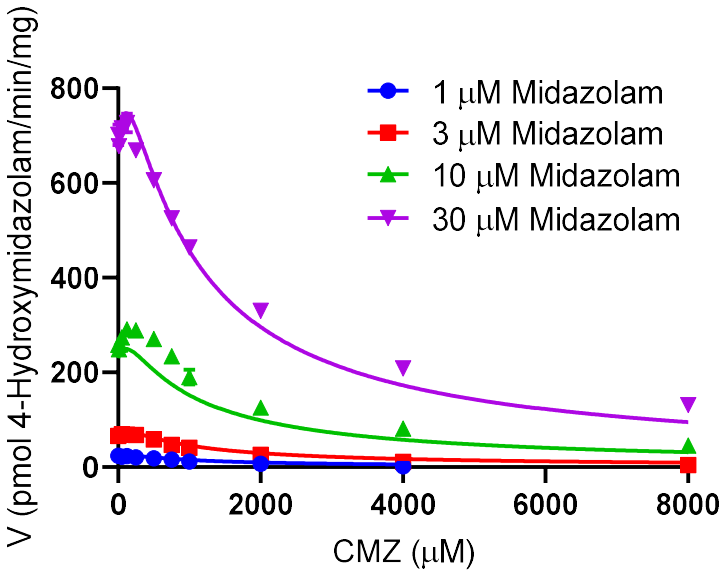

Figure 2.10 Effect of CMZ upon 4-Hydroxymidazolam Formation in HLM Deficient in CYP3A5 Incubations
The fit was ambiguous so parameters are not reported.

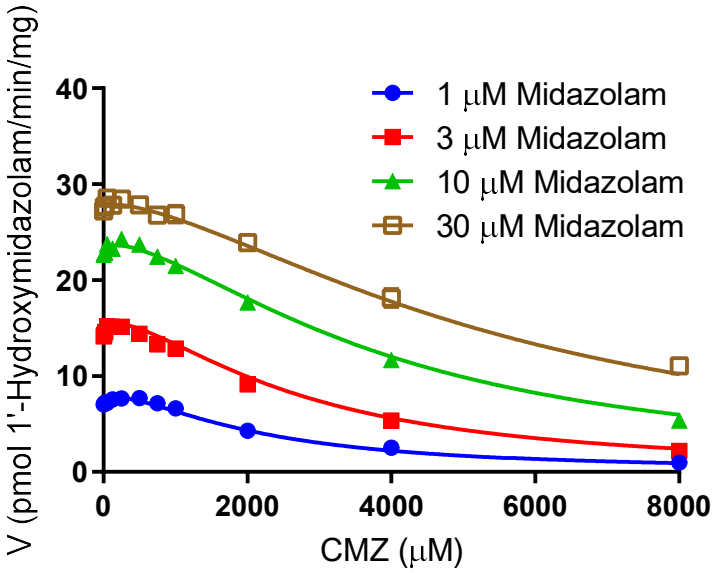

Fit Parameters	
V_{max} (pmol/min/pmol)	30.7
K_m (μM)	3.37
Hill Coefficient	1.592
K_i (μM)	1811
Alpha (Inhibition)	11.28
K_{allo} (μM)	101
A	1
B	0.81

Figure 2.11 Effect of CMZ upon 1'-Hydroxymidazolam Formation in CYP3A4 Supersomes™ Incubations

V_{max} and K_m apply to 1'-hydroxymidazolam formation. The Hill coefficient applies to the inhibition and allosteric binding of CMZ. Alpha is indicative of the mode of inhibition since this was fit with a modified mixed inhibition model. A is the modifier for V_{max} by the binding of the allosteric modulation site, and B is the modifier for K_m by the binding of the allosteric site.

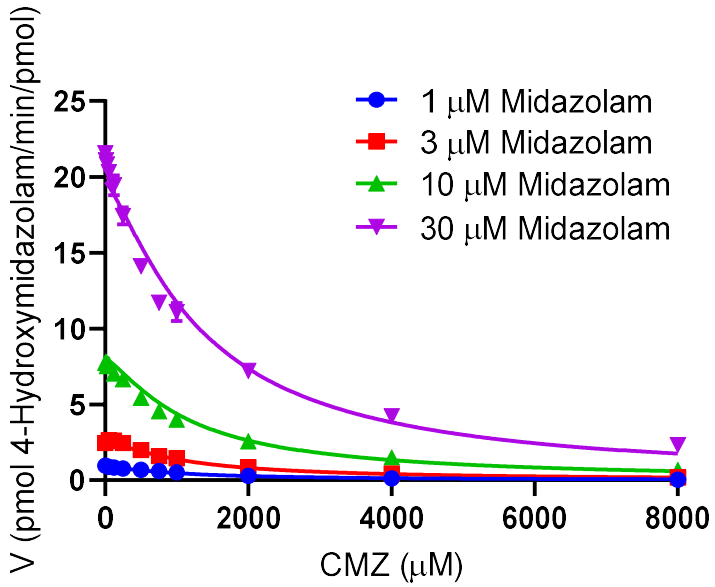

Figure 2.12 Effect of CMZ upon 4-Hydroxymidazolam Formation in CYP3A4 Supersomes™ Incubations
The fit was ambiguous so parameters are not reported.

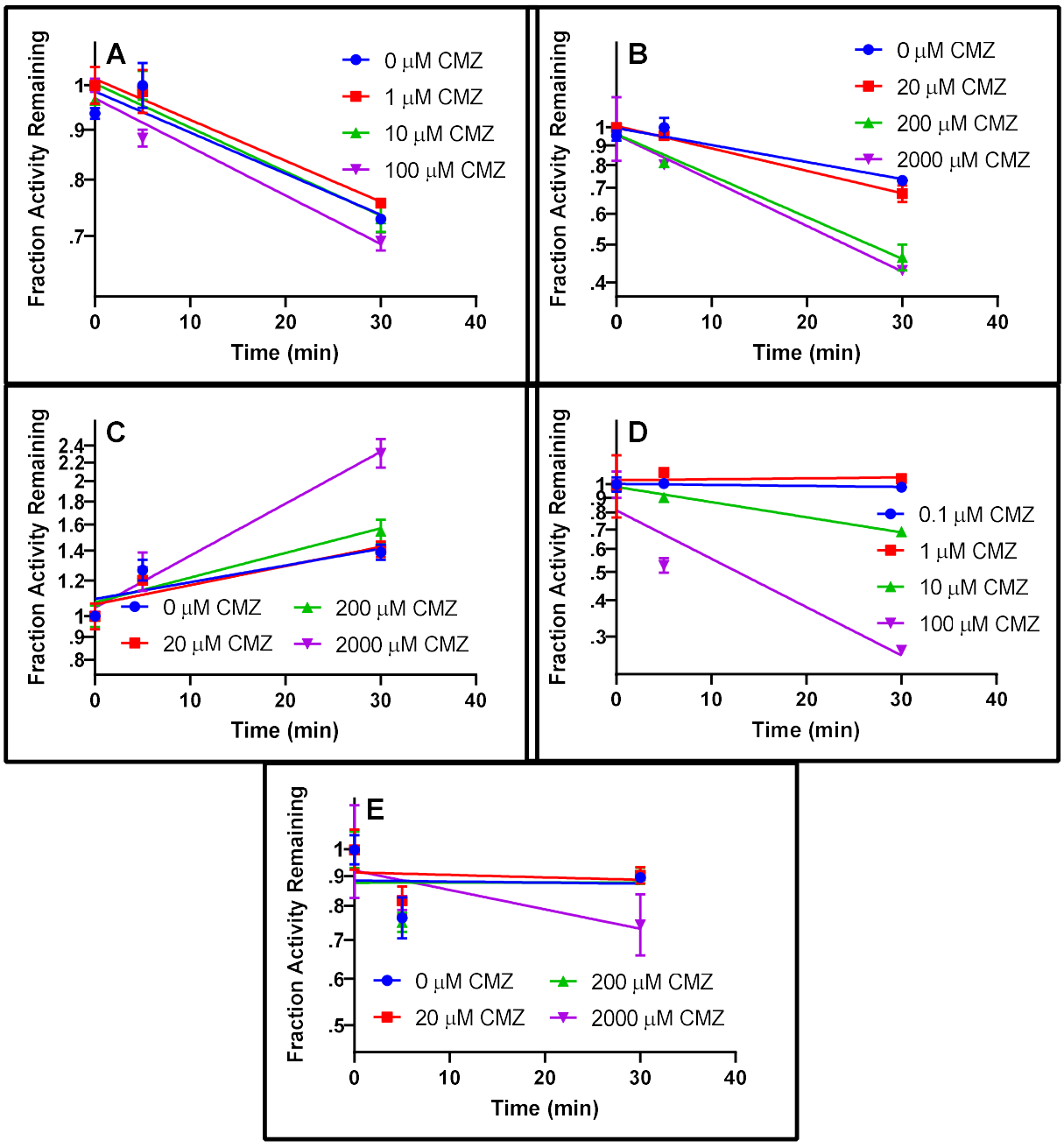

Figure 2.13 Dilution Assay TDI Screening of CYP2A6 (A), CYP2B6 (B), CYP2C19 (C), CYP2E1 (D), CYP3A4/5 (E)
These are first order degradation plots generated for screening of potential TDI from dilution experiments performed with HLM.

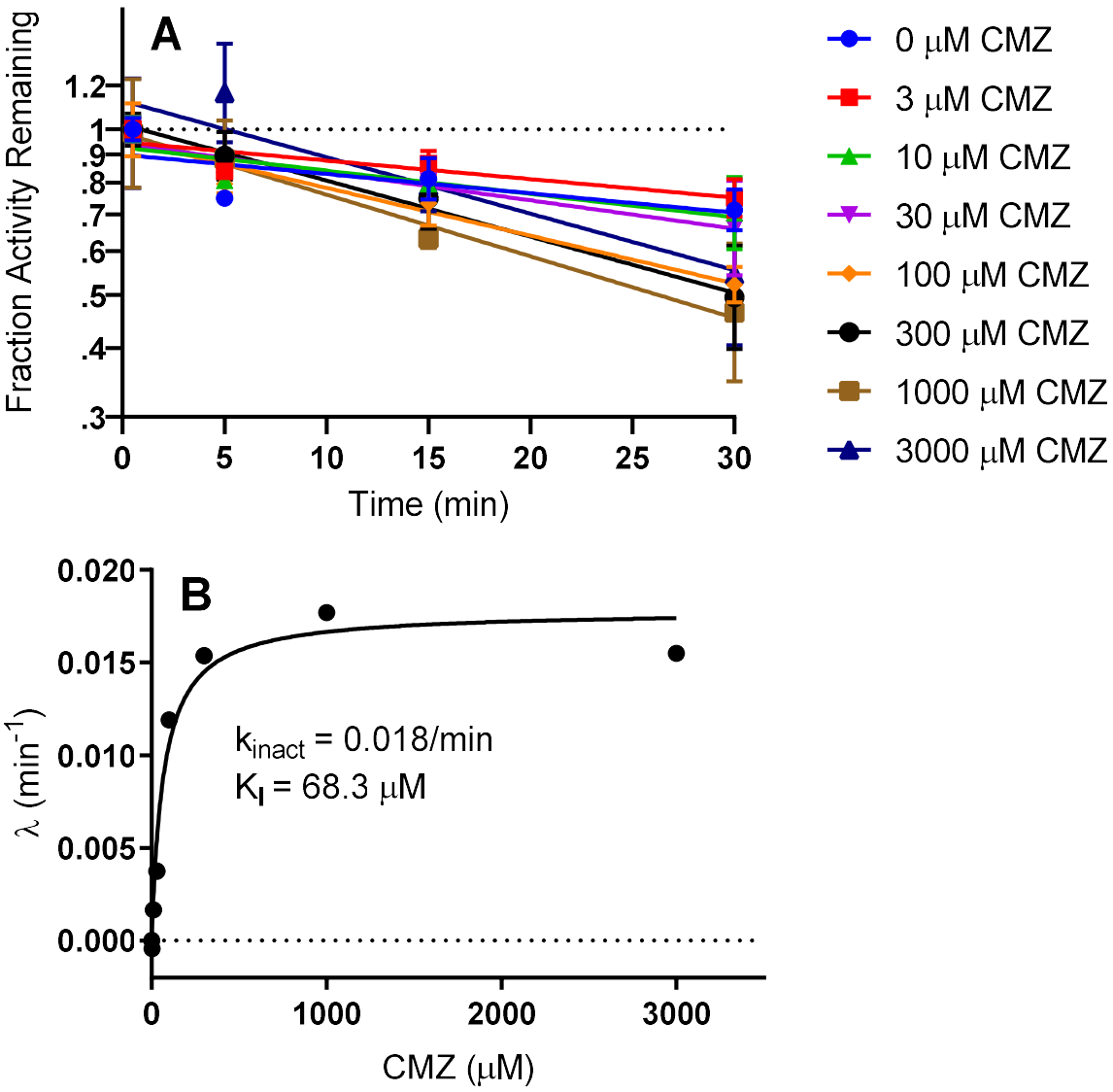

Figure 2.14 Kinetic Determination of TDI for CYP2B6
Part A depicts the linear regression of the CYP2B6-mediated hydroxybupropion activity remaining after natural log transformation. Part B depicts the non-linear regression fit of Michaelis-Menten model using the normalized λ values.

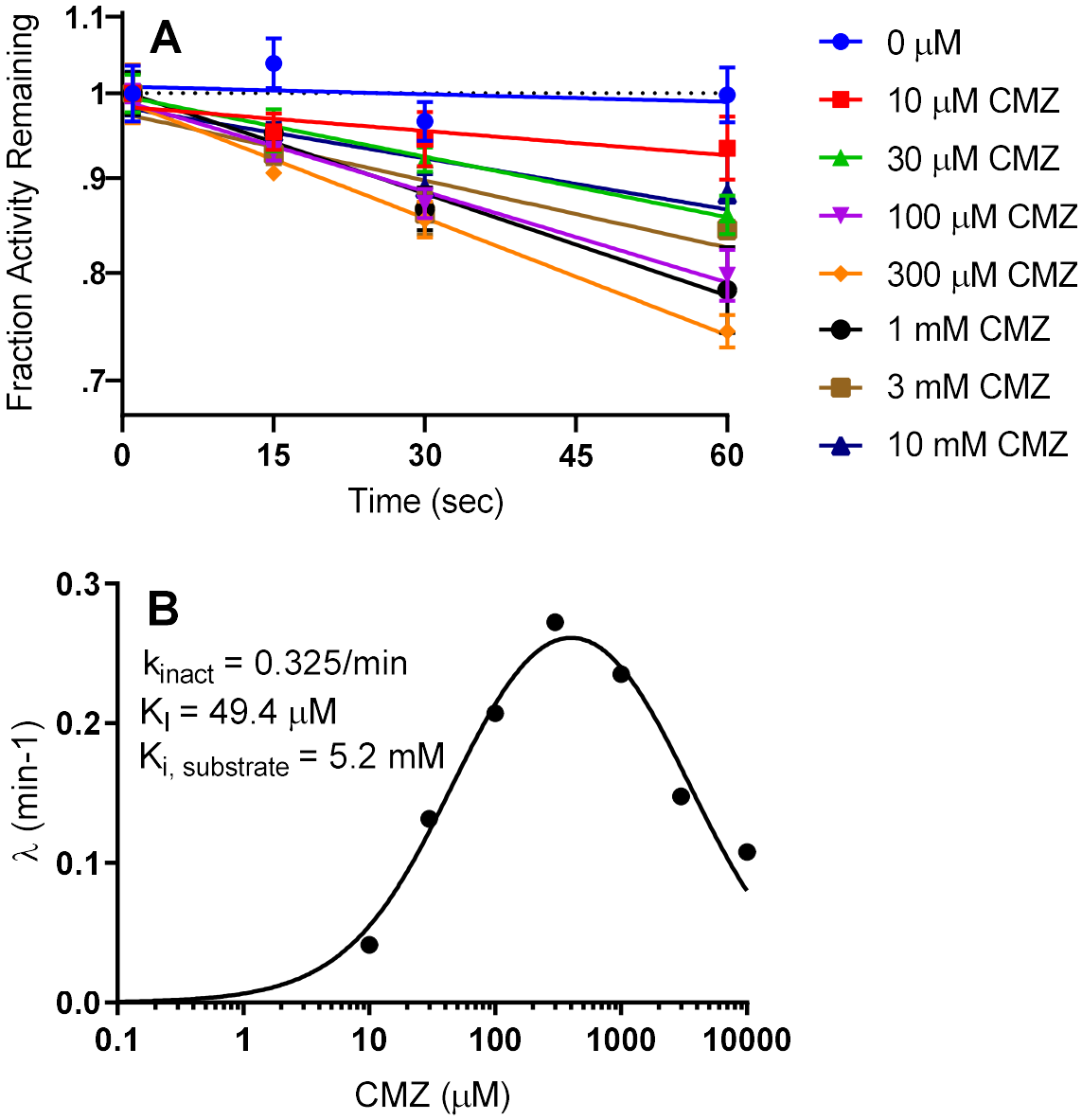

Figure 2.15 Kinetic Determination of TDI for CYP2E1
Part A depicts the linear regression of the CYP2E1-mediated 6-hydroxychlorzoxazone activity remaining after natural log transformation. Part B depicts the non-linear regression fit of substrate inhibition model using the normalized λ values. The X-axis is depicted in a log base 10 format to more easily depict the wide range of concentrations in the experiment.

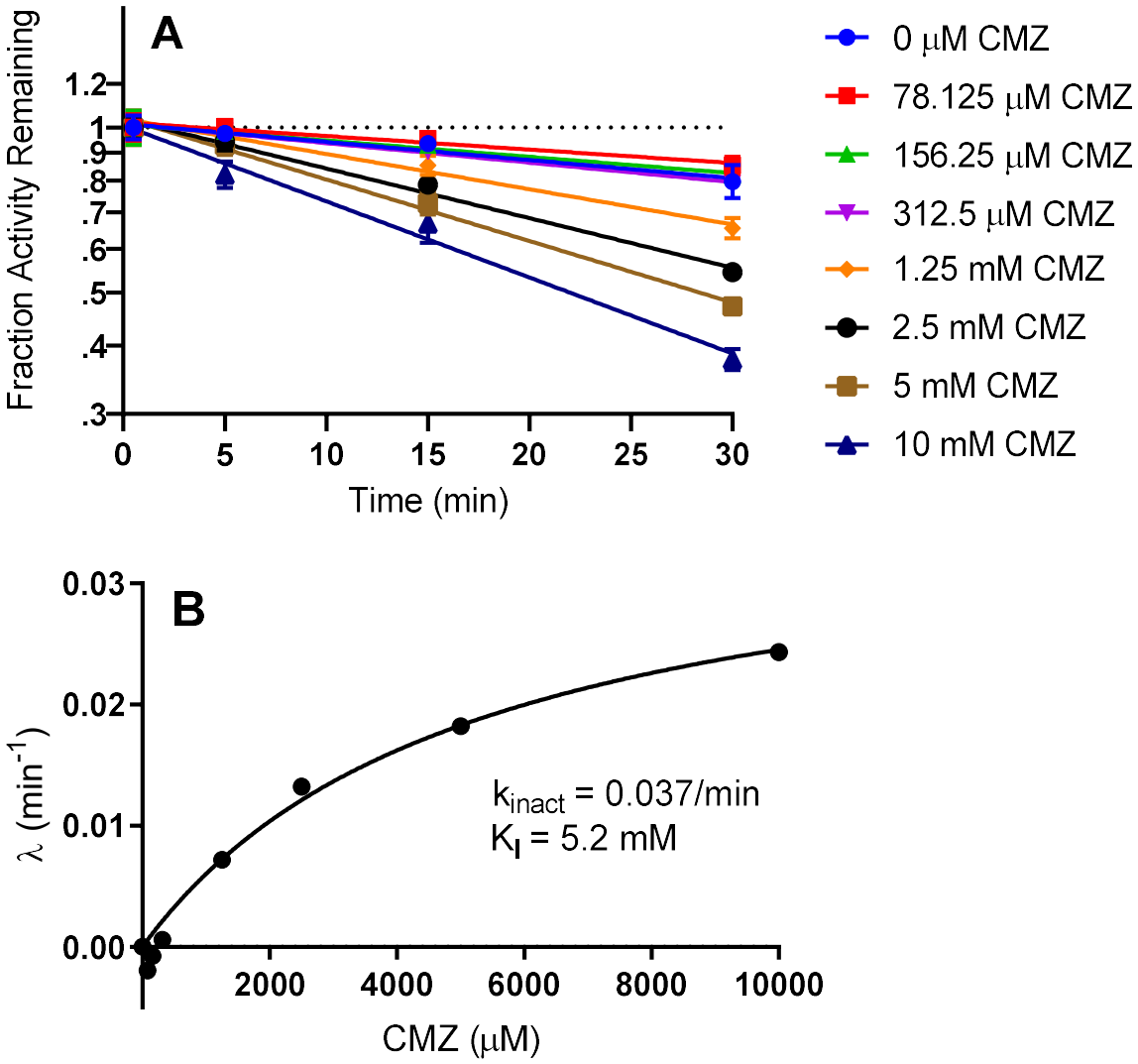

Figure 2.16 Kinetic Determination of TDI for CYP3A4/5
Part A depicts the linear regression of the activity remaining after natural log transformation. Part B depicts the non-linear regression fit of Michaelis-Menten model using the normalized λ values.

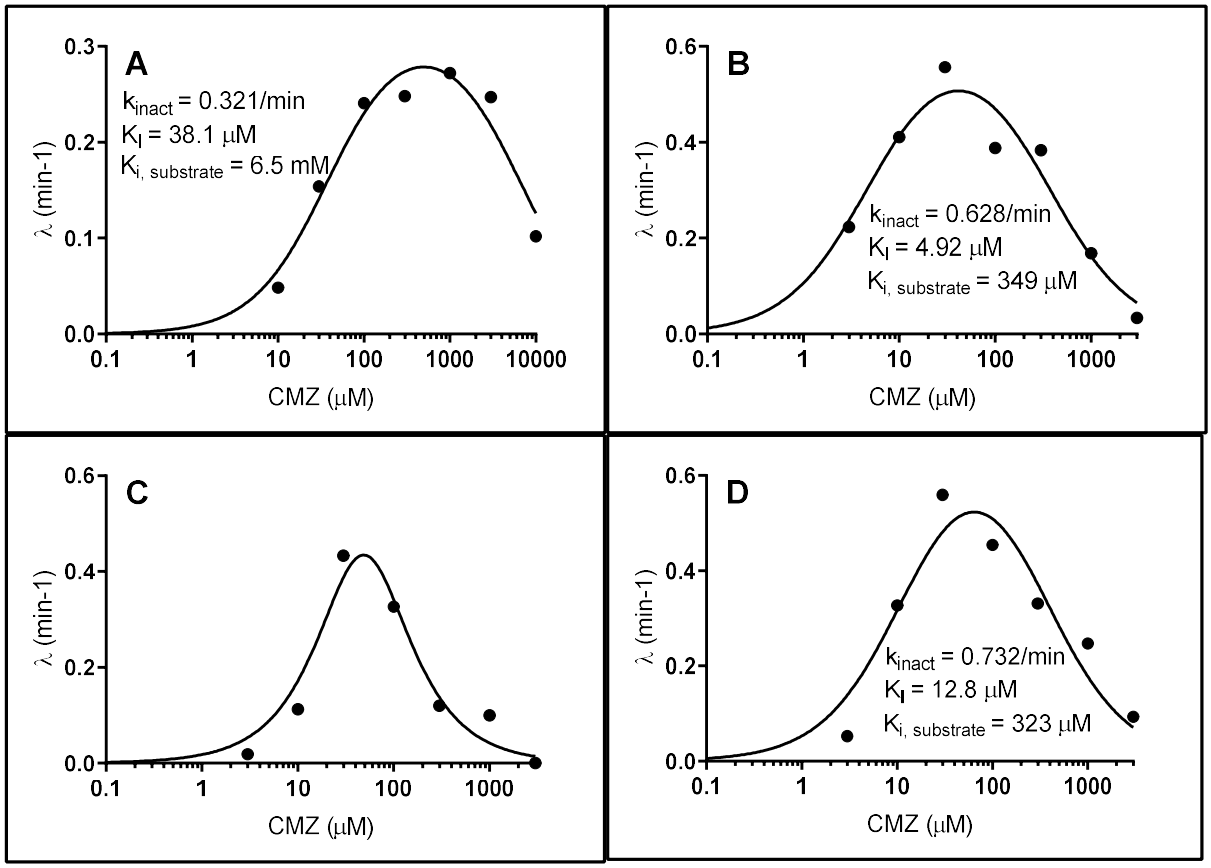

Figure 2.17 TDI Kinetics in Plated Human Hepatocytes (A), in Mouse Liver Microsomes with Chlorzoxazone as a Substrate (B), Plated Mouse Hepatocytes with Chlorzoxazone as a Substrate (C), and Plated Mouse Hepatocytes with Para-Nitrophenol as a Substrate (D) All were fit with substrate inhibition models. The fit for plated mouse hepatocytes with chlorzoxazone was ambiguous so the parameters are not reported.

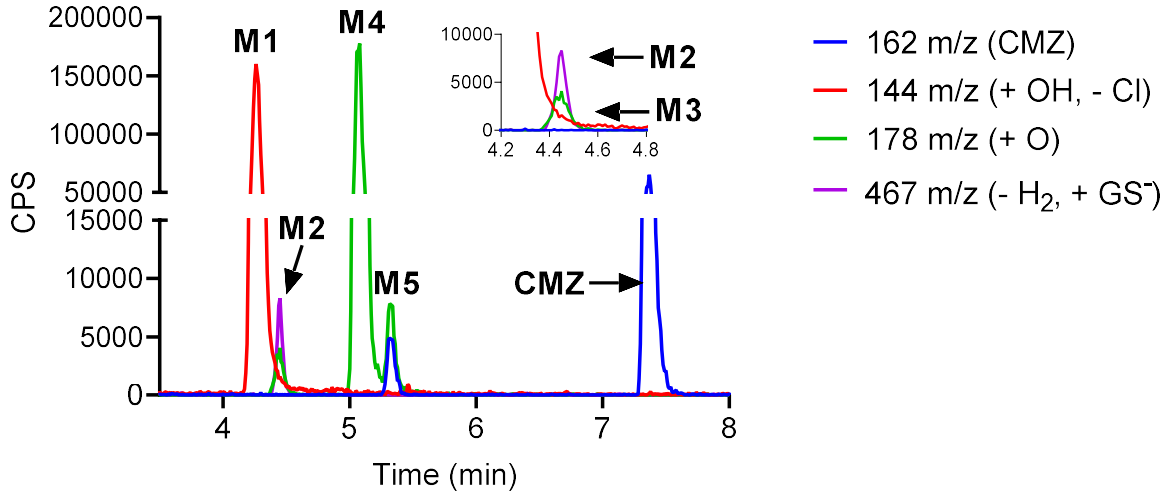

Figure 2.18 Overlay of Extracted Ion Current of Parent and Metabolite m/z from HLM Metabolite Identification

Overlay is composed of extract ion current mass ranges of all found metabolites and parent. M1 is a dechlorinated ethyl alcohol metabolite. M2 is dehydrogenated glutathione adduct. M3 is a N-oxide metabolite. M4 is likely C-2 oxidation resulting in a thiocarbamate. M5 is a hydroxylation on the C-4 methyl group. The inset focuses on M2 and M3.

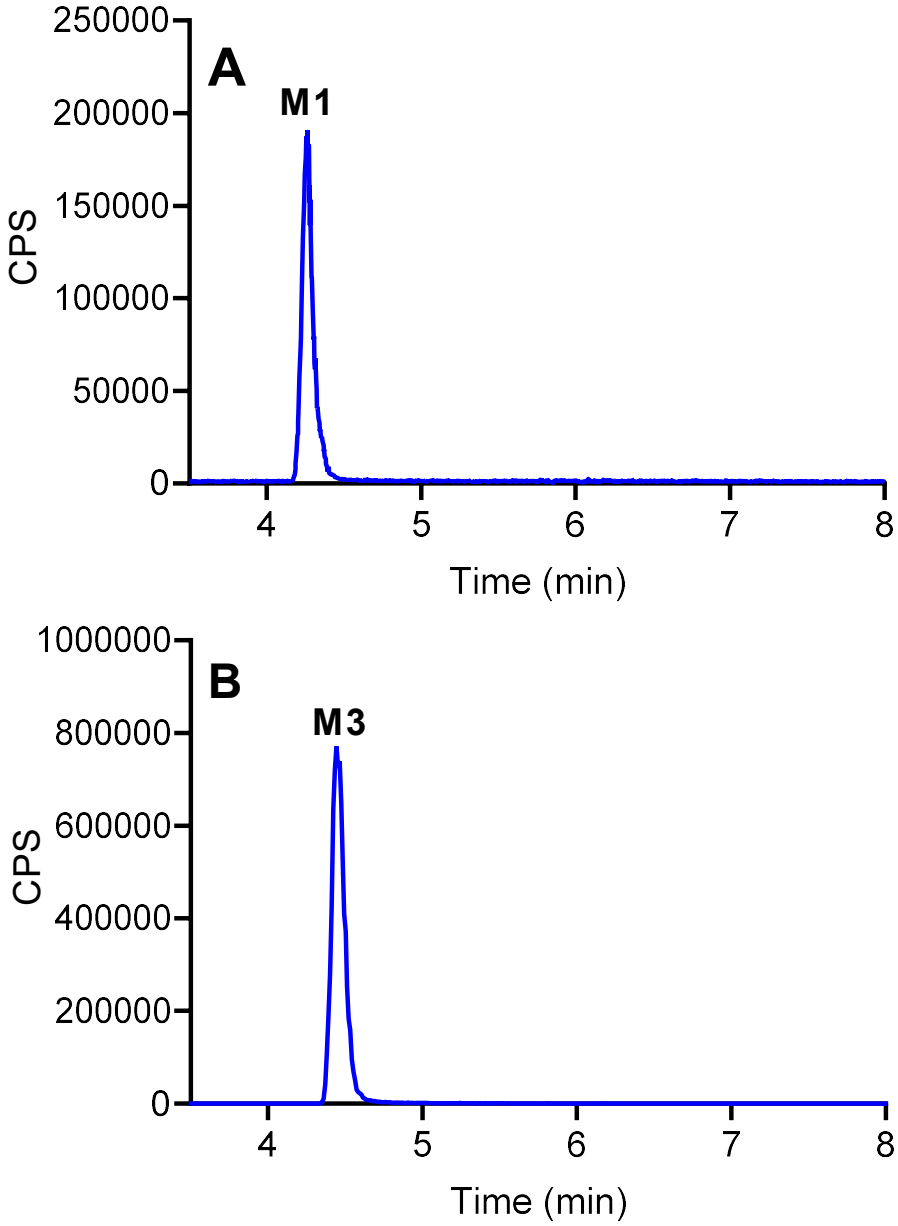

Figure 2.19 Extracted Ion Current of 5(1-Hydroxyethyl) 4-Methylthiazole Standard (A) and CMZ N-Oxide Synthetic Standard

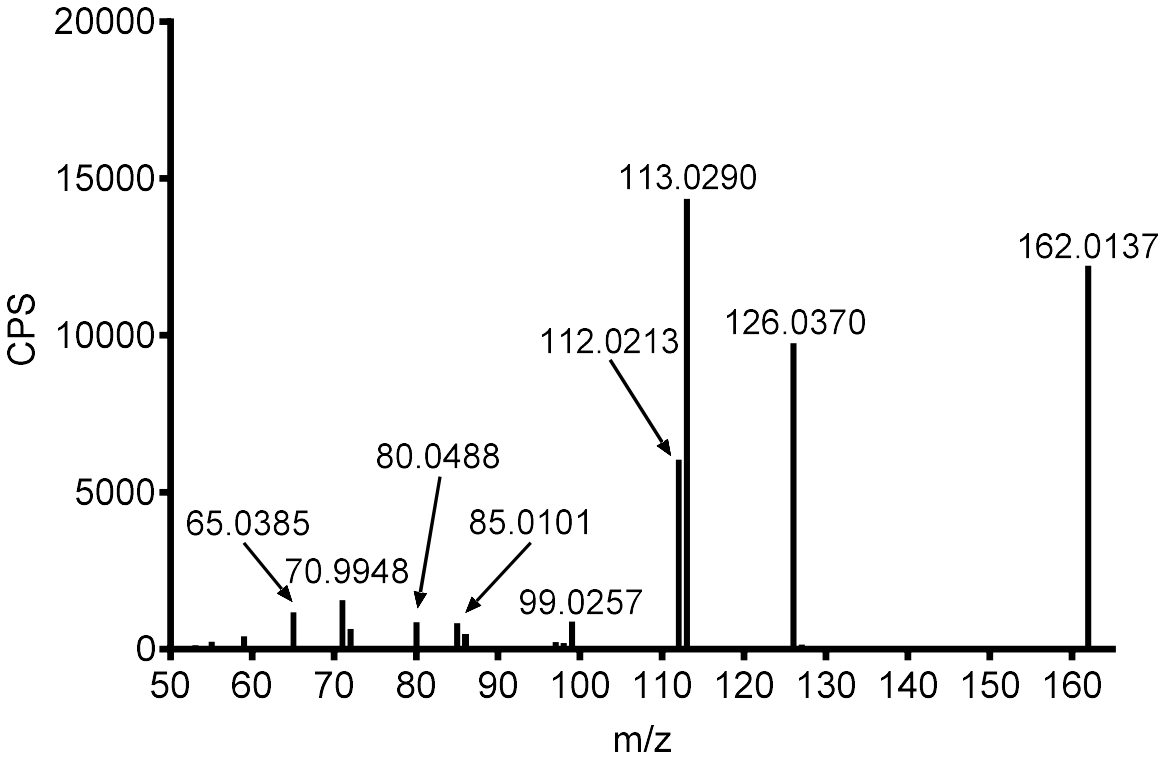

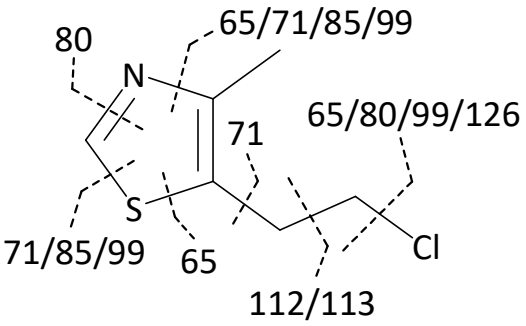

Found Mass	Formula	Predicted Mass	mDa Error
65.0385	$C_5H_5^+$	65.0386	-0.1
70.9948	$C_3H_3S^+$	70.9950	-0.2
80.0488	$C_5H_6N^+$	80.0495	-0.7
85.0101	$C_4H_5S^+$	85.0106	-0.5
99.0257	$C_5H_7S^+$	99.0263	-0.6
112.0213	$C_5H_6NS^+$	112.0215	-0.2
113.0290	$C_5H_7NS^+$	113.0294	-0.4
126.0369	$C_6H_8NS^+$	126.0372	-0.3
162.0137	$C_6H_9ClNS^+$	162.0139	-0.2

Figure 2.20 High Resolution Product Ion Spectrum and Proposed Fragmentation of Chlormethiazole from HLM Incubations

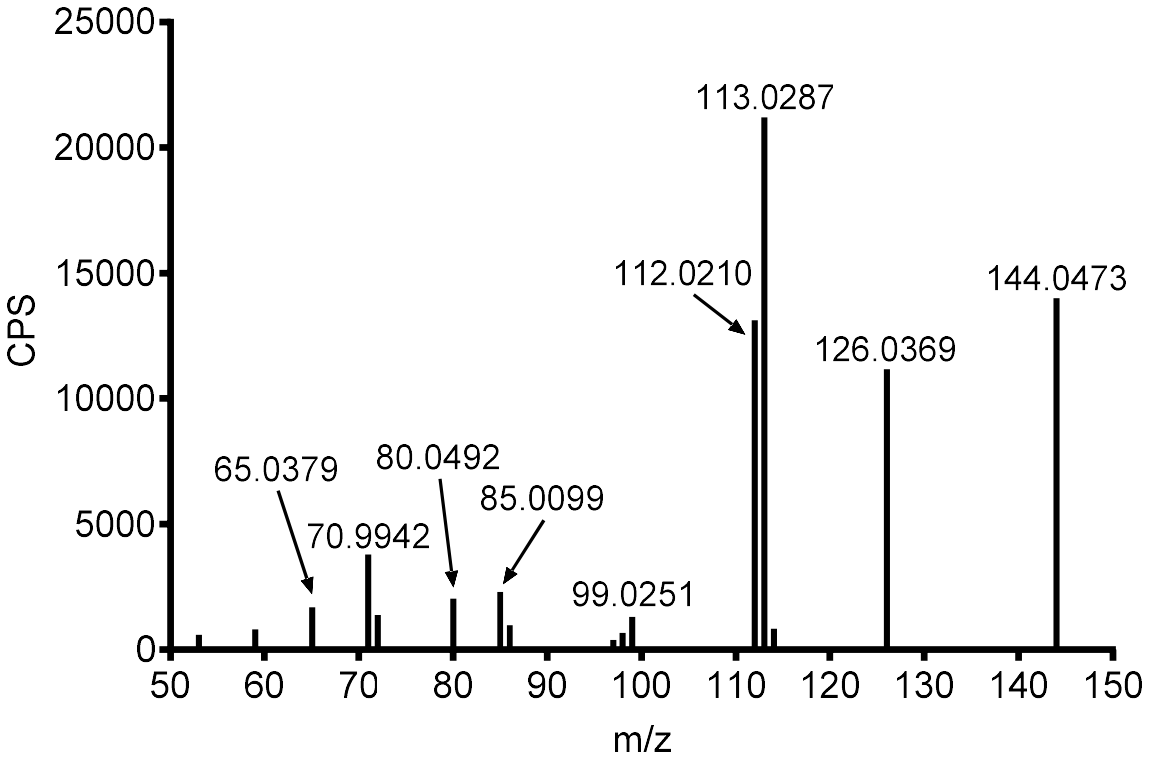

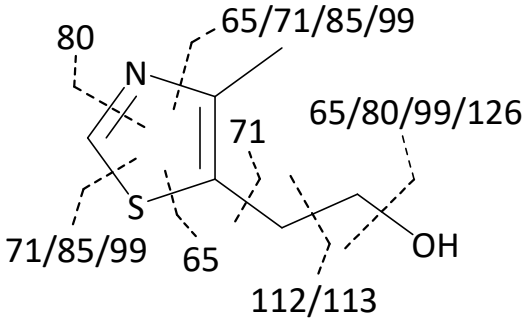

Found Mass	Formula	Predicted Mass	mDa Error
65.0379	$C_5H_5^+$	65.0386	-0.7
70.9942	$C_3H_3S^+$	70.9950	-0.8
80.0492	$C_5H_6N^+$	80.0495	-0.3
85.0099	$C_4H_5S^+$	85.0106	-0.7
99.0251	$C_5H_7S^+$	99.0263	-1.2
112.0210	$C_5H_6NS^+$	112.0215	-0.5
113.0287	$C_5H_7NS^+$	113.0294	-0.7
126.0369	$C_6H_8NS^+$	126.0372	-0.3
144.0473	$C_6H_{10}NOS^+$	144.0478	-0.5

Figure 2.21 Ion Spectrum and Proposed Fragmentation of M1 from HLM Incubations
M1 is proposed to be a deschloro alcohol metabolite.

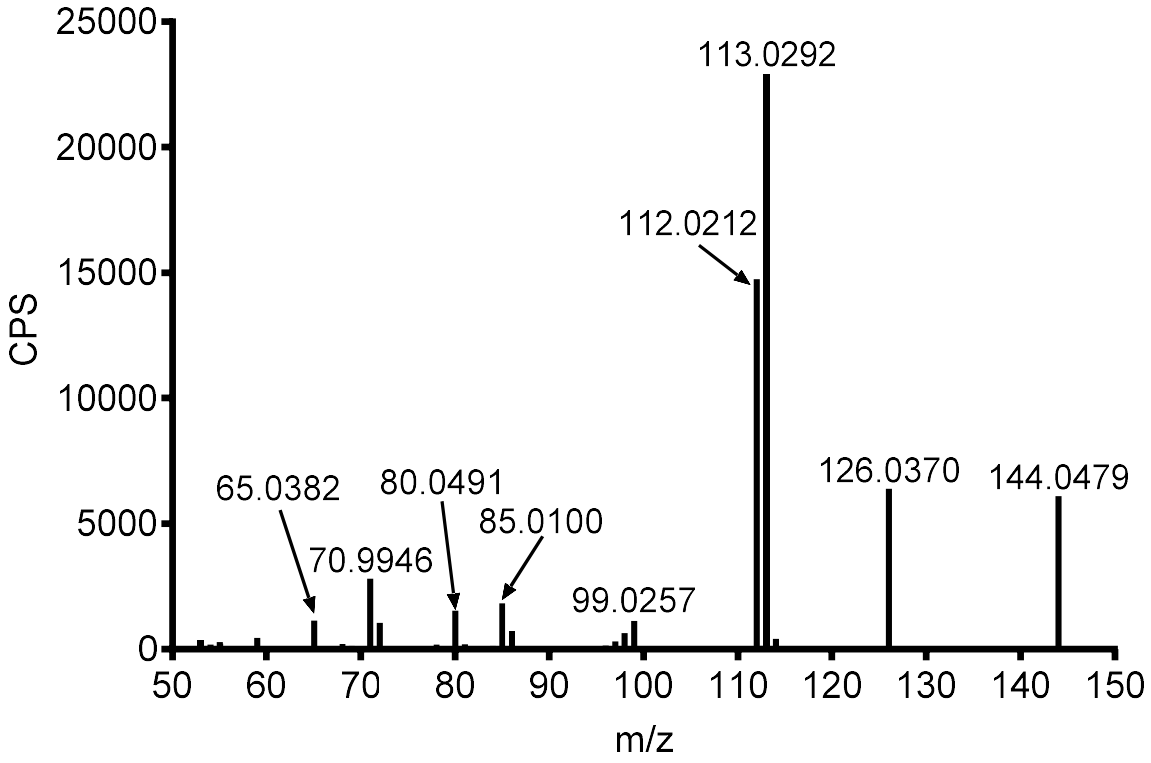

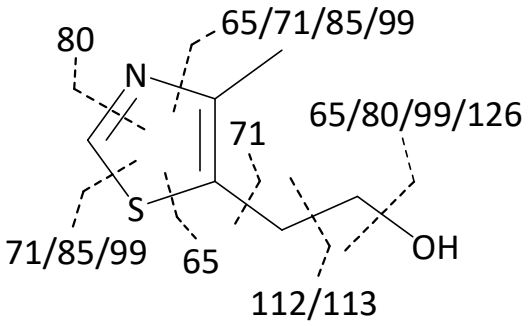

Found Mass	Formula	Predicted Mass	mDa Error
65.0382	$C_5H_5^+$	65.0386	-0.4
70.9946	$C_3H_3S^+$	70.9950	-0.4
80.0491	$C_5H_6N^+$	80.0495	-0.4
85.0100	$C_4H_5S^+$	85.0106	-0.6
99.0257	$C_5H_7S^+$	99.0263	-0.6
112.0212	$C_5H_6NS^+$	112.0215	-0.3
113.0292	$C_5H_7NS^+$	113.0294	-0.2
126.0370	$C_6H_8NS^+$	126.0372	-0.2
144.0479	$C_6H_{10}NOS^+$	144.0478	0.1

Figure 2.22 Ion Spectrum and Proposed Fragmentation of 5(1-Hydroxyethyl) 4-Methylthiazole

These spectra are generated from a commercially available standard.

.

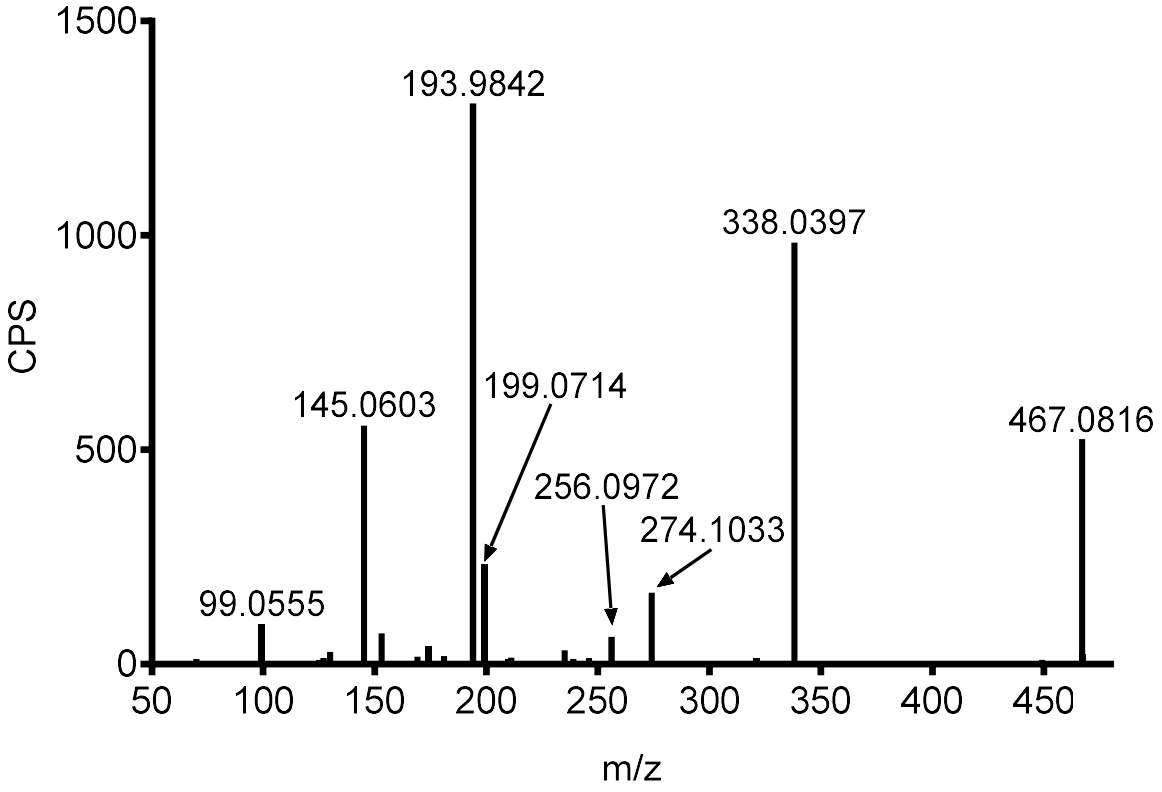

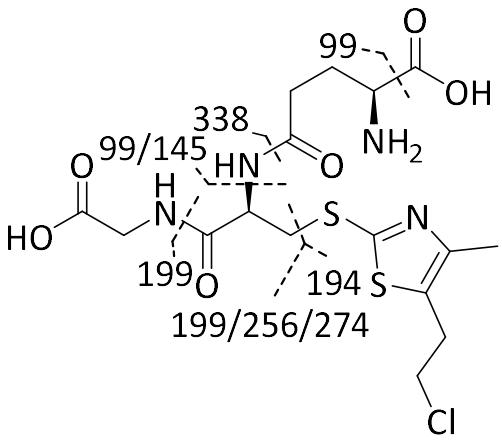

Found Mass	Formula	Predicted Mass	mDa Error
99.0555	$C_4H_7N_2O^+$	99.0553	0.2
145.0603	$C_4H_6NS^+$	145.0608	-0.5
193.9842	$C_6H_9ClNS_2^+$	193.9859	-1.7
199.0714	$C_4H_4NOS^+$	199.0713	0.1
256.0972	$C_{10}H_{14}N_3O_5^+$	256.0928	4.4
274.1033	$C_{10}H_{16}N_3O_6^+$	274.1034	-0.1
338.0397	$C_{11}H_{17}ClN_3O_6S_2^+$	338.0394	0.3
467.0816	$C_{16}H_{24}ClN_4O_6S_2^+$	467.0820	-0.4

Figure 2.23 Product Ion Spectrum and Proposed Fragmentation of M2 from HLM Incubations

M2 is proposed to be a dehydrogenated chlormethiazole glutathione adduct that could be the result of either water loss from hydroxylation at the C4 methyl, N-oxidation, or S-oxidation.

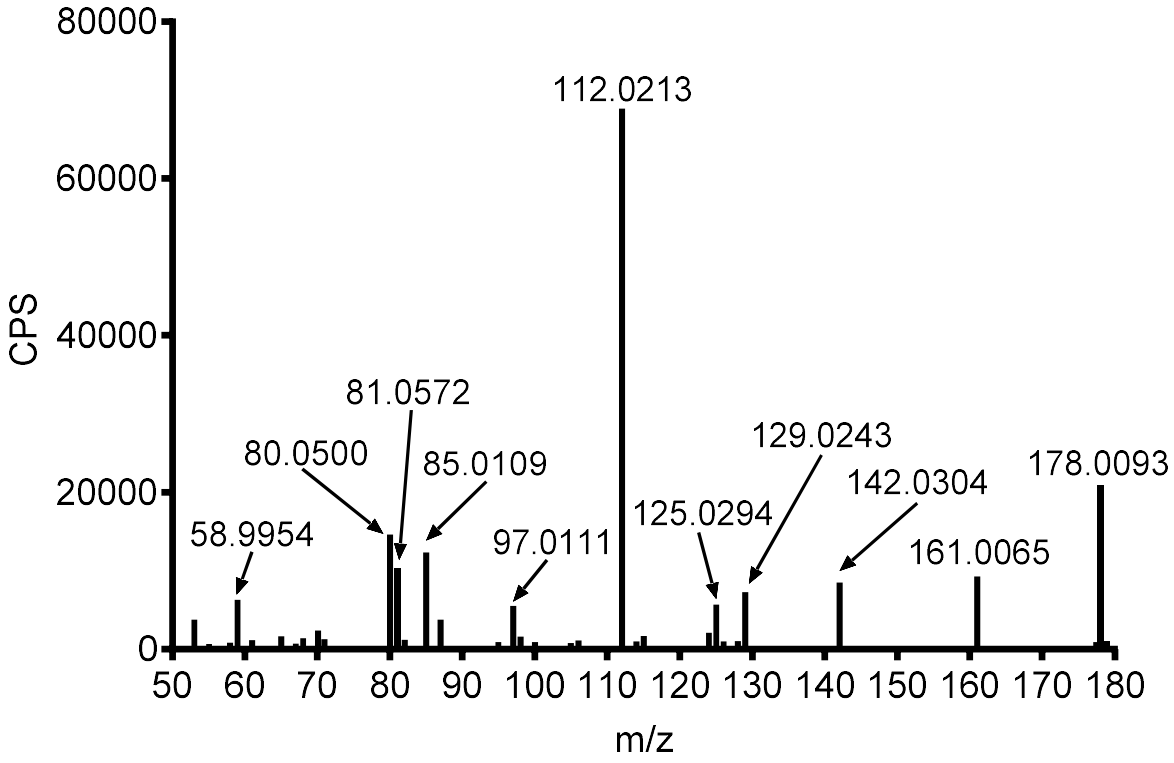

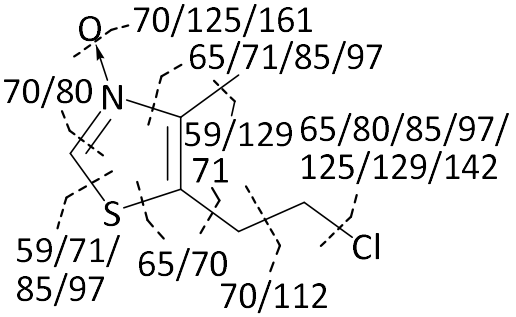

Found Mass	Formula	Predicted Mass	mDa error
53.0388	$C_4H_5^+$	53.0386	0.2
58.9954	$C_2H_3S^+$	58.9950	0.4
65.0388	$C_5H_5^+$	65.0386	0.2
70.0655	$C_4H_8N^+$	70.0651	0.4
70.9949	$C_3H_3S^+$	70.9950	-0.1
80.0500	$C_5H_6N^+$	80.0495	0.5
81.0572	$C_5H_7N^+$	81.0573	-0.1
85.0109	$C_5H_6NS^+$	85.0106	0.3
97.0111	$C_5H_5S^+$	97.0106	0.5
112.0213	$C_5H_6NS^+$	112.0215	-0.2
125.0294	$C_6H_9ClNS^+$	125.0294	0.0
129.0243	$C_5H_7NOS^+$	129.0243	0.0
142.0323	$C_6H_9NOS^+$	142.0321	0.2
161.0065	$C_6H_9ClNS^+$	161.0060	0.5
178.0093	$C_6H_{10}ClNOS^+$	178.0088	0.5

igure 2.24 Product Ion Spectrum and Proposed Fragmentation of Synthetic N-oxide (M3)

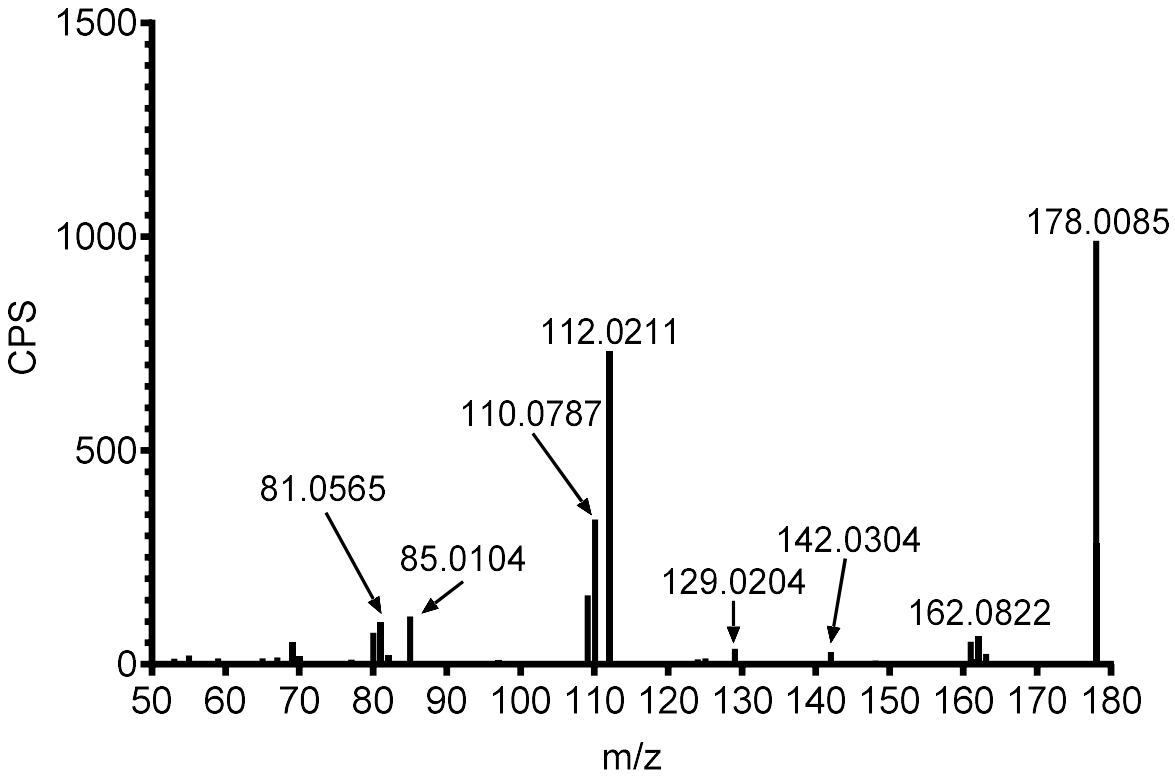

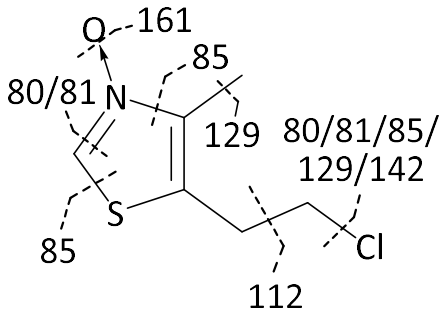

Found Mass	Formula	Predicted Mass	mDa error
80.0500	$C_5H_6N^+$	80.0495	0.5
81.0565	$C_5H_7N^+$	81.0573	-0.8
85.0104	$C_5H_6NS^+$	85.0106	-0.2
112.0211	$C_5H_6NS^+$	112.0215	-0.4
129.0204	$C_5H_7NOS^+$	129.0243	-3.9
142.0304	$C_6H_9NOS^+$	142.0321	-1.7
161.0052	$C_6H_9ClNS^+$	161.0060	-0.8
178.0085	$C_6H_{10}ClNOS^+$	178.0088	-0.3

Figure 2.25 Product Ion Spectrum and Proposed Fragmentation of M3
Due to the small amount of M3 formed in HLM incubations, this spectra appears to contain fragments from another compound as well as the N-oxide. 162.0822 m/z and 110.0787 do not contain mass defects that are consistent with being fragments of M3.

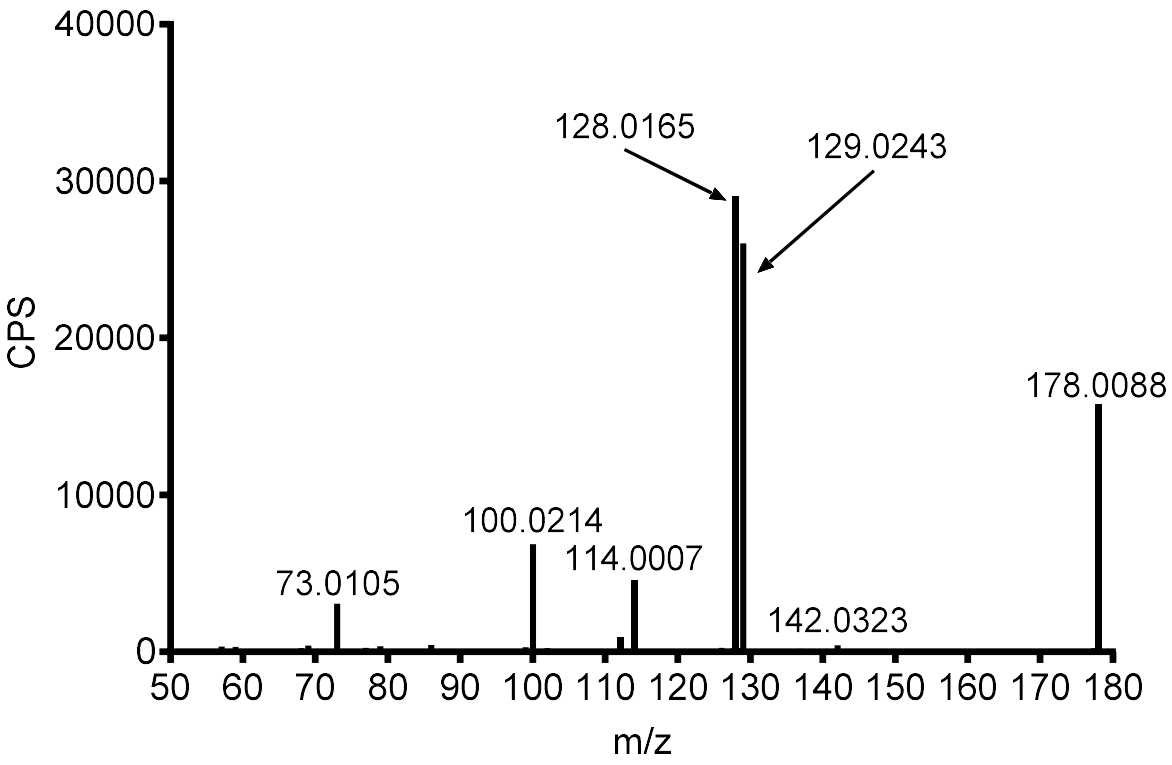

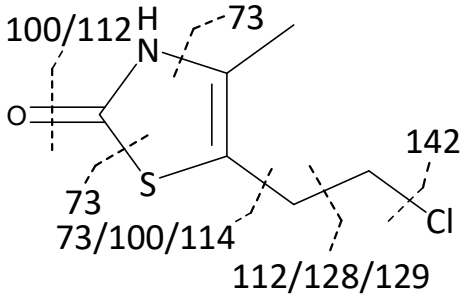

Found Mass	Formula	Predicted Mass	mDa error
73.0105	$C_3H_5S^+$	73.0106	-0.1
100.0214	$C_4H_6NS^+$	100.0215	-0.1
112.0209	$C_5H_6NS^+$	112.0215	-0.6
114.0007	$C_4H_4NOS^+$	114.0008	-0.1
128.0165	$C_5H_6NOS^+$	128.0165	0.0
129.0243	$C_5H_7NOS^+$	129.0243	0.0
142.0323	$C_6H_8NOS^+$	142.0321	0.2
178.0088	$C_6H_{10}ClNOS^+$	178.0088	0.0

Figure 2.26 Product Ion Spectrum and Proposed Fragmentation of M4

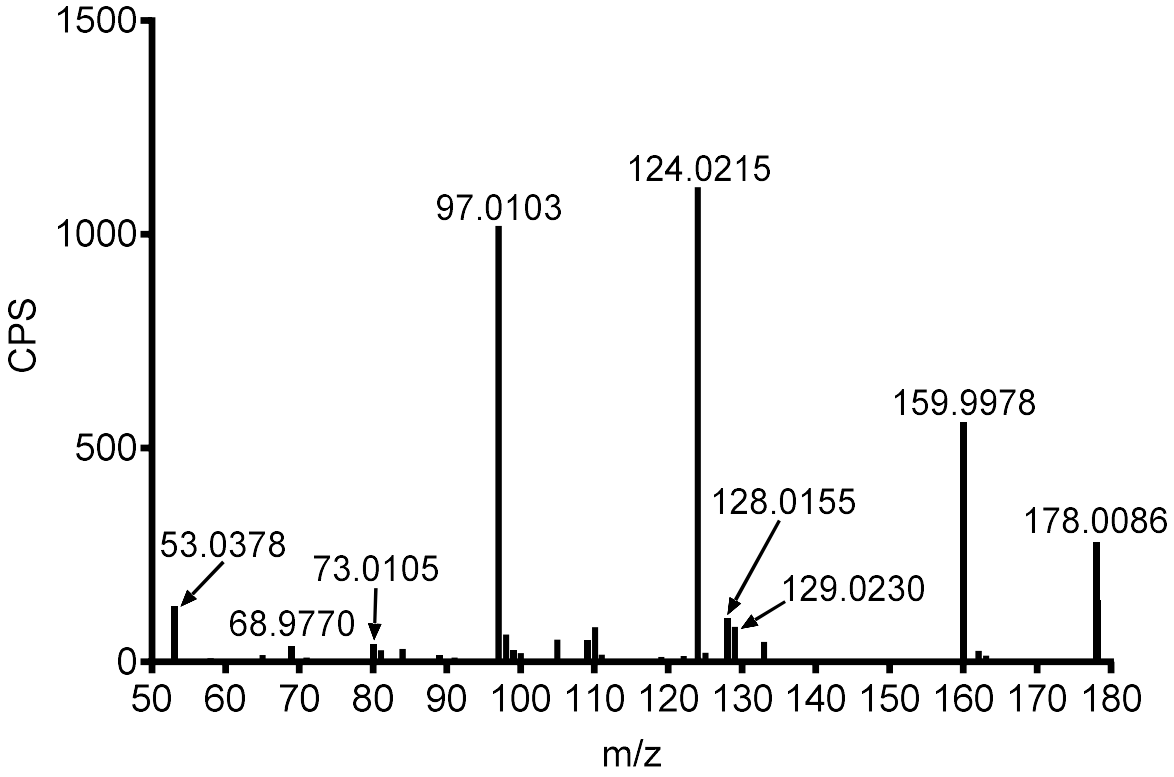

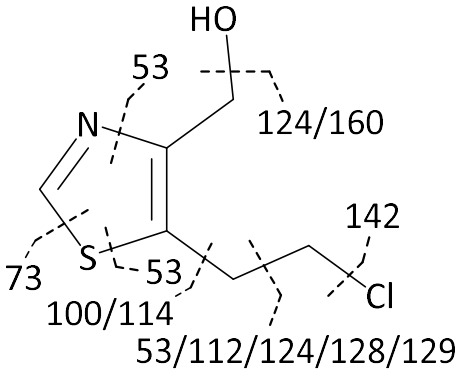

Found Mass	Formula	Predicted Mass	mDa error
53.0378	$C_4H_5^+$	53.0386	-0.8
68.9770	C_3HS^+	68.9793	-2.3
80.0485	$C_5H_6N^+$	80.0495	-1.0
83.9992	$C_5H_6NS^+$	84.0028	-3.6
97.0103	$C_5H_5S^+$	97.0106	-0.3
104.9546	$C_5H_6N^+$	104.9560	-1.4
124.0215	$C_5H_7N^+$	124.0215	0.0
128.0155	$C_5H_6NOS^+$	128.0165	-1.0
129.0230	$C_5H_7NOS^+$	129.0243	-1.3
159.9978	$C_6H_8ClNS^+$	159.9982	-0.4
178.0086	$C_6H_{10}ClNOS^+$	178.0088	-0.2

Figure 2.27 Product Ion Spectrum and Proposed Fragmentation of M5

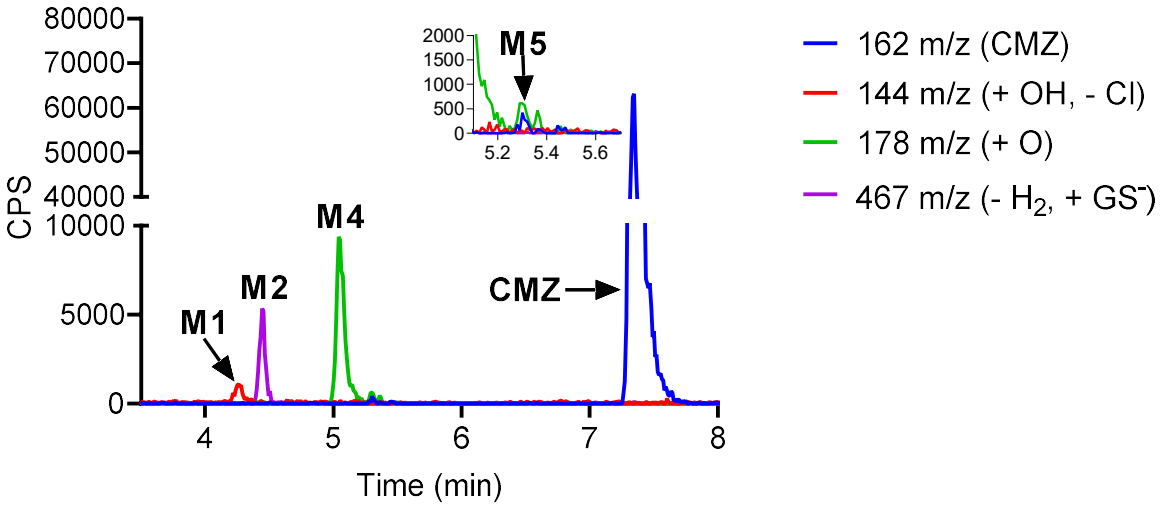

Figure 2.28 Overlay of Extracted Ion Current of Parent and Metabolite m/z from CYP1A2 Metabolite Identification

Overlay is composed of extract ion current mass ranges of all found metabolites and parent. M1 is a dechlorinated ethyl alcohol metabolite. M2 is dehydrogenated glutathione adduct. M3 is a N-oxide metabolite. M4 is likely C-2 oxidation resulting in a thiocarbamate. M5 is a hydroxylation on the C-4 methyl group. The inset focuses upon M5.

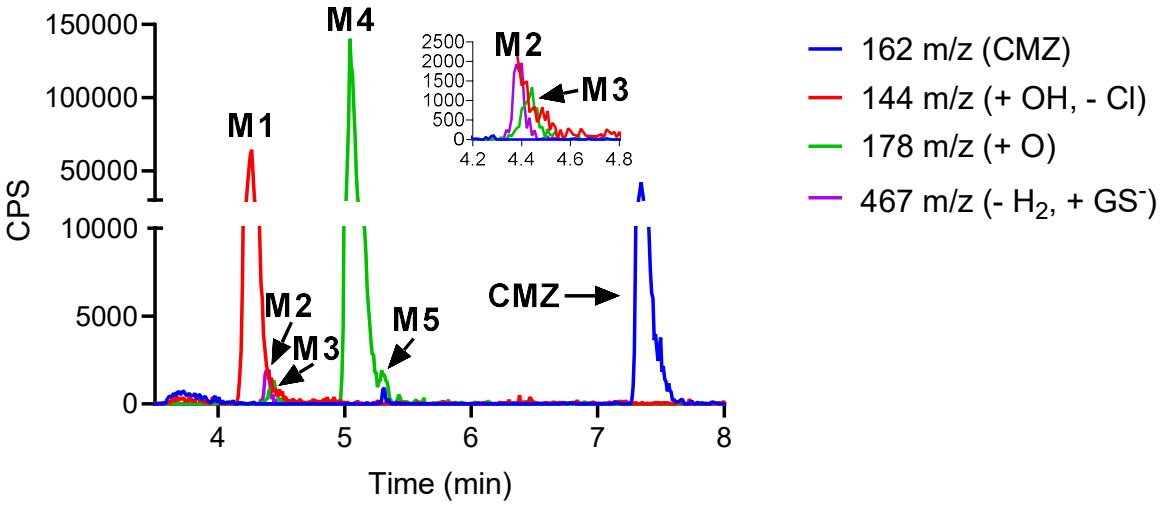

Figure 2.29 Overlay of Extracted Ion Current of Parent and Metabolite m/z from CYP2A6 Metabolite Identification

Overlay is composed of extract ion current mass ranges of all found metabolites and parent. M1 is a dechlorinated ethyl alcohol metabolite. M2 is dehydrogenated glutathione adduct. M3 is a N-oxide metabolite. M4 is likely C-2 oxidation resulting in a thiocarbamate. M5 is a hydroxylation on the C-4 methyl group. The inset focuses upon M2 and M3.

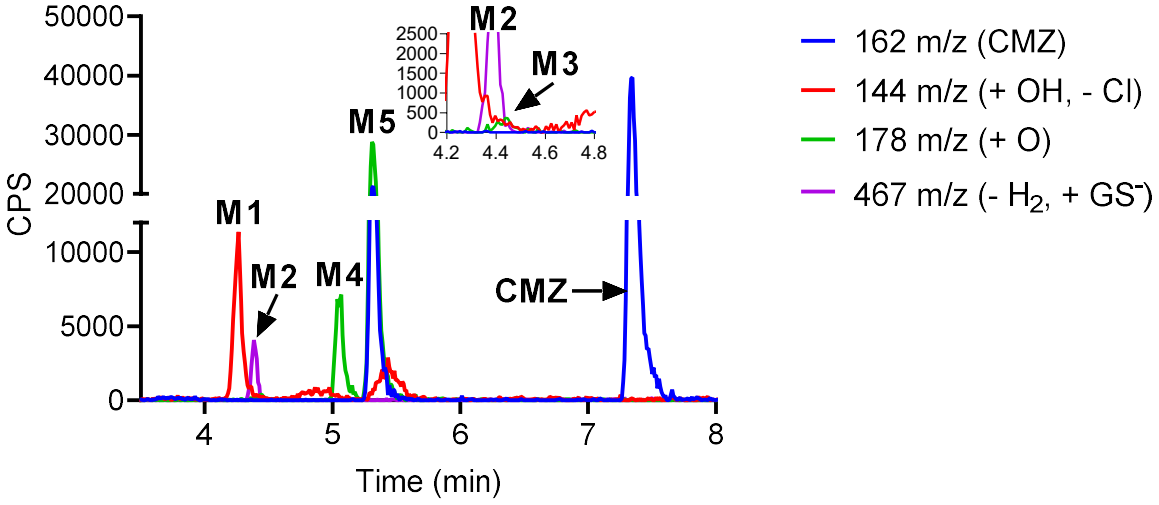

Figure 2.30 Overlay of Extracted Ion Current of Parent and Metabolite m/z from CYP2B6 Metabolite Identification

Overlay is composed of extract ion current mass ranges of all found metabolites and parent. M1 is a dechlorinated ethyl alcohol metabolite. M2 is dehydrogenated glutathione adduct. M3 is a N-oxide metabolite. M4 is likely C-2 oxidation resulting in a thiocarbamate. M5 is a hydroxylation on the C-4 methyl group. The inset focuses upon M2 and M3.

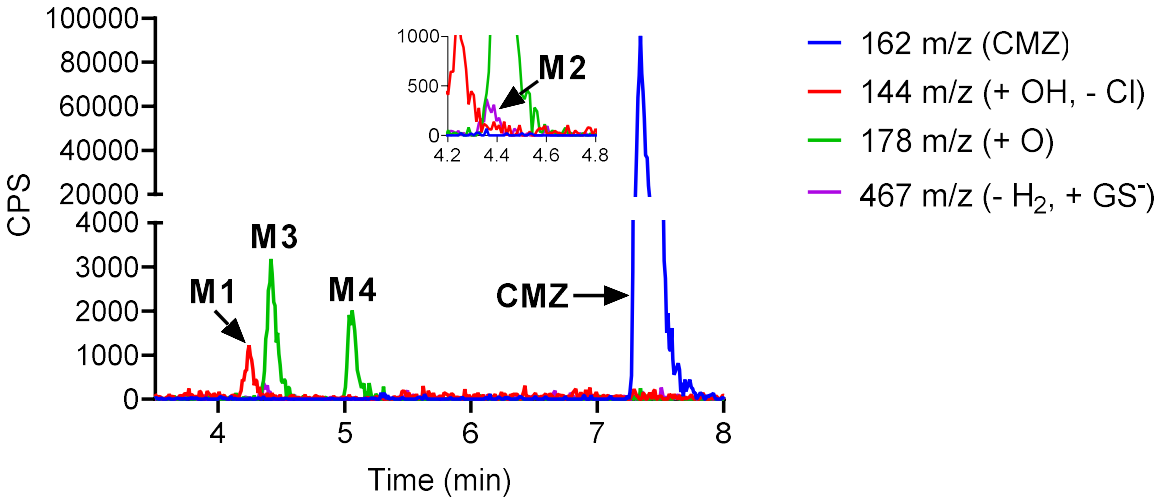

Figure 2.31 Overlay of Extracted Ion Current of Parent and Metabolite m/z from CYP2C8 Metabolite Identification

Overlay is composed of extract ion current mass ranges of all found metabolites and parent. M1 is a dechlorinated ethyl alcohol metabolite. M2 is dehydrogenated glutathione adduct. M3 is a N-oxide metabolite. M4 is likely C-2 oxidation resulting in a thiocarbamate. M5 is a hydroxylation on the C-4 methyl group. The inset focuses upon M2 and M3.

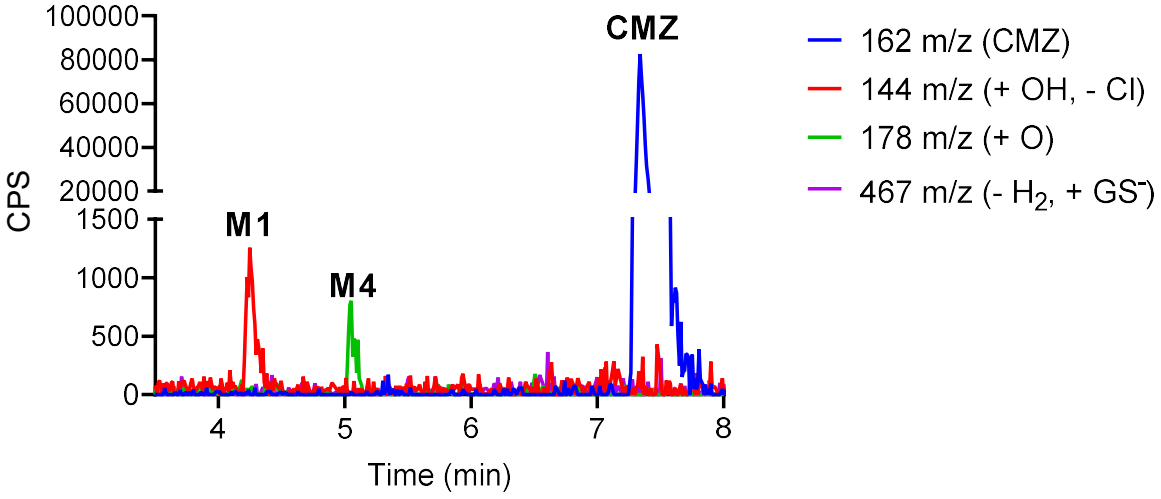

Figure 2.32 Overlay of Extracted Ion Current of Parent and Metabolite m/z from CYP2C9 Metabolite Identification

Overlay is composed of extract ion current mass ranges of all found metabolites and parent. M1 is a dechlorinated ethyl alcohol metabolite. M2 is dehydrogenated glutathione adduct. M3 is a N-oxide metabolite. M4 is likely C-2 oxidation resulting in a thiocarbamate. M5 is a hydroxylation on the C-4 methyl group.

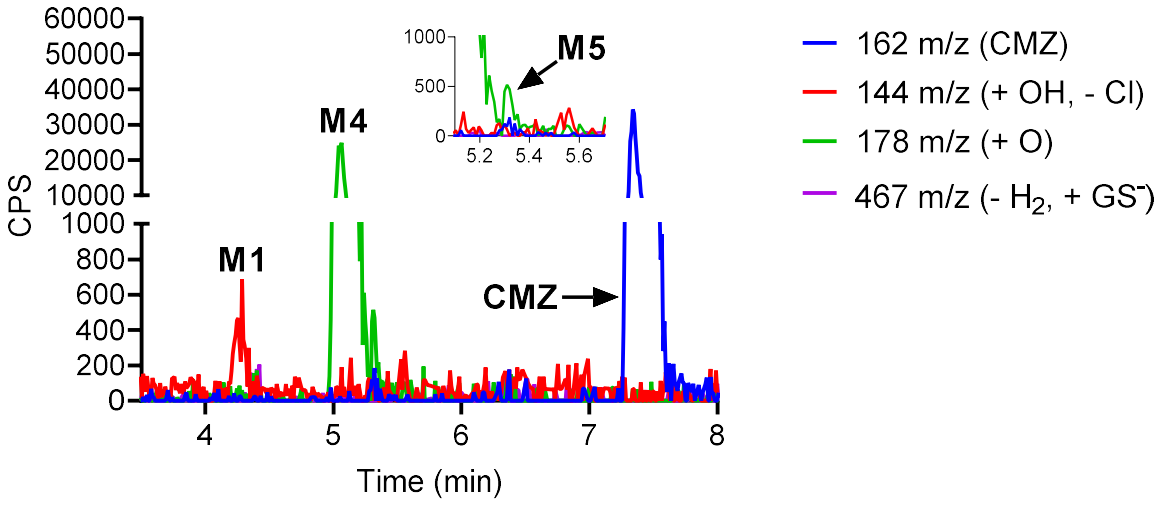

Figure 2.33 Overlay of Extracted Ion Current of Parent and Metabolite m/z from CYP2C19 Metabolite Identification

Overlay is composed of extract ion current mass ranges of all found metabolites and parent. M1 is a dechlorinated ethyl alcohol metabolite. M2 is dehydrogenated glutathione adduct. M3 is a N-oxide metabolite. M4 is likely C-2 oxidation resulting in a thiocarbamate. M5 is a hydroxylation on the C-4 methyl group. The inset focuses upon M5.

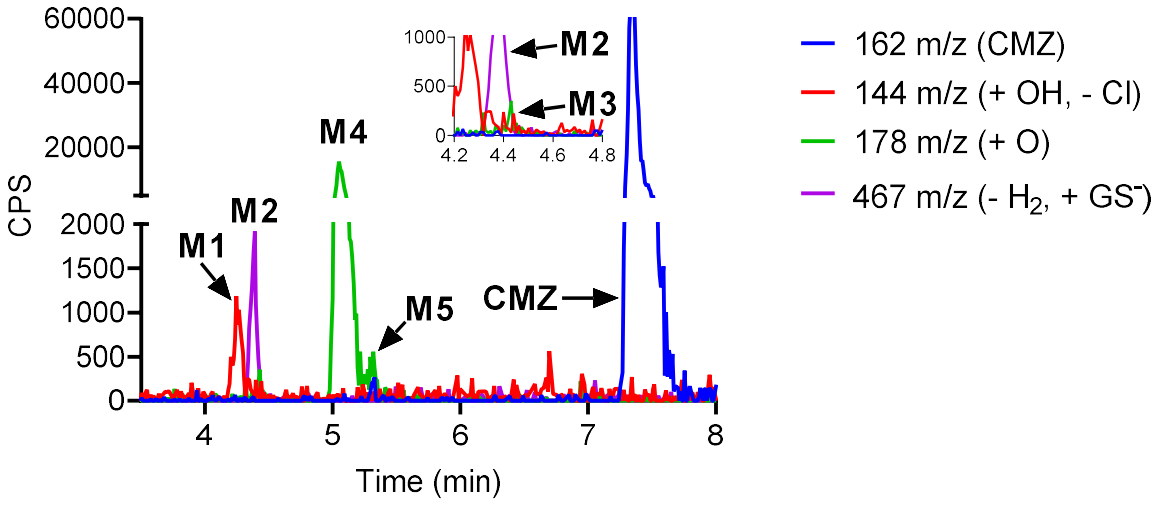

Figure 2.34 Overlay of Extracted Ion Current of Parent and Metabolite m/z from CYP2D6 Metabolite Identification

Overlay is composed of extract ion current mass ranges of all found metabolites and parent. M1 is a dechlorinated ethyl alcohol metabolite. M2 is dehydrogenated glutathione adduct. M3 is a N-oxide metabolite. M4 is likely C-2 oxidation resulting in a thiocarbamate. M5 is a hydroxylation on the C-4 methyl group. The inset focuses upon M2 and M3.

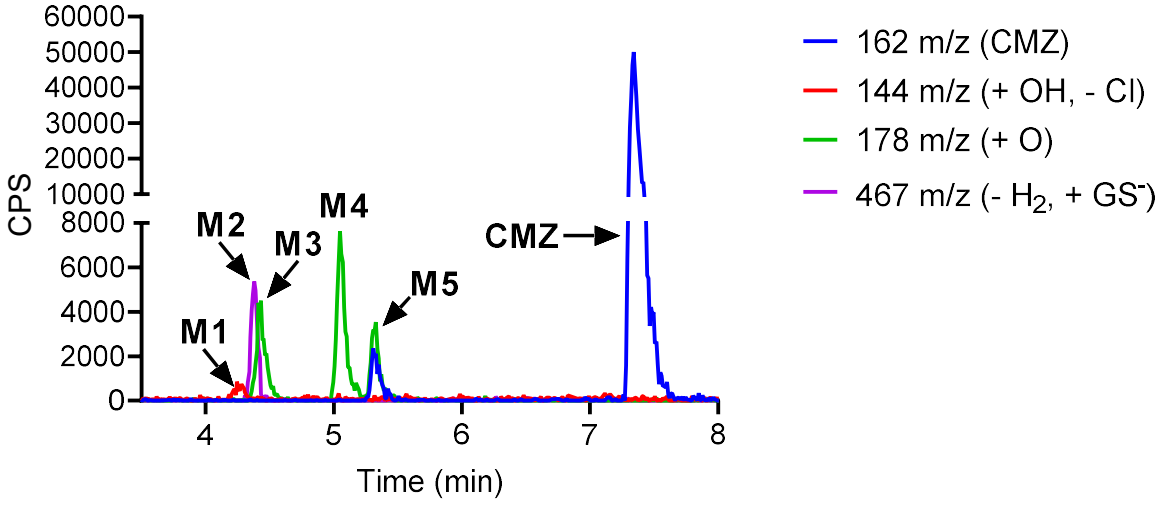

Figure 2.35 Overlay of Extracted Ion Current of Parent and Metabolite m/z from CYP2E1 Metabolite Identification

Overlay is composed of extract ion current mass ranges of all found metabolites and parent. M1 is a dechlorinated ethyl alcohol metabolite. M2 is dehydrogenated glutathione adduct. M3 is a N-oxide metabolite. M4 is likely C-2 oxidation resulting in a thiocarbamate. M5 is a hydroxylation on the C-4 methyl group. The inset focuses upon M2 and M3.

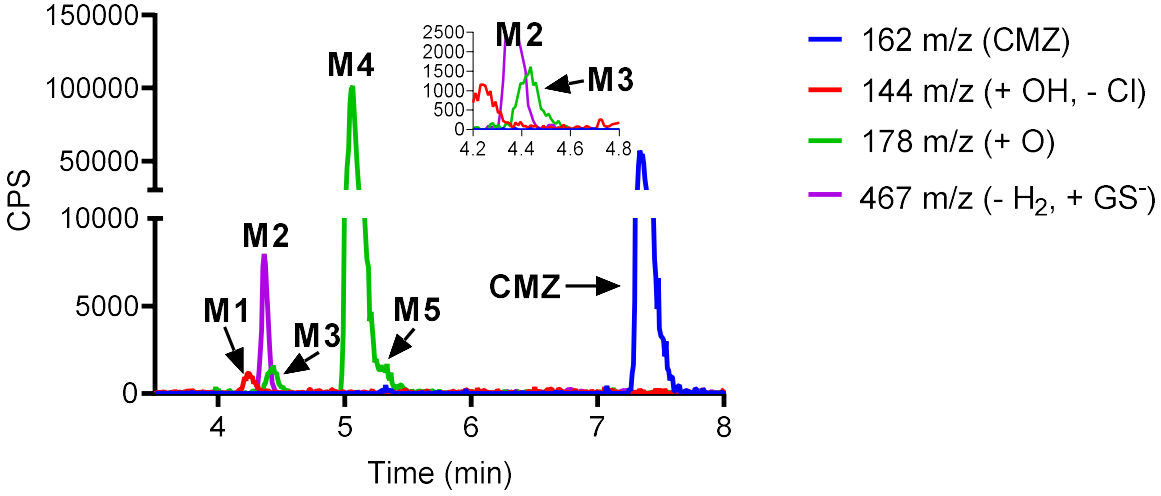

Figure 2.36 Overlay of Extracted Ion Current of Parent and Metabolite m/z from CYP3A4 Metabolite Identification

Overlay is composed of extract ion current mass ranges of all found metabolites and parent. M1 is a dechlorinated ethyl alcohol metabolite. M2 is dehydrogenated glutathione adduct. M3 is a N-oxide metabolite. M4 is likely C-2 oxidation resulting in a thiocarbamate. M5 is a hydroxylation on the C-4 methyl group. The inset focuses upon M2 and M3.

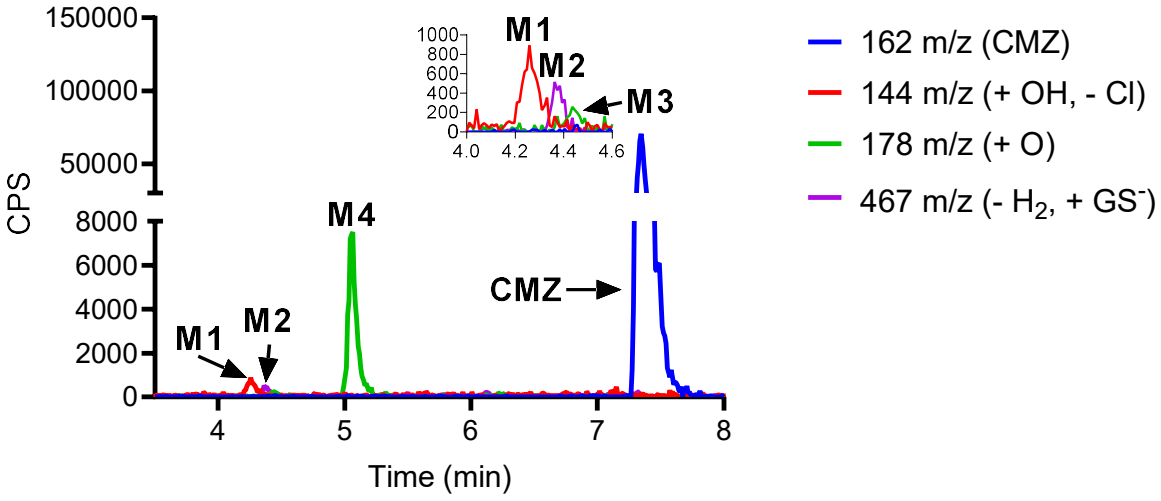

Figure 2.37 Overlay of Extracted Ion Current of Parent and Metabolite m/z from CYP3A5 Metabolite Identification

Overlay is composed of extract ion current mass ranges of all found metabolites and parent. M1 is a dechlorinated ethyl alcohol metabolite. M2 is dehydrogenated glutathione adduct. M3 is a N-oxide metabolite. M4 is likely C-2 oxidation resulting in a thiocarbamate. M5 is a hydroxylation on the C-4 methyl group. The inset focuses upon M1, M2, and M3.

A	Integrated Area of Metabolites					
rCYP	M1	M2	M3	M4	M5	Total Area of All Metabolites
CYP1A2	1091	16493	223	42692	2367	62864
CYP2A6	296578	6195	5519	578132	7616	894039
CYP2B6	46188	11943	1441	33106	130932	223609
CYP2C8	1169	1090	16243	9116	150	27767
CYP2C9	1144	119	33	2774	4	4074
CYP2C19	0	209	138	120032	1314	121693
CYP2D6	300	6029	383	70152	157	77020
CYP2E1	0	20033	21583	34232	16132	91979
CYP3A4	2375	28083	9107	514532	101	554197
CYP3A5	0	1637	684	34752	524	37596

B	Relative % Area of Metabolites for Each Isoform					
rCYP	M1	M2	M3	M4	M5	Total Area of All Metabolites
CYP1A2	1.74%	26.24%	0.35%	67.91%	3.76%	62864
CYP2A6	33.17%	0.69%	0.62%	64.67%	0.85%	894039
CYP2B6	20.66%	5.34%	0.64%	14.81%	58.55%	223609
CYP2C8	4.21%	3.92%	58.50%	32.83%	0.54%	27767
CYP2C9	28.08%	2.91%	0.81%	68.09%	0.11%	4074
CYP2C19	0.00%	0.17%	0.11%	98.63%	1.08%	121693
CYP2D6	0.39%	7.83%	0.50%	91.08%	0.20%	77020
CYP2E1	0.00%	21.78%	23.47%	37.22%	17.54%	91979
CYP3A4	0.43%	5.07%	1.64%	92.84%	0.02%	554197
CYP3A5	0.00%	4.35%	1.82%	92.43%	1.39%	37596

Figure 2.38 Integrated Area (A) and Relative Area of Metabolites (B) for Incubations Using Supersomes™ Recombinant Enzymes

Part A contains the integrated peak areas from a metabolite identification experiment using recombinant major liver drug metabolizing CYP isoforms. Part B presents the percent of total metabolite area response for each metabolite. M1 is a dechlorinated ethyl alcohol metabolite. M2 is dehydrogenated glutathione adduct. M3 is a N-oxide metabolite. M4 is likely C-2 oxidation resulting in a thiocarbamate. M5 is a hydroxylation on the C-4 methyl group. The results are highlighted with colors ranging from red to green to indicate the magnitude of absolute or relative value as compared in the other values in the same column.

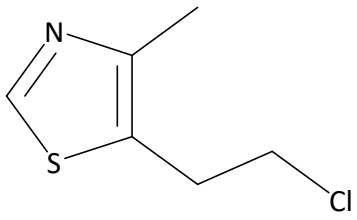

Chlormethiazole

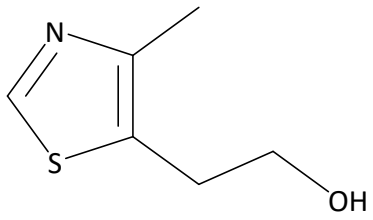

5(1-Hydroxyethyl) 4-methylthiazole

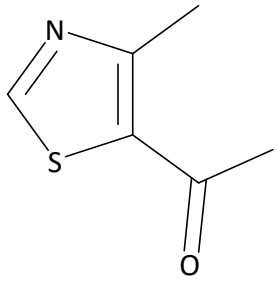

5-Acetyl 4-methylthiazole

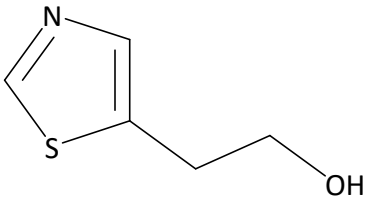

5(1-Hydroxyethyl)thiazole

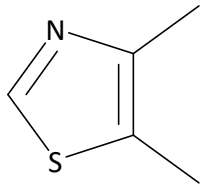

5-Acetyl 4-methylthiazole

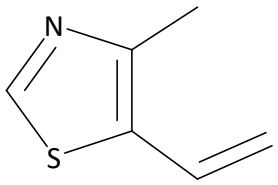

5-Ethenyl 4-methylthiazole

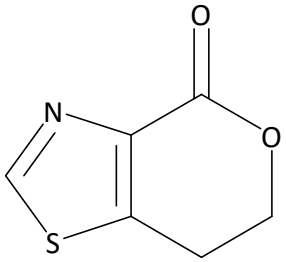

5,4-Ethyl-methyllactone thiazole

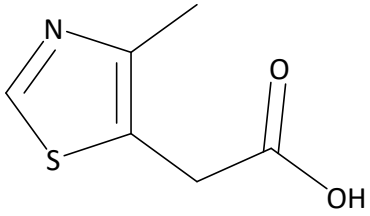

5-(Acetic acid) 4-methylthiazole

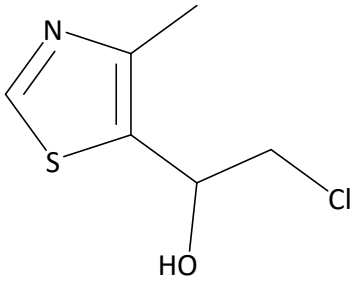

5-(1-Chloro, 4-hydroxyethyl) 4-methylthiazole

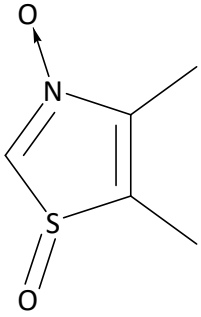

4,5-Dimethylthiazole-N-oxide-S-oxide

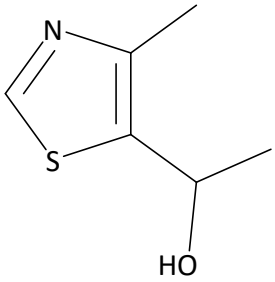

5-(2-Hydroxyethyl) 4-methylthiazole

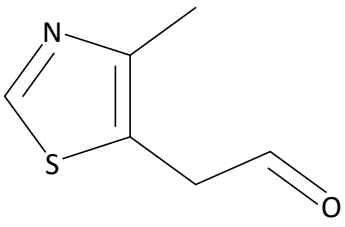

5-(Ethylaldehyde), 4-methylthiazole

Figure 2.39 Summary of Previously Reported In Vivo Metabolites
These structures are adapted from Ende et al, Witts et al, and Offen et al.

Chlormethiazole 1H-NMR

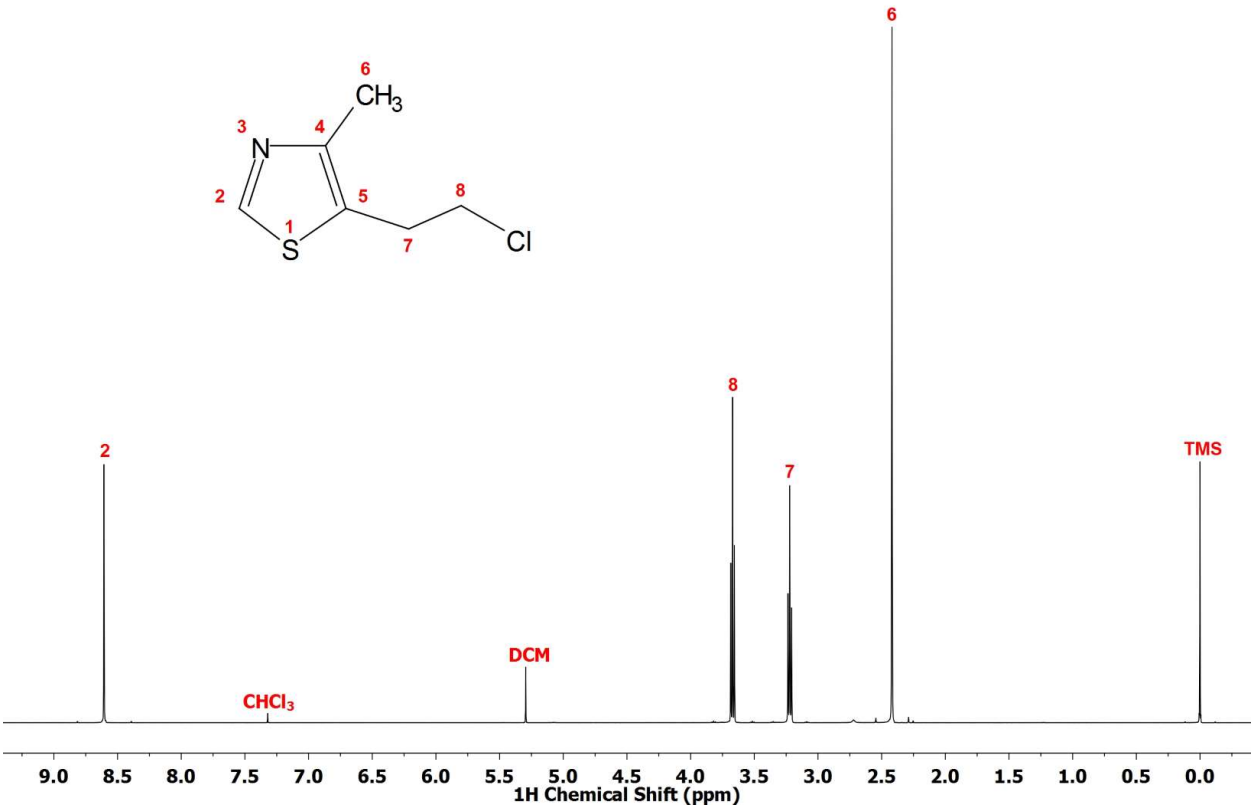

Figure S2.1 ^{1}H-NMR of Synthetic Chlormethiazole

Chlormethiazole N-Oxide 1H-NMR

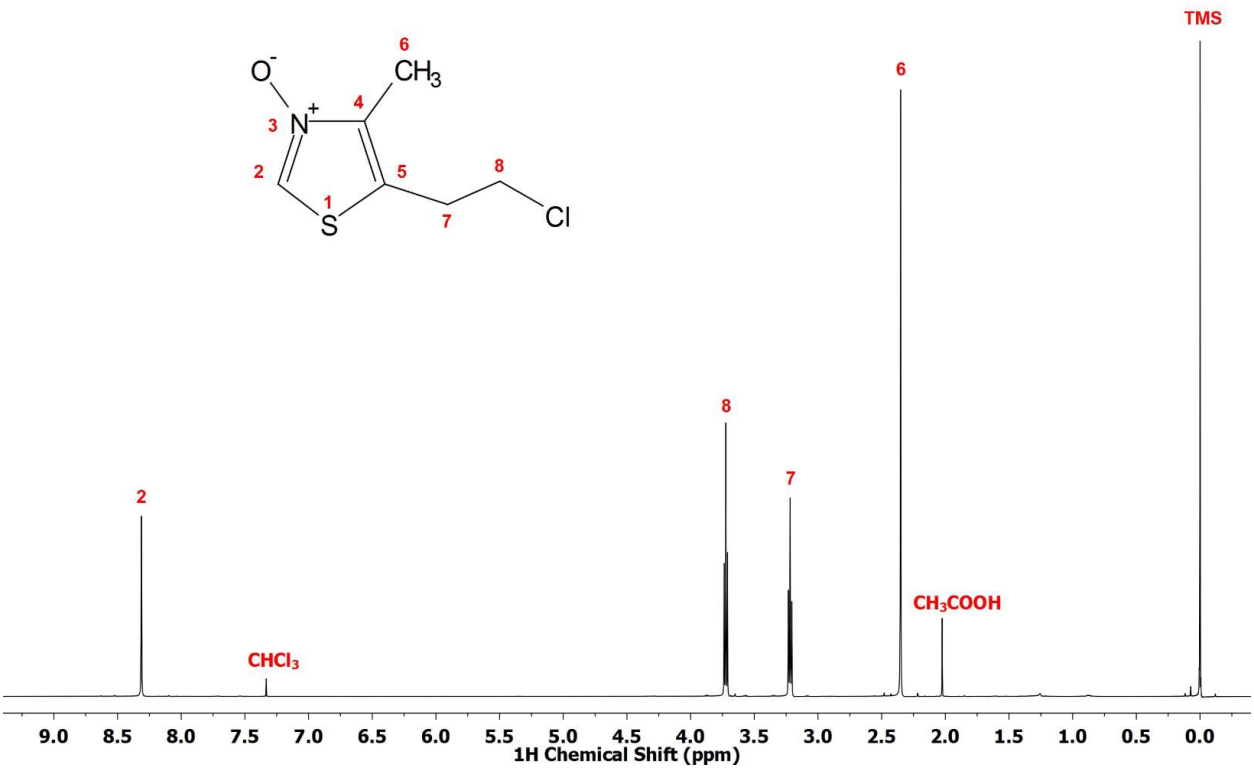

Figure S2.2 ^{1}H-NMR of Synthetic Chlormethiazole N-oxide

Chlormethiazole 13C-NMR

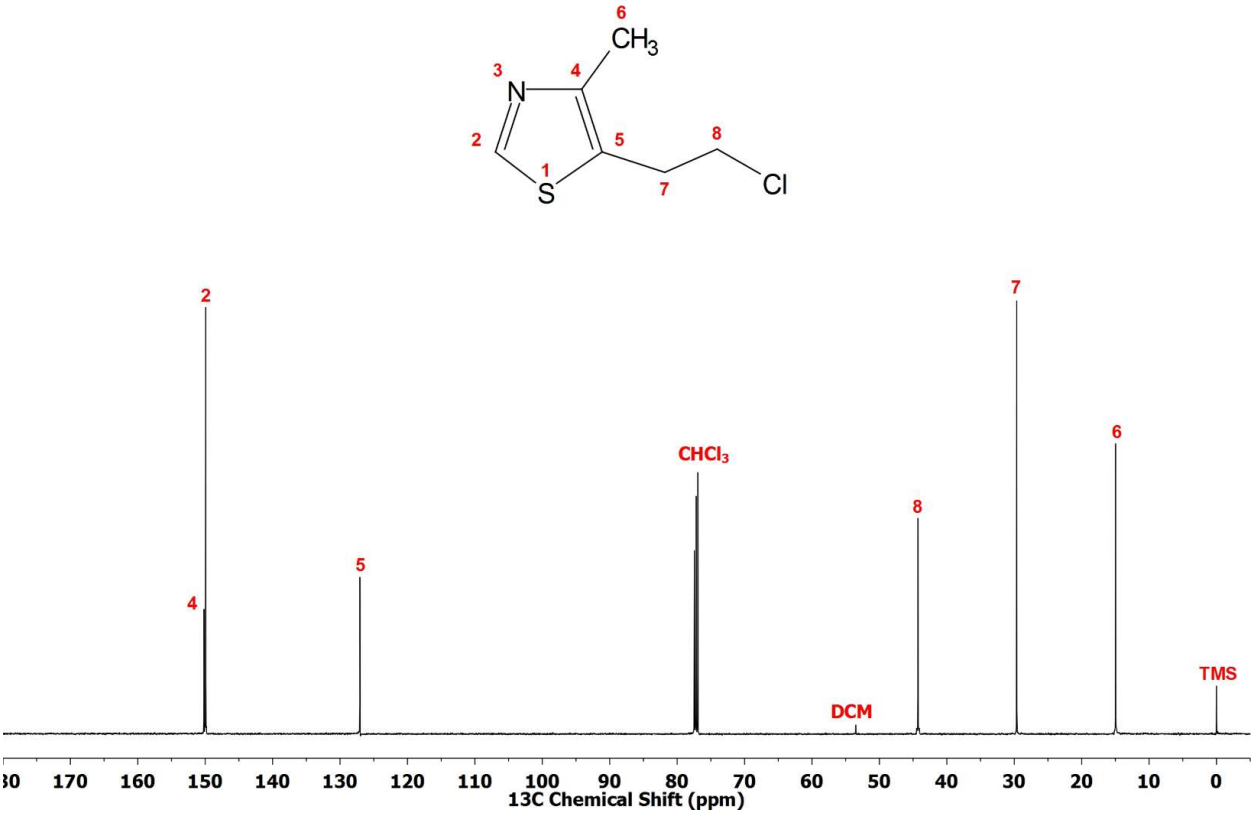

Figure S2.3 ^{13}C-NMR of Synthetic Chlormethiazole

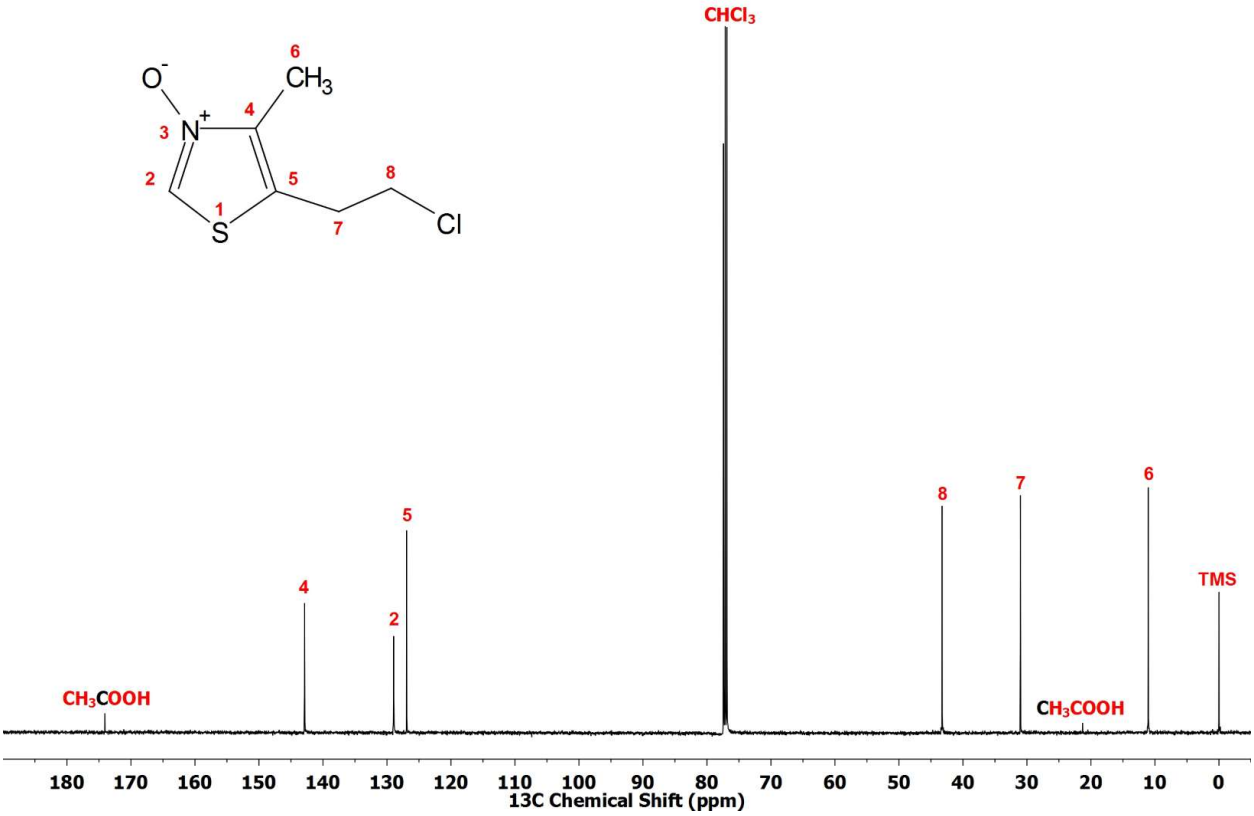

Figure S2.4 ^{13}C-NMR of Synthetic Chlormethiazole N-oxide

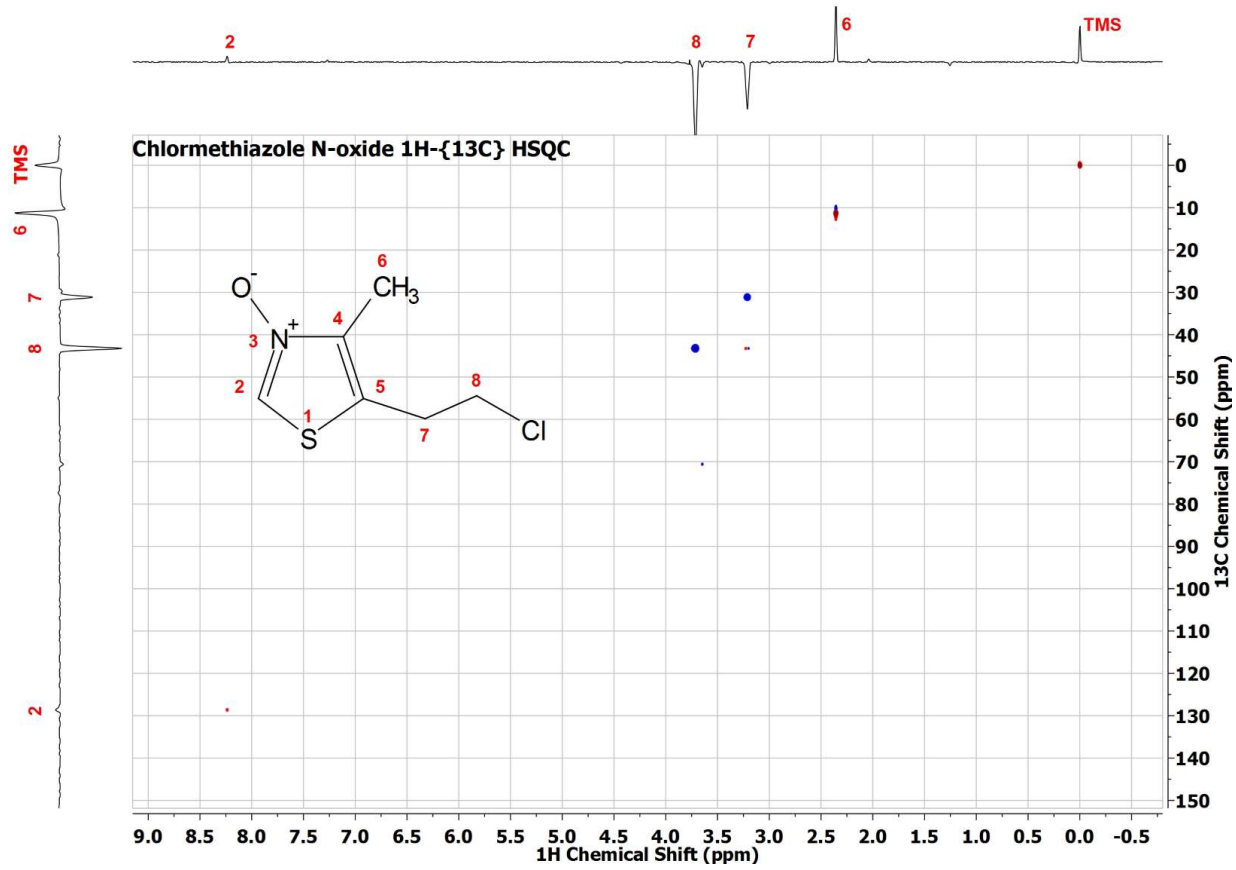

Figure S2.5 ^{1}H-^{13}C-HSQC NMR of Synthetic Chlormethiazole N-oxide

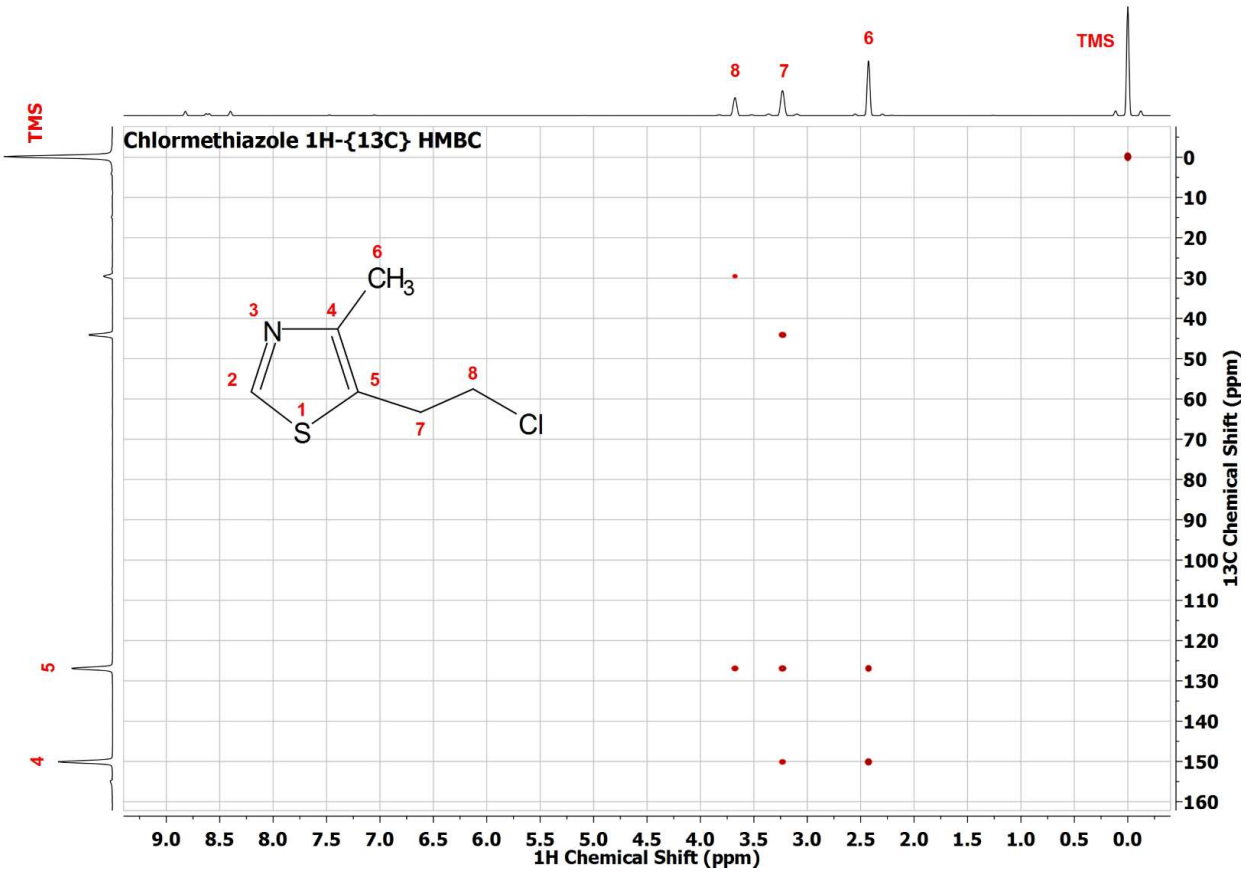

Figure S2.6 ^{1}H-^{13}C-HMBC NMR of Synthetic Chlormethiazole

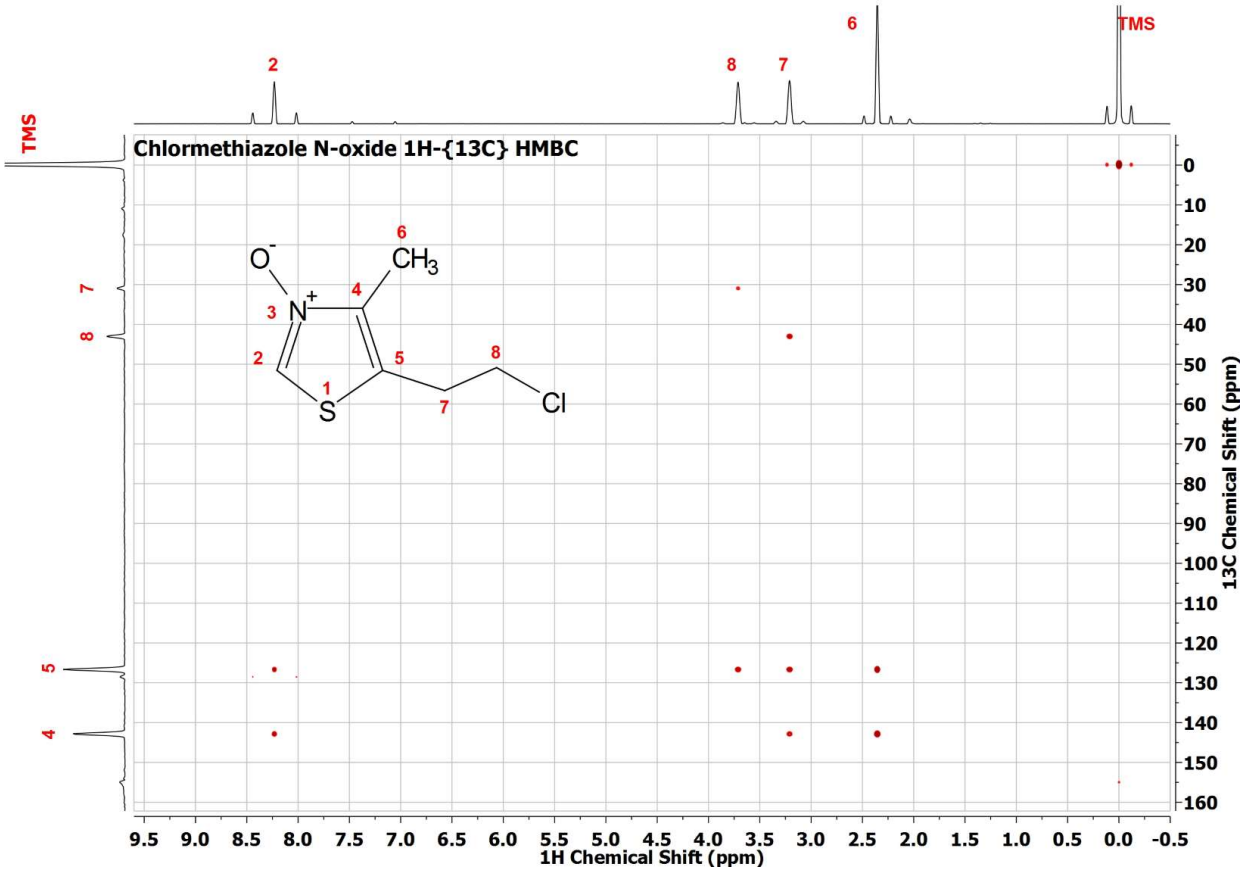

Figure S2.7 ^{1}H-^{13}C-HMBC NMR of Synthetic Chlormethiazole N-oxide

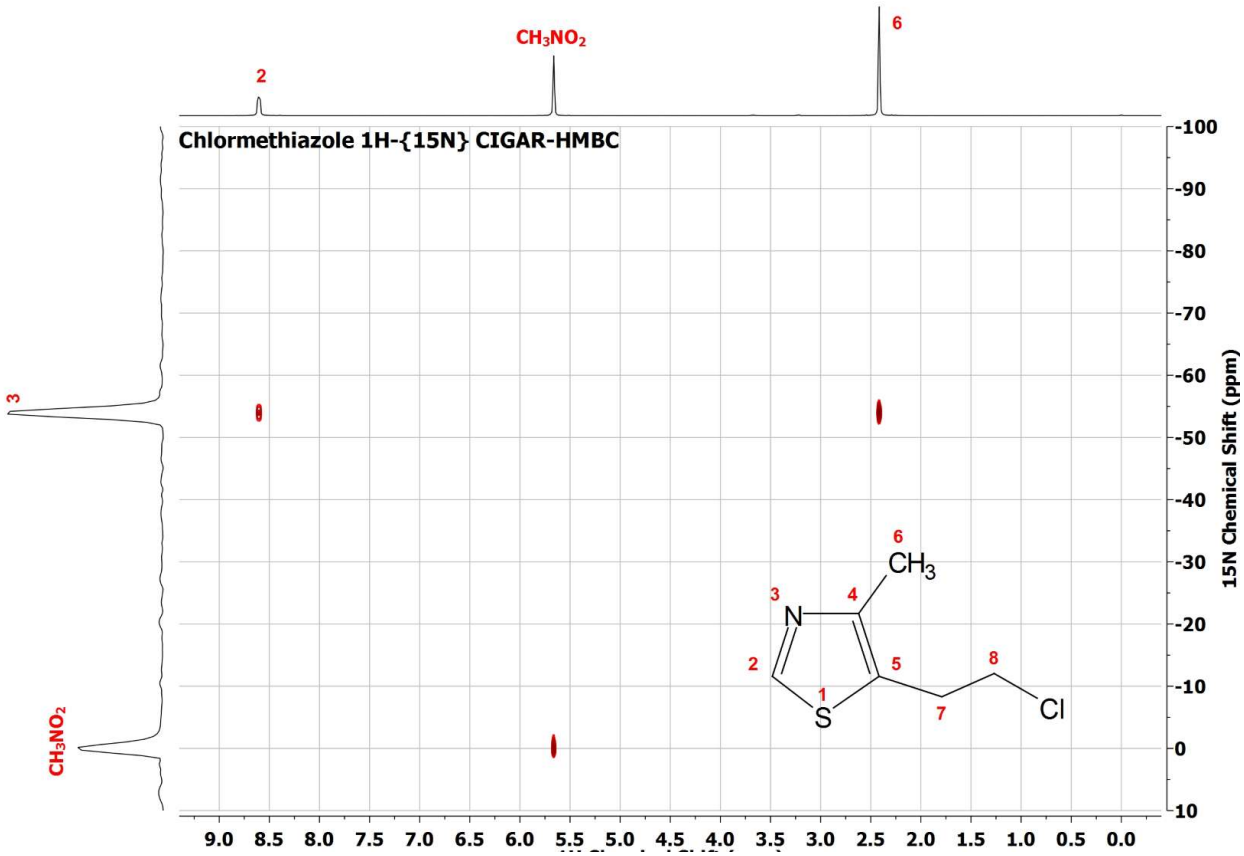

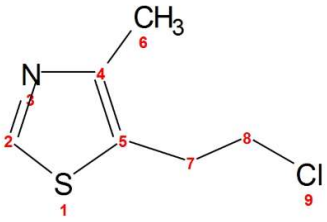

Atom		Chemical Shift*
1	S	
2	C	149.93
	H	8.61
3	N	-53.98
4	C	150.19
5	C	127.04
6	C	14.97
	H3	2.42
7	C	29.63
	H2	3.22
8	C	44.28
	H2	3.67
9	Cl	

* 1H, 13C chemical shifts referenced to internal TMS
15N chemical shifts referenced to external neat CH_3NO_2

Figure S2.8 ^{1}H-^{15}N-CIGAR HMBC NMR of Synthetic Chlormethiazole

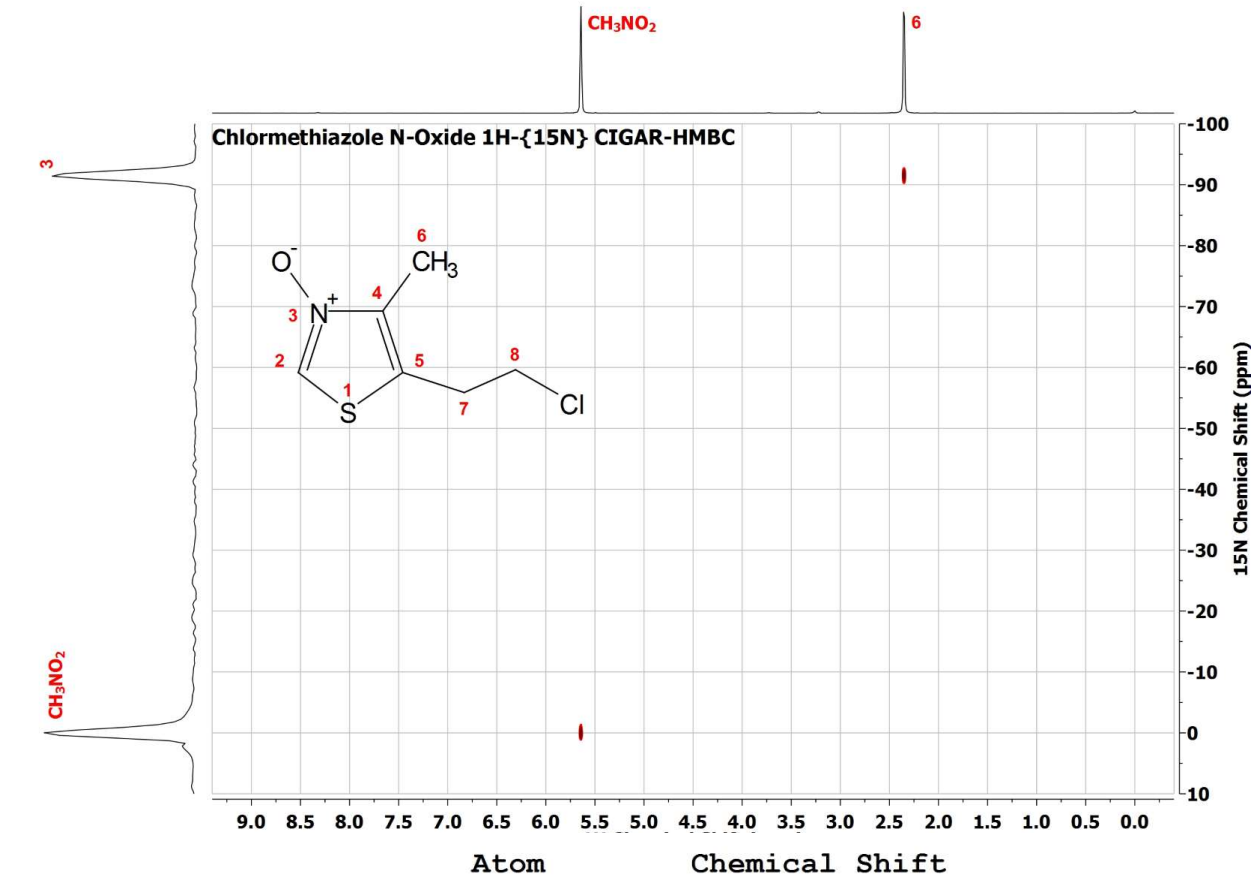

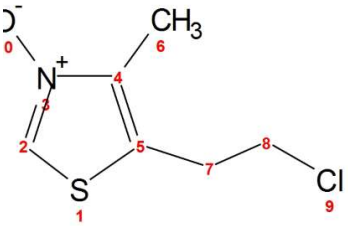

Atom		Chemical Shift
1	S	
2	C	128.96
	H	8.31
3	N	-91.49
4	C	142.87
5	C	126.92
6	C	11.04
	H3	2.35
7	C	31.02
	H2	3.22
8	C	43.25
	H2	3.72
9	Cl	
10	O	

* 1H, 13C chemical shifts referenced to internal TMS
15N chemical shifts referenced to external neat CH_3NO_2

Figure S2.9 ^{1}H-^{15}N-CIGAR HMBC NMR of Synthetic Chlormethiazole N-oxide

Chapter 3: Development of LC/MS Based Methods for the Detection of Heme Adducts and of Heme B Quantitation

3.1 Introduction

Heme is a family of iron containing porphyrins that serve as a functional prosthetic group in several types of (hemo)proteins that have important biological functions in living organisms. Heme can function as a molecular oxygen and carbon dioxide carrier as seen with heme B in hemoglobin and myoglobin and heme S in marine worms, and this is the first function that was described in the literature.(231-233) Hemoproteins are also peroxidases, electron transfer partners, and diatomic gas detectors, but the activation of molecular oxygen for catalysis is the function that is most relevant to this work. Dysregulation of heme homeostasis through multiple mechanisms lead to a number of disease states that have been of interest for several decades.(234-237)

Heme homeostasis and synthesis is regulated by several enzymes in the cytosol and mitochondria.(231-233,238) Heme is generated in a series of steps starting with the reaction of glycine and succinyl-CoA to 5-aminolevulinic acid (5-ALA) in the mitochondria catalyzed by δ-aminolevulinic acid synthase-1 or -2 (ALAS1/ALAS2). ALAS1 is expressed in nearly all tissues while ALAS2 is expressed only in erythroid tissue. 5-ALA is then converted to porphobilinogen by Δ-aminolevulinic acid dehydratase (ALAD), and 4 porphobilinogen units are joined by hydroxymethylbilane synthase (HMBS), which is also known as porphobilinogen deaminase (PBGD), to form hydroxymethylbilane. Uroporphyrinogen III decarboxylase (UROD) converts hydroxymethylbilane to uroporphyrinogen III which is the first intermediate with a complete porphyrin ring system. Uroporphyrinogen III is converted by UROD, coproporphyrinogen-III oxidase (CPOX), and protoporphyrinogen oxidase (PPOX) to protoporphyrin IX (PPIX) which is the last step before incorporation of iron by ferrochelatase (FECH) to complete the synthesis of

heme B. The synthetic process of PPIX and heme B in mammalian cells is summarized in Figure 3.1. Heme B is either incorporated in a hemoprotein or destroyed by heme oxygenase, which generates biliverdin, and the mechanism of heme oxygenase 1 is summarized in Figure 3.2.(239-241) Biliverdin is reduced to bilirubin by biliverdin reductase, and bilirubin is metabolized by UGT1A1 to prepare bilirubin for excretion.(242,243)

Accumulation of PPIX can occur through multiple mechanisms and is potentially toxic.(238) PPIX accumulation can be a consequence of iron deficiency, disruption of normal transport due to mutations, increases in 5-ALA through direct administration or increases in ALAS1, or inhibition of ALAD, PPOX, or FECH. Excess PPIX can chelate zinc, which forms a zinc PPIX species capable of generating reactive oxygen species when exposed to light. As a result, protoporphyrin IX accumulation has been shown to cause photosensitivity and damage skin or other tissues near the surface of the skin such as muscle. Accumulation of PPIX also can cause liver damage through a disruption of biliary secretion. Unmodified PPIX is not readily excreted from the kidney and is eliminated primarily through biliary excretion in the liver by breast cancer resistance protein (BCRP) which is involved in excretion of bile acids. 3,5-Diethoxycarbonyl-1,4-dihydrocollidine (DDC) and griseofulvin are suicide substrates of CYP that generate N-alkylated PPIX, which inhibits FECH and induce ALAS1.(114,244,245) Griseofulvin is known to cause hepatic injury and aplastic anemia, presumably via PPIX accumulation. Griseofulvin and DDC were originally identified as causing porphyria, but the mechanisms were not initially known. Investigation into the mechanisms by which they caused porphyria led to research into CYP mediated heme destruction.

Isozyme members of the cytochrome P450 (CYP) superfamily all contain a prosthetic heme B (Fig 3.3) that performs mostly oxidation reactions and occasionally reduction reactions with endogenous and exogenous compounds.(39,246) With some exceptions, heme B is anchored to the apoprotein of CYPs *via* thiolate from a cysteine residue, which serves as the fifth ligand to

the iron, and a group of positively charged residues that have ionic interactions with the two propionate groups from heme B. In the canonical reaction cycle of CYP, the redox state of the iron-containing porphyrin system is altered to create reactive oxygen species that perform mostly oxidative reactions upon the substrates of the enzymes. The exact masses and structures of heme B and important related species, such as PPIX, are depicted in Figure 3.3. The general reaction cycle of CYP enzymes has been well described in numerous publications.(246) The resulting oxidation reactions may generate reactive products that can be radicals or otherwise electrophilic in nature. These reactive species have the potential to modify the CYP apoprotein or prosthetic heme, and such modifications can inhibit the function of the enzyme.(16,96)

The covalent modification of the apoprotein or heme of CYP enzymes can cause time-dependent or mechanism-based inhibition (TDI and MBI, respectively), and these have been the subject of much research because they can cause drug-drug interactions that have serious implications for human health. Xenobiotic-protein adducts have been known since at least 1947, when it was discovered that aminodiazo-dyes could be bioactivated to reactive species that bound covalently to liver proteins.(247,248) The first clear instances of covalent adduction of apoprotein causing destruction of CYP were described by Halpert and Neal following bioactivation of chloramphenicol and parathion.(106,249) Other work in the 1970's and 1980's by de Matteis, Franklin, Mansuy, and Ortiz de Montellano revealed that modification of heme could cause inactivation of CYP enzymes and also led to some understanding of the mechanisms of heme modification.(49,52,54,84,88,103-105,108,112,116,118,250,251) Of particular interest, in the context of this thesis research with CMZ, various types of carbene reactive species were identified as potential inhibitors of CYP function through heme modification. Since these initial findings, numerous clinically relevant drug-drug interactions that have dramatic effects upon patients' health have been identified, and some important examples were covered in Chapter 1.

The first isolation and characterization of heme B dates back more than 150 years, with the earliest recorded isolation of heme crystals by Teichmann in 1853.(252-254) Most experimental approaches isolated heme B from hemoglobin or myoglobin, but similar procedures have been used to isolate this prosthetic group from CYP enzymes present in tissue fractions or purified systems.(2,3,231) In heme-containing proteins, the propionate groups are usually bound to a set of positively charged or hydrophobic residues. For example, the propionate groups of the heme of CYP2E1 interact with Arg100, Lys103, Trp122, Asn367, His370, and Arg435.(255) Additionally, the heme iron can be penta- or hexa-coordinate. For example, cytochrome b5 is hexacoordinate with histidine as both the proximal and distal ligand. In CYPs (and chloroperoxidase), the proximal ligand in the resting state is cysteine and a loosely held water molecule serves as the sixth ligand. With the notable exception of a few CYP4 enzymes, all CYPs are tethered in the active site cavity by non-covalent interactions with the apoprotein.(97,256)

The majority of heme isolation methods involve the addition of a strong acid to protonate the propionate moieties and any residues of the protein serving as either fifth or sixth ligands.(2,3,257-261) Acidification disrupts these weak interactions such that the heme can be released from the protein. The heme is then typically extracted with various organic solvents and can be purified by crystallization or esterified to facilitate preparative chromatography by normal and reversed phase methods.(252,254,257-259) Additionally, a combination of UV, NMR and mass spectrometry analyses have been used to detect and characterize heme and related protoporphyrin IX products after purification.(3,9,107-109,262,263) However, there are issues with these older methods that may limit their utility in characterizing a wide scope of heme and protoporphyrin IX adducts.

The majority of the older methods that rely upon the use of strong acids - typically mineral acids, hydrochloric or trifluoroacetic acid (TFA) - have two potential complications. Since the pH of the solution reaches 1-2 during treatment with strong acids, the stability of an adduct to heme

or protoporphyrin IX could be adversely affected. Low pH values are known to lead to ejection of the iron from the protoporphyrin IX ring, which underscores the instability of heme and protoporphyrin adducts under such conditions.(3,117) The other potential issue is that mineral acids and TFA are known ion suppressors that can dramatically reduce signal during mass spectrometric analysis.(264) While TFA is volatile, it is often difficult to remove completely from a sample by quickly drying or under a vacuum and so complete removal of either TFA or mineral acids would likely require further processing of the sample, further jeopardizing the nature of an adduct.

The older extraction methods require extensive sample handling. Most of the solvents used to extract heme, such as chloroform and butanone, are not compatible with reversed phase LC/MS chromatography.(265) The organic layer must be dried, which takes time and may require heating to remove the solvent adequately. These requirements for solvent removal may lead to the degradation of unstable adducts prior to analysis. Finally, the sample must be reconstituted in a compatible solvent for LC/MS analysis, but the reconstitution conditions may not be adequate for all types of heme adducts to be resolvated.

Chromatography for LC/MS analysis of heme B, protoporphyrin IX, and heme adducts is also another concern. Heme related compounds tend to be difficult to chromatograph under normal and reversed phase contributions due to the presence of propionic acid groups, the pyrroles of the porphyrin ring, and the ability of heme to make polymers including μ oxo dimers (Figure 3.3).(266) To alleviate these issues, past work in this area has generally been conducted using two general approaches. The first approach involves the use of derivatization methods, such as esterification, to prepare the heme-related species for chromatography.(3) The second approach uses reversed phase columns designed specifically for chromatography of large biomolecules so the intact protein can be injected onto the LC system.(4) Both of these methods

have potential complications even though they facilitate chromatography of heme-related compounds.

Derivatization methods including esterification can mask functional groups that cause poor chromatography. The potential for heme derivative species to be zwitterionic leads, at near neutral pH, to complications during chromatography due to the presence of propionic acid side chains and pyrroles that can function as bases.(266) Furthermore, when the iron is still present in the porphyrin, propionic acid groups can act as a ligand for the porphyrin ring leading to the μ oxo dimer. This polymerization can cause solubility issues as a result of difficulties with solvation of the polymers, and poor chromatography, such as peak broadening, due to the heterogenous nature of the heme polymers. Esterification of the propionic acid groups reduces the problems associated with acidic side chains and μ oxo dimers, but requires use of strong acids to drive the esterification that can lead to further degradation of isolated products. Studies using esterification typically involved large amounts of protein to obtain the target heme and protoporphyrin IX adducts, which is probably a function of multiple issues including the levels of sensitivity of the instrumentation at the time of the study and the stability of heme adducts being isolated.(52,104,105,107,108,117)

The second method involves the use of reverse phase filtration columns such as Poros R1 and R2 that can separate the heme or PPIX from the apoprotein during chromatography with the proper selection of mobile phase components, which is an important advantage of this type of chromatography.(256) However, these columns do not allow high flow rates and can require mobile phase components that are not compatible with LC/MS analysis. When inorganic salts such as NaCl or KCl are used during the LC separation, they must be removed before MS analysis through solid phase extraction or liquid-liquid extraction. Additionally, it is not clear that these columns can separate isomers of various adducts or multiple closely-related adducts due the large size of the particles in these columns that are needed to separate large biomolecules.

The focus of this chapter is the development and validation of extraction and LC/MS methods for the detection of heme adducts and quantification of intact heme. A major aim was to generate an extraction method for heme-related species from various CYP enzyme preparations that is gentler and faster to perform. Another important goal was to greatly reduce the amount of protein required for LC/MS analysis and hopefully detect (unstable) adducts not previously described. As part of the LC/MS method development, we wanted to be able to chromatograph heme-related species without the need for derivatization to further speed analysis of adducts with low stability. Finally, we wanted to improve the speed and efficiency of detecting heme adducts by employing mass defect filtering, which has been used in small molecule metabolite identification for more than 15 years.

Mass defect filtering is a powerful addition to the armamentarium of metabolite identification because it enables the rapid detection of expected and unexpected metabolites present in complex matrices when a mass spectrometer of sufficient resolution and mass accuracy is used.(5,7,267) The concept relies upon the strong tendency of the decimal value of the m/z for most metabolites to exhibit only modest differences when compared to the parent molecule. In fact, most phase I biotransformations result in changes less than 50 mDa, and even phase II biotransformations, such as glutathione conjugation exhibit changes up to only 68 mDa. With newer generations of mass spectrometer technology, instruments such as the AB Sciex 5600 and 6600 TripleTOF^{TM} can now perform data-dependent acquisition based upon one or more mass defect filters that can trigger subsequent scans for mass features of interest. We applied this technology together with our chromatography methods to improve the detection of heme adducts from CYP reactions.

We also validated the heme quantitation assay and the heme adduct detection methods. An intraday experiment was performed to assess the accuracy and precision of our quantitation method. The heme adduct detection method was validated using compounds known to generate

heme and protoporphyrin IX adducts, and the structures of these compounds are presented in Figure 3.4. We were able to achieve relatively high sensitivity and reproduce the results seen previously by others using a diverse set of adduct forming compounds.

3.2 Experimental

3.2.1 Materials.

All chemicals from commercial sources were of analytical grade or better where possible. Optima LC-MS grade acetonitrile, formic acid, and methanol, glacial acetic acid, ammonium hydroxide, 5-aminolevulinic acid (5-ALA), 1-ethynyl-1-cyclohexanol, hexanes, hydrochloric acid, sulfuric acid, isopropyl alcohol, isopropyl β-D-1-thiogalactopyranoside, peptone, trifluoroacetic acid, tryptone, and yeast extract were purchased from Thermo Fisher Scientific (Waltham, MA). All water was distilled, deionized using a house distilled water followed by a Barnstead NANOpure UV system (Thermo Fisher Scientific). Human and rabbit liver microsomes were obtained from Xenotech, LLC (Lenexa, Kansas). Aminobenzotriazole, ammonium formate, ammonium acetate, ammonium bicarbonate, ampicillin, bilirubin, biliverdin, butanone, 3,5-diethoxycarbonyl-1,4-dihydrocollidine, EDTA, glycerol, hemin, hemoglobin, imidazole, 1-octene, phenylacetylene, phenylhydrazine, potassium chloride, potassium phosphate monobasic, potassium phosphate dibasic, protoporphyrin IX, and sodium chloride were purchased from Sigma-Aldrich (St. Louis, MO). Cymal-5 was obtained from Anatrace (Maumee, OH). The internal standard, hemin-d_5, was purchased from Frontier Scientific (Logan, UT). NADPH was obtained from OYC Americas (Vista, CA). All other chemicals were from Sigma-Aldrich unless specified.

3.2.2 Expression and Purification of Recombinant CYP2E1.

The expression vector for CYP2E1 was a gift from Dr. Emily Scott (University of Michigan) and followed Dr. Emily Scott and followed the purification protocol described in Porubsky et al. with some modification.(255,268) We used C41(DE3) cells instead of TOPP3 and using a

previously described CYP3A4 expression protocol for expression.(269) A single isolated colony was used to inoculate LB-ampicillin media, which was cultivated with shaking at 37 °C overnight and then diluted 1:100 in Terrific Broth containing 0.4% glycerol, 1 mg/L of ampicillin, 1 mM thiamine, and trace elements (6.75 mg/mL $FeCl_3 \cdot 6\ H_2O$, 0.5 mg/mL $ZnCl_2 \cdot 4\ H_2O$, 0.5 mg/mL $CoCl_2 \cdot 6$ H2O, 0.5 mg/mL $Na_2MoO_4 \cdot 2\ H_2O$, 0.5 mg/mL CaCl · 2 H_2O, 0.25 mg/mL $CuCl_2$, 0.125 mg/mL H_3BO_3).(270) Cultures were incubated at 37º C until reaching an OD_{600} of 0.4. Cultures were induced by the addition of 0.238 g/mL IPTG and 500 µM 5-ALA, and the temperature was lowered to 27º C and allowed to incubate for 40 hours. Cells were pelleted and frozen at -80º C until further use.

Cells were resuspended with 100 mM potassium phosphate with 0.2 mg/mL lysozyme, 20% glycerol, 1 M NaCl, and protease inhibitor mixture from Promega, and stirred at 4° C for 1 hour. Cells were then manually disrupted with a Potter-Elvehjem homogenizer on ice. Cellular debris was removed by centrifugation at then 4.8 mM Cymal-5 was added. The supernatant was allowed to stir for 60 minutes at 4º C, and the solution was centrifuged at 80,000 g for 60 minutes. The supernatant was then added to a Nickel-NTA column via a peristaltic pump. The column was washed with a 100 mM potassium phosphate (pH 7.4), 4.8 mM Cymal-5, 300 mM NaCl solution and then with a 100 mM potassium phosphate (pH 7.4), 4.8 mM Cymal-5, 200 mM NaCl solution, 15 mM imidazole solution. CYP2E1 was eluted with 50 mM potassium phosphate (pH 7.4), 4.8 mM Cymal-5, 100 mM NaCl, 150 mM imidazole, 10 mM EDTA solution. The fractions containing CYP2E1 were diluted 5-fold with a 5 mM potassium phosphate (pH 7.4), 1 mM EDTA, and 4.8 mM Cymal-5, and loaded by gravity onto a CM Sephadex C-50 column. The column was washed with 5 mM potassium phosphate (pH 7.4)/1 mM EDTA, and then the protein was eluted with a 50 mM potassium phosphate (pH 7.4), 500 NaCl, and 1 mM EDTA solution. The eluted protein was then dialyzed with 120 mM potassium phosphate (pH 7.4) containing 500 mM sucrose and stored

in -80° C. Heme concentration was assessed by a pyridine hemochromogen assay, and P450 content was assessed using UV/Vis spectroscopy.(271,272)

3.2.3 Intraday Validation for Heme Quantification Assay

Standard curve and quality control samples were prepared by serial dilution of CYP2E1 in 0.1 M potassium phosphate, pH 7.4. A stock solution of 5 mM hemin-D_5 was prepared by the addition of 1% ammonium hydroxide to methanol and stored at -20° C. 5 mM hemin-D_5 was diluted in 1:1 acetonitrile/methanol to 500 nM to generate the internal standard/'crash' solution. Formic acid was added to final concentration of 1% was added to the internal standard solution prior to use. The internal standard solution was added in an equal volume to standard or quality control samples, and the samples were vortexed for 1 minute. Samples were then centrifuged in microcentrifuge for 2 minutes, and the supernatants were transferred to the injection plate for LC/MS analysis using the method described in Appendix 14.

3.2.4 Analysis of Porphyrin Adducts

Samples were prepared by incubating 1 mg/mL of either human or rabbit liver microsomes in 0.1 M potassium phosphate (pH 7.4) with 2 mg/mL NADPH for 60 minutes under low light conditions in the presence or absence of 100 µM test compound. The incubation was terminated by the addition of 1% formic acid in acetonitrile/methanol at 1:1 volume. Samples were vortexed for 1 minute and centrifuged for 2 minutes in a microcentrifuge. Supernatants were transferred to LC vials for analysis under the method in Appendix 15. The mass defect filter was adjusted by adding the elemental composition of the test compound to that of heme and to that of PPIX. The LC gradient for all validation compounds is as described in Appendix 15 which is: 0% B(0 - 1 min), 100% B(14-15 min), 0% B(15.1-20 min)

3.3 Results

3.3.1 Development of Extraction Conditions

We started with common heme/PPIX extraction methods, such as 10% TFA/butanone and HCl/acetone.(2,109) Hemoglobin and purified CYP preparations were used to assess the recovery from those hemoproteins by UV/Vis spectroscopy, LC/UV, and LC/MS. It was found that the recovery by these methods was similar to previously described reports, but difficulties were encountered when LC/MS analysis was attempted. When a known amount of hemin was processed through the extraction and reconstitution procedure with TFA/butanone, the loss of signal in LC/MS was >95% even though UV detection suggested better than 80% overall recovery. Similar effects were seen with the use of mineral acids such as HCl, which would not be ameliorated by evaporation. Therefore, we attempted combinations of organic solvents with more LC/MS-'friendly' acids such as formic acid and acetic acid.

Neither formic acid nor acetic acid with butanone provided a phase separation with the aqueous layer. Ethyl acetate and hexanes were substituted for butanone with formic acid, but extraction efficiency was poor by visual inspection when concentrations of hemin and hemoglobin were used that were visually observable. Therefore, we decided to attempt a simpler sample preparation.

Finally, we attempted to use protein precipitation to extract the heme from purified CYP2E1 and HLM. Since acid is a requirement for protonation of the cysteine thiolate and the propionic acid side chains of heme, we used 1% formic acid in our precipitation 'crash' solution. This changed the apparent pH of the solution to approximately 4 when added in a 1:1 ratio to 100 mM potassium phosphate in water that was originally at pH 7.4. Our testing of this combination of 1% formic acid in 1:1 acetonitrile/methanol as our 'crash' solution recovered approximately 75% of the heme by UV after mixing for 5 seconds, so we decided this was sufficient for moving ahead in the method development.

3.3.2 Development of HPLC Methodology for Heme Adduct Detection

As was mentioned previously, heme B and related species can be difficult to chromatograph so we set about testing various common mobile phases and column types to optimize the conditions for effective heme chromatography. The following aqueous mobile phases were used: 0.1% formic acid, 10 mM ammonium formate (pH ~ 4), 10 mM ammonium acetate (pH ~ 5), 10 mM ammonium bicarbonate (pH ~7), 0.1% ammonium hydroxide (pH ~ 10.5). Acetonitrile, methanol, and isopropyl alcohol were used as the base solvents for the organic portion of the mobile phase. When formic acid or ammonium hydroxide was used in the aqueous mobile phase, they were matched to the same percentage in the organic mobile phase, but the organic mobile phase was not modified for other combinations. Various reversed phase columns of 5 to 10 cm in length with a 2.1 mm bore size were used in efforts to optimally chromatograph a known amount of hemin, including Waters T3, Phenomenex HydroRP, and Agilent Zorbax XDB-C18.

The peak shape was poor with all columns under acidic conditions, but improved as the pH was increased. The chromatography was also improved by the use of methanol and best with the use of isopropyl alcohol. Most HPLC and UPLC columns are not stable when exposed to solutions with pH values over 9 for extended periods of time. Zorbax XDB-C8 and XDB-C18 columns are stable up to, but not beyond, that pH. When tested with 0.1% ammonium hydroxide in water and 0.1% ammonium hydroxide in isopropyl alcohol, these columns returned an adequate peak shape, but further analysis suggested that even higher pH values may be required to reduce analyte carryover when quantification is a goal. Since carryover is not really a concern in simply detecting adducts, and stronger base could even degrade any adducts, we proceeded with 0.1% ammonium hydroxide in water and 0.1% ammonium hydroxide in isopropyl alcohol. To allow for higher concentrations of ammonium hydroxide in the analysis a Waters XBridge C8 column was tested and showed better peak shape than the either Zorbax XDB-C18 or XDB-C8.

An example of a chromatogram for heme B extracted from a recombinant CYP2E1 sample is presented in Figure 3.5. The corresponding fragmentation is presented in Figure 3.6

3.3.3 Development of Quantitative Method for Heme B

To develop a quantitative assay for heme, an appropriate internal standard is required, and the carryover issue that was discovered during testing of the LC conditions must be reduced. A commercially available deuterated (D_4) version of heme B was purchased. However, the experimentally determined deuterium composition was not consistent with the label value provided by the manufacturer, but rather existed as a distribution of isotopomers. D_5 was the highest intensity peak (Figure 3.4), and so this isotope was used as the internal standard. Fragmentation of heme B and of the D_5 isotope of the heme B internal standard are shown in Figure 3.7.

Initial testing suggested that carryover of heme B from injection to injection was approximately 5%, and so this had to be reduced for a desired analytical range of 10-1000 nM. We increased the concentration of ammonium hydroxide to 2% and increased the concentration of base in the needle wash to 10% ammonium hydroxide. Carryover was reduced to approximately 0.5%, which was sufficiently minimal for the range of the assay.

An intraday validation using recombinant CYP2E1 as the standard was performed. While it appeared that the integrating parent mass ranges from the TOF scan could also be validated, we only validated the product ion based assay based upon the transition from 616.2 to 557.1634 and 621.2 to 562.1948. A range from 10-1000 nM was validated, and the data is presented in Figure 3.5. The curve fit was not linear and was fit to a Hill (exponential?) model. Carryover during the validation was estimated to be 0.4%.

3.3.4 Development and Validation of a Mass Defect Filter Driven Method for Heme and Protoporphyrin Adducts

The ABI Sciex TripleTOF™ series of Q-TOF mass spectrometers allow for data-dependent acquisition of product ion spectra based upon defined mass ranges and multiple mass defects. All data can also be filtered after acquisition. To attempt to utilize the defect filter during data-dependent acquisition for the detection of heme and protoporphyrin adducts, we added the chemical composition of heme B or protoporphyrin IX to that of the compound of interest to determine the appropriate target mass defect. This set the mass defect range to an 80 mDa window with a mass range of 400 m/z . We tested the method with several known adduct forming compounds including 1-aminobenzotriazole, diethyl 1,4-dihydro-2,4,6-trimethyl-3,5-pyridinedicarboxylate (DDC), 1-ethynyl-1-cyclohexanol, 1-octene, phenylacetylene, and phenylhydrazine.(49,88,107,108,111-113,117,118,263,273-276)

1-Aminobenzotriazole (ABT) is a known alkylator of heme for various CYP isoforms. Alkylation of CYP by a benzyne species generated during the CYP-dependent metabolism of ABT was first described by Ortiz de Montellano and Mathews.(111) In HLM incubations, we observed a series of isomers of 637.2808 m/z, which are likely to be N-N bridged porphyrin adducts, and we also observed benzyne adducts still containing the iron in the porphyrin with a m/z of 692.2083. The chromatogram for ABT adducts and interpretation of the fragmentation of the found adducts are presented in Figure 3.9.

DDC is a known methylator of heme *via* a methyl radical transfer.(107,114) In Figure 3.10, the chromatogram of the N-methylated protoporphyrin IX yielded a parent mass of 577.2808 m/z, and the fragmentation and interpretation are presented. We could clearly identify only a single peak with the standardized gradient that we used for this method validation. However, that peak appeared to have minor peak splitting which suggests that there may be a second species of the same m/z that was not resolved by the chromatography.

1-Ethynyl-1-cyclohexanol is a known heme alkylator that likely alkylates through the epoxidation of the terminal alkyne.(112) We resolved two peaks at 2.90 min and 3.11 min of m/z of 703.3478. The extracted ion current chromatogram, associated product ion spectra, and interpretation of the product ion spectra for 1-ethynyl-1-cyclohexanol related adducts in HLM incubations are presented in Figure 3.11.

1-Octene is one example of terminal alkenes that are known to alkylate heme after metabolic activation by CYP enzymes.(108,117) We found a single peak at m/z 691.3846 that is likely the adduct at the terminal (ω) carbon with an alcohol generated from the ring-opened epxide at the ω-1 position. The extracted ion chromatogram, product ion spectrum, and interpretation of the product ion spectrum of the N-alkylated protoporphyrin IX species are presented in Figure 3.12.

Phenylacetylene is one of a number of terminal alkyne containing compounds shown to form heme adducts when metabolized by CYP enzymes.(49,112,117) Bioactivation of the terminal alkyne can result in a N-alkylated porphyrin adduct, and several related compounds have been characterized by field desorption mass spectrometry.(49,117) The predicted m/z for phenylacetylene adducts, 734.2186 for heme B and 681.3107 for protoporphyrin IX, were found, and the data are presented in Figure 3.13.

Phenylhydrazine and phenyldiazene, the latter an oxidation product of phenylhydrazine, are known to be bioactivated by hemoglobin and CYP enzymes to form various types of heme adducts.(88,263,275-277) The adducts are thought to be formed following the generation of a phenyl radical that is the result of oxidation of phenylhydrazine. We found two types of adducts in HLM incubations. One species is a phenyl modified heme B adduct of 693.2216 m/z, and the second species is a phenyl modified verdoheme with m/z 696.2068.(231,239,278-280) The extracted ion current, fragmentation, and interpretations of the fragmentation are presented in Figure 3.14.

3.3.5 Detection of Heme Degradation to Biliverdin and Bilirubin Isomers

While there is substantial literature surrounding the catabolism of heme B by the heme oxygenase family of enzymes that results mostly in biliverdin IXα, only a small amount of biliverdin IXα and numerous other smaller degradation products, such propentdyopents, were found previously in liver microsomal incubations.(231,239,262,278-282) Our analytical methods allowed us to acquire data related to heme degradation in incubations with HLM as the enzyme source.

In Figure 3.15, a commercial preparation of biliverdin is compared to the biliverdin species found in HLM incubations along with the fragmentation for the commercial biliverdin peak and each of the four biliverdin peaks in the HLM incubations. The four biliverdin peaks in the HLM incubations suggest that all four meso bridges can be broken and each of them has distinct fragmentation patterns. Due to the symmetry of heme B structure, the most direct way to determine the structure of each of the biliverdin isomers is to consider the relationship of the amide functional groups formed during the breaking of the meso bridge to the propionic acid groups. The interpretation of biliverdin fragmentation is presented in Figure 3.16.

We were also able to detect at least two isomers of bilirubin at 2.09 minutes and 2.62 minutes from the HLM incubation, and the chromatogram and fragmentation are presented in Figure 3.17. The peak at 2.09 minutes has more fragments ca. 300 m/z than the peak at 2.62, but none appear to directly confirm the identity of either species. Both contain fragments of 299.1390 m/z which are consistent with one amide being on the same side as the propionic acid side chain. Therefore, we suggest that the two species are likely bilirubin IXα and bilirubin IXγ. There are differences between the two species in terms of fragmentation, but none of the fragments can be used to definitively assign which peaks are bilirubin IXα and bilirubin IXγ.

3.4 Discussion

3.4.1 Chapter Overview and Hypothesis.

Our data for CMZ metabolism indicated that both heme and protein are possible targets of reactive metabolites generated by CYP2B6, 2E1, and 3A4 that could result in inactivation of the enzyme. Therefore, we need a set of assays to detect potential heme adducts and protein adducts. LC/MS analysis of proteins either by whole protein analysis or peptide analysis has become more robust and common practice, but there have been very few improvements in regards to analysis of heme. Our goals for this portion of work were to develop a set of robust and broadly applicable LC/MS assays to quantify heme B and to identify heme and protoporphyrin adducts using modern high resolution mass spectrometry techniques such as mass defect filtering. Additionally, we sought to greatly simplify sample preparation of the heme containing samples to preserve fragile heme adducts and to avoid using chromatography techniques that were slow and/or poorly compatible with LC/MS analysis.

Mass defect filtering in drug metabolism applies the parent molecular composition as a reference point for selection of an appropriate mass range and mass defect for potential metabolites.(5-7) Our adaptation of this technique involves using the elemental composition and isototopic distribution of heme B or protoporphyrin IX in addition to that of the potential adduct forming compound since the adduct should be related in m/z and mass defect to the combination of both species. Typically, mass defect filtering is performed as a post-acquisition analysis technique, but the AB Sciex 5600 TripleTOF^{TM} takes this concept even further by allowing the use of the mass defect filter to trigger data-dependent scans. Product ion scans triggered from the mass defect allow us to confirm the identity of the heme or protoporphyrin adduct. We validated this detection system with a diverse set of compounds that are known to generate a plethora of heme and/or protoporphyrin IX adducts.

3.4.2 Development of the Extraction Method and Chromatography for Heme B.

We developed a simplified extraction method for heme B and a common reverse phase chromatography platform for heme B and related compounds. As mentioned previously, we used an acidified protein precipitation for the extraction method. Our reverse phase chromatography system required ammonium hydroxide, isopropyl alcohol, and HPLC columns stable under basic conditions. The combination of these two components lead to the successful development of the heme B quantification and adduct detection methods.

We encountered two primary issues during the development of the extraction method. Older methods employed TFA or mineral acids to break the ionic interactions of the heme propionates with the protein, and but these acids are known to be ion suppressors in mass spectrometry. (2,109,257,258) When we tested TFA/butanone and HCl/chloroform extraction solvent systems with samples dried under nitrogen, we observed over 90% suppression of signal as compared to similar unextracted hemin even though the extraction methods appeared to be efficient by UV or visual inspection. We also encountered extraction efficiency problems with other solvent systems. It appears that heme and protoporphyrin IX have fairly limited solubility in various organic solvents such as ethyl acetate and hexanes, and acid or strong base is required to extract the heme from protein. There were also concerns about the reconstitution solution during these tests, and it was found that alcohols appeared to be the best choice for organic solvents in terms of solvating heme and PPIX.(257,258) These issues suggested that liquid-liquid method development may not be the most viable path for our intended process.

It should be noted that we did not try the preparation commonly used by the Ortiz de Montellano lab which uses 5% H_2SO_4/methanol as the extraction solvent for 18 hours followed by several steps including TLC and HPLC to purify the extracted porphyrins.(3) This method results in demetallated methyl esterified porphyrin adducts and requires over a day of sample preparation. We wanted a relatively short extraction procedure that would minimize the amount

of material needed and limit long term exposure of porphyrin adducts since it would limit the detection of unknown adducts to those that are acid stable.

After experiencing issues with liquid-liquid extraction, we decided to try a protein precipitation, and our choice of components in the protein precipitation solution contributed to the success of the extraction method. The use of 1% formic acid enabled relatively gentle extraction of the heme from CYP enzymes that do not have covalent linkages to their heme by lowering the sample pH of 0.1 M potassium phosphate containing incubations from 7.4 to approximately 4.0. This pH is higher than what would be expected from 5% sulfuric acid or any of the trifluoroacetic extraction (1%+) containing extractions so it would be expected that the formic acid extraction should be more gentle to acid labile species. The major concern would be reduced efficiency of extraction due to the pH being insufficient to protonate the proprionate groups. However, using a pH of 4.0 should protonate the majority of the propionate groups because the pK_a of propionic acid is reported to be 4.87. Acetonitrile serves to denature the protein, and methanol is a good solvent for heme B. While this method could possibly be improved with other solvents such as isopropyl alcohol, we did not pursue other options after confirmation that the extraction efficiency was above 70%.

The use of base and isopropyl alcohol were critical to the development of our chromatography platform.(257,258) Heme can form different complexes and oligomeric states that can cause issues with chromatography and mass spectrometric detection. μ Oxo dimers require the deprotonation of the propionic acid groups to propionate in order to make an ionic interaction with another heme molecule. There is also a possibility of hydrophobic interactions or so-called π stacking of heme molecules in water that could also limit solubility in an aqueous environment. The increase in concentration of hydroxide likely serves to outcompete the propionate as a ligand for the iron, and prevents stacking of the heme by providing bulk and a polar interaction that would oppose hydrophobic interactions. Isopropyl alcohol was also

necessary for the chromatography of heme since peak shape was significantly better than with acetonitrile and methanol. Isopropanol is a protic solvent but also is more lipophilic than methanol. This combination of characteristics likely allows the best combination of solvent properties to interact with the polar and nonpolar functionalities of heme. While better organic solvents may exist for heme, isopropanol is likely the best and only option for reversed phase chromatography of non-derivatized heme.

The choice of column is also important in the chromatography system to a certain extent. Most reverse phase columns that are used for LC/MS applications are more resistant to acidic conditions than basic conditions so the number of column options for using base in the mobile phase is limited. The first two columns we tried with the base-containing mobile phases were Agilent Zorbax XDB-C18 and C8 columns. These columns are stable at mildly basic conditions and gave reasonable peak shape, but they are an older column technology. There was not much of a difference in retention, peak shape, or carryover with either C_{18} or C_8. We switched to a Water XBridge C8 column that allows pH ranges up to 12 and is a newer technology. The peak shape was improved with the newer column, which can also tolerate increases in ammonium hydroxide that will be required to minimize the amount of carryover in the quantification assay.

3.4.3 Development and Validation of Heme Quantification Method.

Many previous heme quantification methods are based upon the UV/Vis absorbance of heme, and often required derivatization or harsh conditions.(9,10,260,271) While mammalian systems contain mostly heme B, HLM contains mitochondrial contamination which introduces heme A from cytochrome C oxidase, and heme C from cytochrome C.(231,232) All three heme molecules have similar absorbance profiles so a UV/Vis assay cannot effectively distinguish these heme species from one another. LC/MS can readily distinguish them and other heme species from one another. The harsh conditions in many other assays could also remove any potential adducts from the heme B moiety that serve as a false negative for heme loss. By using LC/MS

with our extraction and chromatography system, we were able to develop and validate a heme B quantification method.

While we were able to obtain reasonable peak shape with 0.1% ammonium hydroxide in water and 0.1% ammonium hydroxide in isopropanol for mobile phases with the XBridge C_8 column, we had to resolve other issues in regards to developing a viable LC/MS quantification method using our base chromatography system. Carryover was an issue since the use of 0.1% ammonium hydroxide appeared to result in approximately 5% carryover. An appropriate internal standard is required for any LC/MS assay and must be selected to achieve acceptable assay performance. We also needed to sharpen the gradient so the run time could be shortened to a time that can achieve sufficient throughput.

To alleviate the carryover issue, we modified the needle wash conditions and modified ammonium hydroxide concentrations in the mobile phases. During our testing, increased ammonium hydroxide concentrations in the needle wash solutions and mobile phases reduced carryover. This pattern is consistent with heme B being more soluble at higher pH. We increased the concentrations to 10% ammonium hydroxide in the needle wash and to 2% in the mobile phases which are near the limit for column and LC system. With that increase, we were able to substantially reduce carryover, but could not completely eliminate the issue. We did not have access to a bio inert LC system so we did not evaluate whether using such a system would further reduce carryover.

Stable labeled internal standards are the preferred internal standard for most LC/MS assays, and we were able to acquire such a standard from Frontier Scientific. The manufacturer claimed that the compound was a contained a uniform isotope pattern, but we found it to be a distribution of mostly 3 isotope labelling levels with D_5 being the most abundant. We chose D_5 heme B for the compound to be monitored as the IS, and determined the appropriate daughter ion for both labeled and unlabeled heme B.

While our system could detect heme B concentrations below 10 nM, we validated a range of 10-1000 nM as shown in Figure 3.5. To limit carryover, we injected only 1 µL of sample so there is potential sensitivity for far lower concentrations of heme B. However, our analytical range was limited by carryover, and we determined 10 nM was the lowest concentration we could measure reliably. Even with this limitation, our sensitivity was still better than we experienced with UV/Vis detection (50 nM). Reduction of carryover through the use of bio inert materials or other methods might further improve the assay and result in even lower limits of quantification.

3.4.4 Development and Validation of Heme Adduct Detection Method.

We sought to implement mass defect filtering with the simplified extraction and heme chromatography platform to develop a robust and flexible method for detecting a variety of heme and protoporphyrin adducts. The AB Sciex 5600 TripleTOF^{TM} allows data dependent acquisition of product ion scans based upon multiple mass defect filters so we used two filters for each compound. The first filter for each compound consists of the composition of heme B added to the composition of the target compound with an allowed defect of 80 mDa and an allowed mass range of ± 200 m/z relative to the combined mass of heme and the target compound. The second filter was set similarly except substituting protoporphyrin IX for heme B. We also allowed for product ion scan acquisition of the species with the highest mass spectrometer response. We employed a 15 minute gradient that provided adequate separation of heme and protoporphyrin species under most circumstances. To test the robustness and applicability of the method, we used different six compounds known to form differet types of heme.

As shown in Figure 3.9, we detected multiple heme adducts from HLM-catalyzed turnover of 1-aminobenzotriazole (ABT). In the original paper on ABT adducts, Ortiz de Montellano et al identified modified N-N bridged porphyrins with a m/z of 665 after isolation from liver tissue and esterification with methanol.(111) We detected at least two adducts of 637.2808 m/z that would correspond to the 665 m/z adducts where the mass difference is a consequence of the lack of

esterification of both proprionate groups using our method. We also detected at least one adduct still containing iron in the porphyrin ring, which was not reported in the original paper. The fragmentation of the demetalated adducts only appears to involve the proprionate side chains, but the product ion spectra of the iron containing adduct consists of several other fragments. One cleavage releases the benzyne adduct to regenerate the mass of heme B, which suggests that the adduct is likely interacting with the iron, but we are unsure of the actual nature of bonding of the benzyne to heme in the rest of the structure. We have assigned the loss of a methyl substituent from the adduct to the vinyl groups since it is likely that the disruption of the heme B π system could cause isomerization of vinyl groups that would allow the terminal carbon to be cleaved. Overall, these data are consistent with previous ABT results.

We incubated DDC with HLM, and the data presented in Figure 3.10 is consistent with previous reports.(107,114,115,245) The parent mass for the dimethyl ester of the N-methylated protoporphyrin IX species under electron impact (EI) conditions was 604 m/z. Under our positive mode electrospray (ESI) method N-methylated protoporphyrin IX yielded a parent mass of 577.2808 m/z. These masses are consistent with the differences in ionization and sample preparation since dimethyl esterification would add 28 Da, but ESI would cause protonation during ionization. Our method only clearly detected a single adduct, although the peak is slightly split. The split peak suggests that there could be at least one other adduct contained in the 577.2808 m/z peak which would be consistent with the multiple adducts reported previously. The fragmentation was not informative about the structure beyond confirming that the methyl group was likely attached to a pyrrole nitrogen since the 562.2672 m/z fragment corresponds exactly to the loss of a methyl group.

Our data with incubations of HLM and ethynyl-1-cyclohexanol in Figure 3.11 are consistent with the adducts reported by Kunze et al.(112) These workers reported two adducts with 730 m/z after methyl esterification. We found two adducts of 703.3478 m/z corresponding to

protoporphyrin IX adducts resulting from the bioactivation of the acetylene functional group. The mass difference is a result of the same differences in methods and detection as seen with DDC. The fragmentation yielded 563.2582 m/z, which is consistent with the loss of alkylating species from PPIX.

We also replicated the formation of adducts of 1-octene reported by Kunze et al., as shown in Figure 3.12.(105) They reported an adduct of 719 m/z after methyl esterification using field desorption ionization. In HLM incubations, we found a single adduct of 691.3898 m/z and acquired product ion spectra consistent with a N-alkylated PPIX adduct since a fragment consistent with PPIX itself was produced. Again, our detected adduct m/z differs from previous reports only by the lack of methyl esterification. We assigned the position of the 1-octene adduct by using the reported NMR data from the original publication.

Data from our incubations of rabbit liver microsomes and phenylacetylene incubations are consistent with the predicted adducts described by Kunze et al.(49,112,117) Covalent modification of heme by terminal acetylene containing compounds is thought to occur through an oxidation of the alkyne that results in a radical on the terminal carbon of the triple bonded carbon pair and a positive charge on the other carbon of the triple bond. The oxygen attached to heme iron attacks the positively charged carbon while the carbon radical forms a bond with one of the pyrrole nitrogens. Finally, the oxygen forms a double bond with the carbon while leaving the heme iron, and the resulting adduct is only attached to the porphyrin at a pyrrole nitrogen. It was mentioned in another manuscript from the Ortiz de Montellano lab that the metal free N-alkylated porphyrin adduct of phenylacetylene was very unstable and could not be characterized, while the addition of zinc allowed determination of the UV/Vis spectra. As shown in Figure 3.13, we acquired peaks with m/z consistent with those of other terminal acetylenes that were characterized by mass spectrometry. Taking into account the mass differences due to sample preparation, these are 734.2175 for the heme B species and 681.3071 for the protoporphyrin IX

species. While the peak shape of the iron containing adduct was superior to that of the protoporphyrin IX adduct, we obtained fragmentation only for the protoporphyrin IX adduct. The lack of fragmentation is likely a result of the small peak size of the heme adduct and the overlap in retention time between heme B and the heme adduct. The small peak size of all of the detected species may be a consequence of the relative instability of adducted species. We were likely only able to see these adducts due to the relatively gentle and rapid nature of our sample preparation and to the significant advances in mass spectrometer technology. We assigned the position of the adduct based upon Kunze et al for all the other acetylenic substrates.

Phenylhydrazine was the final compound tested with HLM to validate our system.(88,263,275,277,283) Even though phenylhydrazine has been used in attempts to model the active site space near the heme in CYP enzymes using NMR, we could not find literature with expected m/z values for adducts of phenylhydrazine with heme B in CYP enzymes. However, we did find phenylhydrazine/protoporphyrin IX adduct mass spectrometric data with hemoglobin and myoglobin, and those data suggest phenyl bridged meso adducts with biliverdin Ixα and N-phenylprotoporphyrin IX adducts. As shown in Figure 3.14, the peaks from our data have m/z values that are consistent with the formation of a phenyl adduct with heme B (693.2216 m/z) and verdoheme IX (696.2068 m/z). The extracted ion current for verdoheme suggests at least two species due to the appearance of incompletely separated peaks. There is only one phenyl heme adduct so it is not clear if that single peak contains multiple adducts that were not separated with our chromatography conditions. The fragmentation of all of the detected adducts regenerates heme B (616.1820) or verdoheme (619.1653 m/z) so it is likely that phenyl adduct is associated with the iron, but that iron-adduct interaction is not certain. Overall, our data are at least consistent with the proposed bioactivation mechanism of phenylhydrazine, but our incubations were done in HLM so the results are more difficult to correlate with individual purified enzymes.

It is interesting to note that the verdoheme adduct occurred at all. Even though we have identified biliverdin and bilirubin being generated in our incubations, we did not detect the presence of verdoheme in any other incubations. The presence of verdoheme suggests that it is capable of still being catalytically active with regards to bioactivation of phenylhydrazine, but verdoheme is also inactivated by a similar process to heme.

3.4.5 Detection of Heme Degradation in HLM Incubations.

Our method was able to detect biliverdin and bilirubin isomers that are the result of NADPH-dependent degradation of heme.(239,241,262,278-282) By using a TOF survey scan and data dependent product ion scans with our chromatography system, we were able to acquire the exact mass and fragmentation information for those degradation products of heme, and assign structural features to the isomers that were detected. The extracted ion current data, product ion scan data, and proposed fragmentation for these degradation products are presented in Figures 3.15 and 3.16. The lack of available standards for biliverdin IXβ and biliverdin IXΔ and lack of definitive fragmentation did not allow us to assign those peaks, but we were able to assign biliverdin IXα and biliverdin IXλ. Similarly, we could not completely assign the isomers of bilirubin due to the lack of standards.

In order to assign the structure of the positional isomers of biliverdin, a line of symmetry can be drawn between the two propionic acid groups attached to the C and D rings, and, as a result, each biliverdin isomer will have 0, 1, or 2 amides on each side of the line of symmetry. For biliverdin IXα and biliverdin IXγ, one amide will exist on each side of the line of symmetry, but biliverdin IXβ and biliverdin IXΔ will have two amides on one side, but none on the other. The fragment that corresponds to having one amide on one side of the line of symmetry is 297.1234 m/z, and that fragment is found in the product ion spectra of the 2.24 and 2.85 minute peaks. To determine which peak of 2.24 min and 2.85 min is biliverdin IXα, a fragment containing the C and D rings with no amides would be necessary, and the expected fragments 330.1574 and 344.1731

m/z are present in the 2.24 minute peak product ion spectra. The 2.24 minute peak being biliverdin IXα is consistent with expectations since the commercial preparation of biliverdin should mostly be biliverdin IXα. One major peak was evident from commercial biliverdin at 2.24 minutes with a minor peak at 2.55 minutes that overlap with two of the peaks. The fragmentation of the major peak from commercial biliverdin and the 2.24 minute peak from HLM matched well suggesting they are the same species. There are subtle differences between the fragmentation of the 2.45 min and 2.56 min peaks, but there is no fragment that can differentiate the two species without a synthetic standard since they are nearly mirror images of each other. To confirm that the 2.44 and 2.55 min peaks are biliverdin IXβ and biliverdin IXΔ, there is a fragment of 343.1288 m/z that corresponds to one amide being on either the C or D ring. Therefore, we have generally assigned all 4 isomers of biliverdin, but we were only able to specifically assign biliverdin IXα and biliverdin IXλ.

We also were able to detect the formation of bilirubin IXα and bilirubin IXγ, but could not identify which peak corresponds to which isomer. The extracted ion current, product ion spectra, and proposed structures with fragmentation are presented in Figure 3.17. Both spectra are highly suggestive of the α or λ meso bridge not being present since the pairing of 299.1392 and 285.1223 fragments indicate that one of the amides and one of the propionates is present on each side of the break of the remaining α or λ meso bridge. It is likely that the first peak is bilirubin IXα since biliverdin IXα eluted at a similar retention time. Also, the larger diversity in fragmentation of the 2.09 minute peak is more consistent with the destruction of the distal meso bridge relative to the propionic acid groups. The assignment of bilirubin IXα could be confirmed with a commercial bilirubin standard, but there are no available commercial standards for the other 3 isomers of bilirubin.

The detection, separation, and classification of these heme degradation products demonstrate the utility of this method and of these technologies in revisiting questions in heme

biochemistry that could not be answered completely due to the limited technology available at the time they were first investigated. For example, heme oxygenase is known to generate mostly biliverdin IXα which is the largest biliverdin IX peak we identified, but we see a total of 4 biliverdin isomers at fairly similar levels, which likely correspond to each of the possible biliverdin IX isomers. Those other isomers are likely the product of uncoupled CYP reactions that lead to degradation of the heme, but analysis of the heme degradation products from purified enzymes that normally exist in HLM is required to support this conjecture.

3.5 Conclusions

In this chapter, we have described the successful development of sensitive assays for quantifying heme and for identifying heme adducts and the products of heme destruction. Due to the implementation of modern LC/MS technology and a simplified extraction method that avoids reagents that are detrimental to LC/MS analysis, we were able to achieve much higher levels of sensitivity than had been possible previously, and enable rapid identification of possible heme adducts and heme degradation products. As a result, we were able to use very limited amounts of complex enzyme preparations (100 µg liver microsomes/incubation) and still detect heme and protoporphyrin IX adducts and heme degradation products. While it is unclear whether our simplified extraction methodology would still function with non-CYP enzymes or CYP enzymes with covalent linkages to their heme, these assays should be applicable to the majority of CYP enzymes, including the primary drug metabolizing isoforms.

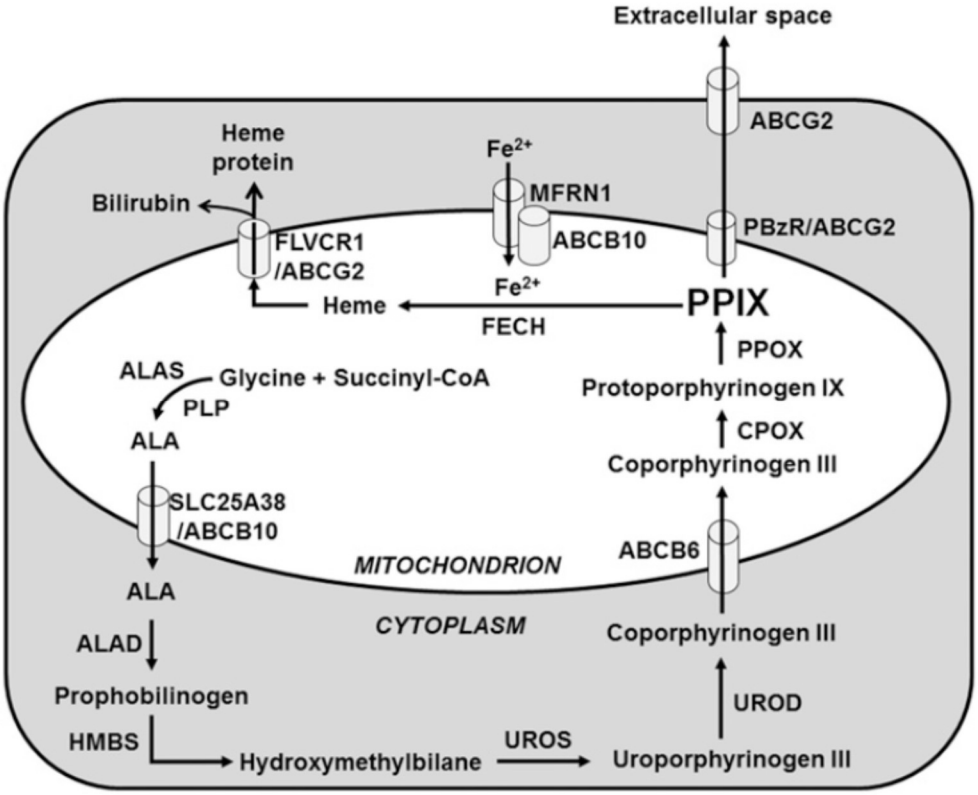

Figure 3.1 Biosynthesis and Disposition of Protoporphyrin IX (PPIX) and Heme in Mammalian Cells

This figure is adapted from Sachar et al.(238) CPOX, coproporphyrinogen oxidase; FLVCR1, feline leukemia virus subgroup c receptor 1; HMBS, hydroxymethylbilane synthase; PLP, pyridoxal phosphate; SLC25A38, solute carrier family 25 member 38; UROD, uroporphyrinogen decarboxylase; UROS, uroporphyrinogen III synthase.

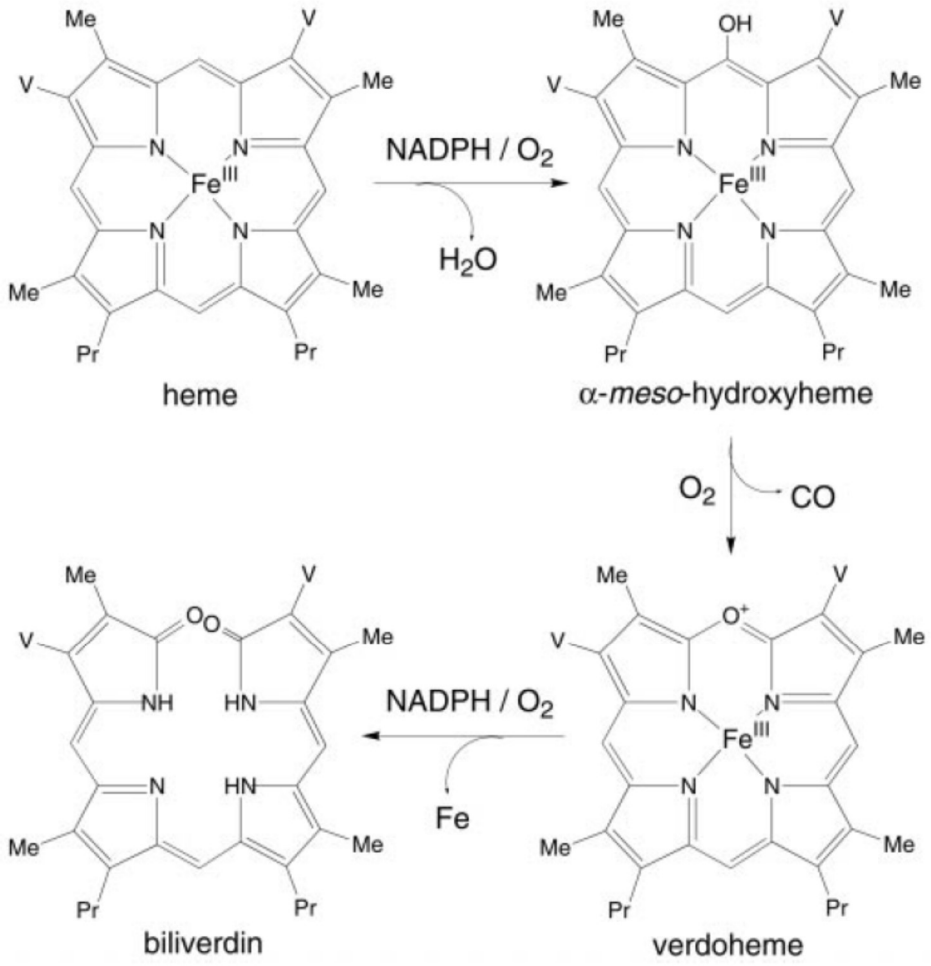

Figure 3.2 Mechanism and Intermediates of Heme Oxygenase I
This figure is adapted from Liu et al.(241). Pr are propionate groups, and V are vinyl groups.

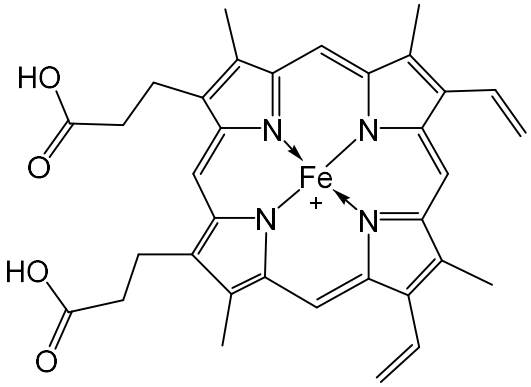

Heme B
Chemical Formula: $C_{34}H_{32}FeN_4O_4^+$
Exact Mass: 616.1767

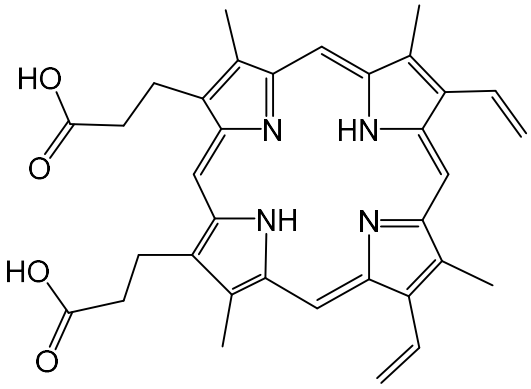

Protoporphyrin IX
Chemical Formula: $C_{34}H_{34}N_4O_4$
Exact Mass: 562.2580

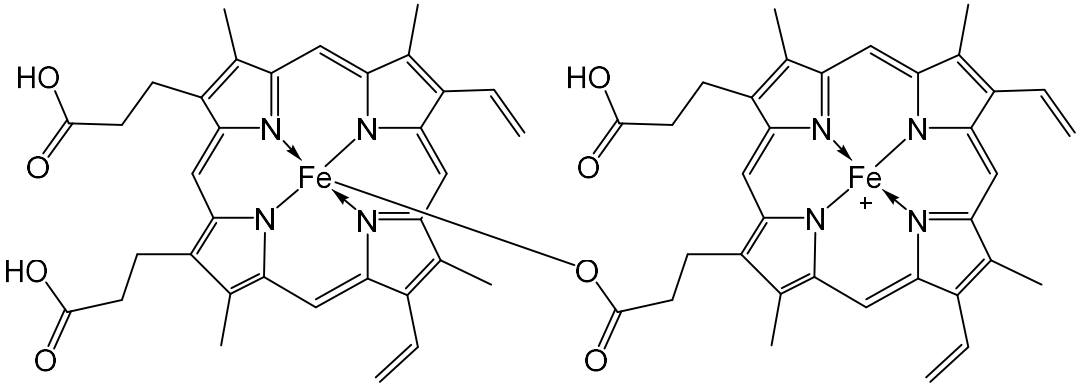

μ Oxo Dimer
Chemical Formula: $C_{68}H_{63}Fe_2N_8O_8^+$
Exact Mass: 1231.3462

Figure 3.3 Structures of Heme B, Protoporphyrin IX, and the μ Oxo Dimer of Heme B

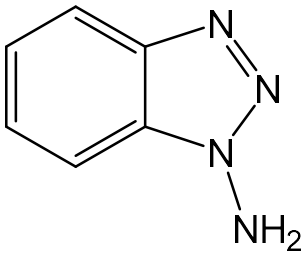

1-Aminobenzotriazole
Chemical Formula: $C_6H_6N_4$
Exact Mass: 134.0592

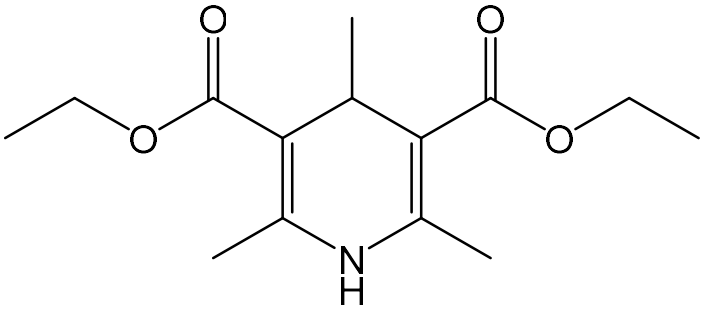

DDC
Chemical Formula: $C_{14}H_{21}NO_4$
Exact Mass: 267.1471

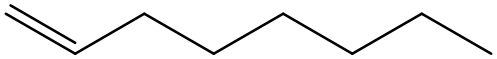

1-Octene
Chemical Formula: C_8H_{16}
Exact Mass: 112.1252

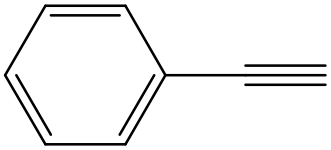

Phenylacetylene
Chemical Formula: C_8H_6
Exact Mass: 102.0470

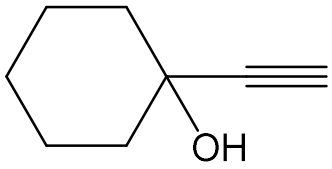

1-Ethynyl-1-Cyclohexanol
Chemical Formula: $C_8H_{12}O$
Exact Mass: 124.0888

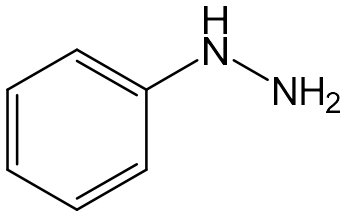

Phenylhydrazine
Chemical Formula: $C_6H_8N_2$
Exact Mass: 108.0687

Figure 3.4 Heme Adduct Detection Method Validation Set

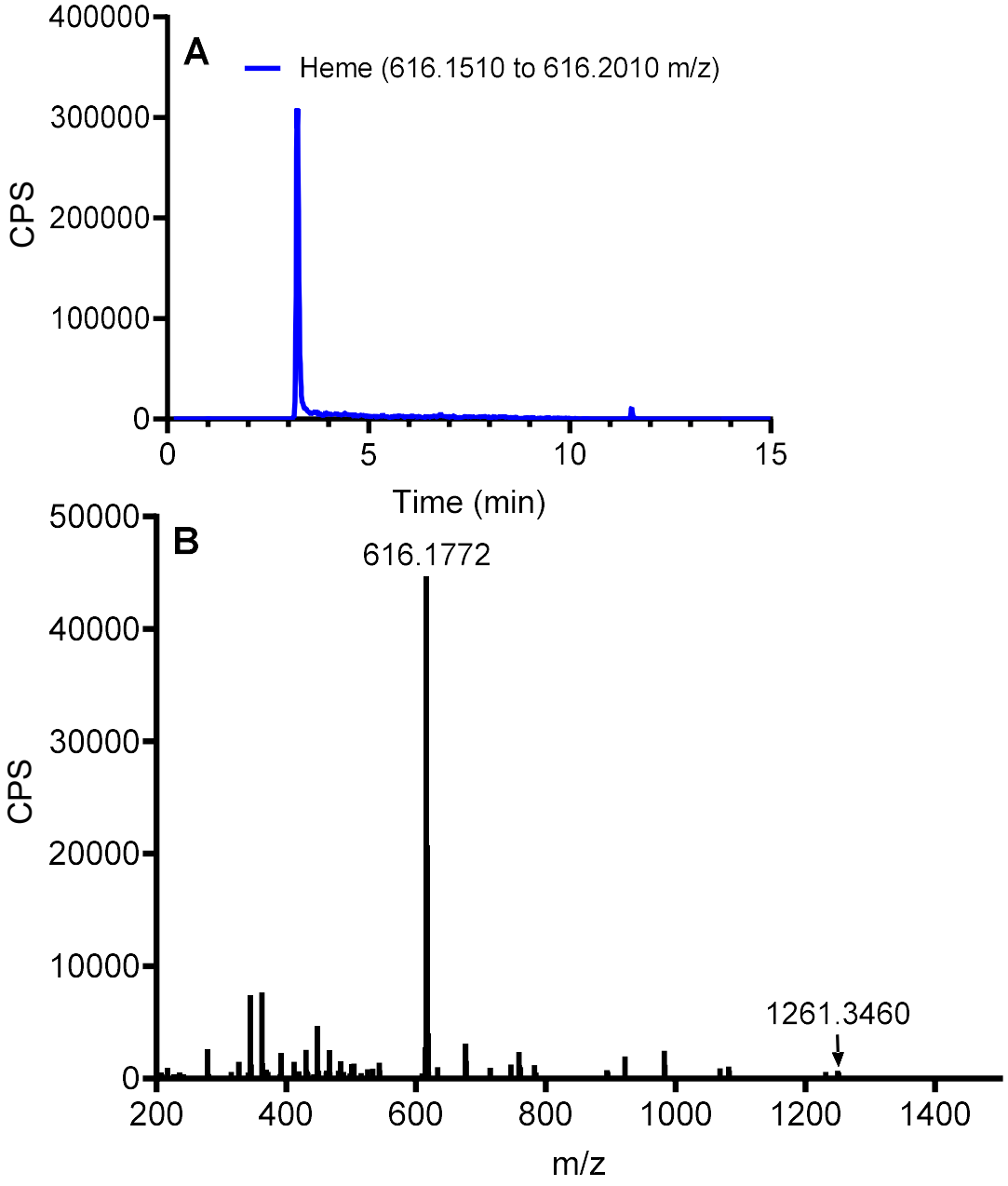

Found Mass	Formula	Predicted Mass	mDa Error
616.1772	$C_{34}H_{32}FeN_4O_4^+$	616.1767	0.5
1231.3460	$C_{68}H_{63}Fe_2N_8O_8^+$	1231.3462	-0.2

Figure 3.5 Extracted Ion Chromatogram (A) and Spectrum (B) of Heme B Extracted from Purified Recombinant CYP2E1
Panel B shows the spectrum that presumably contains a heme dimer which is possibly the μ oxo dimer.

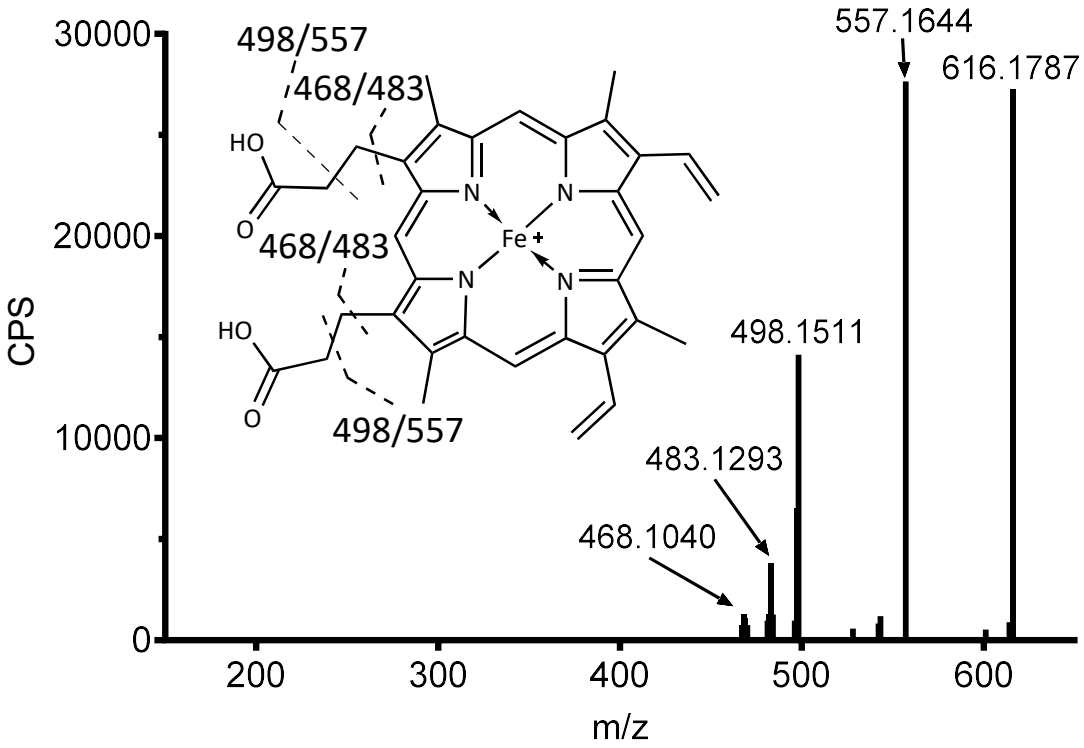

Found Mass	Formula	Predicted Mass	mDa Error
468.1040	$C_{28}H_{20}FeN_4^+$	468.1032	0.8
483.1293	$C_{29}H_{23}FeN_4^+$	483.1267	2.6
498.1511	$C_{30}H_{26}FeN_4^+$	498.1501	1.0
557.1644	$C_{32}H_{29}FeN_4O_2^+$	557.1634	1.0
616.1787	$C_{34}H_{32}FeN_4O_4^+$	616.1767	2.0

Figure 3.6 Product Ion Spectrum of Heme B Extracted from Purified Recombinant CYP2E1

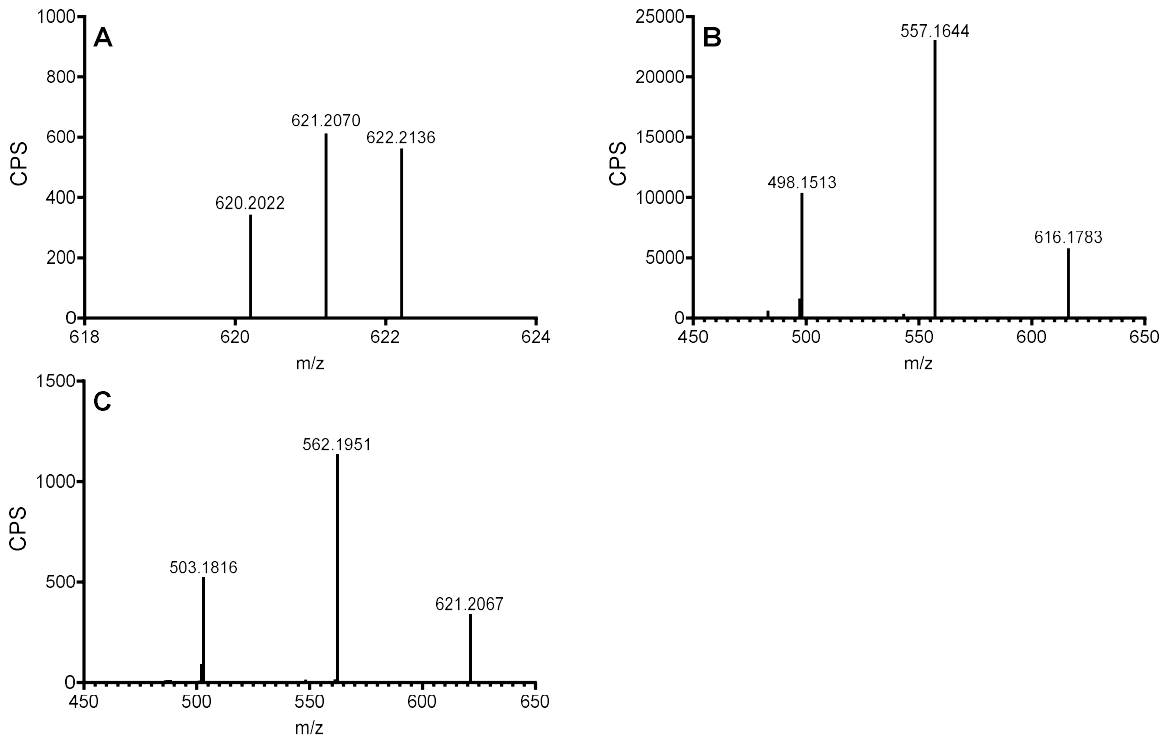

Figure 3.7 Spectra of Commercial Heme B-D_4 (A), Product Ion Spectrum of Heme B (B) and Product Ion Spectrum of Commercial Heme B-D_4

A Standard Accuracy

Nominal (nM)	Found (nM)	% Accuracy
10	10.20	102.04
25	24.78	99.12
50	44.06	88.13
100	113.30	113.27
250	242.60	97.03
500	478.90	95.78
1000	1060.00	106

B Quality Control Accuracy

Nominal (nM)	Found (nM)					% Accuracy
10	12.1	10.7	8.5	8.5	9.5	98.6
25	26.9	24.3	27.3	26.8	25.4	104.5
250	238.9	223.5	231.2	222.2	216.9	90.6
1000	1094.0	1116.0	1095.0	1092.0	1076.0	109.5

Figure 3.8 Intraday Validation Accuracy for Heme B Quantification Assay
Panel A presents the standard curve statistics for accuracy for the intraday validation for heme B quantification. Panel B presents the intraday statistics for the quality control samples.

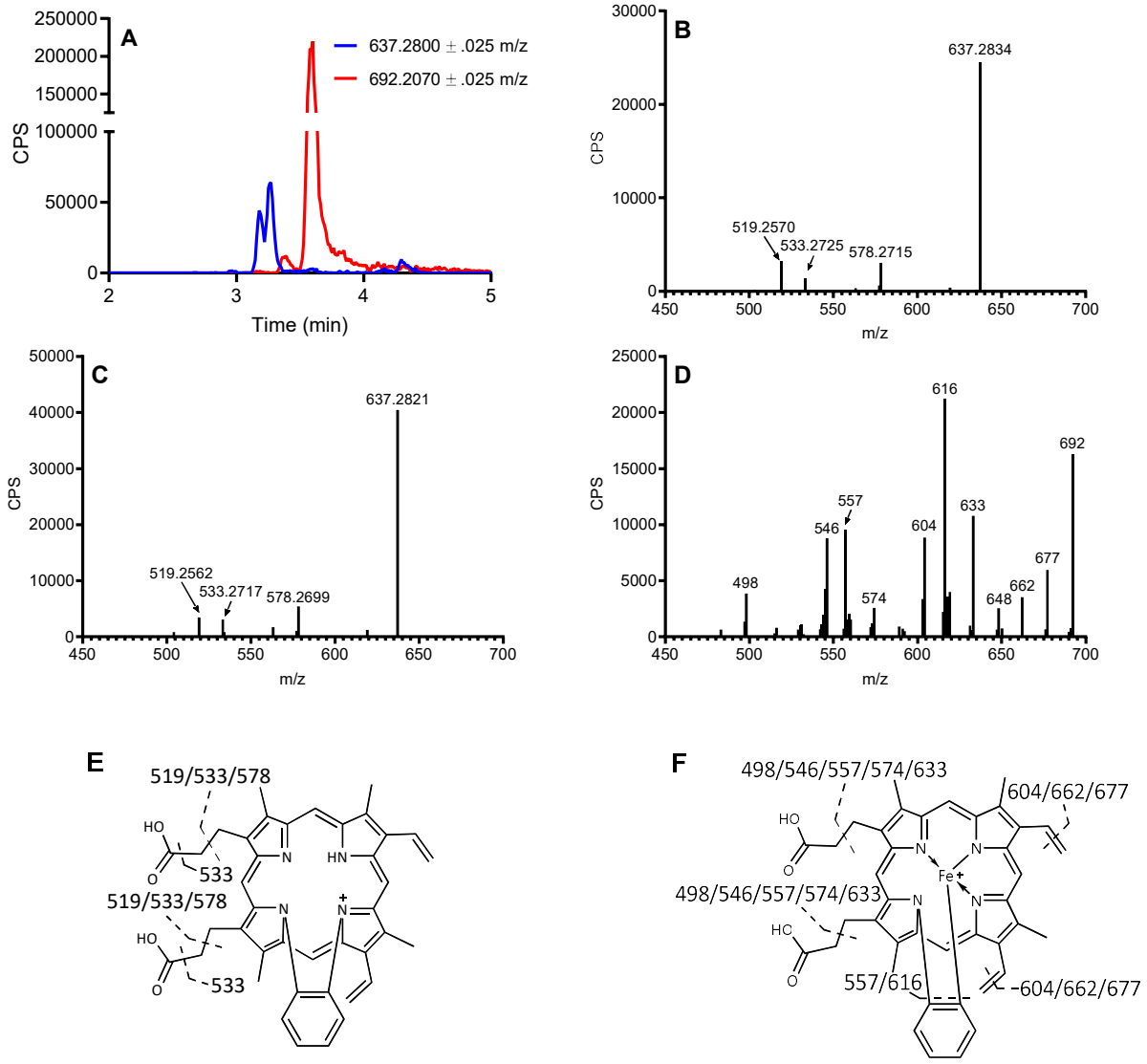

Figure 3.9 Detected Heme and Protoporphyrin IX Related Adducts from Incubations of ABT with HLM

Panel A is an extracted ion current overlay of the m/z ranges of the heme/protoporphyrin adducts. Panel B and C are product ion spectra of 637 m/z for the 3.17 and 3.27 min peaks, respectively, and panel E is a proposed fragmentation pattern for 637 m/z. Panel D is product ion spectra of 692 m/z for the 3.58 min peak, and panel F is a proposed fragmentation pattern for 692 m/z.

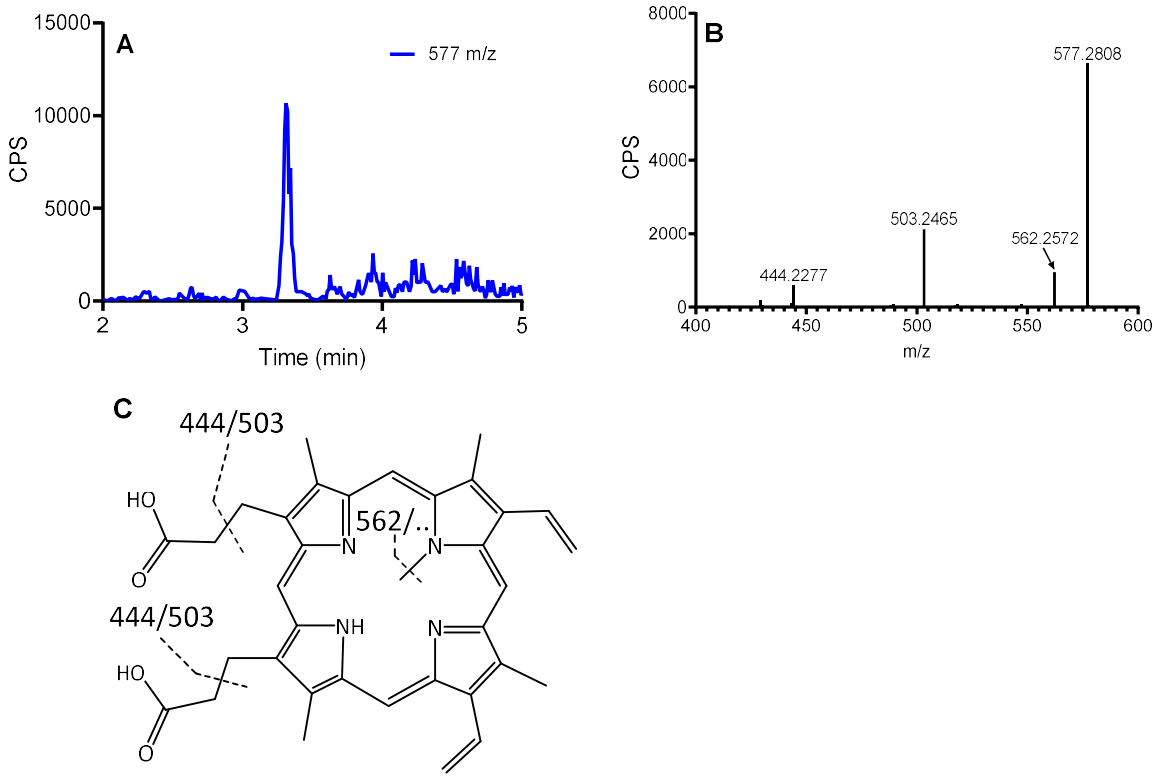

Figure 3.10 Detected Heme and Protoporphyrin IX Related Adducts from Incubations of DDC with HLM

Panel A is an extracted ion current overlay of the m/z ranges of the heme/protoporphyrin adducts. Panel B is a product ion spectra of 577 m/z, and panel C is a proposed fragmentation pattern for 577 m/z.

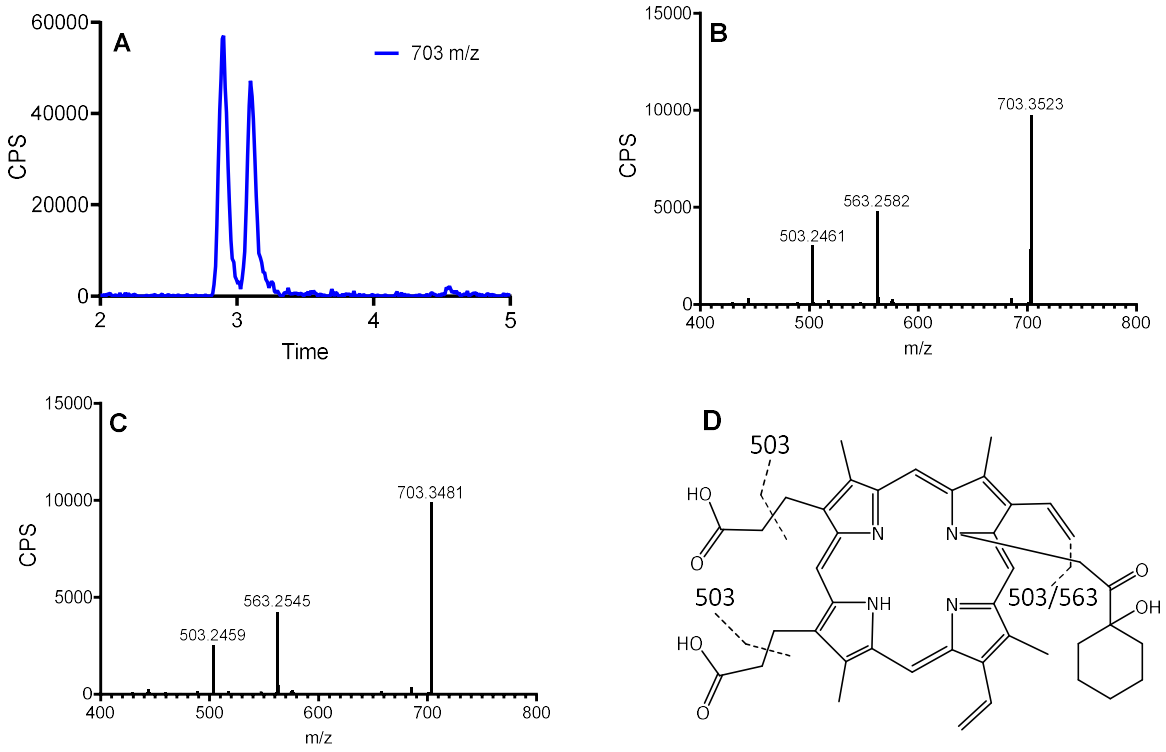

Figure 3.11 Detected Heme and Protoporphyrin IX Related Adducts from Incubations of 1-Ethynyl-1-Cyclohexanol with HLM

Panel A is an extracted ion current overlay of the m/z ranges of the heme/protoporphyrin adducts. Panel B and C are a product ion spectra of 703 m/z at 2.90 and 3.10, respectively. Panel D is a proposed fragmentation pattern for 703 m/z.

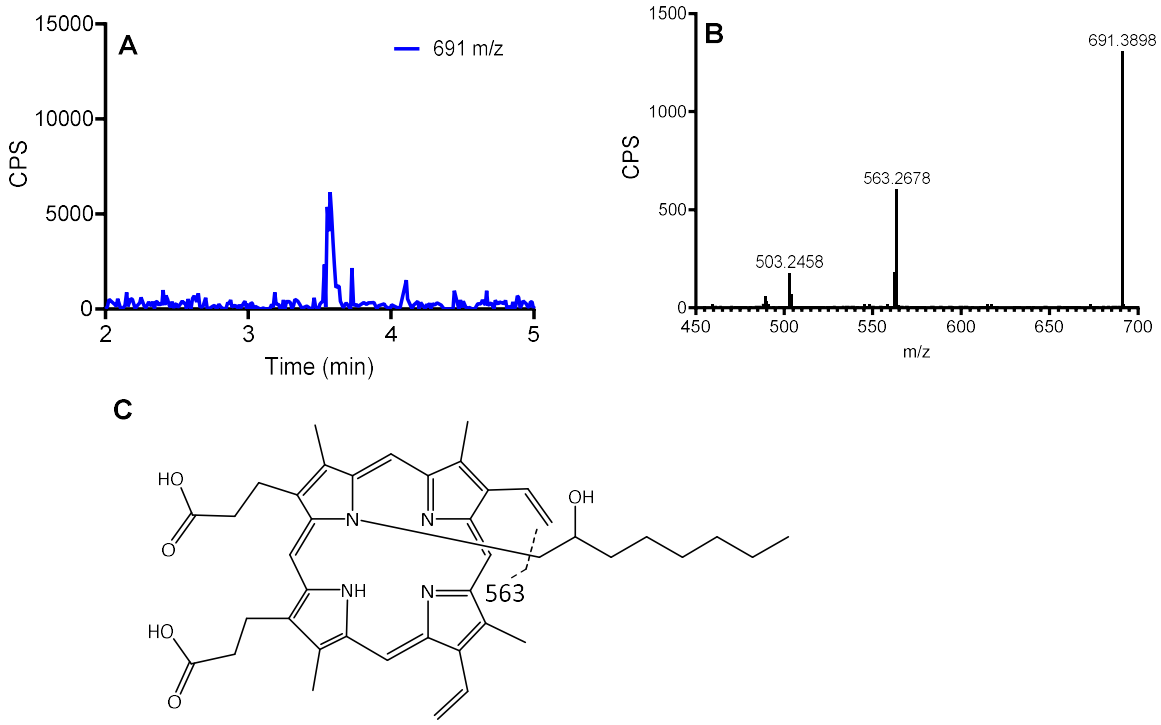

Figure 3.12 Detected Heme and Protoporphyrin IX Related Adducts from Incubations of 1-Octene with HLM

Panel A is an extracted ion current overlay of the m/z ranges of the heme/protoporphyrin adducts. Panel B is the product ion spectra of 691 m/z. Panel C is a proposed fragmentation pattern for 691 m/z based upon the position determined by Kunze et al.

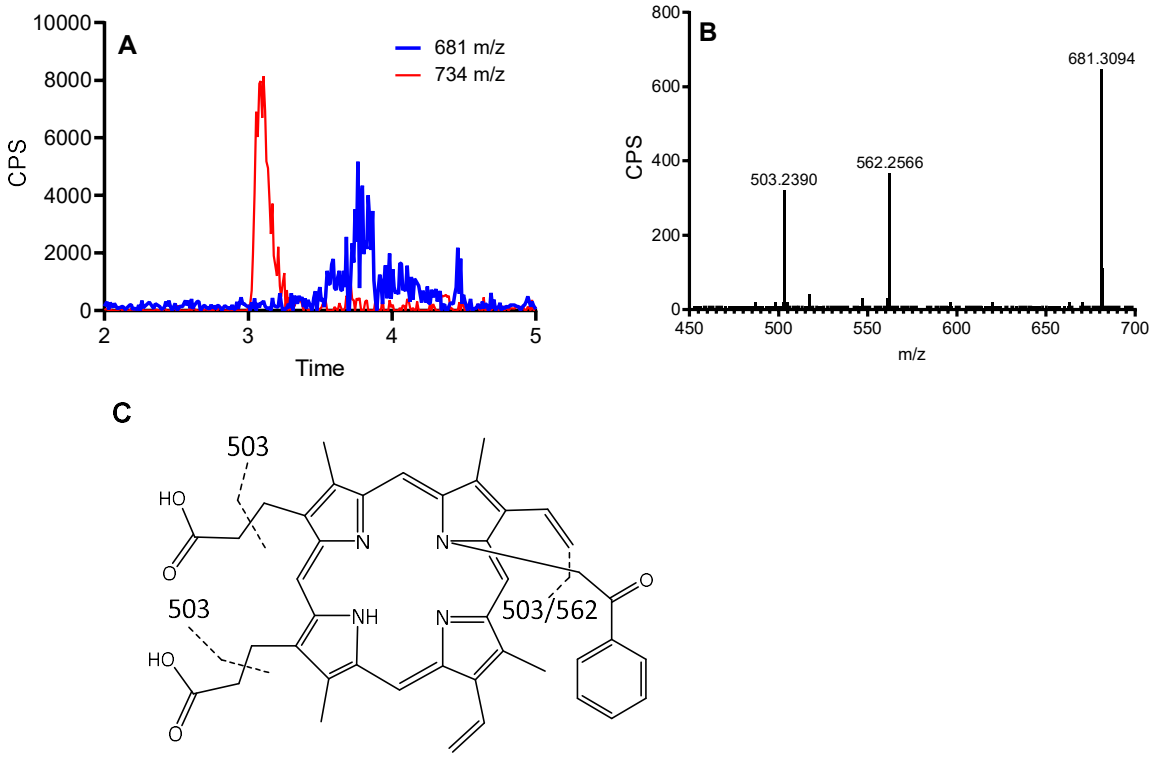

Figure 3.13 Detected Heme and Protoporphyrin IX Related Adducts from Incubations of Phenylacetylene with Rabbit LM

Panel A is an extracted ion current overlay of the m/z ranges of the heme/protoporphyrin adducts. Panel B is the product ion spectra of 681 m/z. Panel C is a proposed fragmentation pattern for 681 m/z based upon the position determined by Kunze et al.

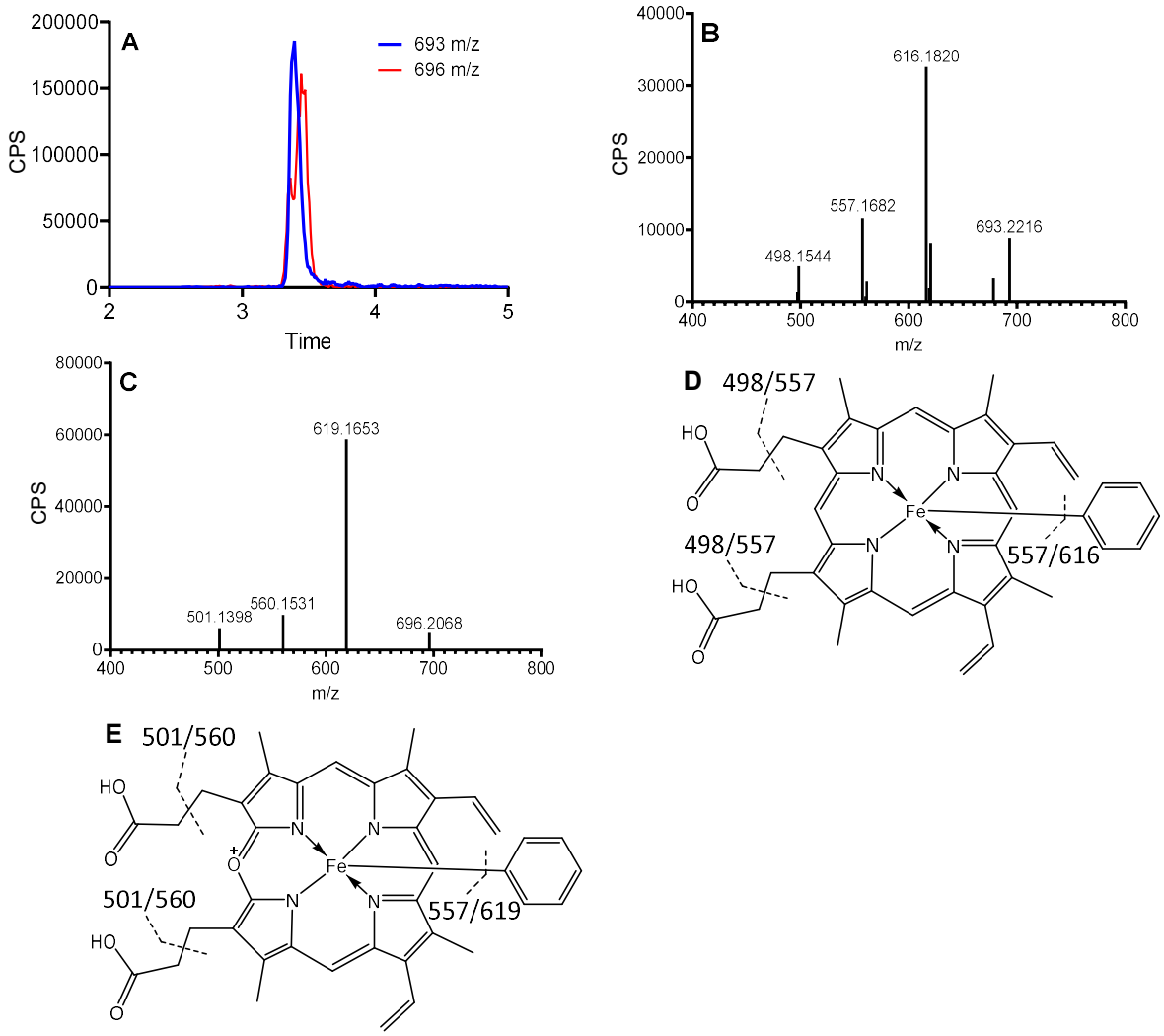

Figure 3.14 Detected Heme and Protoporphyrin IX Related Adducts from Incubations of Phenyhydrazine with HLM

Panel A is an extracted ion current overlay of the m/z ranges of the heme/protoporphyrin related adducts. Panel B is the product ion spectra of 693 m/z. Panel C is the product ion spectra of 696 m/z. Panel D is a proposed fragmentation pattern for 693 m/z,a nd Panel E is a proposed fragmentation pattern of 696 m/z.

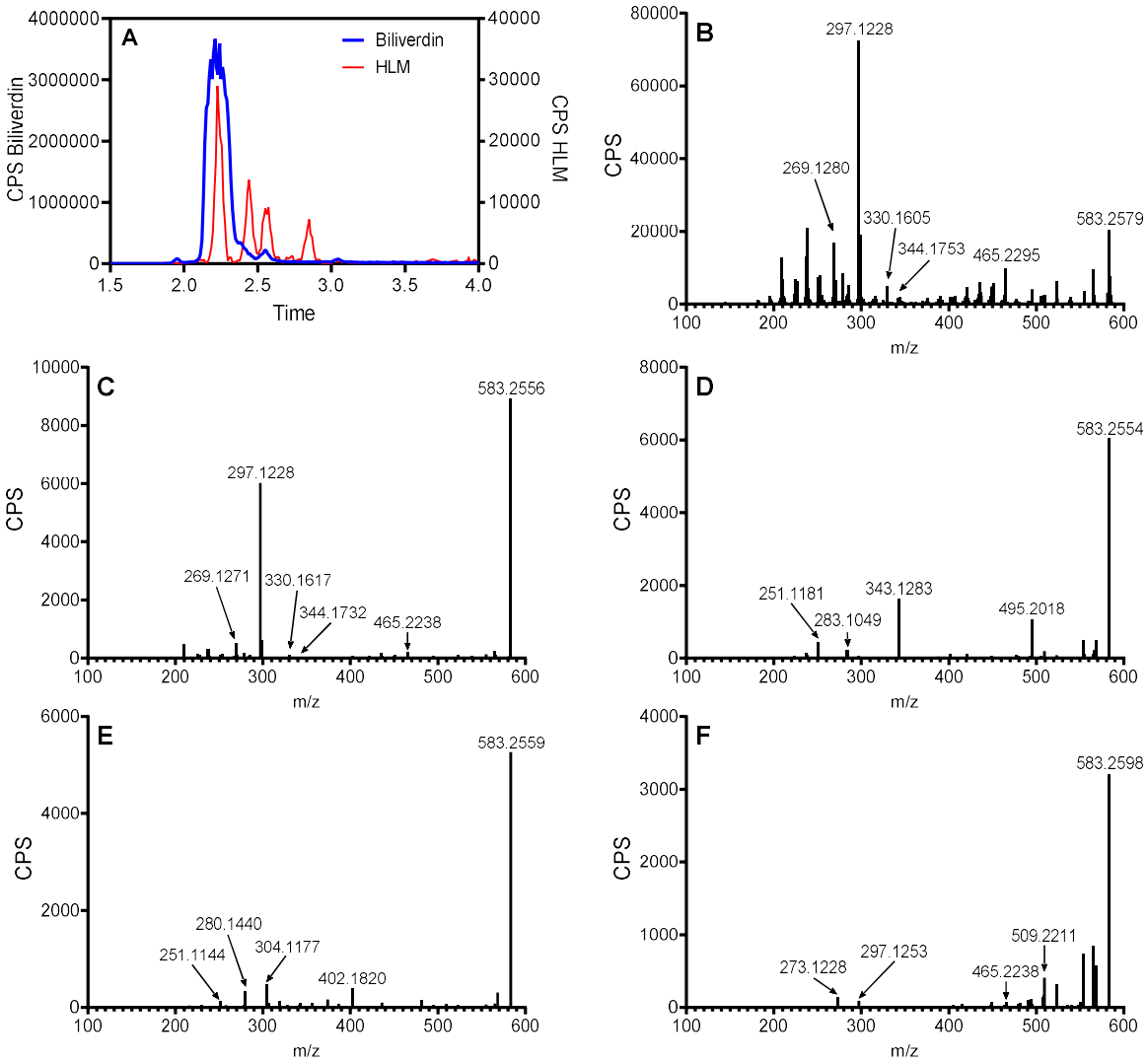

Figure 3.15 Isomers of Biliverdin Detected in Human Liver Microsome Incubations
Panel A is an extracted ion current overlay of a commercial standard of biliverdin and the biliverdin isomers found in HLM incubations. Panel B depicts the product ion spectra of the major (2.24 min) peak contained the biliverdin standard. Panel C depicts the product ion spectra of the 2.24 min peak in the HLM incubation. Panel D depicts the product ion spectra of the 2.45 min peak in the HLM incubation. Panel E depicts the product ion spectra of the 2.55 min peak in the HLM incubation. Panel F depicts the product ion spectra of the 2.85 min peak in the HLM incubation.

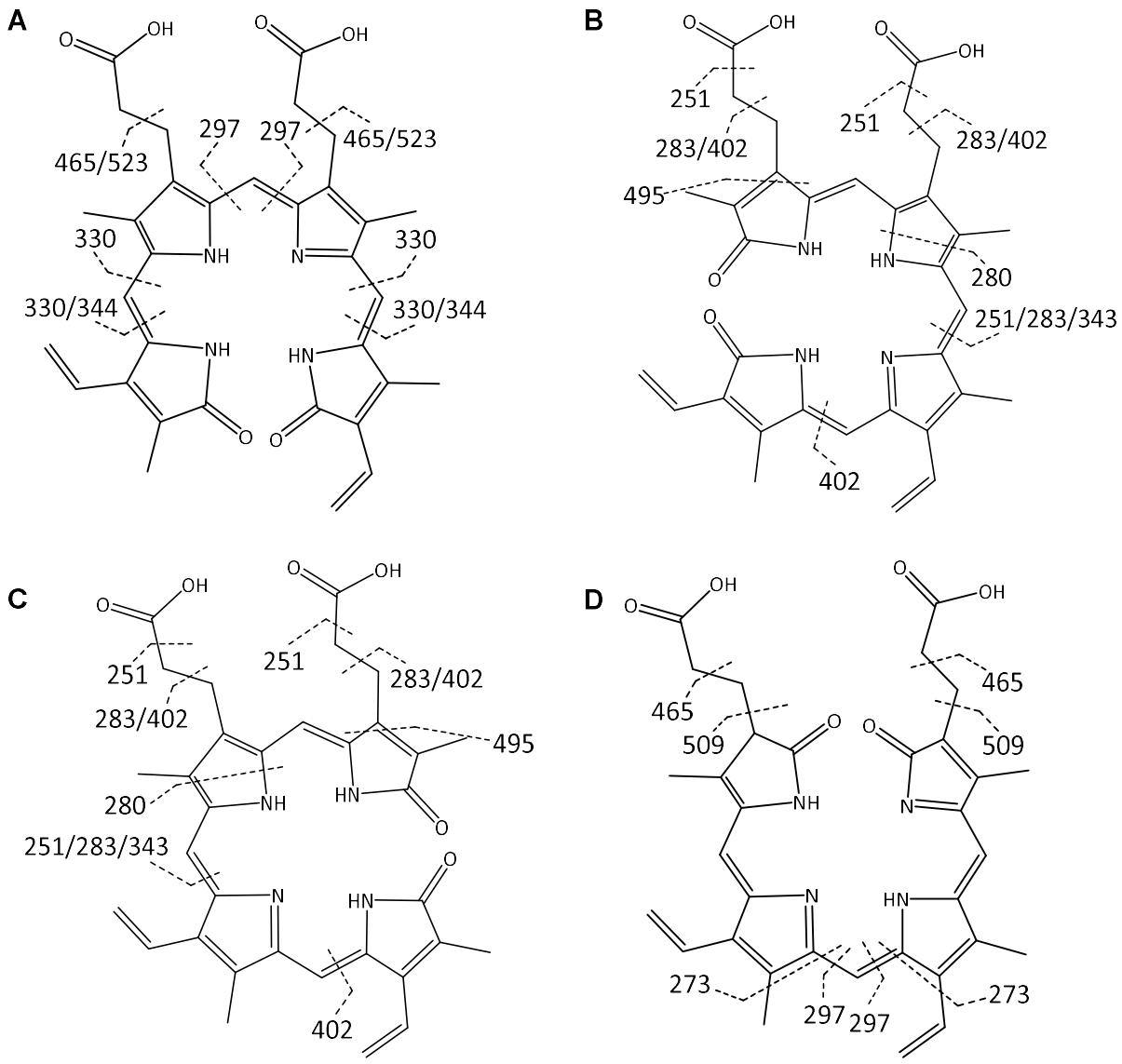

Figure 3.16 Proposed Fragmentation of Biliverdin Isomers
Panel A depicts the proposed fragmentation of biliverdin Ixα which corresponds to the 2.24 min peak in HLM. Panel B depicts the proposed fragmentation of biliverdin IXβ, and panel C depicts the proposed fragmentation of biliverdin IXΔ. The peaks of 2.45 and 2.55 minutes could correspond to either biliverdin IXβ and biliverdin IXΔ. Panel D depicts the proposed fragmentation of biliverdin IXγ which corresponds to the 2.85 min peak in HLM.

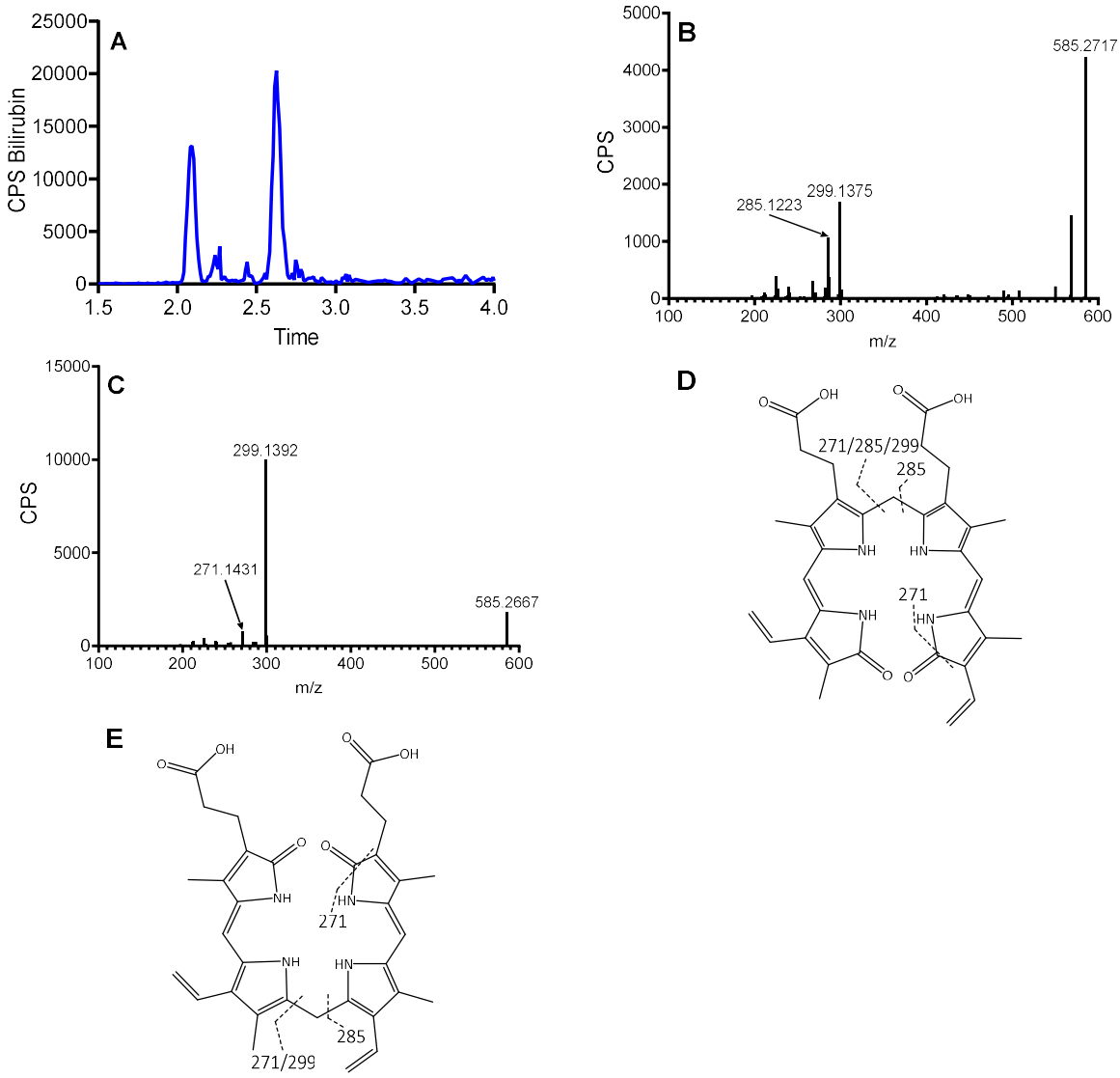

Figure 3.17 Isomers of Bilirubin Detected in HLM Incubations
Panel A is an extracted ion current of bilirubin. Panel B is the product ion spectra of the 2.09 peak, and panel C is the product ion spectra of the 2.62 min peak. Panel D is a proposed fragmentation pattern for bilirubin IXα and panel E is a proposed fragmentation pattern for bilirubin IXγ.

Chapter 4: Mechanistic Analysis of Time Dependent Inhibition of CYP2B6, 2E1, and 3A4/5 by Chlormethiazole

4.1 Introduction

In Chapter 2, we assessed the selectivity of CYP inhibition by chlormethiazole (CMZ) utilizing both co-incubation and time dependent inhibition (TDI) experiments. We showed that CMZ inhibits several CYP isoforms in different mechanisms, including a time-dependent mechanism. In addition to time-dependency, we established that CYP2B6, 2E1, and 3A4/5 were inhibited in a manner consistent with enzymatic turnover. We also investigated the metabolites generated by each isoform in an attempt to identify potential reactive species that could explain the apparent TDI. Since there are numerous causes and types of time-dependent inhibition and each situation can lead to different outcomes in terms of drug-drug interactions (DDI) and possibly toxicity, the mechanisms of TDI must be evaluated for each of the isoforms affected by CMZ.(75,76,79,99,187) To investigate the mechanism of TDI for CYP2B6, CYP2E1, and CYP3A4/5, we will use Silverman's Criteria for a mechanism based inhibitor, mentioned previously in Chapter 1, and will attempt to identify the potential molecular target(s) of the inhibiting species.(11)

A mechanism based inhibitor (MBI), as defined by Richard Silverman, is a special case of time-dependent inhibition in that a reactive species is generated by the normal function of the enzyme and inactivates the enzyme by binding to it in a manner that disrupts catalytic function.(11) An MBI would be expected to be one the simplest cases of TDI to predict DDI since the bioactivation process for the MBI and the binding of the inhibitor would all have to occur within the active site. This localization of the entire enzyme inactivation process would eliminate many potential variables that can complicate other TDI mechanisms such as detoxification or further

metabolism that removes intermediates required for TDI. Silverman's criteria for a MBI are as follows:

8. Time-dependent loss of enzyme activity.
9. The rate of enzyme inactivation is saturable at high concentrations of inactivator (i.e. The rate of the reaction follows Michaelis-Menten enzyme kinetics.)
10. Inactivation is slowed in the presence of an alternative substrate (i.e. The inhibition can be competitively inhibited.)
11. Dialysis or dilution do not restore enzyme activity (i.e. The inactivation is irreversible.)
12. A 1:1 stoichiometry of inhibitor bound to enzyme is observed.
13. A catalytic step by the enzyme is required for inactivation to occur.
14. Inactivation occurs before release of the reactive species (Inactivation occurs in the active site.)

These criteria allow us to investigate the nature of the TDI in a manner that can classify the mode of TDI and, therefore, can identify any potential complications in DDI prediction.

Due to the complex nature of CYP enzymes, the two most difficult criteria to investigate are the stoichiometry of the inhibitor to enzyme and if inactivation occurs prior to product release. In order to assess the stoichiometry, one must be able to detect a stable adduct to either the heme or apo protein, and have a method that enables at least a semi-quantitative assessment of stoichiometry. Typically, the preferred method for assessing stoichiometry would involve radiolabeling of the inhibitor, and monitoring the specific radioactivity adducted to a preparation of CYP enzyme.(284-286) We did not have access to radiolabeled CMZ so this technique is not available for this analysis.

Proving that enzyme inactivation occurs before product release requires multiple factors to be investigated. Since CYP enzymes are capable of releasing reactive oxygen species (ROS) that could inactivate the enzyme in the active site and outside of the active site, exogenous superoxide dismutase (SOD) and catalase (CAT) can be used to block formation of these ROS before they can covalently modify the enzyme outside of the active site.(12,19,287-289) However, using SOD and CAT does not exclude ROS from inactivating the enzyme from within the active site.(290,291) The use of trapping agents can also help to clarify the point of modification by the reactive metabolite.(44-48,230,292) It is thought that large, polar trapping agents, such as glutathione, are incapable of entering the active site so attenuation or elimination of inactivation should indicate that inactivation of the enzyme is at least partially the result of binding of a reactive species outside of the active site. Therefore, direct detection of potential adducts is the preferred method for identifying the location of the adduct, but direct detection is not always possible due to numerous reasons including the stability of the adduct.

In this chapter, we investigate the TDI mechanisms for each isoform individually by a host of techniques while following Silverman's criteria as a guide.(11) Enzymatic activity assays were used to evaluate the effects of competing substrates, dialysis, exogenous detoxification enzymes, and exogenous trapping agents upon the activity of each isoform. By using UV/Vis spectroscopy, we hoped to uncover any changes in absorbance associated with the loss of enzymatic activity that could be associated with the mechanism of inhibition.(12,272) High resolution mass spectrometry techniques were also used to detect potential heme and apo protein adducts.(4,293)

4.2 Experimental

4.2.1 Materials.

All chemicals from commercial sources were of analytical grade or better where possible. Optima LC-MS grade acetonitrile, formic acid, and methanol, dithionite, ACS Plus grade isopropyl

alcohol, para-nitrophenol were purchased from Thermo Fisher Scientific (Waltham, MA). All water was distilled, deionized using a house distilled water followed by a Barnstead NANOpure UV system (Thermo Fisher Scientific). Human liver microsomes (HLM) were prepared from liver samples obtained from the University of Washington Liver Bank. Purified human recombinant CYP2E1 was prepared as described in Chapter 3. Purified human recombinant CYP2B6 was provided by Dr. Rheem Totah, and purified human recombinant CYP3A4 was provided by Michelle Redhair.(294,295) 100x Lipid reconstitution mixture was provided by Michelle Redhair according to Shaw et al.(296) Purified rat cytochrome P450 oxidoreductase (CPR) was provided by John Kowalski, Michelle Redhair, and Dr. Mariko Nakano. Catalase, chlorzoxazone, coumarin, 7-hydroxycoumarin, p-nitrocatechol, midazolam, 1'-hydroxymidazolam, 1'-hydroxymidazolam-D_4, potassium cyanide, potassium phosphate monobasic, potassium phosphate dibasic, reduced glutathione, superoxide dismutase (SOD) testosterone were purchased from Sigma-Aldrich (St. Louis, MO). CMZ, bupropion, hydroxybupropion, hydroxybupropion-D_6, 6-hydroxychlorazoxazone, 6-hydroxychlorzoxazone-$^{13}C_6$ and 4-hydroxymidazolam were purchased from Toronto Research Chemicals (Toronto, ON, Canada). NADPH was obtained from OYC Americas (Vista, CA). CMZ N-oxide was synthesized as described in Chapter 2.

4.2.2 HLM Incubations using dilution assays and Dialysis to Determine the Effect of Various conditions on CMZ TDI of CYP2B6, 2E1, and 3A4/5

These assays consist of four steps which are: pre-incubation, incubation, dialysis, and secondary incubation to determine remaining activity. Pre-incubations consisted of total volume 100 µL containing 0.1 M potassium phosphate buffer and 0.5 mg/mL pooled human liver microsomes with various combinations of the following components including 2 mg/mL NADPH, CMZ dissolved in water, 5 mM GSH, SOD/CAT (2,000 U/mL SOD/50 µg/mL CAT), 500 µM bupropion, 400 µM CHZ, 110 mM ethanol, and 400 µM testosterone. Some reactions were pre-incubated for 5 minutes before the addition of NADPH in a 37º C water bath. For CYP2B6, pre-

incubations lasted 30 minutes, and the concentration of CMZ was 100 μM. For CYP2E1, the pre-incubation concentration of CMZ was 100 μM. The pre-incubation time for the set of samples where CMZ was used as the competing substrate for CMZ was 10 minutes, while the pre-incubation for the set of samples where ethanol was competing the substrate lasted 5 minutes. After pre-incubation samples were transferred to 3500 MW cutoff Slide-a-Lyzer Mini (100 μL size) dialysis cups that were floating in 500 mL of ice cold 0.1 M potassium phosphate (pH 7.4). The buffer was exchanged 10 minutes after the addition of the samples to the dialysis cups, and then three more exchanges were performed over 18 hours. The secondary incubations contained 200 μM bupropion for CYP2B6, 400 μM CHZ for CYP2E1, or 40 μM midazolam for CYP3A4/5 as the substrate, and the incubation times were 10 minutes for CYP2B6, 5 minutes for CYP2E1, and 5 minutes for CYP3A4/5. Standards were prepared as described in Chapter 2, and all samples were analyzed using the methods described in Appendix 3, 8, and 10.

4.2.3 Reconstitution of Purified CYP2B6, 2E1, and CYP3A4 with or without Purified CPR.

A 100x solution of the lipid reconstitution solution described by Shaw et al was provided by Michelle Redhair.(296) Final concentrations of lipids were the following: 0.5 mg CHAPS/mL, 0.1 mg/mL liposomes [L-α-dilauroyl-sn-glycero-3-phosphocholine, L-α-diloleoyl-sn-glycero-3-phosphocholine, L-α-dilauroyl-sn-glycero-3-phosphoserine (1:1:1, w/w/w per mL), 3.0 mM GSH, and 50 mM potassium HEPES, pH 7.4]. During the experiments, we used various ratios of CPR to P450 including: 0:1, 0.5:1, 1:1, and 2:1. CPR was added to the purified CYP and gently mixed at 4° C for 5 minutes on a Nutator™ before the addition of lipid mix. Lipid mix was added to the enzyme mix and allowed to mix at 4° C for at least 60 minutes on a Nutator™ before use.

4.2.4 UV/Vis Spectroscopy of CMZ or CMZ N-oxide Binding with CYP2B6, 2E1, or 3A4/5.

All UV spectroscopy was performed using a modernized Aminco DW-2 UV/Vis spectrophotometer (Olis, Inc., Bogart, Georgia) with a Julabo circulating bath (Seelbach,

Germany) to control sample temperature. The scan range was from 350-700 nm, and each took approximately 2 minutes. The sample cuvette initially contains 400 µL of 0.125 M potassium phosphate (pH 7.4) containing 1.25 µM of reconstituted CYP without CPR, and the reference cuvette contains 400 µL of 0.125 M of potassium phosphate (pH 7.4) to allow for the addition of various components in water up to 100 µL while maintaining at least 0.1 M potassium phosphate. CMZ and CMZ N-oxide were solubilized in water at 50 mM to make the initial stock solution. Any component added to the sample side was balanced by addition to the reference lacking enzyme, and both sides were mixed after the addition of any component. After the addition of CMZ or CMZ N-oxide, dithionite was added to reach 1 mg/mL as the final concentration. The calculated difference spectra was generated by comparison to enzyme alone to determine the binding mode of CMZ or CMZ N-oxide by using GraphPad Prism 8.2. Interpretation of spectra was performed by comparison with previous literature regarding CYP heme absorbance, flavin absorbance, and heme adduct absorbances.(3,12,49,52,54,84,105,111,117,297,298)

4.2.5 UV/Vis Spectroscopy of CMZ Inactivation of CYP2B6, 2E1, or 3A4/5.

All UV spectroscopy was performed using a modernized Aminco DW-2 UV/Vis spectrophotometer (Olis, Inc., Bogart, Georgia) with a Julabo circulating bath (Seelbach, Germany) to control sample temperature. The scan range was from 350-700 nm, and each scan took approximately 2 minutes. The solutions in the reference and sample cuvette were prepared as described above except NADPH. NADPH was added to a final concentration of 1 mg/mL was added to start the reaction, and scans were repeated to capture the time course of inactivation. Difference spectra were calculated as above. Interpretation of spectra was performed using previous literature regarding CYP heme absorbance, flavin absorbance, and heme adduct absorbances.(3,12,49,52,54,84,105,111,117,297,298)

4.2.6 Heme Adduct Analysis.

CYP2B6, 2E1, or 3A4 was reconstituted with 1:1 CPR to CYP, and CYP2E1 was also reconstituted with 0.5:1 and 2:1 CPR to CYP using the method described above. Two μM reconstituted enzyme was incubated with 0.1 M potassium phosphate (pH 7.4), 2 mg/mL NADPH, and CMZ (100 μM for CYP2B6/CYP2E1 or 1 mM for CYP3A4) for 5 minutes under low ambient light conditions. Samples were terminated and analyzed as described in Chapter 3 using the elemental composition of CMZ with heme B and CMZ with PPIX as the mass defect filter target masses. Due to the potential instability of the adduct, the samples were injected within 5 minutes of termination.

4.2.7 Whole Protein Adduct Analysis.

CYP2B6, 2E1, or 3A4 was reconstituted with 1:1 CPR to CYP using the method described above. Two μM reconstituted enzyme was incubated in 0.1 M potassium phosphate (pH 7.4), 2 mg/mL NADPH, and CMZ (100 μM for CYP2B6/CYP2E1 or 1 mM for CYP3A4) for 15 minutes. Samples were injected using the method described in Appendix 16.

4.3 Results

4.3.1 Effects of Dialysis, Exogenous Trapping Agents, Exogenous Detoxification Enzymes, and Exogenous Substrates on CYP2B6 inactivation

To begin our mechanistic analysis of CYP2B6, we performed a series of activity assays to assess the effects of various experimental conditions upon the inactivation of CYP2B6 by CMZ.

In Figure 4.1, a dilution assay was performed with all samples being preincubated with 100 μM CMZ. The activity of CYP2B6 was reduced by 52.8% by the addition of NADPH during the preincubation as compared to preincubation without NADPH, thus confirming NADPH requirement for CMZ-dependent TDI. The combination of SOD/CAT did not have any significant

effects on inactivation as indicated by the similar reduction of activity when SOD/CAT (48.6%) was added to samples preincubated with NADPH and CMZ compared to those lacking SOD/CAT. Interestingly, the addition of reduced glutathione (GSH) to a NADPH-containing incubation markedly reduced the magnitude of inhibition (32.4% vs. 52.8%).

In Figure 4.2, bupropion, CMZ, or both bupropion and CMZ were incubated with pooled HLM and NADPH for 30 minutes then the incubations were dialyzed. The remaining activity was then assessed using CYP2B6-mediated bupropion hydroxylation. Incubation with CMZ reduced CYP2B6 activity by 74% as compared to the bupropion control. The co-incubation of CMZ with bupropion resulted in a 45.6% reduction in activity as compared to bupropion alone.

4.3.2 UV/Vis Spectroscopy of CMZ/CMZ N-oxide Binding and Inactivation of CYP2B6

UV/Vis spectroscopy of CYP2B6 reconstituted in lipid mixture in the presence or absence of rat cytochrome P450 reductase (CPR) was performed in order to detect any possible absorbance changes related to loss or modification of the prosthetic heme. We performed an experiment to examine the effects of ligand binding to CYP2B6 reconstituted with lipid only and CMZ and CMZ N-oxide in the presence or absence of the reducing agent, dithionite. We also performed a time course of reconstituted CYP2B6/CPR incubated with CMZ and NADPH to capture absorbance changes during the inactivation of CYP2B6.

In Figure 4.3, we present the calculated difference binding spectrum of CMZ with CYP2B6 in the presence and absence of dithionite. The type of binding spectra for CMZ is not clear from these data since there is no increase in absorbance at any of the wavelengths measured. The loss of absorbance at 416 nm is somewhat consistent with a Type I binding mode, but there is no corresponding increase near 390 nm. The addition of dithionite results in an even greater loss of absorbance at 416 nm and additional loss of absorbance at 363 nm. The expected merger of α and β bands due to reduction of heme that results in a 550 nm peak occurred. There may be a

slight increase in absorbance at 452 nm when dithionite is added to CMZ with CYP2B6, but there is a dramatic decrease at both 361 nm and 417 nm.

In Figure 4.4, we present the data of a change in absorbance time course when CMZ and NADPH are incubated with CYP2B6 that is reconstituted with rat CPR (1:1) and lipid mixture. During the time course, there is a loss of absorbance at 376 nm over time, but there is no detectable corresponding increase in absorbance.

In Figure 4.5, a binding spectra of CMZ N-oxide in the presence or absence of dithionite is presented. The addition of N-oxide resulted in a loss of absorbance at 416 nm with no corresponding increase of any absorbance. The addition of dithionite results in a greater loss of the band at 416 nm, and a broad absorbance increase centered around 466 nm appears. Absorbance at 550 nm corresponding to reduction of heme also occurred.

4.3.3 LC/MS Analysis of CYP2B6 Heme and CYP2B6 Apo Protein after Inactivation

We attempted to detect any covalent modification of either the heme or apo protein via high resolution mass spectroscopy. We employed the mass defect filtering technique described in Chapter 3 with reconstituted CYP2B6 to attempt to identify heme adducts that may have been formed during the inactivation process. Incubation of CMZ with reconstituted CYP2B6 also did not yield any detectable adducts to apo protein.

4.3.4 Effects of Dialysis, Exogenous Trapping Agents, Exogenous Detoxification Enzymes, and Exogenous Substrates upon CYP2E1 Activity

As for CYP2B6, we performed a series of activity experiments after preincubation with various components and subsequent dialysis to obtain mechanistic information about the mechanism of CYP2E1 inactivation. We performed one experiment focused on the effects of NADPH, GSH, and co-incubation of chlorzoxazone (CHZ) upon CMZ inactivation of CYP2E1, and

one experiment focused on the effects of SOD/CAT and co-incubation with ethanol. The complete results for these experiments are presented in in Figure 4.6 and Figure 4.7.

The results for CMZ co-incubation with ethanol and SOD/CAT are presented in Figure 4.6. Ethanol was able to block inactivation by CMZ at concentrations 10-fold higher than the reported K_m, but SOD/CAT had little or no apparent effect upon CMZ inactivation of CYP2E1. Interestingly, treatment of HLM with ethanol in absence of NADPH resulted in the same activity as treatment with NADPH and ethanol + NADPH.(36,37) In Figure 4.6, preincubation with NADPH alone caused an increase in activity so ethanol maybe displacing the inhibitory compound from the CYP2E1 active site.

In Figure 4.7, the effects of NADPH and GSH are more complicated than expected. Preincubation of HLM with NADPH caused an increase in chlorzoxazone 6-hydroxylase activity after dialysis, and GSH appears to also cause a smaller increase in activity combined with NADPH. This effect of GSH seems to be eliminated when preincubated with CHZ. These complications require comparisons with different controls to assess the contribution to changes in CMZ mediated inactivation of CYP2E1. In Figure 4.8, we normalized and matched the appropriate controls from Figure 4.8 to the corresponding test samples to assess the effects of these variables, then applied a one way ANOVA with Dunnett's test to assess statistical significance as compared NADPH with CMZ normalized to incubation with NADPH alone. Even though there was some reduction in inactivation in presence of GSH (12.6%) and CHZ (4.3%) individually, those components did not affect inactivation in a statistically significant manner. The effects of the GSH and CHZ combination were cumulative (28.2%) and resulted in a statistically significant change. Even though CHZ concentration was ~10-fold over K_m, CHZ was not effective in competing CMZ during the CMZ inactivation of CYP2E1.

4.3.5 UV/Vis Spectroscopy of CMZ/CMZ N-oxide Binding and Inactivation of CYP2E1

The binding spectra of CMZ with CYP2E1 is presented in Figure 4.9 in absence of dithionite and in Figure 4.10 in presence of dithionite. As shown in Figure 4.11, we acquired spectra of CYP2E1 reconstituted with lipid and CPR incubated with CMZ and NADPH. Figures 4.12 and Figure 4.13 depict the spectra of CMZ N-oxide binding to CYP2E1 and illustrate the changes caused in that spectrum by dithionite.

The addition of CMZ to CYP2E1 resulted in a clear change in absorbance in a concentration dependent manner. There was a decrease in absorbance at 390 nm and an increase at 430 nm, and these changes are consistent with a type II binding mode. The addition of dithionite did not alter this pattern (Figure 4.10).

The spectral changes caused by incubation of CMZ and NADPH with CYP2E1 reconstituted with lipid and CPR are presented in Figure 4.11. There are two regions where losses in absorbance increase over time. The loss 430 nm corresponds to loss of heme in the type II binding mode with CMZ, but the second region does not have a minimum that we can clearly correlate to heme.

Figures 4.12 and 4.13 depict the binding spectra of CMZ N-oxide with CYP2E1. The binding spectra of the N-oxide is that of a type II binding mode with a minimum of 390 nm and a maximum at 430 nm. The addition of dithionite did cause an absorbance change with the appearance of a new absorbance peak around 450 nm and the reduction of the 430 nm peak.

4.3.6 LC/MS Analysis of CYP2E1 Heme and CYP2E1 Apo Protein after Inactivation

Although a UV/Vis active species was detected with the addition of CMZ N-oxide and dithionite to CYP2E1, the data from UV/Vis did not clearly indicate any potential MIC or formation of another UV/Vis active species during the incubation of CMZ and NADPH with reconstituted

enzyme. Because there was no clear mechanism suggested by these data, we employed LC/HRMS techniques to analyze for any heme or apo protein adducts.

We employed methods described in Chapter 3, and found a mass consistent with a protoporphyrin IX adduct of CMZ to CYP2E1 that was mono-oxygenated. The extracted ion current, spectra, and proposed structure of the putative adduct are presented in 4.14. The m/z was approximately 2.7 ppm different from the expected m/z of 738.2511. We also found two additional m/z species that were consistent with the ^{13}C and ^{37}Cl isotope distributions expected from the chemical composition, and those species further strengthen the identity of the adduct. This adduct appears to be unstable as reinjection of the same sample after 2 hours resulted in no detectable adduct. The signal was also not sufficient to obtain fragmentation so no structural information is available beyond the elemental composition. No protein adduct was detected even though we were able to detect the protein adduct of diethyldithiocarbamate first reported by Pratt-Hyatt.(102)

4.3.7 Effects of Dialysis, Exogenous Trapping Agents, Exogenous Detoxification Enzymes, and Exogenous Substrates upon CYP3A4/5 Activity

As we did for CYP2B6 and CYP2E1, we performed a series of activity experiments after preincubation with various components and subsequent dialysis to obtain mechanistic information about the inactivation of CYP3A4/5 using midazolam 1'-hydroxylation as the reporter activity. We performed one experiment focused on the effects of NADPH, GSH, and SOD/CAT upon CMZ inactivation of CYP3A4/5, and one experiment focused upon the effects of co-incubation of CMZ with testosterone. The complete results for these experiments are presented in in Figure 4.15 and Figure 4.16.

In Figure 4.15, the effects of preincubation with NADPH, GSH, and SOD/CAT are examined. The inhibition appears to be NADPH dependent but resistant to dialysis. There is statistically significant apparent reduction of inhibition by GSH, and it appears that SOD/CAT may

reduce inhibition. The reduction by SOD/CAT alone though is not statistically different, but the effect appears to be additive with GSH.

Figure 4.16 depicts a competition experiment between testosterone and CMZ to identify if another CYP3A4/5 substrate can compete with the TDI caused by CMZ. The concentration of testosterone in the assay is approximately 10-fold above the reported K_m value while the concentration of CMZ is only 5-fold above K_I.(299) However, co-incubation with testosterone did not block any of the apparent TDI by CMZ. Due to solubility, testosterone concentrations could not be increased further.

4.3.8 UV/Vis Spectroscopy of CMZ/CMZ N-oxide Binding and Inactivation of CYP3A4/5

The binding spectra of CMZ with CYP3A4 is presented in Figure 4.17. As shown in Figure 4.18, we acquired spectra of CYP3A4 reconstituted with lipid and CPR incubated with CMZ and NADPH. Figures 4.19 depict the spectra of CMZ N-oxide binding with CYP3A4 along with the changes caused in that spectra by dithionite.

The calculated difference binding spectrum of CMZ with CYP3A4 is similar to that of CYP2B6. There was a clear decrease in absorbance at 417 nm, but there was no corresponding increase at any absorbance. Therefore, we cannot classify the binding mode of CMZ with CYP3A4.

The spectral changes caused by incubation of CMZ and NADPH with CYP3A4 reconstituted with lipid and CPR are presented in Figure 4.18. Over time, there is a clear increase of absorbance in the 451 nm and a decrease at 389 nm. Due to the shape of the loss of absorbance below 451 nm, there may also be a loss of absorbance peak around 418 nm in this region.

Figures 4.19 depict the binding spectra of CMZ N-oxide with CYP3A4 in the presence and absence of dithionite. The binding spectra of the CMZ N-oxide most resembles a type II binding mode with a maxima of 427 nm, but there was no corresponding loss of absorbance elsewhere

in the region. The addition of dithionite did cause an absorbance change with the appearance of a new absorbance peak around 448 nm.

4.3.9 LC/MS Analysis of CYP3A4 Heme and CYP3A4 Apo Protein after Inactivation

The UV/Vis absorbance data indicates that the formation of a MIC or sigma complex is occurring, but that does not rule out the possibility of other heme or apo protein modifications. Therefore, we employed the heme adduct detection method described in Chapter 3 and performed whole protein LC/HRMS. However, neither of these methods detected any other species that could be related to inactivation by CMZ. In summary, we could not detect any covalent modification of CYP3A4 by CMZ.

4.4 Discussion

4.4.1 Chapter Overview and Hypothesis.

The overall goal of the entire study was to determine the probable mechanisms of TDI for CYP isoforms by CMZ. To achieve this goal, we used Silverman's criteria for an MBI as a guide for examining the nature of the TDI, and we also employed techniques to directly address the molecular target of inhibition. By combining the metabolite identification data with this additional information, we aimed to propose rational mechanisms of inhibition.

In view of the data in Chapter 2, heme and protein could be targets of CMZ reactive metabolites generated by CYP2B6, 2E1, and 3A4 that could result in inactivation of the enzyme. The formation of glutathione adducts is indicative of the formation of a reactive metabolite that is at least capable of reacting with thiol groups which are present in cysteine residues in most proteins such as CYP enzymes. We also found an N-oxide metabolite that is a quasi-stable carbene.(168,212,300) Numerous examples of carbenes forming either MIC or alkylating heme exist in the literature, e.g. 1,3-benzodioxazole-containing and diaromatic vinylidene

compounds.(52,54,84) Therefore, we had to investigate the possibility that the apo protein and heme could be targets of CMZ reactive metabolites.

In order to investigate the formation of apo protein adducts, two methods are typically available. Performing studies using a radiolabeled version of the compound of interest is one of the easiest methods to at least detect the formation of an adduct to the protein. The radiolabel can be used to detect a potential adduct through numerous methods such as SDS-PAGE followed by autoradiography or scintillation. However, in the absence of radiolabeled CMZ, we turned to high resolution mass spectrometry. By measuring either whole protein or digested protein via LC/HRMS, we can search for shifts in mass corresponding to potential CMZ adducts.

To investigate the potential of heme being the target of CMZ metabolism mediated inhibition, there are three methods that could be employed. Similar to apo proteins, heme adducts can be investigated by HRMS and we have developed the methodology for detecting heme adducts, which is described in Chapter 3. Additionally, one of the more traditional methods that is used is UV/Visible absorbance. MICs typically do not survive extraction methods for heme and protoporphyrin IX adducts since they likely require the thiol ligand of cysteine to be stable, but these complexes have a characteristic absorbance around 455 nm.(12,54,75,76,187) Heme and protoporphyrin that are the result of alkylations of the pyrroles or meso bridges can have disparate UV/Vis spectra, but should be detectable if the scan range is sufficiently wide.(105,111,117,301) The combination of these techniques can be used to attempt to identify any potential modification of heme that could be causing the apparent TDI.

The identification of the molecular target of inhibition is essential to proposing rational inhibition mechanisms for all three enzymes we examined. If we are able to acquire HRMS data of the adducted apo protein or heme, the exact masses should give the elemental composition of the adducted species. It is possible that fragmentation of the adducted species could result in

some structural information as well. Additionally, the identification of UV/Vis active species related to inhibition will also allow us to propose a reasonable mechanism.

4.4.2 Potential Molecular Target(s) and Mechanism(s) of CYP2B6 TDI by CMZ.

Before performing these mechanism directed studies, there was no information on the molecular target or mechanism for CYP2B6 inhibition. The metabolite identification data in Chapter 2 indicated that CYP2B6 produced both the glutathione adduct (M2) and the N-oxide (M3) metabolite. Since M2 is likely the result of an S-oxide or similar species, the formation of M2 is probably more indicative of protein adduction. It is also possible that M2 formation is related to a radical species that could attack the heme. M3 is most likely to be a heme modifier by either MIC or heme adduct formation since it is a quasi-stable carbene. Therefore, we have to employ other data to suggest a potential mechanism of inhibition.

The activity data from HLM incubations regarding the effects of dialysis, NADPH, GSH, and SOD/CAT give some information regarding the mechanism. The inhibition observed was not reversible by dialysis but was NADPH dependent. The addition of SOD/CAT did not reduce the percent of inhibition, but GSH did cause a statistically significant decrease in inhibition. The most likely interpretation of GSH-mediated reduction of inhibition is that GSH has trapped a reactive species that has left the active site which is at least partially reasonable for the TDI observed. A target of this potential reactive species could be outside of the active site of CYP2B6, but it is not clear since there is no evidence that GSH is unable enter the active site of CYP2B6 or any other CYP enzyme.

The UV/Vis absorbance data suggest that changes at the heme may be possible, but it is not conclusive. There is evidence that the heme is being destroyed during the incubation of reconstituted CYP2B6 with CMZ and NADPH. The loss of absorbance at 377 nm which could be consistent with the loss of high spin character, but there is no corresponding increase of absorbance that could suggest some sort of complex or adduct. As was shown in Chapter 3 and

other sources, CYP enzymes can destroy their own heme through uncoupled reactions which could explain most if not all of the spectral changes that were observed with the NADPH incubation.(262,282) The reduction of CYP2B6 in the presence of CMZ and CMZ N-oxide resulted in changes that may suggest some sort of MIC or sigma complex formation. The addition of dithionite results in a loss of absorbance at 360 and 417 nm with a broad increase around 450 nm and smaller increase consistent with heme reduction at 550 nm. The addition of dithionite to CYP2B6 with CMZ N-oxide resulted in a loss at 417 nm with a broad peak forming at approximately 465 nm and the heme reduction peak at 550 nm. The addition of dithionite could result in metabolism of CMZ by CYP2B6 to a metabolite such as the N-oxide and then a subsequent formation of MI complex or sigma complex. However, we do not have evidence to support this supposition. Additionally, this analysis is complicated by the possibility of DTT being able to reduce CMZ N-oxide. It is known that some heme alkylations can result in UV/Vis active species that are higher than 450 nm so it is possible that dithionite addition to the N-oxide caused a heme alkylation.(52,104,114) Both the CMZ and CMZ N-oxide related absorbance peaks are not large even though we used 1 μM of enzyme so it is possible that the amount formed is low or these species UV/Vis active species are unstable.

We generated LC/HRMS data of both the apo protein and heme after incubation of reconstituted CYP2B6 with CPR and CMZ, but there was no direct detection of any adduct. The rate of inactivation of CYP2B6 by CMZ is not particularly fast which would allow unstable adducts to degrade rapidly in solution or be at such low levels that issues such as in source fragmentation are sufficient to eliminate any detectable signal. Since we used concentrations of 1-2 μM CYP2B6, which are at the upper limit of the dynamic range for the AB Sciex 5600 and Waters Synapt G2 instruments for heme and apo protein detection, and the adducts are potentially unstable, it is unlikely that we can improve our methods substantially to detect possible adducts.

When taken together, these data do not exclude apo protein or heme as potential targets, but it is possible that the apo protein is one target. The addition of glutathione results in a reduction of inactivation by CMZ. This reduction of inhibition is consistent with the reactive species leaving the active site and adducting a target outside of the active site since it is believed that GSH is not able to enter the active site. M2 is the result of a GSH trapping so it is the most likely species we have identified that is related to the inactivation of CYP2B6. One of the most likely species for this type of reactivity is an S-oxide, and reaction scheme for thiol from either a protein or GSH is presented in Figure 4.20.(174,175) This indirect evidence suggests that protein could be a target, but it does not exclude heme also being effected.

4.4.3 Potential Molecular Target(s) and Mechanism(s) of CYP2E1 TDI by CMZ.

Similar to CYP2B6, the previous data did not exclude apo protein or heme from being the molecular target of CMZ TDI with CYP2E1. M2 and M3 were both present in the recombinant incubations which would be consistent with either protein or heme as a target. Therefore, other assays were necessary to identify the molecular target of inhibition.

We measured the remaining activity from HLM incubations that after preincubation with various components, such as GSH, other CYP2E1 substrates, NADPH, and SOD/CAT, and dialysis, and the data from those assays were more complex than that of CYP2B6. Preincubation with NADPH and GSH appear to increase the activity of CYP2E1 after dialysis unless ethanol is added to the preincubation. The addition of NADPH likely leads to metabolism of an endogenous inhibitor in the HLM which is displaced or solvated by ethanol so that could be removed from the microsomes in the incubation. The solubilized inhibitor could then have been removed by the dialysis step. GSH appears to cause increases in activity with or without NADPH also in the preincubation. Therefore, GSH may not just trap reactive species, but GSH may also serve as a post translational modification (PTM) or a regulator of PTM.(302-307) Glutathionylation is a known PTM that can occur with cells undergoing oxidative stress that can alter the function of

proteins, such as those in the mitochondria. It is possible that CYP2E1 in our HLM preparation may be glutathionylated and the addition of GSH removes the glutathionylation by forming GSSG. It is possible that this removal of the PTM could result in higher activity of CYP2E1 as was seen with our incubations. These complications led us to the paired normalizations that we used to interpret our results from these assays.

Our results from these activity assays indicate that the majority of the inhibition for CYP2E1 is likely due to a NADPH dependent species that does not leave the activity site, and that CYP2E1 possibly fits Silverman's criteria for an MBI. The addition of SOD/CAT appeared to have no detectable effect upon the inhibition by CMZ so uncoupled reactive oxygen species released from CYP2E1 have little or no contribution to CYP2E1 TDI. It appears GSH has a very mild effect upon the apparent TDI by CMZ that is only statistically significant when combined with the co-incubation NADPH and chlorzoxazone (CHZ), a CYP2E1 substrate so the inactivation of CYP2E1 by CMZ is mostly due to the formation of the inactivating species in the active site without release. We used two CYP2E1 substrates, chlorzoxazone and ethanol, at concentrations at least 10-fold above their reported K_m to attempt to compete against the inactivating reaction of CYP2E1 TDI, and only ethanol was truly successful. It is not clear whether this is a result of binding site differences or insufficient concentrations of CHZ to compete against CMZ inactivation of CYP2E1, but inactivation by CMZ can be inhibited by a substrate of CYP2E1. All of these parameters for the inactivation fit with Silverman's criteria for a MBI.

Even though the HLM activity data indicated that the target was likely in the active site, further experiments were required to determine the molecular target of inhibition. We performed UV/Vis experiments and LC/HRMS experiments of apo protein and heme to identify the molecular target of inhibition similarly to CYP2B6. While the UV/Vis data is inconclusive, the LC/HRMS data indicate heme is a target of CMZ inactivation of CYP2E1.

The UV/Vis absorbance data for CYP2E1 was slightly more indicative of the mechanism and molecular target of inhibition, but it was inconclusive. Unlike CYP2B6, we were able to generate CMZ and CMZ N-oxide binding spectra that were clearer in their interpretation. CMZ and CMZ N-oxide produced clear Type II spectra with CYP2E1. Dithionite had no discernable effect upon CMZ binding but did cause the formation of an increase in absorbance at 448 nm when N-oxide is present. The presence of the 448 nm species would be consistent with the formation of an MI complex or sigma complex from the N-oxide metabolite.(54,83,84,110) However, the incubation of reconstituted CYP2E1 with CMZ only yielded the loss of absorbance at 430 nm and no increase in absorbance at any wavelength including 448 nm. These data indicate that CMZ N-oxide, which is generated by CYP2E1, can form a complex with heme in CYP2E1, but it is not clear whether that complex forms or is stable when generated by metabolic turnover.

The HRMS data indicate that heme is likely the only molecular target of inhibition by CMZ. We could not detect any protein adducts from CMZ incubations in multiple attempts by both whole protein and trypsin digests even though we could reproduce the protein adducts of diethyldithiocarbamate.(102) However, we did detect a PPIX adduct consistent with the addition oxygen to CMZ. Since CMZ N-oxide is a stable carbene, the N-oxide metabolite could have formed a MI complex then migrated to the nitrogen of a pyrrole or bridged two pyrroles which resulted in the loss of iron as depicted in Figures 4.14 and 4.21. These adducts are not stable and will degrade rapidly at room temperature as evidenced by their disappearance after 2 hours when the same sample is reinjected (data not shown). The optimal incubation time for generating these adducts appeared to be 5 minutes since longer incubation times led to lack of detectable adducts, but shorter times also led to even lower signal. The probable structures of a CMZ N-oxide related heme adduct contains 3 or 4 electronegative heteroatoms directly attached to the carbon where the carbene would initially exist. These configurations would leave the carbon

highly electrophilic and could lead to the apparent instability of the adduct. While it is possible that there is an unstable protein adduct, we are able to clearly detect an unstable PPIX adduct that would explain the inactivation of CYP2E1 by CMZ.

4.4.4 Potential Molecular Target(s) and Mechanism(s) of CYP3A4/5 TDI by CMZ.

As with CYP2B6 and CYP2E1, CYP3A4 and CYP3A5 generated both M2 and M3 so we were unable to propose the molecular target of inhibition by CMZ from data in Chapter 2. Therefore, we had to employ the same activity assays, UV/Vis methods, and HRMS methods used with CYP2B6 and CYP3A4 to identify the potential targets of inhibition and to propose a mechanism of inhibition.

We employed similar activity assays with HLM as we did with CYP2B6 and CYP2E1 to examine the influence of various factors upon CMZ inactivation of CYP3A4/5. The inactivation of CYP3A4/5 by CMZ was shown to be NADPH dependent and resistant to dialysis. The addition of SOD/CAT to the preincubation may have caused a slight increase in activity, but it was not statistically significant. The addition of GSH to the preincubation did cause a statistically significant reduction in apparent inhibition by CMZ. In the case of CYP3A4/5, it is most likely that GSH is trapping a reactive species that has left the active site which is lowering the overall inhibition, but we do not have evidence to fully exclude other possibilities. There are at least two possible alternative explanations for the apparent changes in activity. It is possible that glutathionylation can alter CYP3A4/5 activity in a substrate specific manner which results in lowering CMZ inactivation but changing not 1'-hydroxymidazolam formation. Also, midazolam is a known TDI, but the mechanism is not known. GSH may serve to protect CYP3A4/5 from reactive species generated from midazolam metabolism that would retain 1'-hydroxymidazolam activity. Since midazolam is a known TDI, we avoided midazolam and used testosterone as the competitive substrate for the competition experiment with CMZ inactivation.(32,98) We did not see any effect of testosterone upon the apparent inhibition which could be the result of multiple

factors including: the lack of a shared active site between testosterone metabolism and CMZ metabolism that results in inactivation, insufficiently high concentrations of testosterone to compete with the CMZ concentration used in the assay, and the multiple site binding nature of testosterone simultaneously enhancing the rate of inactivation when CMZ is bound in the active site and competing at the binding site of CMZ bioactivation. These activity results suggest apo protein could be a target, but we required more evidence for determining the molecular target of inhibition.

In the case of CYP3A4, the UV/Vis absorbance data indicate that heme is a molecular target of CMZ inhibition of CYP3A4. The binding spectra of reconstituted CYP3A4 is similar to that of CYP2B6 with a loss of absorbance at 417 nm and no corresponding increase at any wavelength. The binding spectra of CMZ N-oxide is similar to Type II with absorbance increasing at 429 nm, but there is no corresponding decrease in absorbance. When dithionite is added, the 429 nm absorbance peak decrease, but a new maximum appears at 451 nm. The time course of reconstituted CYP3A4 with CPR and incubated with NADPH and CMZ resulted in a loss of absorbance at 389 nm and a broad increase in absorbance at 451 nm. These changes in absorbance are consistent with the loss of high spin and the gain of a MI or Sigma complex, and the appearance of the 451 nm maximum closely resembles the spectra of CYP3A4 in the CMZ N-oxide and dithionite.(54,83,84,110) Since CYP3A4 can produce the CMZ N-oxide metabolite and the 451 nm absorbance peak exists in the time course of CMZ inactivation, we propose that CYP3A4 is inhibited by CMZ at least partially through the generation of an N-oxide metabolite which then forms a MI or sigma complex with CYP3A4.

To further investigate the nature of CMZ inactivation, we performed LC/HRMS analysis of apo protein and heme as we did with the other isoforms. Our analysis of whole protein and heme did not yield any detectable adducts. Again, the lack of detectable adducts using our methods

does not exclude the possibility of unstable species being formed that did not survive our analysis procedure.

We suggest that CYP3A4 undergoes a process of inhibition similar to CYP2E1, as presented in Figure 4.21. It is clear that we have formation of a heme modification that is very likely to be a MI or sigma complex formed with M3, but it is not clear why this complex does not rearrange into detectable amounts of a heme or PPIX adduct as is likely the case with CYP2E1. It is possible that the active site topology of CYP3A4 could restrict migration of CMZ N-oxide to pyrrole nitrogens or otherwise stabilize the MI or sigma complex that is initially formed. Additionally, the rate of CYP3A4/5 inactivation is far slower than that of CYP2E1 so it is also possible that the rearranged product does not build up to sufficient concentrations that are detectable.

4.5 Conclusions

In this chapter, we have investigated the mechanisms of apparent TDI for CYP2B6, CYP2E1, and CYP3A4/5. Even though the depth and strength of evidence that can be employed to propose mechanisms of inhibition vary significantly from isoform to isoform, these isoforms have common elements in their inhibition by CMZ. Each of these isoforms is inhibited by NADPH dependent processes that follow an enzyme kinetic model for inactivation and the inhibition is not reversible via dialysis. The reduction of inhibition by the addition of GSH with all three isoforms suggests the possibility of reactive metabolites inhibiting these enzymes after release from the active site. If this supposition is true then none of these enzymes are undergoing a process that is a true MBI as set forth by Silverman's criteria.(11) However, we have not found direct evidence that apo protein is the target of CMZ inhibition, and other explanations can be applied to explain at least some of the apparent reduction of activity loss. Additionally, SOD/CAT had no influence upon any of the inactivation seen with any of the isoforms so the release of reactive oxygen

species from the active site plays no discernable role in the process of inhibiting any of these isoforms by CMZ.

The weakest level of mechanistic evidence for inhibition of the isoforms is that of CYP2B6. The data for CYP2B6 is somewhat conflicted and weak since we have only indirect evidence that can suggest that apo protein or heme. Both M2 and M3 are formed by CYP2B6 metabolism of CMZ which leave both targets as being possible. Reduction of CMZ inhibition by GSH would be consistent with an apo protein modification since catalytically relevant heme exists only in the active site, but there are potential caveats such as glutathionylation. The UV/Vis spectral data are fairly weak since the inactivation of the enzyme does not yield any UV/Vis active peak that is informative. The data related to dithionite reduction of CYP2B6 does show that there may be interactions of CMZ and M3, but the absorbance changes are not as large or dramatic as was seen with CYP2E1 and especially CYP3A4. The HRMS analysis of CYP2B6 apo protein and heme yielded no adduct so we cannot definitively assign whether the mechanism from Figures 4.20 and 4.21 or another mechanism are operating during the inactivation process.

We have direct evidence for the inhibition of CYP2E1 and CYP3A4/5 that are consistent with the modification of heme and the inhibition of these isoforms is likely due, at least in part, by the formation of the N-oxide metabolite (M3). In the case of CYP2E1, we directly measured an unstable PPIX adduct corresponding to the m/z of mono oxygenated CMZ and protoporphyrin IX. For CYP3A4/5, we matched the UV/Vis maxima peak of the M3 in a reduced CYP3A4 complex with the spectra from a time course of inactivation of reconstituted CYP3A4 with CPR. Since M3 is a quasi stable carbene, it is likely that CYP2E1 and CYP3A4 initially form the same complex with M3 that either mostly remains as an MI or Sigma complex, as in the case of CYP3A4, or rapidly rearranges to a protoporphyrin IX adduct, as in the case of CYP2E1. These data are the first to strongly support the idea of thiazole N-oxides irreversibly inhibiting CYP enzymes, and this discovery can serve to inform drug design in the future.

4.6 Future Directions

Potential directions for the further investigation of CMZ are numerous. We did not generate sufficient data to strongly suggest the mechanism of CYP2B6 inhibition by CMZ, and we did not rule out other contributors to the inactivation of CYP2E1 and CYP3A4/5 so it is possible to further investigate CMZ in this regard. We have only scratched the surface of allosterism with CYP3A4/5 since our model is only really descriptive. Also, we have not used our selectivity data to assess the potential impact and dosing of CMZ upon DDI and CYP2E1 mediated toxicity, such as acetaminophen and alcohol induced steatosis.(1,17,63,204,205,207,308-314)

Even though we have substantial support for the involvement of the N-oxide in the inactivation of CYP2E1 and CYP3A4/5, we do not have clear mechanistic evidence for inhibition of CYP2B6, and we cannot exclude the contribution of other metabolites to the inactivation of these isoforms. Since we used high concentrations of purified enzymes to perform our analyses, it is unlikely we can choose a better system to perform these experiments. Therefore, we have only two avenues available to us that could improve our chances at detecting potential adducts. The first is the further optimization of our current methods for generating and detecting apo protein and heme adducts, and the second is the generation of site specific labeled or modified versions of chlormethiazole that can alter the rates or even mechanisms of inactivation.

During our studies, we found that heme adducts in purified reconstituted systems tended to form rapidly, but often would degrade when incubation times were extended beyond 5 to 10 minutes. Additionally, increasing the CPR to CYP ratio also appeared to be deleterious in some cases. Adducts formed in microsomal incubations tended to require longer incubation times and appeared to be more stable. This observation is in line with the lower CPR to CYP ratio in LM as compared to reconstituted systems. It is possible that we did not test sufficient conditions to optimize the conditions for CYP2B6 or CYP3A4 to detect heme adducts nor did we optimize the incubation times for apo protein sufficiently. More testing with various known adduct forming

compounds could be done to more fully optimize the conditions for a broad selection of compounds, and those conditions could be applied to these enzymes to improve the chances of detecting any adduct.

Modification of CMZ by isotope labeling or other means could be useful in determining the mechanism of inhibition for CMZ for CYP2B6 and in adding more mechanistic information for CYP2E1 and CYP3A4/5, but there are other issues. We have attempted to synthesis the deuterated C-4 methyl analog, but we had encountered three major issues. The incorporation of deuterium was one of the biggest roadblocks since the deuterium must be incorporated early in the total synthesis of the compound and the deuterium must be retained during the rest of the process. We have mostly alleviated this issue with 97% deuterium content at that C-4 methyl, but issues of purification and yield still remain. There is a contaminant of similar mass and chromatographic properties that is present in the preparation we have so far. Even though CMZ is the major species, any detectable contaminant of similar mass could raise issues with the interpretation of experiments comparing the labeled and unlabeled compounds, such as kinetic isotope experiments. Even though we had used flash chromatography to prepare the compound, we were unable to remove the contaminating species during this purification. It is possible that we need to use reversed phase chromatography to remove the contaminant. As also mentioned, the yield was low from our process as about 1 gram of starting material yielded only 21 mg of D_3 sample. Further optimization maybe required in order to generate sufficient material for further purification and use in subsequent experiments. The deuterium labeling of the C-2 carbon and chlorethyl carbons should be possible, but these processes will need substantial optimization. We do not have a means of blocking or dramatically slowing the rate of oxidation at nitrogen or sulfur without dramatic changes that could cause difficulty interpretation. Isotope labeling of nitrogen would not result in a detectable change in inactivation rates and alkylation would cause the formation of ylide that can act in a similar manner as the N-oxide. Isotope labeling of sulfur is

practically useless since the percentage change in mass between sulfur isotopes is even smaller than nitrogen. Selective alkylation or oxidation of the sulfur does not seem possible with our current synthesis route so there may not be a viable path forward.

There is much work that could be done in regards to the effects of CMZ allosterism with CYP3A4/5. The identification of the binding sites could be investigated through methods such NMR, crystallography, or hydrogen-deuterium exchange mass spectrometry. Binding site affinities could be investigated by the use of kinetics of metabolite formation of CMZ or other binding methods such as surface plasmon resonance (SPR).(28,269,315-321) Since it is possible that the increase in 1'-hydroxymidazolam turnover could be a function of better coupling or changes in CYP3A4 structure that increases in rates of metabolite formation, these avenues can be investigated as well.

Most studies that employ CMZ to inhibit CYP2E1 in vitro or in vivo do so without regard to concentrations required to selectively inhibit CYP2E1 as cleanly as possible.(1,151,204-207,322,323) The ideal dosing regimen for CMZ should maintain concentrations high enough to suppress CYP2E1 activity nearly completely, but those same concentrations should not substantially affect the activity of other CYPs and should not approach the concentrations required for $GABA_A$ agonism.(140,142,324,325) With our in vitro kinetic data and in vivo data of CMZ disposition, we should be able to estimate dosing regimens using PBPK modelling that would fulfill those requirements and validate those regimens. It would then be finally possible to interpret the real effects of CYP2E1 inhibition upon any disease or condition mediated by CYP2E1 metabolism.

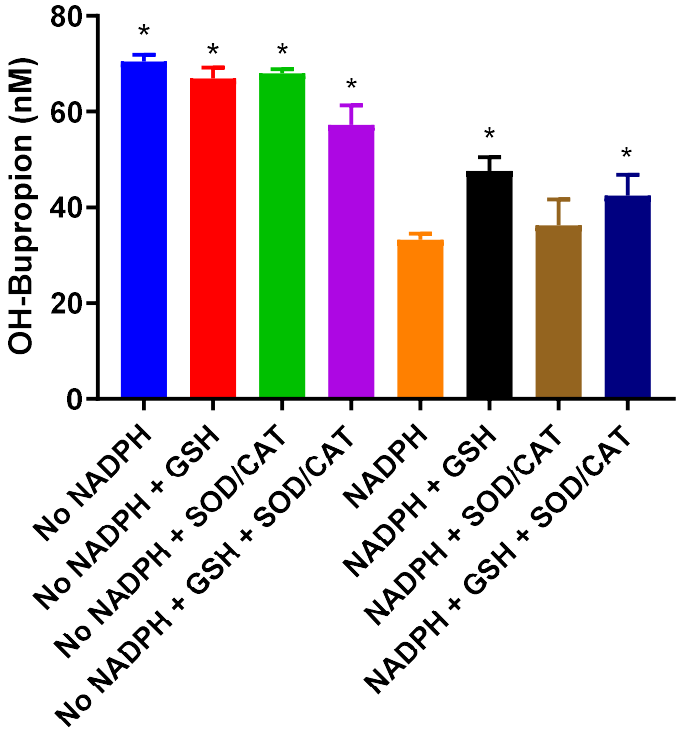

Figure 4.1 Effects of NADPH, GSH, and SOD/CAT upon CYP2B6 Inactivation in HLM Incubations

100 μM CMZ preincubated with HLM in various combinations of NADPH, GSH, and SOD/CAT and the remaining CYP2B6-mediated bupropion hydroxylase activity was assessed after dialysis.

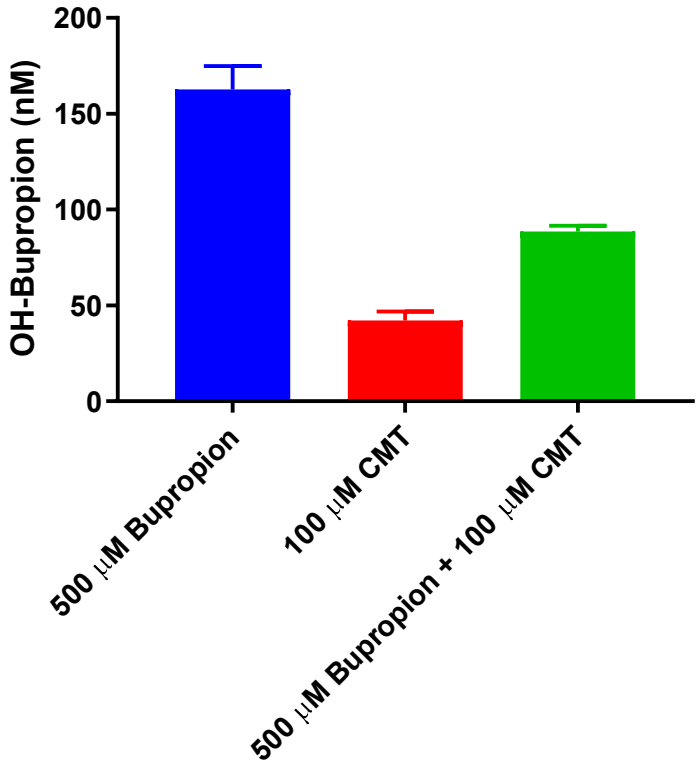

Figure 4.2 Effects of Dialysis and Co-incubation of CMZ with Bupropion upon TDI of CYP2B6 in HLM Incubations
100 μM CMZ, 500 μM bupropion, or both were preincubated with HLM and the remaining CYP2B6-mediated bupropion hydroxylase activity was assessed after dialysis.

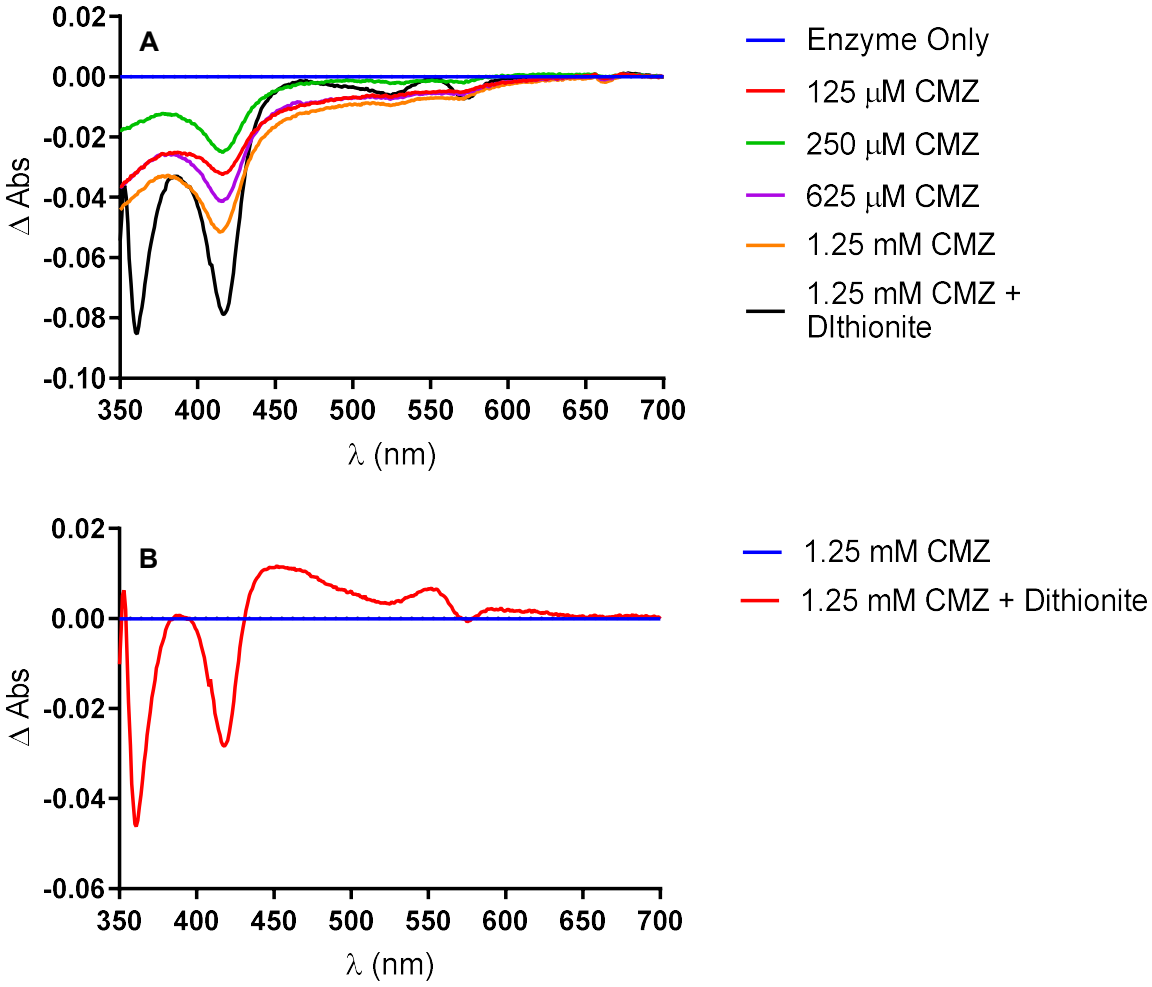

Figure 4.3 Calculated Difference Binding Spectra of CMZ with CYP2B6 Reconstituted with Lipid

CMZ was added at various concentration to detect spectral changes associated with CMZ binding. The reference cuvette contains all of the same components as the sample cuvette except CYP2B6 reconstituted with lipid only. In panel A, all spectra were calculated in reference to the enzyme only scan that was set as the baseline. In panel B, the spectra for 1.25 mM CMZ were used as a reference to identify changes caused by dithionite.

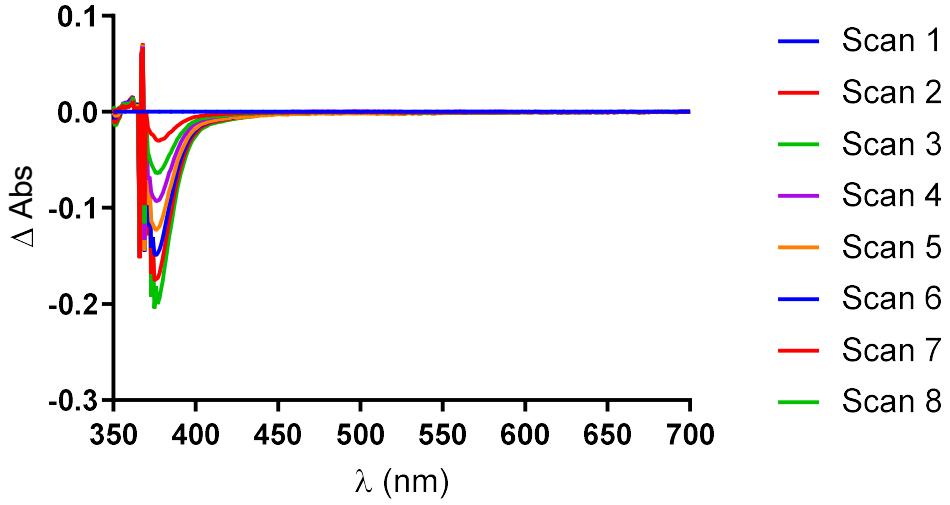

Figure 4.4 Time Course of Calculated Difference Spectra of CYP2B6 Inactivation by CMZ To detect time dependent changes of CYP2B6 UV/Vis spectra related to CMZ inactivation, 1.25 mM of CMZ was added to CYP2B6 reconstituted with lipid and CPR, and the reaction was initiated with NADPH. The reference cuvette contained all components except reconstituted enzyme. The initial scan was obtained after the addition of NADPH, and each subsequent scan is normalized against that scan to show time dependent effects related to CMZ inactivation of CYP2B6.

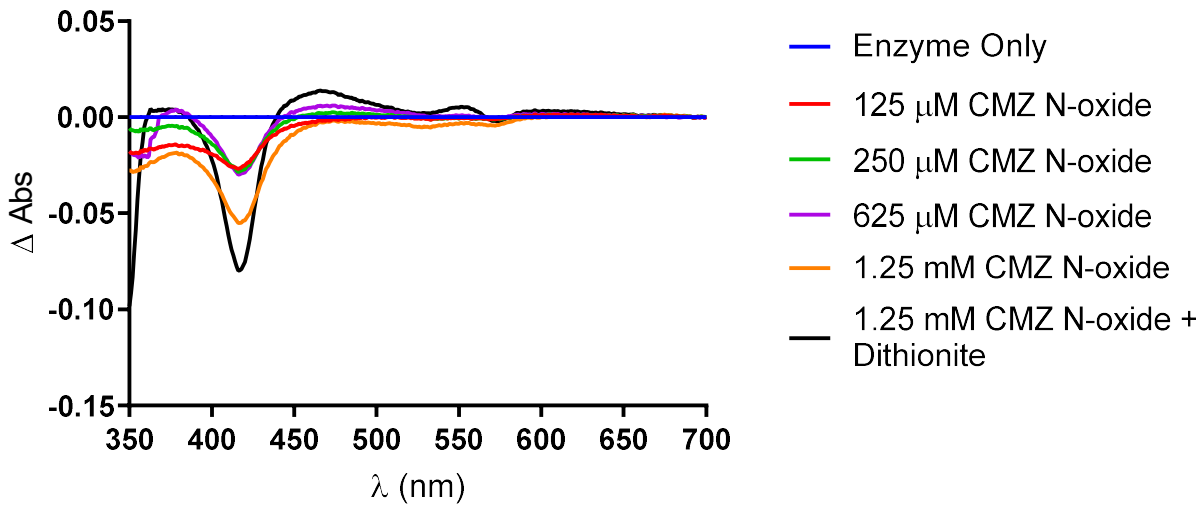

Figure 4.5 Calculated Difference Spectra of CMZ N-oxide with CYP2B6 Reconstituted with Lipid

CMZ N-oxide and dithionite were added to CYP2B6 reconstituted with only lipid to identify the binding mode of CMZ N-oxide and to explore whether CMZ N-oxide could form a MI or sigma complex wth CYP2B6. The reference cuvette contains all of the same components as the sample cuvette except CYP2B6 reconstituted with lipid only. All spectra were calculated in reference to the enzyme only scan that was set as the baseline.

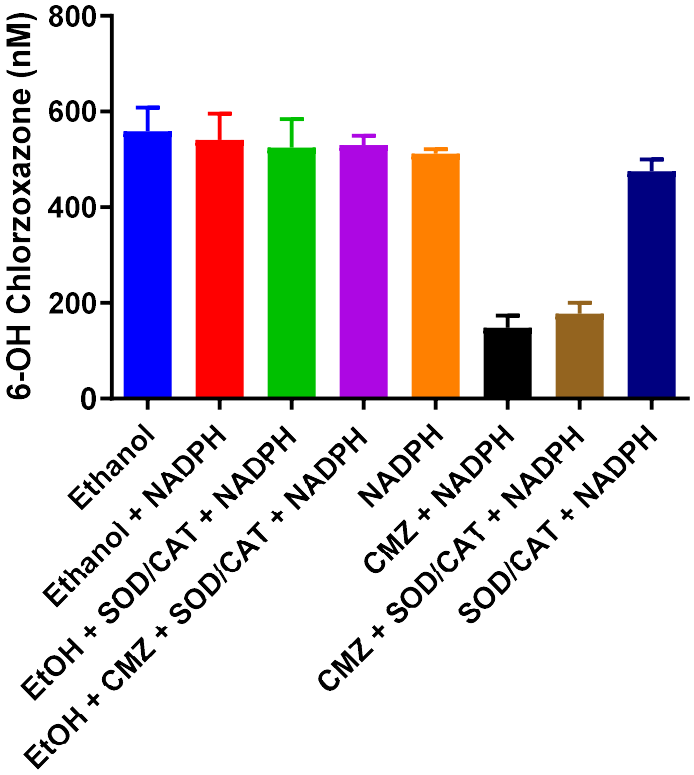

Figure 4.6 Effects of Dialysis, Ethanol, and SOD/CAT upon CMZ Inactivation of CYP2E1 in HLM Incubations

100 μM CMZ, 110 mM ethanol, NADPH, and SOD/CAT were preincubated with HLM in various combinations, and the remaining CYP2E1-mediated chlorzoxazone 6-hydroxylase activity was assessed after dialysis.

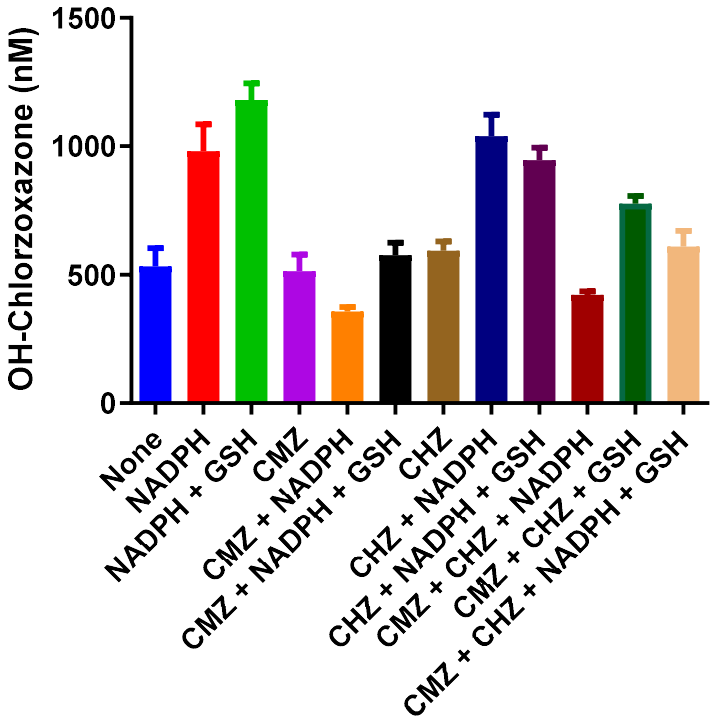

Figure 4.7 Effects of Dialysis, NAPDH, GSH, and CHZ upon CMZ Inactivation of CYP2E1 in HLM Incubations

100 μM CMZ, 500 μM chlorzoxazone, NADPH, GSH, and SOD/CAT were preincubated with HLM in various combinations, and the remaining CYP2E1-mediated chlorzoxazone 6-hydroxylase activity was assessed after dialysis.

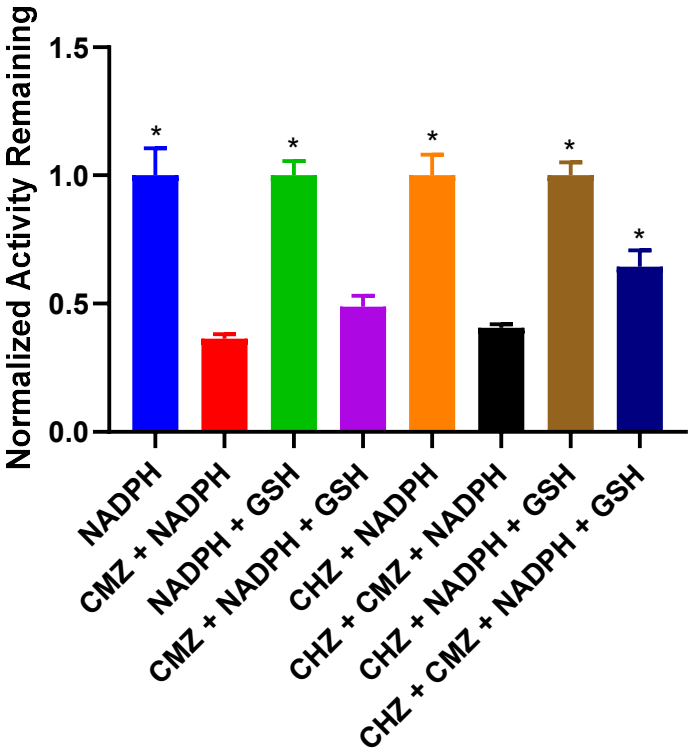

Figure 4.8 Effect upon Normalized Activity of Various Preincubation Components upon CMZ Inactivation of CYP2E1 in HLM Incubations

Activities from Figure 4.6 were normalized in pairwise by matching incubation components to the member of the pair not containing CMZ being set as 100% activity.

*: Indicates statistical significance ($p < 0.05$) as compared to CMZ + NADPH sample

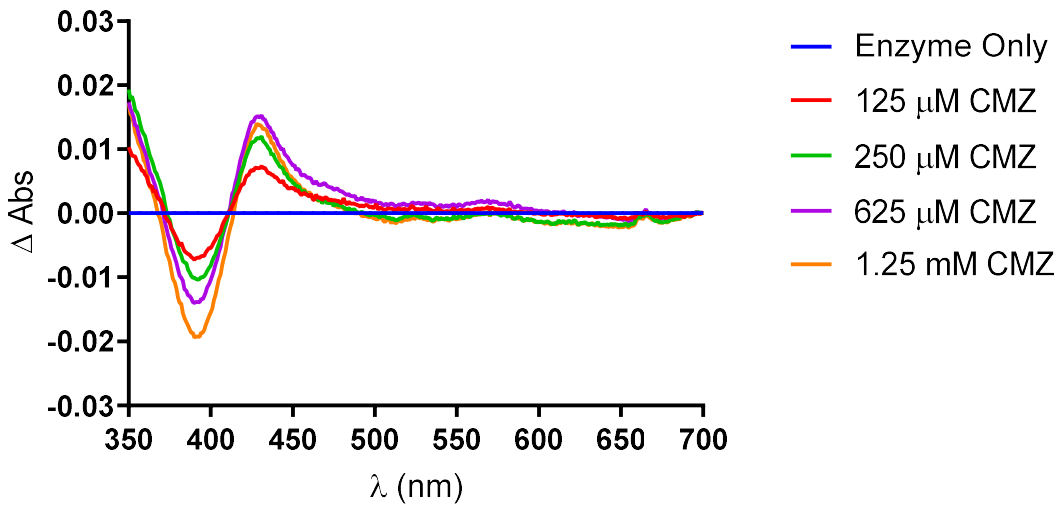

Figure 4.9 Calculated Difference Binding Spectra of CMZ with CYP2E1 Reconstituted with Lipid

CMZ was added at various concentration to detect spectral changes associated with CMZ binding. The reference cuvette contains all of the same components as the sample cuvette except CYP2E1 reconstituted with lipid only. All spectra were calculated in reference to the enzyme only scan that was set as the baseline.

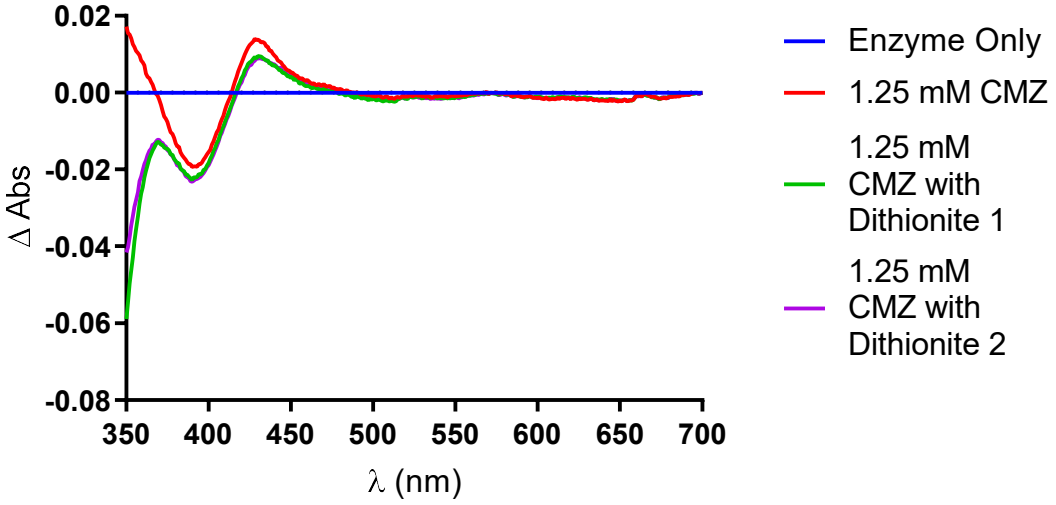

Figure 4.10 Effect of Dithionite upon Calculated Difference Binding Spectra of CMZ with CYP2E1 Reconstituted with Lipid

Dithionite was added to CYP2E1 was added to detect spectral changes associated with heme reduction and CMZ binding. The reference cuvette contains all of the same components as the sample cuvette except CYP2E1 reconstituted with lipid only. All spectra were calculated in reference to the enzyme only scan that was set as the baseline.

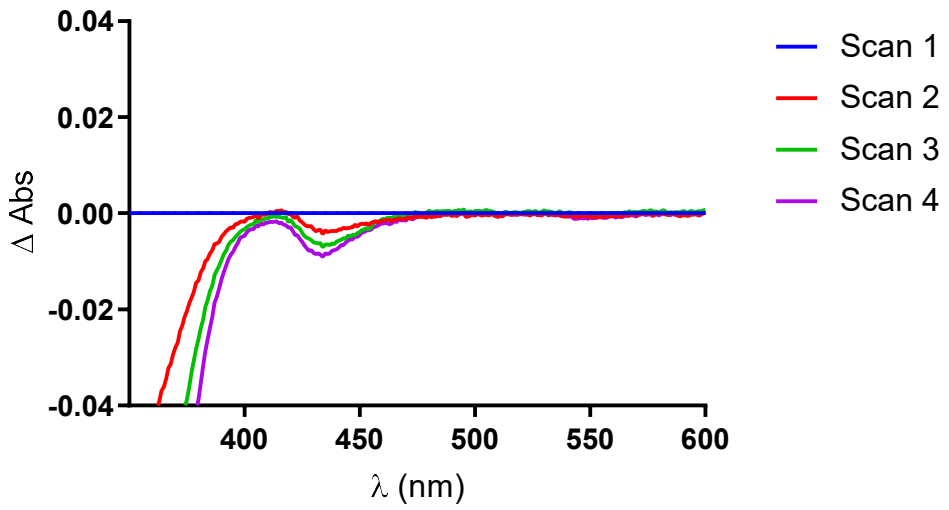

Figure 4.11 Time Course of Calculated Difference Spectra of CYP2E1 Inactivation by CMZ

To detect time dependent changes of CYP2E1 UV/Vis spectra related to CMZ inactivation, 1 mM of CMZ was added to CYP2E1 reconstituted with lipid and CPR, and the reaction was initiated with NADPH. The reference cuvette contained all components except reconstituted enzyme. The initial scan was taken after the addition of NADPH, and each subsequent scan is normalized against that scan to show time dependent effects related to CMZ inactivation of CYP2E1.

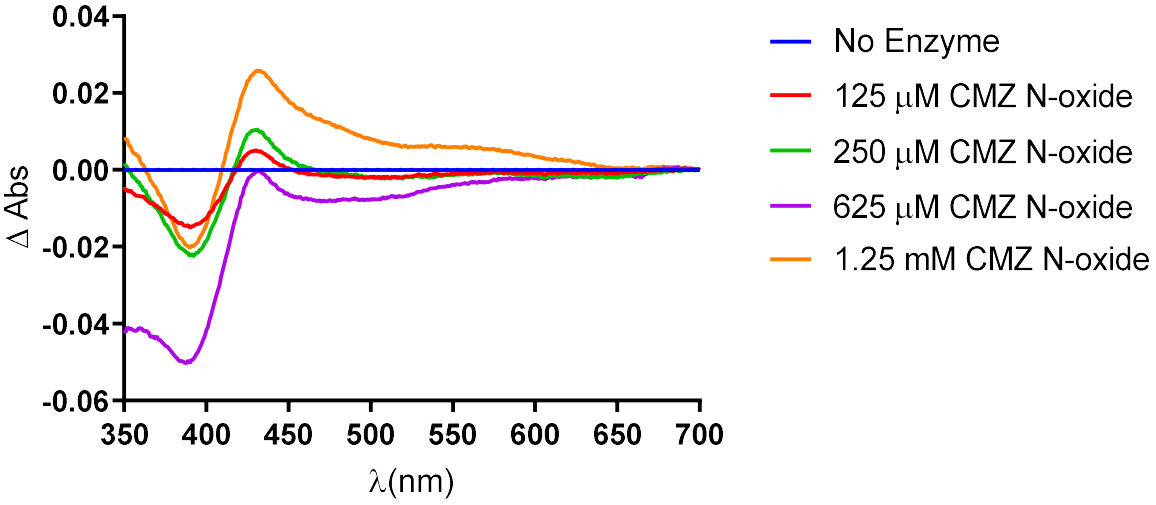

Figure 4.12 Calculated Difference Binding Spectra of CMZ N-oxide with CYP2E1 Reconstituted with Lipid Alone

CMZ N-oxide and dithionite were added to CYP2E1 reconstituted with only lipid to identify the binding mode of CMZ N-oxide with CYP2E1. The reference cuvette contains all of the same components as the sample cuvette except CYP2E1 reconstituted with lipid only. All spectra were calculated in reference to the enzyme only scan that was set as the baseline.

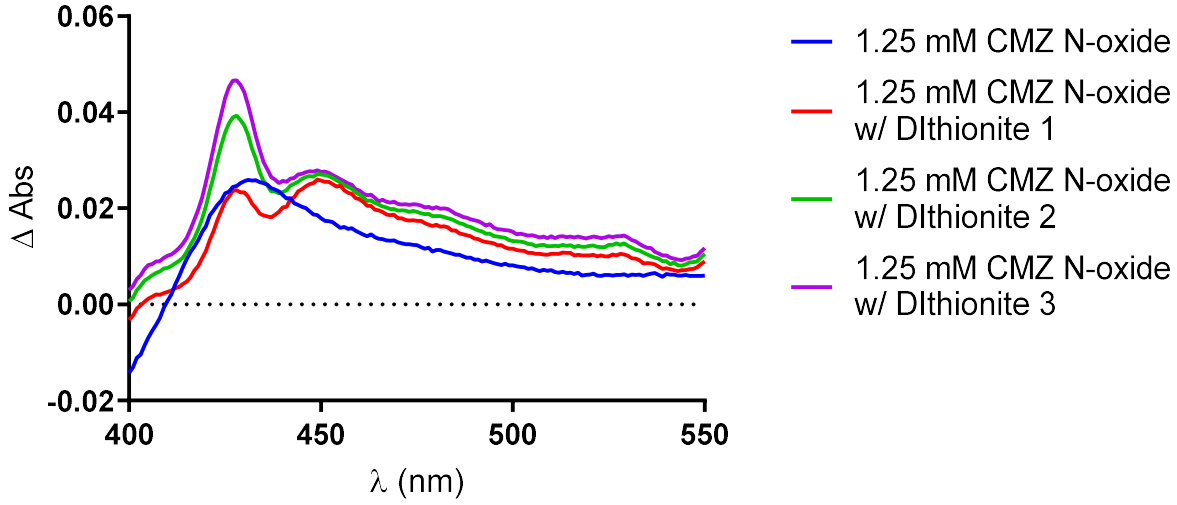

Figure 4.13 Effect of Dithionite upon Calculated Difference Binding Spectra of CMZ N-oxide with CYP2E1 Reconstituted with Lipid

CMZ N-oxide and dithionite were added to CYP2E1 reconstituted with only lipid to identify the binding mode of CMZ N-oxide and to explore whether CMZ N-oxide could form a MI or sigma complex wth CYP2B6. The reference cuvette contains all of the same components as the sample cuvette except CYP2B6 reconstituted with lipid only. All spectra were calculated in reference to the enzyme only scan that was set as the baseline.

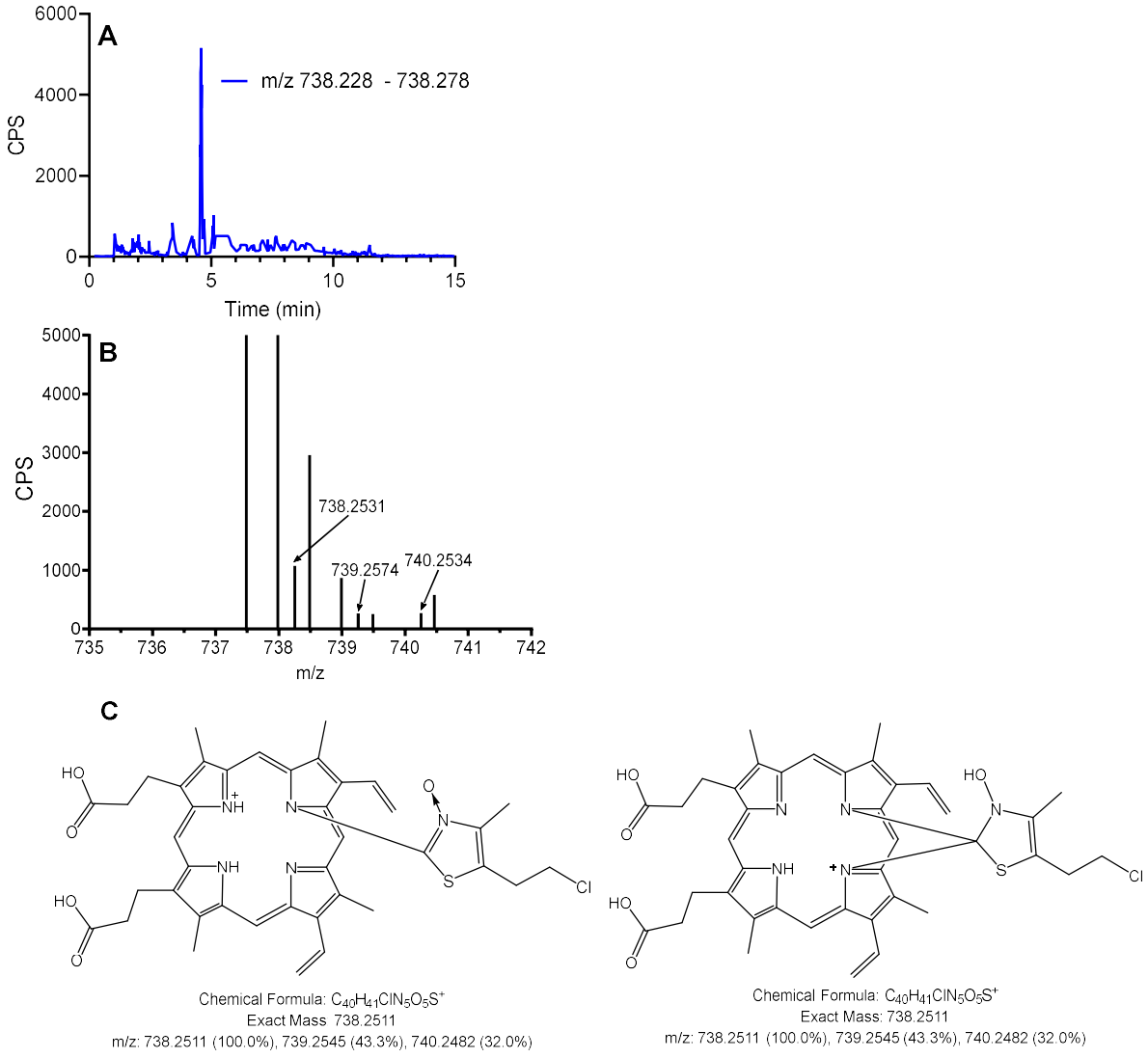

Figure 4.14 Extracted Ion Current (A), TOF Spectra (B), and Proposed Structure of the Putative CMZ N-oxide Protoporphyrin IX Adducts from Reconstituted CYP2E1 Incubation (C)

CYP2E1 reconstituted with lipid and CPR was incubated with CMZ for 5 minutes, and the heme adduct detection method from Chapter 3 was applied. Panel A is the extracted ion current (XIC) of the only species consistent with a CMZ related heme or protoporphyrin IX adduct. Panel B shows the spectra from the peak identified in the XIC. Panel C depicts two possible configurations of a N-oxide related adduct that match the putative adduct.

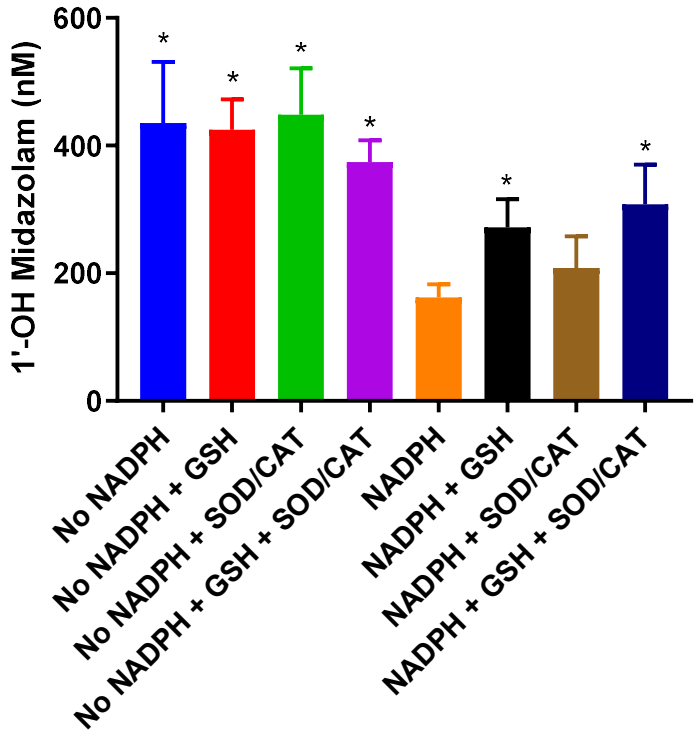

Figure 4.15 Effects of NADPH, GSH, and SOD/CAT upon CYP3A4/5 Inactivation in HLM Incubations

10 mM of CMZ was preincubated with HLM in various combinations of NADPH, GSH, and SOD/CAT and the remaining CYP3A4/5-mediated midazolam 1'-hydroxylase activity was assessed aftfer dialysis.

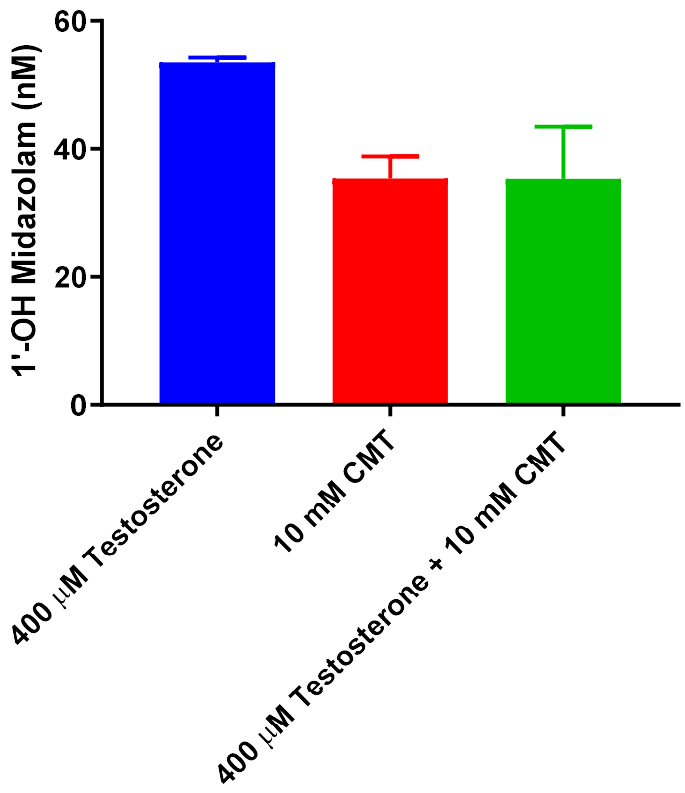

Figure 4.16 Effects of Dialysis and Co-incubation of CMZ with Testosterone upon TDI of CYP3A4/5 in HLM Incubations
10 mM CMZ, 400 µM testosterone, or both were preincubated with HLM and the remaining CYP3A4/5-mediated midazolam 1'-hydroxylase activity was assessed after dialysis.

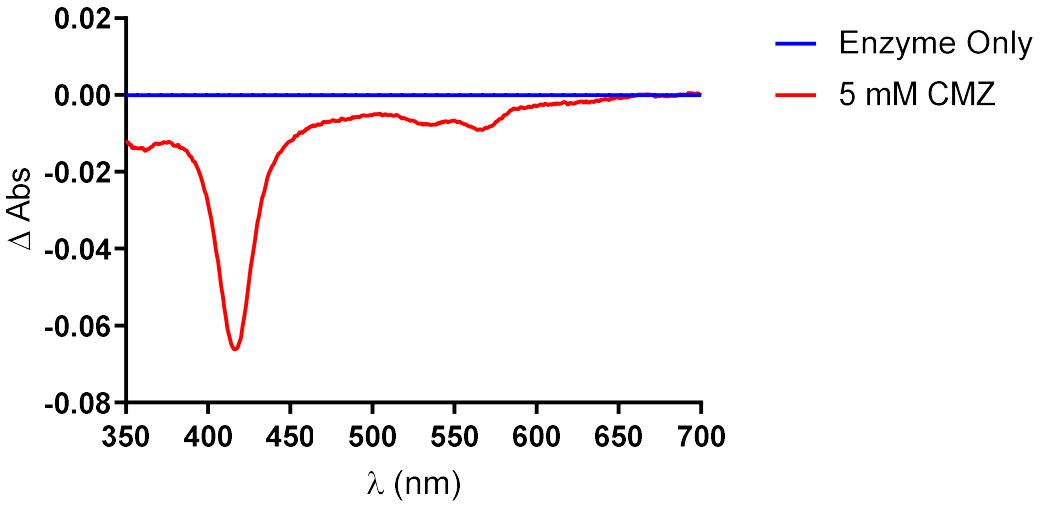

Figure 4.17 Calculated Difference Spectrum of CMZ Binding with CYP3A4 Reconstituted with Lipid

5 mM CMZ was added to detect spectral changes associated with CMZ binding. The reference cuvette contains all of the same components as the sample cuvette except CYP3A4 reconstituted with lipid only. All spectra were calculated in reference to the enzyme only scan that was set as the baseline.

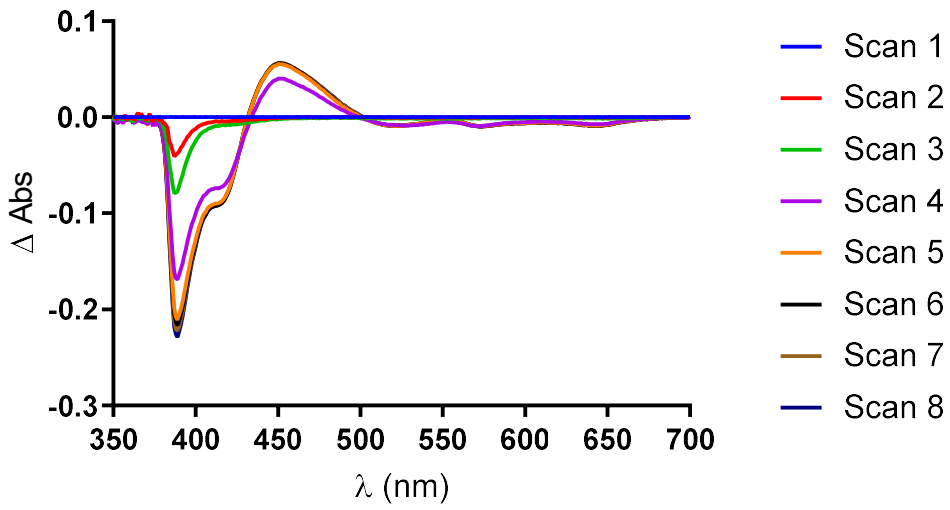

Figure 4.18 Calculated Difference Spectrum of CYP3A4 Reconstituted with Lipid and CPR Incubated with 5 mM CMZ and NADPH
To detect time dependent changes of CYP3A4 UV/Vis spectra related to CMZ inactivation, 5 mM of CMZ was added to CYP3A4 reconstituted with lipid and CPR, and the reaction was initiated with NADPH. The reference cuvette contained all components except reconstituted enzyme. The initial scan was taken after the addition of NADPH, and each subsequent scan is normalized against that scan to show time dependent effects related to CMZ inactivation of CYP3A4.

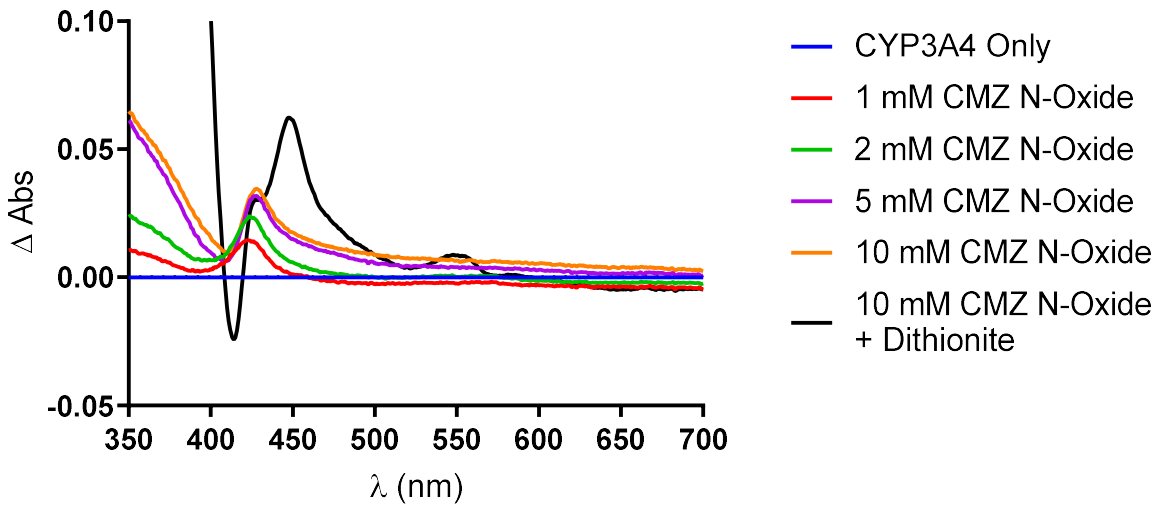

Figure 4.19 Effect of Dithionite upon Calculated Difference Binding Spectra of CMZ N-oxide with CYP3A4 Reconstituted with Lipid

CMZ N-oxide and dithionite were added to CYP3A4 reconstituted with only lipid to identify the binding mode of CMZ N-oxide and to explore whether CMZ N-oxide could form a MI or sigma complex wth CYP3A4. The reference cuvette contains all of the same components as the sample cuvette except CYP3A4 reconstituted with lipid only. All spectra were calculated in reference to the enzyme only scan that was set as the baseline.

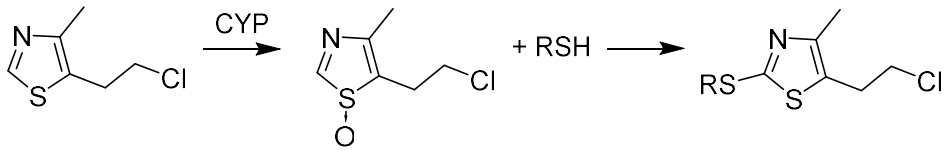

Figure 4.20 Proposed Reactivity of CMZ S-Oxide

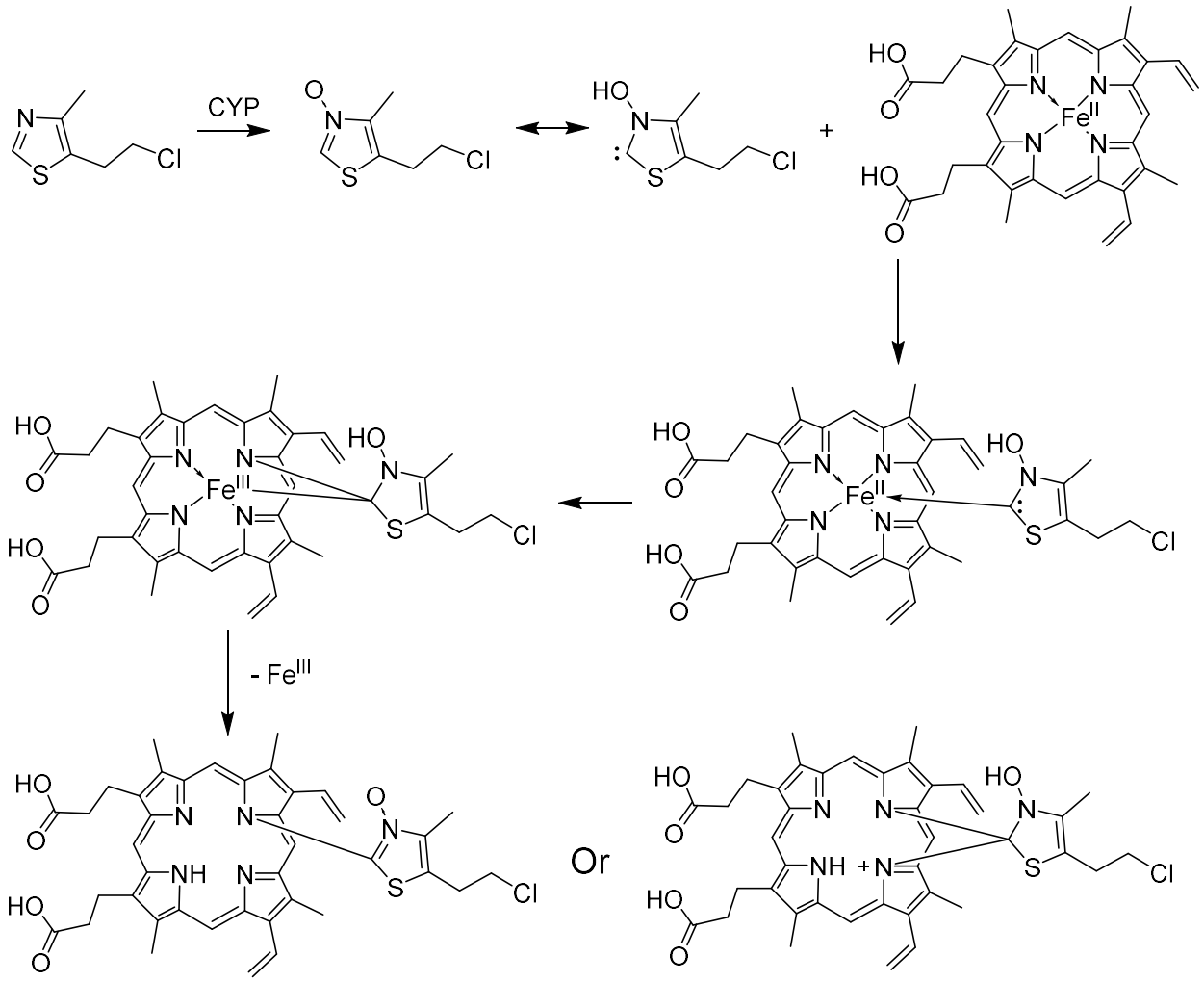

Figure 4.21 Proposed Schemes of Inactivation of CYP via CMZ N-oxide

Appendix 1 LC/MS/MS Conditions for Phenacetin O-Deethylase Assay

The LC/MS system was composed of an UHPLC (Waters H Class, Milford, MA) and a triple quadrupole mass spectrometer (SCIEX API-4000 QTrap, Applied Biosystems, Framingham, MA). Peak areas of acetaminophen and acetaminophen-D_3 were collected and integrated by Analyst (version 1.6, Applied Biosystems, Framingham, MA). The details were as follows:

LC Conditions	
Column:	Agilent Zorbax XDB-C18 2.1 × 50 mm, 5 µ (Santa Clara, CA)
Column Temperature:	Ambient
Needle Wash:	Acetonitrile/methanol
Mobile Phases:	(A) 0.1% formic acid in water
	(B) 0.1% formic acid in acetonitrile
Gradient:	(B) 0% (0 – 1.3 min), 100% (1.6 - 4 min), 0% (4.1 - 7 min)
Flow Rate:	500 µL/min
IS:	Acetaminophen-D_3 (100 nM)
Sample Tray Temperature:	4°C
Sample Injection Volume:	10 µL
MS Conditions	
Ionization Mode	Positive
Curtain Gas:	35
Temperature:	600°C
GAS1:	60
GAS2:	60
Ion Spray Voltage:	5000 V
CAD Gas:	Medium

Multiple Reaction Monitor (MRM) Conditions:							
	Q1 m/z	Q3 m/z	Time (ms)	DP	EP	CE	CXP
Acetaminophen	152.1	110.0	75	60	10	25	15
Acetaminophen-D_3	155.1	111.0	75	60	10	25	15

Appendix 2 LC/MS/MS Conditions for Coumarin 7-Hydroxylase Assay

The LC/MS system was composed of an UHPLC (Waters H Class, Milford, MA) and a triple quadrupole mass spectrometer (SCIEX API-4000 QTrap, Applied Biosystems, Framingham, MA). Peak areas of 7-OH coumarin and 7-OH-coumarin-$^{13}C_5$ were collected and integrated by Analyst (version 1.6, Applied Biosystems, Framingham, MA). The details were as follows:

LC Conditions	
Column:	Agilent Zorbax XDB-C18 2.1 × 50 mm, 5 µ (Santa Clara, CA)
Column Temperature:	Ambient
Needle Wash:	Acetonitrile/methanol
Mobile Phases:	(A) 0.1% formic acid in water
	(B) 0.1% formic acid in acetonitrile
Gradient:	(B) 0% (0 – 0.8 min), 100% (3.0 min), 0% (3.1 - 6 min)
Flow Rate:	500 µL/min
IS:	7-OH-Coumarin-$^{13}C_5$ (100 nM)
Sample Tray Temperature:	4°C
Sample Injection Volume:	10 µL
MS Conditions	
Ionization Mode	Negative
Curtain Gas:	35
Temperature:	600°C
GAS1:	60
GAS2:	60
Ion Spray Voltage:	-4500 V
CAD Gas:	Medium

Multiple Reaction Monitor (MRM) Conditions:							
	Q1 m/z	Q3 m/z	Time (ms)	DP	EP	CE	CXP
7-OH-Coumarin	160.9	133.0	150	-86	-10	-28	-21
7-OH-Coumarin-$^{13}C_5$	166.0	138.0	150	-86	-10	-28	-21

Appendix 3 LC/MS/MS Conditions for Bupropion Hydroxylase Assay

The LC/MS system was composed of an UHPLC (Waters H Class, Milford, MA) and a triple quadrupole mass spectrometer (SCIEX API-4000 QTrap, Applied Biosystems, Framingham, MA). Peak areas of OH-bupropion and OH-bupropion-D_6 were collected and integrated by Analyst (version 1.6, Applied Biosystems, Framingham, MA). The details were as follows:

LC Conditions	
Column:	Agilent Zorbax XDB-C18 2.1 × 50 mm, 5 µ (Santa Clara, CA)
Column Temperature:	Ambient
Needle Wash:	Acetonitrile/methanol
Mobile Phases:	(A) 0.1% formic acid in water
	(B) 0.1% formic acid in acetonitrile
Gradient:	(B) 0% (0 – 0.8 min), 100% (3.0 min), 0% (3.1 - 6 min)
Flow Rate:	500 µL/min
IS:	OH-Bupropion-D_6 (100 nM)
Sample Tray Temperature:	4°C
Sample Injection Volume:	10 µL
MS Conditions	
Ionization Mode	Positive
Curtain Gas:	35
Temperature:	600°C
GAS1:	60
GAS2:	60
Ion Spray Voltage:	5000 V
CAD Gas:	Medium

Multiple Reaction Monitor (MRM) Conditions:							
	Q1 m/z	Q3 m/z	Time (ms)	DP	EP	CE	CXP
OH-Bupropion	256.1	131.1	100	60	10	35	11
OH-Bupropion-D_6	262.1	138.0	100	60	10	35	11

Appendix 4 LC/MS/MS Conditions for Amodiaquine O-Deethylase Assay

The LC/MS system was composed of an UHPLC (Waters H Class, Milford, MA) and a triple quadrupole mass spectrometer (SCIEX API-4000 QTrap, Applied Biosystems, Framingham, MA). Peak areas of desethylamodiaquine and desethylamodiaquine-D_5 were collected and integrated by Analyst (version 1.6, Applied Biosystems, Framingham, MA). The details were as follows:

LC Conditions	
Column:	Thermo Fisher Hypurity C_4 2.1 × 50 mm, 5 μ (Waltham, MA)
Column Temperature:	Ambient
Needle Wash:	0.3% Formic Acid in Acetonitrile
Mobile Phases:	(A) 0.3% formic acid in water
	(B) 0.3% formic acid in acetonitrile
Gradient:	(B) 0% (0 – 0.8 min), 100% (3 - 4 min), 0% (4.1 - 7 min)
Flow Rate:	500 μL/min
IS:	Desethylamodiaquine-D_5 (100 nM)
Sample Tray Temperature:	4°C
Sample Injection Volume:	10 μL
MS Conditions	
Ionization Mode	Positive
Curtain Gas:	35
Temperature:	600°C
GAS1:	60
GAS2:	60
Ion Spray Voltage:	5000 V
CAD Gas:	Medium

Multiple Reaction Monitor (MRM) Conditions:							
	Q1 m/z	Q3 m/z	Time (ms)	DP	EP	CE	CXP
Desethylamodiaquine	256.1	131.1	100	70	10	27	16
Desethylamodiaquine-D_5	262.1	138.0	100	70	10	27	16

Appendix 5 LC/MS/MS Conditions for Tolbutamide Hydroxylase Assay

The LC/MS system was composed of an UHPLC (Waters H Class, Milford, MA) and a triple quadrupole mass spectrometer (SCIEX API-4000 QTrap, Applied Biosystems, Framingham, MA). Peak areas of OH-tolbutamide and OH-tolbutamide-D_9 were collected and integrated by Analyst (version 1.6, Applied Biosystems, Framingham, MA). The details were as follows:

LC Conditions	
Column:	Agilent Zorbax XDB-C18 2.1 × 50 mm, 5 µ (Santa Clara, CA)
Column Temperature:	Ambient
Needle Wash:	Acetonitrile/methanol
Mobile Phases:	(A) 0.1% formic acid in water
	(B) 0.1% formic acid in acetonitrile
Gradient:	(B) 0% (0 – 0.8 min), 100% (3 - 4 min), 0% (4.1 - 7 min)
Flow Rate:	500 µL/min
IS:	Hydroxytolbutamide-D_9 (100 nM)
Sample Tray Temperature:	4°C
Sample Injection Volume:	10 µL
MS Conditions	
Ionization Mode	Positive
Curtain Gas:	35
Temperature:	600°C
GAS1:	60
GAS2:	60
Ion Spray Voltage:	5000 V
CAD Gas:	Medium

Multiple Reaction Monitor (MRM) Conditions:							
	Q1 m/z	Q3 m/z	Time (ms)	DP	EP	CE	CXP
OH-Tolbutamide	287.1	188.2	100	70	10	17	0
OH-Tolbutamide-D_9	296.1	188.2	100	70	10	17	0

Appendix 6 LC/MS/MS Conditions for Mephenytoin Hydroxylase Assay

The LC/MS system was composed of an UHPLC (Waters H Class, Milford, MA) and a triple quadrupole mass spectrometer (SCIEX API-4000 QTrap, Applied Biosystems, Framingham, MA). Peak areas of OH-mephenytoin and OH-mephenytoin -D_6 were collected and integrated by Analyst (version 1.6, Applied Biosystems, Framingham, MA). The details were as follows:

LC Conditions	
Column:	Agilent Zorbax XDB-C18 2.1 × 50 mm, 5 µ (Santa Clara, CA)
Column Temperature:	Ambient
Needle Wash:	Acetonitrile/methanol
Mobile Phases:	(A) 0.1% formic acid in water
	(B) 0.1% formic acid in acetonitrile
Gradient:	(B) 0% (0 – 0.8 min), 100% (3 - 4 min), 0% (4.1 - 7 min)
Flow Rate:	500 µL/min
IS:	Hydroxymephenytoin-D_3 (100 nM)
Sample Tray Temperature:	4°C
Sample Injection Volume:	10 µL
MS Conditions	
Ionization Mode	Positive
Curtain Gas:	35
Temperature:	600°C
GAS1:	60
GAS2:	60
Ion Spray Voltage:	5000 V
CAD Gas:	Medium

Multiple Reaction Monitor (MRM) Conditions:							
	Q1 m/z	Q3 m/z	Time (ms)	DP	EP	CE	CXP
OH-Mephenytoin	235.0	150.0	150	80	10	30	14
OH-Mephenytoin-D_3	238.0	150.0	150	80	10	30	14

Appendix 7 LC/MS/MS Conditions for Dextromethorphan O-Demethylase Assay

The LC/MS system was composed of an UHPLC (Waters H Class, Milford, MA) and a triple quadrupole mass spectrometer (SCIEX API-4000 QTrap, Applied Biosystems, Framingham, MA). Peak areas of dextorphan and dextorphan-D_6 were collected and integrated by Analyst (version 1.6, Applied Biosystems, Framingham, MA). The details were as follows:

LC Conditions	
Column:	Agilent Zorbax XDB-C18 2.1 × 50 mm, 5 μ (Santa Clara, CA)
Column Temperature:	Ambient
Needle Wash:	Acetonitrile/methanol
Mobile Phases:	(A) 0.1% formic acid in water
	(B) 0.1% formic acid in acetonitrile
Gradient:	(B) 0% (0 – 1 min), 25% (1.1 min), 35% (2 min), 100% (4 min), 0% (4.1 - 7 min)
Flow Rate:	500 μL/min
IS:	Dextorphan-D_3 (100 nM)
Sample Tray Temperature:	4°C
Sample Injection Volume:	10 μL
MS Conditions	
Ionization Mode	Positive
Curtain Gas:	35
Temperature:	600°C
GAS1:	60
GAS2:	60
Ion Spray Voltage:	5000 V
CAD Gas:	Medium

Multiple Reaction Monitor (MRM) Conditions:							
	Q1 m/z	Q3 m/z	Time (ms)	DP	EP	CE	CXP
Dextorphan	258.1	157.0	75	60	10	25	14
Dextorphan-D_3	261.1	157.0	75	60	10	25	14

Appendix 8 LC/MS/MS Conditions for Chlorzoxazone 6-Hydroxylase Assay

The LC/MS system was composed of an UHPLC (Waters H Class, Milford, MA) and a triple quadrupole mass spectrometer (SCIEX API-4000 QTrap, Applied Biosystems, Framingham, MA). Peak areas of 6-OH chlorzoxazone and 6-OH chlorzoxazone-$^{13}C_6$ were collected and integrated by Analyst (version 1.6, Applied Biosystems, Framingham, MA). The details were as follows:

LC Conditions	
Column:	Agilent Zorbax XDB-C18 2.1 × 50 mm, 5 μ (Santa Clara, CA)
Column Temperature:	Ambient
Needle Wash:	Acetonitrile/methanol
Mobile Phases:	(A) 0.1% formic acid in water
	(B) 0.1% formic acid in acetonitrile
Gradient:	(B) 0% (0 – 0.8 min), 100% (1.8 - 3 min), 0% (3.1 - 5 min)
Flow Rate:	500 μL/min
IS:	6-OH Chlorzoxazone-$^{13}C_6$ (100 nM)
Sample Tray Temperature:	4°C
Sample Injection Volume:	10 μL
MS Conditions	
Ionization Mode	Negative
Curtain Gas:	35
Temperature:	500°C
GAS1:	60
GAS2:	60
Ion Spray Voltage:	-4200 V
CAD Gas:	Medium

Multiple Reaction Monitor (MRM) Conditions:							
	Q1 m/z	Q3 m/z	Time (ms)	DP	EP	CE	CXP
6-OH Chlorzoxazone	184.0	120.0	50	-70	-10	-26	-19
6-OH Chlorzoxazone-$^{13}C_6$	192.0	125.0	50	-80	-10	-26	-19

Appendix 9 LC/MS/MS Conditions for para-Nitrophenol Hydroxylase Assay

The LC/MS system was composed of an UHPLC (Waters H Class, Milford, MA) and a triple quadrupole mass spectrometer (SCIEX API-4000 QTrap, Applied Biosystems, Framingham, MA). Peak areas of p-nitrocatechol and p-nitrocatechol-$^{13}C_6$ were collected and integrated by Analyst (version 1.6, Applied Biosystems, Framingham, MA). The details were as follows:

LC Conditions	
Column:	Agilent Zorbax XDB-C18 2.1 × 50 mm, 5 μ (Santa Clara, CA)
Column Temperature:	Ambient
Needle Wash:	Acetonitrile/methanol
Mobile Phases:	(A) 0.1% formic acid in water
	(B) 0.1% formic acid in acetonitrile
Isocratic:	(B) 30%
Flow Rate:	500 μL/min
IS:	p-Nitrocatechol-$^{13}C_6$ (100 nM)
Sample Tray Temperature:	4°C
Sample Injection Volume:	10 μL
MS Conditions	
Ionization Mode	Negative
Curtain Gas:	35
Temperature:	500°C
GAS1:	60
GAS2:	60
Ion Spray Voltage:	-4200 V
CAD Gas:	Medium

Multiple Reaction Monitor (MRM) Conditions:							
	Q1 m/z	Q3 m/z	Time (ms)	DP	EP	CE	CXP
p-Nitrocatechol	153.8	123.8	100	-80	-10	-24	-9
p-Nitrocatechol-$^{13}C_6$	159.9	130.0	100	-80	-10	-24	-9

Appendix 10 LC/MS/MS Conditions for Midazolam 1'-Hydroxylase and 4-Hydroxylase Assay

The LC/MS system was composed of an UHPLC (Waters H Class, Milford, MA) and a triple quadrupole mass spectrometer (SCIEX API-4000 QTrap, Applied Biosystems, Framingham, MA). Peak areas of 1'-OH midazolam, 4-OH midazolam, and 1'-hydroxymidazolam-D_3 were collected and integrated by Analyst (version 1.6, Applied Biosystems, Framingham, MA). The details were as follows:

LC Conditions	
Column:	Agilent Zorbax XDB-C18 2.1 × 50 mm, 5 µ (Santa Clara, CA)
Column Temperature:	Ambient
Needle Wash:	Acetonitrile/methanol
Mobile Phases:	(A) 0.1% formic acid in water
	(B) 0.1% formic acid in acetonitrile
Gradient:	(B) 0% (0 - 0.8 min), 35% (3 min), 100% (3.5 min), 0% (3.6-6 min)
Flow Rate:	500 µL/min
IS:	1'-OH Midazolam-D_4 (100 nM)
Sample Tray Temperature:	4°C
Sample Injection Volume:	10 µL
MS Conditions	
Ionization Mode	Positive
Curtain Gas:	35
Temperature:	600°C
GAS1:	60
GAS2:	60
Ion Spray Voltage:	5000 V
CAD Gas:	Medium

Multiple Reaction Monitor (MRM) Conditions:							
	Q1 m/z	Q3 m/z	Time (ms)	DP	EP	CE	CXP
1'-OH Midazolam	342.0	203.1	150	80	10	37	14
4-OH Midazolam	342.0	297.0	150	80	10	35	14
1'-OH Midazolam-D_4	346.0	203.1	150	80	10	35	14

Appendix 11 LC/MS/MS Conditions for Testosterone 6β-Hydroxylase Assay

The LC/MS system was composed of an UHPLC (Waters H Class, Milford, MA) and a triple quadrupole mass spectrometer (SCIEX API-4000 QTrap, Applied Biosystems, Framingham, MA). Peak areas of 6β-OH testosterone and 6β-OH testosterone-D_3 were collected and integrated by Analyst (version 1.6, Applied Biosystems, Framingham, MA). The details were as follows:

LC Conditions	
Column:	Agilent Zorbax XDB-C18 2.1 × 50 mm, 5 μ (Santa Clara, CA)
Column Temperature:	Ambient
Needle Wash:	Acetonitrile/methanol
Mobile Phases:	(A) 0.1% formic acid in water
	(B) 0.1% formic acid in acetonitrile
Gradient:	(B) 0% (0 - 0.8 min), 100% (3-4 min), 0% (4.1-7 min)
Flow Rate:	500 μL/min
IS:	6β-OH Testosterone-D_3 (100 nM)
Sample Tray Temperature:	4°C
Sample Injection Volume:	10 μL
MS Conditions	
Ionization Mode	Positive
Curtain Gas:	35
Temperature:	650°C
GAS1:	60
GAS2:	60
Ion Spray Voltage:	5000 V
CAD Gas:	Medium

Multiple Reaction Monitor (MRM) Conditions:							
	Q1 m/z	Q3 m/z	Time (ms)	DP	EP	CE	CXP
6β-OH Testosterone	305.0	269.0	150	60	10	22	11
6β-OH Testosterone-D_3	308.0	272.0	150	60	10	22	11

Appendix 12 LC/MS/MS Conditions for Nifedipine Dehydrogenation Assay

The LC/MS system was composed of an UHPLC (Waters H Class, Milford, MA) and a triple quadrupole mass spectrometer (SCIEX API-4000 QTrap, Applied Biosystems, Framingham, MA). Peak areas of dehydronifedipine and dehydronifedipine-D_6 were collected and integrated by Analyst (version 1.6, Applied Biosystems, Framingham, MA). The details were as follows:

LC Conditions	
Column:	Agilent Zorbax XDB-C18 2.1 × 50 mm, 5 μ (Santa Clara, CA)
Column Temperature:	Ambient
Needle Wash:	Acetonitrile/methanol
Mobile Phases:	(A) 0.1% formic acid in water
	(B) 0.1% formic acid in acetonitrile
Gradient:	(B) 0% (0 - 0.8 min), 100% (3-4 min), 0% (4.1-7 min)
Flow Rate:	500 μL/min
IS:	Dehydronifedipine-D_6 (100 nM)
Sample Tray Temperature:	4°C
Sample Injection Volume:	10 μL
MS Conditions	
Ionization Mode	Positive
Curtain Gas:	35
Temperature:	600°C
GAS1:	60
GAS2:	60
Ion Spray Voltage:	5000 V
CAD Gas:	Medium

Multiple Reaction Monitor (MRM) Conditions:							
	Q1 m/z	Q3 m/z	Time (ms)	DP	EP	CE	CXP
Dehydronifedipine	345.2	284.1	100	70	10	39	14
Dehydronifedipine-D_6	351.2	287.1	100	70	10	39	14

Appendix 13 LC/MS Conditions for Chlormethiazole Metabolite Identification

The LC/MS system was composed of an UHPLC (Waters I Class, Milford, MA) and a hybrid quadrupole/time of flight mass spectrometer (AB SCIEX 5600 TripleTOF, Applied Biosystems, Framingham, MA). Data were collected by Analyst TF (version 1.7.1, Applied Biosystems, Framingham, MA), analyzed with PeakView (version 2.2, Applied Biosystems) and Metabolite Pilot (version 2.0.2, Applied Biosystems) and integrated with MultiQuant (version 3.0.2, Applied Biosystems). The details were as follows:

LC Conditions	
Column:	Waters Sunfire C_{18} 2.1 × 150 mm, 5 µ (Milford, MA)
Column Temperature:	Ambient
Needle Wash:	Acetonitrile/methanol
Mobile Phases:	(A) 10 mM ammonium bicarbonate in water (B) acetonitrile
Gradient:	(B) 0% (0 - 1 min), 100% (14-15 min), 0% (15.1-20 min)
Flow Rate:	500 µL/min
Sample Tray Temperature:	4°C
Sample Injection Volume:	10 µL
MS Conditions	
Ionization Mode	Positive
Curtain Gas:	35
Temperature:	600°C
GAS1:	60
GAS2:	60
ISVF:	4500 V
Survey Scan Settings:	
Scan Range:	50-1000 m/z
Accumulation Time:	0.1 sec
DP:	100
CE:	5
CES:	0
IDA Settings:	
Maximum Scans per cycle:	4 (Product Ion)
Scan Range:	50-1000 m/z
Accumulation Time:	0.1 sec
DP:	100
CE:	35
CES:	20
IDA Trigger Type:	Mass Defect Filter and Largest Peak
Mass Defect Filters:	50 mDa error/400 Da window with C_6H_8ClNS and $C_{16}H_{24}ClN_4S_2O_6$
Exclude previous ions:	1 sec
Minimum CPS for trigger:	300

Appendix 14 LC/MS Conditions for Heme Quantitation Method

The LC/MS system was composed of an UHPLC (Waters I Class, Milford, MA) and a hybrid quadrupole/time of flight mass spectrometer (AB SCIEX 5600 TripleTOF, Applied Biosystems, Framingham, MA). Peak areas of hemin B and hemin-D_4 were collected by Analyst TF (version 1.7.1, Applied Biosystems, Framingham, MA), and integrated with MultiQuant (version 3.0.2, Applied Biosystems). The details were as follows:

LC Conditions	
Column:	Waters XBridge C_8 2.1 × 50 mm, 5 µ (Milford, MA)
Column Temperature:	Ambient
Needle Wash:	10% ammonium hydroxide, 40% water, 50% isopropyl alcohol
Mobile Phases:	(A) 2% ammonium hydroxide in water
	(B) 2% ammonium hydroxide in isopropyl alcohol
Gradient:	(B) 10% (0 - 1 min), 100% (4-5 min), 10% (5.1-8 min)
Flow Rate:	500 µL/min
IS:	Hemin-D_4 (500 nM)
Sample Tray Temperature:	Room temperature
Sample Injection Volume:	10 µL
MS Conditions	
Ionization Mode	Positive
Curtain Gas:	35
Temperature:	600°C
GAS1:	60
GAS2:	60
ISVF:	5000 V
Survey Scan Settings:	
Scan Range:	100-2000 m/z
Accumulation Time:	0.1 sec
DP:	100
CE:	5
CES:	0
Product Ion Settings:	
Parent m/z 1:	616.18
Parent m/z 2:	621.21
PIS Scan Range:	100-2000 m/z
Accumulation Time:	0.1 sec
DP:	100
CE:	55
Scan Range:	100-2000 m/z

Appendix 15 LC/MS Conditions for Base Heme Adduct Method

The LC/MS system was composed of an UHPLC (Waters I Class, Milford, MA) and a hybrid quadrupole/time of flight mass spectrometer (AB SCIEX 5600 TripleTOF, Applied Biosystems, Framingham, MA). Data were collected by Analyst TF (version 1.7.1, Applied Biosystems, Framingham, MA), and were analyzed with PeakView (version 2.2, Applied Biosystems) and Metabolite Pilot (version 2.0.2, Applied Biosystems). The details were as follows:

LC Conditions	
Column:	Waters XBridge C_8 2.1 × 50 mm, 5 µ (Milford, MA)
Column Temperature:	Ambient
Needle Wash:	10% ammonium hydroxide, 40% water, 50% isopropyl alcohol
Mobile Phases:	(A) 0.1% ammonium hydroxide in water (B) 0.1% ammonium hydroxide in isopropyl alcohol
Gradient:	(B) 0% (0 - 1 min), 100% (14-15 min), 0% (15.1-20 min)
Flow Rate:	500 µL/min
Sample Tray Temperature:	Room temperature
Sample Injection Volume:	10 µL
MS Conditions	
Ionization Mode	Positive
Curtain Gas:	35
Temperature:	600°C
GAS1:	60
GAS2:	60
ISVF:	4500 V
Survey Scan Settings:	
Scan Range:	100-2000 m/z
Accumulation Time:	0.1 sec
DP:	100
CE:	5
CES:	0
IDA Settings:	
Maximum Scans per cycle:	4 (Product Ion)
Scan Range:	100-2000 m/z
Accumulation Time:	0.1 sec
DP:	100
CE:	35
CES:	20
IDA Trigger Type:	Mass Defect Filter and Largest Peak
Mass Defect Filters:	70 mDa error/400 Da window with $C_{34}H_{34}N_4O_4$ + Compound Formula and $C_{34}H_{32}N_4O_4Fe$ + Compound Formula
Exclude previous ions:	1 sec
Minimum CPS for trigger:	200

Appendix 16 LC/MS Conditions for Whole Protein Analysis

The LC/MS system was composed of an UHPLC (Waters I Class, Milford, MA) and a hybrid quadrupole/time of flight mass spectrometer (Waters Synapt G2 Si, Milford, MA). Data were collected and analyzed by MassLynx (version 4.1, Waters, Milford, MA). The details were as follows:

LC Conditions	
Column:	Agilent PLRP-S 2.1 × 50 mm, 300Å (Santa Clara, CA)
Column Temperature:	Ambient
Needle Wash:	Acetonitrile/Methanol
Mobile Phases:	(A) 0.1% formic acid in water
	(B) 0.1% formic acid in acetonitrile
Gradient:	(B) 5% (0 min), 20% (1 min), 50% (3 min), 95% (4 min), 5% (4.1-5.5 min)
Flow Rate:	500 µL/min (0 min), 300 µL/min (1-5.5 min)
Sample Tray Temperature:	Room temperature
Sample Injection Volume:	10 µL
MS Conditions	
Ionization Mode	Positive
Desolvation Gas:	800 L/hr
Desolvation Temperature:	325°C
Source Temperature:	100°C
Capillary Voltage:	3 kV
Reference Cone Voltage:	40 V
Resolution Setting:	Resolution Mode
Scan Range:	400-4000 m/z
Accumulation Time:	0.1 sec

References

1. Lee, H. C., Jung, S. A., Jung, H. K., Yi, S. Y., Kim, D. Y., Moon, I. H., and Park, S. S. (1999) Protective effect of chlormethiazole, a sedative, against acetaminophen-induced liver injury in mice. *The Korean journal of internal medicine* **14**, 27-33
2. Fronticelli, C., and Bucci, E. (1963) Acetone extraction of heme from myoglobin and hemoglobin at acid pH. *BBA - Biochimica et Biophysica Acta* **78**, 530-531
3. Ortiz de Montellano, P. R. (1991) [52] Mechanism-based inactivation of cytochrome P450: Isolation and characterization of N-alkyl heme adducts. *Methods in Enzymology* **206**, 533-540
4. Rock, B. M., Hengel, S. M., Rock, D. A., Wienkers, L. C., and Kunze, K. L. (2014) Characterization of ritonavir-mediated inactivation of cytochrome P450 3A4. *Mol Pharmacol* **86**, 665-674
5. Zhu, M. S., Ma, L., Zhang, D. L., Ray, K., Zhao, W. P., Humphreys, W., Skiles, G., Sanders, M., and Zhang, H. (2006) Detection and characterization of metabolites in biological matrices using mass defect filtering of liquid chromatography/high resolution mass spectrometry data. *Drug Metab. Dispos.* **34**, 1722-1733
6. Zhu, M., Ma, L., Zhang, H., and Humphreys, W. G. (2007) Detection and structural characterization of glutathione-trapped reactive metabolites using liquid chromatography--high-resolution mass spectrometry and mass defect filtering.(Technical report). *Analytical Chemistry* **79**, 8333
7. Zhang, H., Zhang, D., Ray, K., and Zhu, M. (2009) Mass defect filter technique and its applications to drug metabolite identification by high-resolution mass spectrometry. *Journal of Mass Spectrometry* **44**, 999-1016
8. Mirsky, A. E., and Anson, M. L. (1929) On pyridine hemochromogen. *Journal of General Physiology* **12**, 581-586
9. Urry, D. W. (1967) The heme chromophore in the ultraviolet. *Journal of Biological Chemistry* **242**, 4441-4448
10. Marcero, J. R., Piel Iii, R. B., Burch, J. S., and Dailey, H. A. (2016) Rapid and sensitive quantitation of heme in hemoglobinized cells. *BioTechniques* **61**, 83
11. Silverman, R. B. (1988) *Mechanism-based enzyme inactivation : chemistry and enzymology*, CRC Press, Boca Raton, FL
12. Ortiz de Montellano, P. R. (2015) *Cytochrome P450 : structure, mechanism, and biochemistry*, 4th edition. ed., Cham : Springer, Cham
13. Cerny, M. A. (2016) Prevalence of Non-Cytochrome P450-Mediated Metabolism in Food and Drug Administration-Approved Oral and Intravenous Drugs: 2006-2015. *Drug metabolism and disposition: the biological fate of chemicals* **44**, 1246
14. Zanger, U. M., and Schwab, M. (2013) Cytochrome P450 enzymes in drug metabolism: Regulation of gene expression, enzyme activities, and impact of genetic variation. *Pharmacology and Therapeutics* **138**, 103-141
15. Kalgutkar, A. S., Gardner, I., Obach, R. S., Shaffer, C. L., Callegari, E., Henne, K. R., Mutlib, A. E., Dalvie, D. K., Lee, J. S., Nakai, Y., O'Donnell, J. P., Boer, J., and Harriman, S. P. (2005) A comprehensive listing of bioactivation pathways of organic functional groups. *Curr Drug Metab* **6**, 161-225
16. Kalgutkar, A., Obach, R., and Maurer, T. (2007) Mechanism-based inactivation of cytochrome P450 enzymes: Chemical mechanisms, structure-activity relationships and relationship to clinical drug-drug interactions and idiosyncratic adverse drug reactions. *Curr. Drug Metab.* **8**, 407-447

17. Cheung, C., Yu, A. M., Ward, J. M., Krausz, K. W., Akiyama, T. E., Feigenbaum, L., and Gonzalez, F. J. (2005) The cyp2e1-humanized transgenic mouse: role of cyp2e1 in acetaminophen hepatotoxicity. *Drug metabolism and disposition: the biological fate of chemicals* **33**, 449-457
18. Dey, A. (2013) *Cytochrome P450 2E1: its role in disease and drug metabolism*, Springer, Dordrecht
19. Hrycay, E. G., and Bandiera, S. M. (2015) Involvement of Cytochrome P450 in Reactive Oxygen Species Formation and Cancer. *Advances in pharmacology (San Diego, Calif.)* **74**, 35
20. FDA. (2016) Preventable Adverse Drug Reactions: A Focus on Drug Interactions. https://www.fda.gov/drugs/developmentapprovalprocess/developmentresources/druginteractionslabeling/ucm110632.htm
21. Marzolini, C., Gibbons, S., Khoo, S., and Back, D. (2016) Cobicistat versus ritonavir boosting and differences in the drug–drug interaction profiles with co-medications. *Journal of Antimicrobial Chemotherapy* **71**, 1755-1758
22. Sim, S. C., and Ingelman-Sundberg, M. (2010) The Human Cytochrome P450 (CYP) Allele Nomenclature website: a peer-reviewed database of CYP variants and their associated effects.(http://www.cypalleles.ki.se/)(Website overview). **4**
23. Wienkers, L. C., and Heath, T. G. (2005) Predicting in vivo drug interactions from in vitro drug discovery data. *Nat Rev Drug Discov* **4**, 825-833
24. Saravanakumar, A., Sadighi, A., Ryu, R., and Akhlaghi, F. (2019) Physicochemical Properties, Biotransformation, and Transport Pathways of Established and Newly Approved Medications: A Systematic Review of the Top 200 Most Prescribed Drugs vs. the FDA-Approved Drugs Between 2005 and 2016. *Clinical pharmacokinetics*, <xocs:firstpage xmlns:xocs=""/>
25. Dong, D., Wu, B., Chow, D., and Hu, M. (2012) Substrate selectivity of drug-metabolizing cytochrome P450s predicted from crystal structures and in silico modeling. Taylor & Francis
26. Korzekwa, K. R., Krishnamachary, N., Shou, M., Ogai, A., Parise, R. A., Rettie, A. E., Gonzalez, F. J., and Tracy, T. S. (1998) Evaluation of atypical cytochrome P450 kinetics with two-substrate models: evidence that multiple substrates can simultaneously bind to cytochrome P450 active sites. *Biochemistry* **37**, 4137-4147
27. Korzekwa, K. (2014) Enzyme kinetics of oxidative metabolism: cytochromes P450. *Methods Mol Biol* **1113**, 149-166
28. Sevrioukova, I. F., and Poulos, T. L. (2017) Structural basis for regiospecific midazolam oxidation by human cytochrome P450 3A4. *Proceedings of the National Academy of Sciences of the United States of America* **114**, 486
29. Ueng, Y. F., Kuwabara, T., Chun, Y. J., and Guengerich, F. P. (1997) Cooperativity in oxidations catalyzed by cytochrome P450 3A4. *Biochemistry* **36**, 370-381
30. Wang, R. W., Newton, D. J., Liu, N., Atkins, W. M., and Lu, A. Y. (2000) Human cytochrome P-450 3A4: in vitro drug-drug interaction patterns are substrate-dependent. *Drug metabolism and disposition: the biological fate of chemicals* **28**, 360-366
31. Williams, J. A., Ring, B. J., Cantrell, V. E., Jones, D. R., Eckstein, J., Ruterbories, K., Hamman, M. A., Hall, S. D., and Wrighton, S. A. (2002) Comparative metabolic capabilities of CYP3A4, CYP3A5, and CYP3A7. *Drug metabolism and disposition: the biological fate of chemicals* **30**, 883
32. Khan, K. K., He, Y. Q., Domanski, T. L., and Halpert, J. R. (2002) Midazolam oxidation by cytochrome P450 3A4 and active-site mutants: an evaluation of multiple binding sites and of the metabolic pathway that leads to enzyme inactivation. *Molecular pharmacology* **61**, 495

33. Mäenpää, J., Hall, S. D., Ring, B. J., Strom, S. C., and Wrighton, S. A. (1998) Human cytochrome P450 3A (CYP3A) mediated midazolam metabolism: The effect of assay conditions and regioselective stimulation by α-naphthoflavone, terfenadine and testosterone. *Pharmacogenetics* **8**, 137-155
34. Hartman, J. H., Boysen, G., and Miller, G. P. (2012) CYP2E1 metabolism of styrene involves allostery. *Drug metabolism and disposition: the biological fate of chemicals* **40**, 1976-1983
35. Hartman, J. H., Boysen, G., and Miller, G. P. (2013) Cooperative effects for CYP2E1 differ between styrene and its metabolites. *Xenobiotica; the fate of foreign compounds in biological systems* **43**, 755-764
36. Bell, L. C., and Guengerich, F. P. (1997) Oxidation kinetics of ethanol by human cytochrome P450 2E1. Rate-limiting product release accounts for effects of isotopic hydrogen substitution and cytochrome b5 on steady-state kinetics. *The Journal of biological chemistry* **272**, 29643-29651
37. Bell-Parikh, L. C., and Guengerich, F. P. (1999) Kinetics of cytochrome P450 2E1-catalyzed oxidation of ethanol to acetic acid via acetaldehyde. *The Journal of biological chemistry* **274**, 23833-23840
38. Guengerich, F. (2001) Common and uncommon cytochrome P450 reactions related to metabolism and chemical toxicity. *Chem. Res. Toxicol.* **14**, 611-650
39. Guengerich, F., and Munro, A. (2013) Unusual Cytochrome P450 Enzymes and Reactions. *J. Biol. Chem.* **288**, 17065-17073
40. Guengerich, F. (2018) Mechanisms of Cytochrome P450-Catalyzed Oxidations. *ACS Catal.* **8**, 10964-10976
41. Pearson, R. (2005) Chemical hardness and density functional theory. *[Formerly: Proceedings (Chemical Sciences)]* **117**, 369-377
42. Pearson, R. G. (2005) *Chemical Hardness*,
43. Mayr, H., Breugst, M., and Ofial, A. (2011) Farewell to the HSAB Treatment of Ambident Reactivity. *Angew. Chem.-Int. Edit.* **50**, 6470-6505
44. Argoti, D., Liang, L., Conteh, A., Chen, L., Bershas, D., Yu, C.-P., Vouros, P., and Yang, E. (2005) Cyanide trapping of iminium ion reactive intermediates followed by detection and structure identification using liquid chromatography-tandem mass spectrometry (LC-MS/MS). *Chemical research in toxicology* **18**, 1537
45. Zhang, C., Wong, S., Delarosa, E. M., Kenny, J. R., Halladay, J. S., Hop, C. E., and Khojasteh-Bakht, S. C. (2009) Inhibitory properties of trapping agents: glutathione, potassium cyanide, and methoxylamine, against major human cytochrome p450 isoforms. *Drug metabolism letters* **3**, 125
46. Pelkonen, O., Pasanen, M., Tolonen, A., Koskinen, M., Hakkola, J., Abass, K., Laine, J., Hakkinen, M., Juvonen, R., Auriola, S., Storvik, M., Huuskonen, P., Rousu, T., and Rahikkala, M. (2015) Reactive metabolites in early drug development: predictive in vitro tools. *Curr Med Chem* **22**, 538-550
47. Grillo, M. P. (2015) Detecting reactive drug metabolites for reducing the potential for drug toxicity. *Expert opinion on drug metabolism & toxicology* **11**, 1281-1302
48. Kalgutkar, A. S. (2017) Liabilities Associated with the Formation of "Hard" Electrophiles in Reactive Metabolite Trapping Screens. *Chemical research in toxicology* **30**, 220-238
49. Ortiz de Montellano, P. R., Kunze, K. L., Beilan, H. S., and Wheeler, C. (1982) Destruction of Cytochrome P-450 by Vinyl Fluoride, Fluroxene, and Acetylene. Evidence for a Radical Intermediate in Olefin Oxidation. *Biochemistry* **21**, 1331-1339
50. Serron, S. C., Dwivedi, N., and Backes, W. L. (2000) Ethylbenzene Induces Microsomal Oxygen Free Radical Generation: Antibody-Directed Characterization of the Responsible Cytochrome P450 Enzymes. *Toxicology and Applied Pharmacology* **164**, 305-311

51. Smith, M. (2013) *March's advanced organic chemistry : reactions, mechanisms, and structure*, 7th edition / Michael B. Smith, Professor of Chemistry. ed., Hoboken : Wiley, Hoboken
52. Lange, M., & Mansuy, D. . (1981) N-substituted porphyrins formation from carbene iron-porphyrin complexes: A possible pathway for cytochrome P450 heme destruction. . *Tetrahedron Letters* **22**, 4
53. Riener, K., Haslinger, S., Raba, A., Hogerl, M. P., Cokoja, M., Herrmann, W., and Kuhn, F. (2014) Chemistry of Iron N-Heterocyclic Carbene Complexes: Syntheses, Structures, Reactivities, and Catalytic Applications. *Chem. Rev.* **114**, 5215-5272
54. Franklin, M. R. (1977) Inhibition of Mixed-Function Oxidations by Substrates Forming Reduced Cytochrome P-450 Metabolic-Intermediate Complexes. *Pharmac Ther A* **2**, 19
55. Dahlin, D. C., and Nelson, S. D. (1982) Synthesis, decomposition kinetics, and preliminary toxicological studies of pure N-acetyl-p-benzoquinone imine, a proposed toxic metabolite of acetaminophen. *Journal of medicinal chemistry* **25**, 885
56. Lauterburg, B. H., Corcoran, G. B., and Mitchell, J. R. (1983) Mechanism of action of N-acetylcysteine in the protection against the hepatotoxicity of acetaminophen in rats in vivo. *J Clin Invest* **71**, 980-991
57. Rosen, G. M., Rauckman, E. J., Ellington, S. P., Dahlin, D. C., Christie, J. L., and Nelson, S. D. (1984) Reduction and glutathione conjugation reactions of N-acetyl-p-benzoquinone imine and two dimethylated analogues. *Molecular Pharmacology* **25**, 151-157
58. Dahlin, D. C., Miwa, G. T., and Nelson, S. D. (1984) N-acetyl-p-benzoquinone Imine: A Cytochrome P-450-Mediated Oxidation Product of Acetaminophen. *Proceedings of the National Academy of Sciences of the United States of America* **81**, 1327-1331
59. Potter, D. W., and Hinson, J. A. (1986) Reactions of glutathione with oxidative intermediates of acetaminophen. *Advances in experimental medicine and biology* **197**, 763
60. Streeter, A. J., Harvison, P. J., Nelson, S. D., and Baillie, T. A. (1986) Cross-linking of protein molecules by the reactive metabolite of acetaminophen, N-acetyl-p-benzoquinone imine, and related quinoid compounds. *Advances in experimental medicine and biology* **197**, 727-737
61. Perry, H. E., and Shannon, M. W. (1998) Efficacy of oral versus intravenous N-acetylcysteine in acetaminophen overdose: results of an open-label, clinical trial. *J Pediatr* **132**, 149-152
62. Buckley, N. A., Whyte, I. M., O'Connell, D. L., and Dawson, A. H. (1999) Activated charcoal reduces the need for N-acetylcysteine treatment after acetaminophen (paracetamol) overdose. *J Toxicol Clin Toxicol* **37**, 753-757
63. Whyte, I. M., Francis, B., and Dawson, A. H. (2007) Safety and efficacy of intravenous N-acetylcysteine for acetaminophen overdose: analysis of the Hunter Area Toxicology Service (HATS) database. *Curr Med Res Opin* **23**, 2359-2368
64. Yarema, M. C., Johnson, D. W., Berlin, R. J., Sivilotti, M. L., Nettel-Aguirre, A., Brant, R. F., Spyker, D. A., Bailey, B., Chalut, D., Lee, J. S., Plint, A. C., Purssell, R. A., Rutledge, T., Seviour, C. A., Stiell, I. G., Thompson, M., Tyberg, J., Dart, R. C., and Rumack, B. H. (2009) Comparison of the 20-hour intravenous and 72-hour oral acetylcysteine protocols for the treatment of acute acetaminophen poisoning. *Ann Emerg Med* **54**, 606-614
65. Blackford, M. G., Felter, T., Gothard, M. D., and Reed, M. D. (2011) Assessment of the clinical use of intravenous and oral N-acetylcysteine in the treatment of acute acetaminophen poisoning in children: a retrospective review. *Clin Ther* **33**, 1322-1330
66. Blieden, M., Paramore, L. C., Shah, D., and Ben-Joseph, R. (2014) A perspective on the epidemiology of acetaminophen exposure and toxicity in the United States. *Expert Rev Clin Pharmacol* **7**, 341-348

67. Lee, S. S., Buters, J. T., Pineau, T., Fernandez-Salguero, P., and Gonzalez, F. J. (1996) Role of CYP2E1 in the hepatotoxicity of acetaminophen. *The Journal of biological chemistry* **271**, 12063-12067
68. Chen, W., Koenigs, L. L., Thompson, S. J., Peter, R. M., Rettie, A. E., Trager, W. F., and Nelson, S. D. (1998) Oxidation of acetaminophen to its toxic quinone imine and nontoxic catechol metabolites by baculovirus-expressed and purified human cytochromes P450 2E1 and 2A6. *Chemical research in toxicology* **11**, 295-301
69. Zhao, P., Kalhorn, T. F., and Slattery, J. T. (2002) Selective mitochondrial glutathione depletion by ethanol enhances acetaminophen toxicity in rat liver. *Hepatology* **36**, 326-335
70. Laine, J. E., Auriola, S., Pasanen, M., and Juvonen, R. O. (2009) Acetaminophen bioactivation by human cytochrome P450 enzymes and animal microsomes. *Xenobiotica; the fate of foreign compounds in biological systems* **39**, 11-21
71. Posadas, I., Santos, P., Blanco, A., Munoz-Fernandez, M., and Cena, V. (2010) Acetaminophen induces apoptosis in rat cortical neurons. *PloS one* **5**, e15360
72. Kenneth, E. T., John, T. S., Howard, R., Jenny, Y. C., Sidney, D. N., Kenneth, E. L., and Paul, B. W. (2000) Ethanol and production of the hepatotoxic metabolite of acetaminophen in healthy adults*. *Clinical Pharmacology & Therapeutics* **67**, 591
73. Chen, Y., Liu, L., Nguyen, K., and Fretland, A. J. (2011) Utility of intersystem extrapolation factors in early reaction phenotyping and the quantitative extrapolation of human liver microsomal intrinsic clearance using recombinant cytochromes P450. *Drug metabolism and disposition: the biological fate of chemicals* **39**, 373
74. Mayhew, B. S., Jones, D. R., and Hall, S. D. (2000) An in vitro model for predicting in vivo inhibition of cytochrome P450 3A4 by metabolic intermediate complex formation. *Drug metabolism and disposition: the biological fate of chemicals* **28**, 1031-1037
75. Riley, R. J., Grime, K., and Weaver, R. (2007) Time-dependent CYP inhibition. *Expert opinion on drug metabolism & toxicology* **3**, 51-66
76. Zhou, Z. W., and Zhou, S. F. (2009) Application of mechanism-based CYP inhibition for predicting drug-drug interactions. *Expert opinion on drug metabolism & toxicology* **5**, 579-605
77. Kenny, J. R., Mukadam, S., Zhang, C., Tay, S., Collins, C., Galetin, A., and Khojasteh, S. C. (2012) Drug-drug interaction potential of marketed oncology drugs: in vitro assessment of time-dependent cytochrome P450 inhibition, reactive metabolite formation and drug-drug interaction prediction. *Pharm Res* **29**, 1960-1976
78. Yan, Z., and Caldwell, G. W. (2012) The current status of time dependent CYP inhibition assay and in silico drug-drug interaction predictions. *Curr Top Med Chem* **12**, 1291-1297
79. Riley, R. J., and Wilson, C. E. (2015) Cytochrome P450 time-dependent inhibition and induction: advances in assays, risk analysis and modelling. Informa Healthcare
80. Bjornsson, T. D., Callaghan, J. T., Einolf, H. J., Fischer, V., Gan, L., Grimm, S., Kao, J., King, S. P., Miwa, G., Ni, L., Kumar, G., McLeod, J., Obach, R. S., Roberts, S., Roe, A., Shah, A., Snikeris, F., Sullivan, J. T., Tweedie, D., Vega, J. M., Walsh, J., Wrighton, S. A., Group, P. R. a. M. o. A. P. D. M. C. P. T. W., and (CDER), F. C. f. D. E. a. R. (2003) The conduct of in vitro and in vivo drug-drug interaction studies: a Pharmaceutical Research and Manufacturers of America (PhRMA) perspective. *Drug metabolism and disposition: the biological fate of chemicals* **31**, 815-832
81. Sager, J. E., Lutz, J. D., Foti, R. S., Davis, C., Kunze, K. L., and Isoherranen, N. (2014) Fluoxetine- and Norfluoxetine-Mediated Complex Drug-Drug Interactions: In Vitro to In Vivo Correlation of Effects on CYP2D6, CYP2C19, and CYP3A4. *Clinical pharmacology and therapeutics* **95**
82. Lin, J. H., and Lu, A. Y. (1998) Inhibition and induction of cytochrome P450 and the clinical implications. *Clinical pharmacokinetics* **35**, 361-390

83. Elcombe C.R., B. J., Nimmo-Smith R.H., Werringloer J. (1975) Cumene Hydroperoxide-Mediated Formation of Inhibited Complexes of Methylenedioxyphenyl Compounds with Cytochrome P-450. *Biochemical Society Transactions* **3**, 4
84. Mansuy, D., Beaune, P., Chottard, J. C., Bartoli, J. F., and Gans, P. (1976) The nature of the "455 nm absorbing complex" formed during the cytochrome P450 dependent oxidative metabolism of amphetamine. *Biochemical pharmacology* **25**, 609
85. Bertelsen, K. M., Venkatakrishnan, K., Von Moltke, L. L., Obach, R. S., and Greenblatt, D. J. (2003) Apparent mechanism-based inhibition of human CYP2D6 in vitro by paroxetine: comparison with fluoxetine and quinidine. *Drug metabolism and disposition: the biological fate of chemicals* **31**, 289-293
86. McConn, D. J., Lin, Y. S., Allen, K., Kunze, K. L., and Thummel, K. E. (2004) Differences in the inhibition of cytochromes P450 3A4 and 3A5 by metabolite-inhibitor complex-forming drugs. *Drug metabolism and disposition: the biological fate of chemicals* **32**, 1083
87. Varma, M. V., Pang, K. S., Isoherranen, N., and Zhao, P. (2014) Dealing with the complex drug-drug interactions: towards mechanistic models. *Biopharmaceutics & drug disposition*
88. Battioni, P., Mahy, J. P., Delaforge, M., and Mansuy, D. (1983) Reaction of Monosubstituted Hydrazines and Diazenes with Rat-Liver Cytochrome P450. *European Journal of Biochemistry* **134**, 241-248
89. Hanson, K. L., Vandenbrink, B. M., Babu, K. N., Allen, K. E., Nelson, W. L., and Kunze, K. L. (2010) Sequential metabolism of secondary alkyl amines to metabolic-intermediate complexes: opposing roles for the secondary hydroxylamine and primary amine metabolites of desipramine, (s)-fluoxetine, and N-desmethyldiltiazem. *Drug metabolism and disposition: the biological fate of chemicals* **38**, 963
90. Wynn, R. L. (1993) Erythromycin and ketoconazole (Nizoral) associated with terfenadine (Seldane)-induced ventricular arrhythmias. *General dentistry* **41**, 27
91. Biglin, K., Faraon, M. S., Constance, T., and Liehlai, M. (1994) DRUG-INDUCED TORSADES-DE-POINTES - A POSSIBLE INTERACTION OF TERFENADINE AND ERYTHROMYCIN. *Ann. Pharmacother.* **28**, 282-282
92. Jurima-Romet, M., Crawford, K., Cyr, T., and Inaba, T. (1994) Terfenadine metabolism in human liver. In vitro inhibition by macrolide antibiotics and azole antifungals. *Drug metabolism and disposition: the biological fate of chemicals* **22**, 849
93. Paris, D. G., Parente, T. F., Bruschetta, H. R., Guzman, E., and Niarchos, A. P. (1994) Torsades de pointes induced by erythromycin and terfenadine. *American Journal of Emergency Medicine* **12**, 636-638
94. Shou, M. (2007) *Mechanism-Based CYP Inhibition: Enzyme Kinetics, Assays, and Prediction of Human Drug-Drug Interactions*,
95. Obach, R. S., Walsky, R. L., and Venkatakrishnan, K. (2007) Mechanism-based inactivation of human cytochrome p450 enzymes and the prediction of drug-drug interactions. *Drug metabolism and disposition: the biological fate of chemicals* **35**, 246
96. Hollenberg, P., Kent, U., and Bumpus, N. N. (2008) Mechanism-based inactivation of human cytochromes P450s: Experimental characterization, reactive intermediates, and clinical implications. *Chem. Res. Toxicol.* **21**, 189-205
97. Ortiz De Montellano, P. R. (2008) Mechanism and Role of Covalent Heme Binding in the CYP4 Family of P450 Enzymes and the Mammalian Peroxidases. *Drug Metabolism Reviews* **40**, 405-426
98. Giragossian, C., LaPerle, J., Kosa, R. E., and Gillian, S. (2009) Impact of time-dependent inactivation on the estimation of enzyme kinetic parameters for midazolam. *Drug metabolism letters* **3**, 45-53
99. Kamel, A., and Harriman, S. (2012) Inhibition of cytochrome P450 enzymes and biochemical aspects of mechanism-based inactivation (MBI). *Drug Discovery Today: Technologies* **10**

100. Baer, B. R., Wienkers, L. C., and Rock, D. A. (2007) Time-dependent inactivation of P450 3A4 by raloxifene: identification of Cys239 as the site of apoprotein alkylation. *Chemical research in toxicology* **20**, 954
101. Yukinaga, H., Takami, T., Shioyama, S.-H., Tozuka, Z., Masumoto, H., Okazaki, O., and Sudo, K.-I. (2007) Identification of cytochrome P450 3A4 modification site with reactive metabolite using linear ion trap-Fourier transform mass spectrometry. *Chemical research in toxicology* **20**, 1373
102. Pratt-Hyatt, M., Lin, H. L., and Hollenberg, P. (2010) Mechanism-Based Inactivation of Human CYP2E1 by Diethyldithocarbamate. *Drug Metab. Dispos.* **38**, 2286-2292
103. De Matteis, F. (1971) Loss of haem in rat liver caused by the porphyrogenic agent 2-allyl-2-isopropylacetamide. *The Biochemical journal* **124**, 767
104. Ortiz de Montellano, P. R., and Kunze, K. L. (1980) Inactivation of hepatic cytochrome P-450 by allenic substrates. *Biochemical and Biophysical Research Communications* **94**, 443-449
105. Ortiz de Montellano, P. R., Kunze, K. L., and Mico, B. A. (1980) Destruction of cytochrome P-450 by olefins: N-alkylation of prosthetic heme. *Molecular pharmacology* **18**, 602
106. Halpert, J., Hammond, D., and Neal, R. A. (1980) Inactivation of purified rat liver cytochrome P-450 during the metabolism of parathion (diethyl p-nitrophenyl phosphorothionate). *The Journal of biological chemistry* **255**, 1080
107. Ortiz de Montellano, P. R., Beilan, H. S., and Kunze, K. L. (1981) N-Alkylprotoporphyrin IX formation in 3,5-dicarbethoxy-1,4-dihydrocollidine-treated rats. Transfer of the alkyl group from the substrate to the porphyrin. *The Journal of biological chemistry* **256**, 6708
108. Ortiz de Montellano, P. R., Mangold, B. L., Wheeler, C., Kunze, K. L., and Reich, N. O. (1983) Stereochemistry of cytochrome P-450-catalyzed epoxidation and prosthetic heme alkylation. *The Journal of biological chemistry* **258**, 4208
109. He, K., He, Y. A., Szklarz, G. D., Halpert, J. R., and Correia, M. A. (1996) Secobarbital-mediated inactivation of cytochrome P450 2B1 and its active site mutants. Partitioning between heme and protein alkylation and epoxidation. *The Journal of biological chemistry* **271**, 25864
110. Pessayre, D., Larrey, D., Vitaux, J., Breil, P., Belghiti, J., and Benhamou, J.-P. (1982) Formation of an inactive cytochrome P-450 Fe(II)-metabolite complex after administration of troleandomycin in humans. *Biochemical pharmacology* **31**, 1699-1704
111. Ortiz de Montellano, P. R., and Mathews, J. M. (1981) Autocatalytic alkylation of the cytochrome P-450 prosthetic haem group by 1-aminobenzotriazole. Isolation of an NN-bridged benzyne-protoporphyrin IX adduct. *The Biochemical journal* **195**, 761-764
112. Ortiz de Montellano, P. R., and Kunze, K. L. (1980) Self-catalyzed inactivation of hepatic cytochrome P-450 by ethynyl substrates. *The Journal of biological chemistry* **255**, 5578
113. Ortiz de Montellano, P. R., and Kunze, K. L. (1980) Occurrence of a 1,2 Shift during Enzymatic and Chemical Oxidation of a Terminal Acetylene. *Journal of the American Chemical Society* **102**, 7373-7375
114. Ortiz de Montellano, P. R., Beilan, H. S., and Kunze, K. L. (1981) N-Methylprotoporphyrin IX: chemical synthesis and identification as the green pigment produced by 3,5-diethoxycarbonyl-1,4-dihydrocollidine treatment. *Proceedings of the National Academy of Sciences of the United States of America* **78**, 1490
115. Kunze, K. L., and Ortiz de Montellano, P. R. (1981) N-Methylprotoporphyrin IX. Identification by NMR of the Nitrogen Alkylated in Each of the Four Isomers. *Journal of the American Chemical Society* **103**, 4225-4230
116. Correia, M. A., Farrell, G. C., Olson, S., Wong, J. S., Schmid, R., Ortiz de Montellano, P. R., Beilan, H. S., Kunze, K. L., and Mico, B. A. (1981) Cytochrome P-450 heme moiety. The specific target in drug-induced heme alkylation. *The Journal of biological chemistry* **256**, 5466

117. Kunze, K. L., Mangold, B. L., Wheeler, C., Beilan, H. S., and Ortiz de Montellano, P. R. (1983) The cytochrome P-450 active site. Regiospecificity of prosthetic heme alkylation by olefins and acetylenes. *The Journal of biological chemistry* **258**, 4202
118. De Montellano, P. R. O., Mico, B. A., Mathews, J. M., Kunze, K. L., Miwa, G. T., and Lu, A. Y. H. (1981) Selective inactivation of cytochrome P-450 isozymes by suicide substrates. *Archives of biochemistry and biophysics* **210**, 717-728
119. Rostami-Hodjegan, A. (2012) Physiologically based pharmacokinetics joined with in vitro-in vivo extrapolation of ADME: a marriage under the arch of systems pharmacology. *Clinical pharmacology and therapeutics* **92**, 50-61
120. Sager, J. E., Yu, J., Ragueneau-Majlessi, I., and Isoherranen, N. (2015) Physiologically Based Pharmacokinetic (PBPK) Modeling and Simulation Approaches: A systematic review of published models, applications and model verification. *Drug metabolism and disposition: the biological fate of chemicals*
121. Wagner, C., Zhao, P., Pan, Y., Hsu, V., Grillo, J., Huang, S. M., and Sinha, V. (2015) Application of Physiologically Based Pharmacokinetic (PBPK) Modeling to Support Dose Selection: Report of an FDA Public Workshop on PBPK. *CPT Pharmacometrics Syst Pharmacol* **4**, 226-230
122. McGinnity, D. F., Berry, A. J., Kenny, J. R., Grime, K., and Riley, R. J. (2006) Evaluation of time-dependent cytochrome P450 inhibition using cultured human hepatocytes. *Drug metabolism and disposition: the biological fate of chemicals* **34**, 1291-1300
123. Emery, M. G., Jubert, C., Thummel, K. E., and Kharasch, E. D. (1999) Duration of cytochrome P-450 2E1 (CYP2E1) inhibition and estimation of functional CYP2E1 enzyme half-life after single-dose disulfiram administration in humans. *The Journal of pharmacology and experimental therapeutics* **291**, 213-219
124. Chan, C. Y. S., Roberts, O., Rajoli, R. K. R., Liptrott, N. J., Siccardi, M., Almond, L., and Owen, A. (2018) Derivation of CYP3A4 and CYP2B6 degradation rate constants in primary human hepatocytes: A siRNA-silencing-based approach. *Drug Metabolism and Pharmacokinetics* **33**, 179-187
125. Fowler, S., and Zhang, H. (2008) In vitro evaluation of reversible and irreversible cytochrome P450 inhibition: current status on methodologies and their utility for predicting drug-drug interactions. *AAPS J* **10**, 410-424
126. Lutz, J. D., VandenBrink, B. M., Babu, K. N., Nelson, W. L., Kunze, K. L., and Isoherranen, N. (2013) Stereoselective inhibition of CYP2C19 and CYP3A4 by fluoxetine and its metabolite: implications for risk assessment of multiple time-dependent inhibitor systems. *Drug metabolism and disposition: the biological fate of chemicals* **41**, 2056-2065
127. Einolf, H. J., Chen, L., Fahmi, O. A., Gibson, C. R., Obach, R. S., Shebley, M., Silva, J., Sinz, M. W., Unadkat, J. D., Zhang, L., and Zhao, P. (2014) Evaluation of various static and dynamic modeling methods to predict clinical CYP3A induction using in vitro CYP3A4 mRNA induction data. *Clinical pharmacology and therapeutics* **95**, 179-188
128. Yang, J., Liao, M. X., Shou, M. G., Jamei, M., Yeo, K., Tucker, G., and Rostami-Hodjegan, A. (2008) Cytochrome P450 turnover: Regulation of synthesis and degradation, methods for determining rates, and implications for the prediction of drug interactions. *Curr. Drug Metab.* **9**, 384-393
129. Almond, L., Yang, J., Jamei, M., Tucker, G., and Rostami-Hodjegan, A. (2009) Towards a Quantitative Framework for the Prediction of DDIs Arising from Cytochrome P450 Induction. *Curr. Drug Metab.* **10**, 420-432
130. Glatt, M. M., George, H. R., and Frisch, E. P. (1965) Controlled trial of chlormethiazole in treatment of the alcoholic withdrawal phase. *British medical journal* **2**, 401-404
131. Lechat, P., and Streichenberger, G. (1966) [Pharmacologic study of the possible anti-Parkinson effect of chlormethiazole]. *Therapie* **21**, 1617-1621

132. Condie, R. G., and Tunstall, M. E. (1969) Chlormethiazole as a sedative in normal labour. *Acta Anaesthesiol Scand Suppl* **37**, 192-197
133. Duffus, G. M., Tunstall, M. E., Condie, R. G., and MacGillivray, I. (1969) Chlormethiazole in the prevention of eclampsia and the reduction of perinatal mortality. *J Obstet Gynaecol Br Commonw* **76**, 645-651
134. Hollister, L. E., Prusmack, J. J., and Lipscomb, W. (1972) Treatment of acute alcohol withdrawal with chlormethiazole (Heminevrin). *Dis Nerv Syst* **33**, 247-250
135. Nation, R. L., Vine, J., Triggs, E. J., and Learoyd, B. (1977) Plasma level of chlormethiazole and two metabolites after oral administration to young and aged human subjects. *European journal of clinical pharmacology* **12**, 137-145
136. Stanley, T. V. (1982) Oral chlormethiazole in childhood epilepsy. *Archives of disease in childhood* **57**, 242-243
137. Witts, D. J., Arnold, K., and Exton-Smith, A. N. (1983) The plasma levels of chlormethiazole and two of its metabolites in elderly subjects after single and multiple dosing. *Journal of pharmaceutical and biomedical analysis* **1**, 311-320
138. Lapierre, Y. D., Bulmer, D. R., Oyewumi, L. K., Mauguin, M. L., and Knott, V. J. (1983) Comparison of chlormethiazole (Heminevrin) and chlordiazepoxide (Librium) in the treatment of acute alcohol withdrawal. *Neuropsychobiology* **10**, 127-130
139. Pålsson, A. (1986) The efficacy of early chlormethiazole medication in the prevention of delirium tremens. A retrospective study of the outcome of different drug treatment strategies at the Helsingborg psychiatric clinics, 1975-1980. *Acta Psychiatr Scand Suppl* **329**, 140-145
140. Empson, R. M., Gee, V. J., Sheardown, M. J., and Newberry, N. R. (2000) Chlormethiazole inhibits epileptiform activity by potentiating GABA(A) receptor function. *Brain research* **884**, 31-34
141. Ulrich, S., Danos, P., Baumann, B., Muller, D., Lehmann, D., Treuheit, T. O., and Spieler, M. (2002) Serum concentration of chlormethiazole and therapeutic effect in acute alcohol withdrawal syndrome: an open clinical trial. *Therapeutic drug monitoring* **24**, 446-454
142. Usala, M., Thompson, S. A., Whiting, P. J., and Wafford, K. A. (2003) Activity of chlormethiazole at human recombinant GABA(A) and NMDA receptors. *British journal of pharmacology* **140**, 1045-1050
143. Zingmark, P. H., Ekblom, M., Odergren, T., Ashwood, T., Lyden, P., Karlsson, M. O., and Jonsson, E. N. (2003) Population pharmacokinetics of clomethiazole and its effect on the natural course of sedation in acute stroke patients. *British journal of clinical pharmacology* **56**, 173-183
144. Seifert, J., Peters, E., Jahn, K., Metzner, C., Ohlmeier, M., te Wildt, B., Emrich, H. M., and Schneider, U. (2004) Treatment of alcohol withdrawal: chlormethiazole vs. carbamazepine and the effect on memory performance--a pilot study. *Addiction biology* **9**, 43-51
145. Wilby, M. J., and Hutchinson, P. J. (2004) The pharmacology of chlormethiazole: a potential neuroprotective agent? *CNS Drug Rev* **10**, 281-294
146. AKTIENGESELLSCHAFT, F. H.-L. R. C. (1938) Verfahren zur Darstellung von 4-Methyl-5-B-chloräthylthiazol., Switzerland
147. Moore, R. G., Triggs, E. J., Shanks, C. A., and Thomas, J. (1975) Pharmacokinetics of chlormethiazole in humans. *European journal of clinical pharmacology* **8**, 353-357
148. Stresser, D. M., Perloff, E. S., Mason, A. K., Blanchard, A. P., Dehal, S. S., Creegan, T. P., Singh, R., and Gangl, E. T. (2016) Selective Time- and NADPH-Dependent Inhibition of Human CYP2E1 by Clomethiazole. *Drug metabolism and disposition: the biological fate of chemicals* **44**, 1424-1430
149. Hu, Y., Mishin, V., Johansson, I., von Bahr, C., Cross, A., Ronis, M. J., Badger, T. M., and Ingelman-Sundberg, M. (1994) Chlormethiazole as an efficient inhibitor of cytochrome

P450 2E1 expression in rat liver. *The Journal of pharmacology and experimental therapeutics* **269**, 1286-1291
150. Gouillon, Z., Lucas, D., Li, J., Hagbjork, A. L., French, B. A., Fu, P., Fang, C., Ingelman-Sundberg, M., Donohue, T. M., Jr., and French, S. W. (2000) Inhibition of ethanol-induced liver disease in the intragastric feeding rat model by chlormethiazole. *Proc Soc Exp Biol Med* **224**, 302-308
151. Lu, Y., Zhuge, J., Wang, X., Bai, J., and Cederbaum, A. I. (2008) Cytochrome P450 2E1 contributes to ethanol-induced fatty liver in mice. *Hepatology* **47**, 1483-1494
152. Gebhardt, A. C., Lucas, D., Menez, J. F., and Seitz, H. K. (1997) Chlormethiazole inhibition of cytochrome P450 2E1 as assessed by chlorzoxazone hydroxylation in humans. *Hepatology* **26**, 957-961
153. Dalvie, D. K., Kalgutkar, A. S., Khojasteh-Bakht, S. C., Obach, R. S., and O'Donnell, J. P. (2002) Biotransformation reactions of five-membered aromatic heterocyclic rings. *Chemical research in toxicology* **15**, 269-299
154. Obach, R. S., Kalgutkar, A. S., Ryder, T. F., and Walker, G. S. (2008) In vitro metabolism and covalent binding of enol-carboxamide derivatives and anti-inflammatory agents sudoxicam and meloxicam: insights into the hepatotoxicity of sudoxicam. *Chemical research in toxicology* **21**, 1890-1899
155. Hossain, M. A., Tran, T., Chen, T., Mikus, G., and Greenblatt, D. J. (2017) Inhibition of human cytochromes P450 in vitro by ritonavir and cobicistat. *Journal of Pharmacy and Pharmacology* **69**, 1786-1793
156. Lind, R. C., Gandolfi, A. J., Sipes, I. G., Brown, B. R., and Waters, S. J. (1986) Oxygen concentrations required for reductive defluorination of halothane by rat hepatic microsomes. *Anesthesia and analgesia* **65**, 835
157. Spracklin, D. K., Thummel, K. E., and Kharasch, E. D. (1996) Human reductive halothane metabolism in vitro is catalyzed by cytochrome P450 2A6 and 3A4. *Drug metabolism and disposition: the biological fate of chemicals* **24**, 976
158. Kharasch, E. D., Hankins, D., Mautz, D., and Thummel, K. E. (1996) Identification of the enzyme responsible for oxidative halothane metabolism: implications for prevention of halothane hepatitis. *The Lancet* **347**, 1367-1371
159. Spracklin, D. K., Hankins, D. C., Fisher, J. M., Thummel, K. E., and Kharasch, E. D. (1997) Cytochrome P450 2E1 is the principal catalyst of human oxidative halothane metabolism in vitro. *The Journal of pharmacology and experimental therapeutics* **281**, 400
160. Kharasch, E. D., Hankins, D. C., Fenstamaker, K., and Cox, K. (2000) Human halothane metabolism, lipid peroxidation, and cytochromes P 450 2A6 and P 450 3A4. *European journal of clinical pharmacology* **55**, 853-859
161. Spracklin, D. K., Emery, M. E., Thummel, K. E., and Kharasch, E. D. (2003) Concordance between trifluoroacetic acid and hepatic protein trifluoroacetylation after disulfiram inhibition of halothane metabolism in rats. *Acta anaesthesiologica Scandinavica* **47**, 765-770
162. D, lt, authfull, gt, source, and Science, K. (2002) Product class 17: thiazoles. *Science of Synthesis* **11**, 627-833
163. Chhabria, M., Patel, S., Modi, P., and Brahmkshatriya, P. S. (2016) Thiazole: A Review on Chemistry, Synthesis and Therapeutic Importance of its Derivatives. *Curr. Top. Med. Chem.* **16**, 2841-2862
164. Kashyap, A. (2018) Review on Synthetic Chemistry and Antibacterial Importance of Thiazole Derivatives. *Current Drug Discovery Technologies* **15**, 214-228
165. Stander-Grobler, E., Schuster, O., Strasser, C. E., Albrecht, M., Cronje, S., and Raubenheimer, H. G. (2011) Normal and abnormal carbene complexes derived from thiazole: Preparation and a preliminary investigation of their relative catalytic performance. *Polyhedron* **30**, 2776-2782

166. Kochetov, G., and Solovjeva, O. (2014) Structure and functioning mechanism of transketolase. *BBA-Proteins Proteomics* **1844**, 1608-1618
167. Jennings, G. K., Ritchie, C. M., Shock, L. S., Lyons, C. E., and Hackett, J. C. (2016) N-Heterocyclic Carbene Capture by Cytochrome P450 3A4. *Molecular pharmacology* **90**, 42
168. Campeau, L.-C., Bertrand-Laperle, M., Leclerc, J.-P., Villemure, E., Gorelsky, S., and Fagnou, K. (2008) C2, C5, and C4 azole N-oxide direct arylation including room-temperature reactions. *Journal of the American Chemical Society* **130**, 3276
169. Campeau, L.-C., Stuart, D. R., Leclerc, J.-P., Bertrand-Laperle, M., Villemure, E., Sun, H.-Y., Lasserre, S., Guimond, N., Lecavallier, M., and Fagnou, K. (2009) Palladium-catalyzed direct arylation of azine and azole N-oxides: reaction development, scope and applications in synthesis. *Journal of the American Chemical Society* **131**, 3291
170. Amir, E., and Rozen, S. (2006) Easy access to the family of thiazole N -oxides using HOF·CH 3 CN. *Chemical Communications*, 2262-2264
171. Yan, G., Borah, A. J., and Yang, M. (2014) Recent Advances in Catalytic Functionalization of N -Oxide Compounds via C□H Bond Activation. Weinheim
172. Dince, C. C., Meoded, R. A., and Hilvert, D. (2017) Synthesis and characterization of catalytically active thiazolium gold(i)-carbenes. *Chem. Commun.* **53**, 7585-7587
173. Zeitler, K. (2007) N-heterocyclic carbenes: organocatalysts displaying diverse modes of action. *Ernst Schering Foundation symposium proceedings*, 183-206
174. Kalgutkar, A. S., Driscoll, J., Zhao, S. X., Walker, G. S., Shepard, R. M., Soglia, J. R., Atherton, J., Yu, L., Mutlib, A. E., Munchhof, M. J., Reiter, L. A., Jones, C. S., Doty, J. L., Trevena, K. A., Shaffer, C. L., and Ripp, S. L. (2007) A rational chemical intervention strategy to circumvent bioactivation liabilities associated with a nonpeptidyl thrombopoietin receptor agonist containing a 2-amino-4-arylthiazole motif. *Chemical research in toxicology* **20**, 1954
175. Kalgutkar, A. S., Ryder, T. F., Walker, G. S., Orr, S. T., Cabral, S., Goosen, T. C., Lapham, K., and Eng, H. (2013) Reactive metabolite trapping studies on imidazo- and 2-methylimidazo[2,1-b]thiazole-based inverse agonists of the ghrelin receptor. *Drug metabolism and disposition: the biological fate of chemicals* **41**, 1375-1388
176. Yang, X., and Chen, W. (2005) In vitro microsomal metabolic studies on a selective mGluR5 antagonist MTEP: Characterization of in vitro metabolites and identification of a novel thiazole ring opening aldehyde metabolite. *Xenobiotica; the fate of foreign compounds in biological systems* **35**, 797-809
177. Green, M. D., Yang, X., Cramer, M., and King, C. D. (2006) In vitro metabolic studies on the selective metabotropic glutamate receptor sub-type 5 (mGluR5) antagonist 3-[(2-methyl-1,3-thiazol-4-yl) ethynyl]-pyridine (MTEP). *Neuroscience Letters* **391**, 91-95
178. Sychla, H., Gründer, G., and Lammertz, S. E. (2017) Comparison of Clomethiazole and Diazepam in the Treatment of Alcohol Withdrawal Syndrome in Clinical Practice. *Eur Addict Res* **23**, 211-218
179. Reid, J., and Judge, T. G. (1980) Chlormethiazole night sedation in elderly subjects receiving other medications. *The Practitioner* **224**, 751-753
180. Majumdar, S. K. (1978) The effect of chlormethiazole on hepatic microsomal enzymes. *Pharmatherapeutica* **2**, 27-30
181. Hoensch, H. P. (1986) Effect of chlormethiazole on the hepatic monooxygenase enzyme system. *Acta Psychiatr Scand Suppl* **329**, 66-68
182. Waxman, D. J., Lapenson, D. P., Aoyama, T., Gelboin, H. V., Gonzalez, F. J., and Korzekwa, K. (1991) Steroid hormone hydroxylase specificities of eleven cDNA-expressed human cytochrome P450s. *Archives of biochemistry and biophysics* **290**, 160-166
183. Eap, C. B., Schnyder, C., Besson, J., Savary, L., and Buclin, T. (1998) Inhibition of CYP2E1 by chlormethiazole as measured by chlorzoxazone pharmacokinetics in patients

with alcoholism and in healthy volunteers. *Clinical pharmacology and therapeutics* **64**, 52-57
184. Mudie, D. M., Murray, K., Hoad, C. L., Pritchard, S. E., Garnett, M. C., Amidon, G. L., Gowland, P. A., Spiller, R. C., Amidon, G. E., and Marciani, L. (2014) Quantification of gastrointestinal liquid volumes and distribution following a 240 mL dose of water in the fasted state. *Mol Pharm* **11**, 3039-3047
185. Bjornsson, T. D., Callaghan, J. T., Einolf, H. J., Fischer, V., Gan, L., Grimm, S., Kao, J., King, S. P., Miwa, G., Ni, L., Kumar, G., McLeod, J., Obach, S. R., Roberts, S., Roe, A., Shah, A., Snikeris, F., Sullivan, J. T., Tweedie, D., Vega, J. M., Walsh, J., Wrighton, S. A., and Groups, P. R. a. M. o. A. D. M. C. P. T. W. (2003) The conduct of in vitro and in vivo drug-drug interaction studies: a PhRMA perspective. *J Clin Pharmacol* **43**, 443-469
186. Bourrie, M., Meunier, V., Berger, Y., and Fabre, G. (1996) Cytochrome P450 isoform inhibitors as a tool for the investigation of metabolic reactions catalyzed by human liver microsomes. *The Journal of pharmacology and experimental therapeutics* **277**, 321-332
187. Stresser, D. M., Mao, J., Kenny, J. R., Jones, B. C., and Grime, K. (2014) Exploring concepts of in vitro time-dependent CYP inhibition assays. *Expert opinion on drug metabolism & toxicology* **10**, 157-174
188. Yan, Z., and Caldwell, G. W. (2013) In vitro identification of cytochrome P450 enzymes responsible for drug metabolism. *Methods Mol Biol* **1015**, 251-261
189. Backman, J. T., Filppula, A. M., Niemi, M., and Neuvonen, P. J. (2016) Role of Cytochrome P450 2C8 in Drug Metabolism and Interactions. *Pharmacol Rev* **68**, 168-241
190. FDA. (2015) Drug Interactions & Labeling - Drug Development and Drug Interactions: Table of Substrates, Inhibitors and Inducers.
191. Yuan, R., Madani, S., Wei, X. X., Reynolds, K., and Huang, S. M. (2002) Evaluation of cytochrome P450 probe substrates commonly used by the pharmaceutical industry to study in vitro drug interactions. *Drug metabolism and disposition: the biological fate of chemicals* **30**, 1311-1319
192. Khojasteh, S. C., Prabhu, S., Kenny, J. R., Halladay, J. S., and Lu, A. Y. (2011) Chemical inhibitors of cytochrome P450 isoforms in human liver microsomes: a re-evaluation of P450 isoform selectivity. *European journal of drug metabolism and pharmacokinetics* **36**, 1-16
193. Rosenblatt, D. H., Epstein, T., and Levitch, M. (1953) Some Nuclearly Substituted Catechols and their Acid Dissociation Constants. *Journal of the American Chemical Society* **75**, 3277-3278
194. Kline, M., and Cheatham, S. (2003) A robust method for determining 1 H– 15 N long-range correlations: 15 N optimized CIGAR-HMBC experiments. *Magnetic Resonance in Chemistry* **41**, 307-314
195. Cox, B., and Emili, A. (2006) Tissue subcellular fractionation and protein extraction for use in mass-spectrometry-based proteomics. *Nat Protoc* **1**, 1872-1878
196. Copeland, R. A. (2005) Evaluation of enzyme inhibitors in drug discovery. A guide for medicinal chemists and pharmacologists. *Methods Biochem Anal* **46**, 1-265
197. Copeland, R. A. (2000) *Enzymes : a practical introduction to structure, mechanism, and data analysis*, 2nd ed. ed., New York : Wiley, New York
198. Lucas, D., Ferrara, R., Gonzalez, E., Bodenez, P., Albores, A., Manno, M., and Berthou, F. (1999) Chlorzoxazone, a selective probe for phenotyping CYP2E1 in humans. *Pharmacogenetics* **9**, 377-388
199. Ono, S., Hatanaka, T., Hotta, H., Tsutsui, M., Satoh, T., and Gonzalez, F. J. (1995) Chlorzoxazone is metabolized by human CYP1A2 as well as by human CYP2E1. *Pharmacogenetics* **5**, 143-150
200. Yamamura, Y., Koyama, N., and Umehara, K. (2015) Comprehensive kinetic analysis and influence of reaction components for chlorzoxazone 6-hydroxylation in human liver

microsomes with CYP antibodies. *Xenobiotica; the fate of foreign compounds in biological systems* **45**, 353-360
201. Yamazaki, H., Guo, Z., and Guengerich, F. P. (1995) Selectivity of cytochrome P4502E1 in chlorzoxazone 6-hydroxylation. *Drug metabolism and disposition: the biological fate of chemicals* **23**, 438-440
202. Shou, M., Dai, R., Cui, D., Korzekwa, K. R., Baillie, T. A., and Rushmore, T. H. (2001) A kinetic model for the metabolic interaction of two substrates at the active site of cytochrome P450 3A4. *The Journal of biological chemistry* **276**, 2256-2262
203. Albaugh, D., Farrell, T., Langan, M., and Lai, W. G. (2009) High throughput quantitative assessment of CYP inactivation using 2 concentration points. *Drug metabolism letters* **3**, 78-82
204. Abdelmegeed, M. A., Banerjee, A., Jang, S., Yoo, S. H., Yun, J. W., Gonzalez, F. J., Keshavarzian, A., and Song, B. J. (2013) CYP2E1 potentiates binge alcohol-induced gut leakiness, steatohepatitis, and apoptosis. *Free Radic Biol Med* **65**, 1238-1245
205. Cederbaum, A. I. (2010) Role of CYP2E1 in ethanol-induced oxidant stress, fatty liver and hepatotoxicity. *Dig Dis* **28**, 802-811
206. Chen, Y. Y., Zhang, C. L., Zhao, X. L., Xie, K. Q., and Zeng, T. (2014) Inhibition of cytochrome P4502E1 by chlormethiazole attenuated acute ethanol-induced fatty liver. *Chemico-biological interactions* **222C**, 18-26
207. Wu, D., Wang, X., Zhou, R., Yang, L., and Cederbaum, A. I. (2012) Alcohol steatosis and cytotoxicity: the role of cytochrome P4502E1 and autophagy. *Free Radic Biol Med* **53**, 1346-1357
208. Löfgren, S., Hagbjörk, A. L., Ekman, S., Fransson-Steen, R., and Terelius, Y. (2004) Metabolism of human cytochrome P450 marker substrates in mouse: a strain and gender comparison. *Xenobiotica; the fate of foreign compounds in biological systems* **34**, 811-834
209. Shi, S. M., and Di, L. (2017) The role of carbonyl reductase 1 in drug discovery and development. Taylor & Francis
210. Baillie, T. A., and Davis, M. R. (1993) Mass spectrometry in the analysis of glutathione conjugates. *Biological Mass Spectrometry* **22**, 319-325
211. Murphy, C. M., Fenselau, C., and Gutierrez, P. L. (1992) Fragmentation characteristic of glutathione conjugates activated by high-energy collisions. *Journal of the American Society for Mass Spectrometry* **3**, 815-822
212. Zhu, J., Kong, Y., Lin, F., Wang, B., Chen, Z., and Liu, L. (2015) Copper-Catalyzed Direct Amination of 1,2,3-Triazole N-Oxides by C–H Activation and C–N Coupling. *European Journal of Organic Chemistry* **2015**, 1507-1515
213. Ende, M., Spiteller, G., Remberg, G., and Heipertz, R. (1979) Urinary metabolites of clomethiazole. Detection and structural analysis by gas chromatography-mass spectrometry. *Arzneimittelforschung* **29**, 1655-1658
214. Grupe, A., and Spiteller, G. (1982) Unexpected metabolites produced from clomethiazole. *J Chromatogr* **230**, 335-344
215. Osmundsen, H., Bremer, J., and Pedersen, J. (1991) METABOLIC ASPECTS OF PEROXISOMAL BETA-OXIDATION. *Biochimica Et Biophysica Acta* **1085**, 141-158
216. Bhateria, M., Ramakrishna, R., Puttrevu, S. K., Saxena, A. K., and Bhatta, R. S. (2016) Enantioselective inhibition of Cytochrome P450-mediated drug metabolism by a novel antithrombotic agent, S002-333: Major effect on CYP2B6. *Chemico-biological interactions* **256**, 257-265
217. Bhattacharya, C., Kirby, D., Van Stipdonk, M., and Stratford, R. E. (2019) Comparison of In Vitro Stereoselective Metabolism of Bupropion in Human, Monkey, Rat, and Mouse Liver Microsomes. *European journal of drug metabolism and pharmacokinetics* **44**, 261-274

218. Coles, R., and Kharasch, E. D. (2008) Stereoselective metabolism of bupropion by cytochrome P4502B6 (CYP2B6) and human liver microsomes. *Pharm Res* **25**, 1405-1411
219. Kharasch, E. D., Mitchell, D., and Coles, R. (2008) Stereoselective bupropion hydroxylation as an in vivo phenotypic probe for cytochrome P4502B6 (CYP2B6) activity. *J Clin Pharmacol* **48**, 464-474
220. Sager, J. E., Price, L. S. L., and Isoherranen, N. (2016) Stereoselective metabolism of bupropion to OH-bupropion, threohydrobupropion, erythrohydrobupropion, and 49-OH-bupropion in vitro. *Drug Metabolism and Disposition* **44**, 1709-1719
221. Galetin, A., Clarke, S. E., and Houston, J. B. (2003) Multisite kinetic analysis of interactions between prototypical CYP3A4 subgroup substrates: midazolam, testosterone, and nifedipine. *Drug metabolism and disposition: the biological fate of chemicals* **31**, 1108-1116
222. Kenworthy, K. E., Bloomer, J. C., Clarke, S. E., and Houston, J. B. (1999) CYP3A4 drug interactions: correlation of 10 in vitro probe substrates. *British journal of clinical pharmacology* **48**, 716-727
223. Stresser, D. M., Blanchard, A. P., Turner, S. D., Erve, J. C., Dandeneau, A. A., Miller, V. P., and Crespi, C. L. (2000) Substrate-dependent modulation of CYP3A4 catalytic activity: analysis of 27 test compounds with four fluorometric substrates. *Drug metabolism and disposition: the biological fate of chemicals* **28**, 1440-1448
224. Koley, A. P., Buters, J. T., Robinson, R. C., Markowitz, A., and Friedman, F. K. (1995) CO binding kinetics of human cytochrome P450 3A4. Specific interaction of substrates with kinetically distinguishable conformers. *The Journal of biological chemistry* **270**, 5014-5018
225. Prasad, B., Bhatt, D. K., Johnson, K., Chapa, R., Chu, X., Salphati, L., Xiao, G., Lee, C., Hop, C. E. C. A., Mathias, A., Lai, Y., Liao, M., Humphreys, W. G., Kumer, S. C., and Unadkat, J. D. (2018) Abundance of phase 1 and 2 drug-metabolizing enzymes in alcoholic and hepatitis C cirrhotic livers: A quantitative targeted proteomics study. *Drug Metabolism and Disposition* **46**, 943-952
226. Zhang, H.-F., Li, Z.-H., Liu, J.-Y., Liu, T.-T., Wang, P., Fang, Y., Zhou, J., Cui, M.-Z., Gao, N., Tian, X., Gao, J., Wen, Q., Jia, L.-J., and Qiao, H.-L. (2016) Correlation of Cytochrome P450 Oxidoreductase Expression with the Expression of 10 Isoforms of Cytochrome P450 in Human Liver. *Drug metabolism and disposition: the biological fate of chemicals* **44**, 1193
227. Ishii, Y., Koba, H., Kinoshita, K., Oizaki, T., Iwamoto, Y., Takeda, S., Miyauchi, Y., Nishimura, Y., Egoshi, N., Taura, F., Morimoto, S., Ikushiro, S., Nagata, K., Yamazoe, Y., Mackenzie, P. I., and Yamada, H. (2014) Alteration of the function of the UDP-glucuronosyltransferase 1A subfamily by cytochrome P450 3A4: different susceptibility for UGT isoforms and UGT1A1/7 variants. *Drug metabolism and disposition: the biological fate of chemicals* **42**, 229-238
228. Fisher, M. B., Campanale, K., Ackermann, B. L., VandenBranden, M., and Wrighton, S. A. (2000) In vitro glucuronidation using human liver microsomes and the pore-forming peptide alamethicin. *Drug metabolism and disposition: the biological fate of chemicals* **28**, 560-566
229. Yan, Z., and Caldwell, G. W. (2003) Metabolic assessment in liver microsomes by co-activating cytochrome P450s and UDP-glycosyltransferases. *European journal of drug metabolism and pharmacokinetics* **28**, 223-232
230. Castro-Perez, J., Plumb, R., Liang, L., and Yang, E. (2005) A high-throughput liquid chromatography/tandem mass spectrometry method for screening glutathione conjugates using exact mass neutral loss acquisition. *Rapid Commun Mass Spectrom* **19**, 798-804
231. Hemes in Biology. in *Wiley Encyclopedia of Chemical Biology*. pp 1-10
232. Poulos, T. (2014) Heme Enzyme Structure and Function. *Chem. Rev.* **114**, 3919-3962
233. Kadish, K. M., Smith, K. M., and Guilard, R. (2012) *The Porphyrin Handbook: The Iron and Cobalt Pigments: Biosynthesis, Structure and Degradation*,

234. Ramanujam, V.-M. S., and Anderson, K. E. (2015) Porphyria Diagnostics-Part 1: A Brief Overview of the Porphyrias. *Current protocols in human genetics* **86**, 17.20.11
235. Chiabrando, D., Fiorito, V., Petrillo, S., and Tolosano, E. (2018) Unraveling the Role of Heme in Neurodegeneration. *Front. Neurosci.* **12**
236. discusses the signal transduction and immunomodulatory mechanism in inflammation and summarizes the promising therapeutic strategies based on this pathway in inflammatory and immune, d. (2019) Heme Catabolic Pathway in Inflammation and Immune Disorders. *Frontiers in Pharmacology* **10**
237. Chiang, S. K., Chen, S. E., and Chang, L. C. (2019) A dual role of heme oxygenase-1 in cancer cells. *International Journal of Molecular Sciences* **20**, <xocs:firstpage xmlns:xocs=""/>
238. Sachar, M., Anderson, K., and Ma, X. C. (2016) Protoporphyrin IX: the Good, the Bad, and the Ugly. *J. Pharmacol. Exp. Ther.* **356**, 267-275
239. Yoshida, T., and Migita, C. T. (2000) Mechanism of heme degradation by heme oxygenase. *Journal of Inorganic Biochemistry* **82**, 33-41
240. Liu, Y., and Ortiz de Montellano, P. R. (2000) Reaction intermediates and single turnover rate constants for the oxidation of heme by human heme oxygenase-1. *The Journal of biological chemistry* **275**, 5297
241. Liu, Y., Moënne-Loccoz, P., Loehr, T. M., and Ortiz de Montellano, P. R. (1997) Heme oxygenase-1, intermediates in verdoheme formation and the requirement for reduction equivalents. *The Journal of biological chemistry* **272**, 6909
242. O'brien, L., Hosick, P. A., John, K., Stec, D. E., and Hinds, T. D. (2015) Biliverdin reductase isozymes in metabolism. *Trends in Endocrinology & Metabolism* **26**, 212-220
243. Steventon, G. (2019) Uridine diphosphate glucuronosyltransferase 1A1. *Xenobiotica; the fate of foreign compounds in biological systems*, 1
244. Cole, S. P. C., Ortiz De Montellano, P. R., Kunze, K. L., and Marks, G. S. (1981) Inhibition of hepatic ferrochelatase by N-methylprotoporphyrin. *Pharmacologist* **23**, No. 248
245. Ortiz de Montellano, P. R., Kunze, K. L., Cole, S. P. C., and Marks, G. S. (1980) Inhibition of hepatic ferrochelatase by the four isomers of N-methylprotoporphyrin IX. *Biochemical and Biophysical Research Communications* **97**, 1436-1442
246. Ortiz de Montellano, P. R. (2005) *Cytochrome P450 : structure, mechanism, and biochemistry*, 3rd ed., Kluwer Academic/Plenum Publishers, New York
247. Miller, E. C., and Miller, J. A. (1947) The Presence and Significance of Bound Aminoazo Dyes in the Livers of Rats Fed p-Dimethylaminoazobenzene. *Cancer Research* **7**, 468-480
248. Miller, J. A., and Miller, E. C. (1947) The metabolism and carcinogenicity of p-dimethylaminoazobenzene and related compounds in the rat. *Cancer research* **7**, 39
249. Halpert, J., and Neal, R. A. (1980) Inactivation of purified rat liver cytochrome P-450 by chloramphenicol. *Molecular pharmacology* **17**, 427
250. Bond, E. J., and De Matteis, F. (1969) Biochemical changes in rat liver after administration of carbon disulphide, with particular reference to microsomal changes. *Biochemical pharmacology* **18**, 2531-2549
251. De Matteis, F. (1970) Rapid loss of cytochrome P-450 and haem caused in the liver microsomes by the porphyrogenic agent 2-allyl-2-isopropylacetamide. *FEBS Letters* **6**, 343-345
252. Teichmann, L. K. (1853) Lieber die Kristallisation der organischen Bestandteile des Bluts. *Zeitschrift für rationelle Median* **111**, 375-388
253. Nencki, M., and Zaleski, J. (1900) Untersuchungen über den Blutfarbstoff. *Hoppe-Seyler's Zeitschrift fur Physiologische Chemie* **30**, 384-435
254. Fischer, H. (1941) Hemin. *Organic Syntheses* **21**, 53

255. Porubsky, P. R., Meneely, K. M., and Scott, E. E. (2008) Structures of human cytochrome P-450 2E1. Insights into the binding of inhibitors and both small molecular weight and fatty acid substrates. *The Journal of biological chemistry* **283**, 33698
256. Henne, K. R., Kunze, K. L., Zheng, Y.-M., Christmas, P., Soberman, R. J., and Rettie, a. E. (2001) Covalent linkage of prosthetic heme to CYP4 family P450 enzymes. *Biochemistry* **40**, 12925
257. Morrison, D. B., and Williams, E. F. (1941) The Solubility and Titration of Hemin and Ferrihemic Acid. *Journal of Biological Chemistry* **137**, 461-473
258. Morrison, M., and Stotz, E. (1957) The extraction and paper chromatography of hemins. *The Journal of biological chemistry* **228**, 123-130
259. Morrison, M., and Stotz, E. (1955) Partition chromatography of hemins; separation of the prosthetic groups of cytochromes a and a3. *The Journal of biological chemistry* **213**, 373-378
260. Sinclair, P. R., Gorman, N., and Jacobs, J. M. (2001) Measurement of heme concentration. *Current protocols in toxicology / editorial board, Mahin D. Maines (editor-in-chief) ... [et al.]* **8**, Unit 8.3
261. He, K., Woolf, T. F., and Hollenberg, P. F. (1999) Mechanism-based inactivation of cytochrome P-450-3A4 by mifepristone (RU486). *The Journal of pharmacology and experimental therapeutics* **288**, 791
262. Guengerich, F. P. (1978) Destruction of Heme and Hemoproteins Mediated by Liver Microsomal Reduced Nicotinamide Adenine Dinucleotide Phosphate-Cytochrome P-450 Reductase. *Biochemistry* **17**, 3633-3639
263. Augusto, O., Kunze, K. L., and Ortiz de Montellano, P. R. (1982) N-Phenylprotoporphyrin IX formation in the hemoglobin-phenylhydrazine reaction. Evidence for a protein-stabilized iron-phenyl intermediate. *The Journal of biological chemistry* **257**, 6231
264. Annesley, T. M. (2003) Ion suppression in mass spectrometry. *Clin. Chem.* **49**, 1041-1044
265. Brown, P. R., and Krstulovic, A. M. (1979) Practical aspects of reversed-phase liquid chromatography applied to biochemical and biomedical research. *Analytical Biochemistry* **99**, 1-21
266. Collier, G. S., Pratt, J. M., De Wet, C. R., and Tshabalala, C. F. (1979) Studies on haemin in dimethyl sulphoxide/water mixtures. *The Biochemical journal* **179**, 281
267. Zhang, H., Zhang, D., and Ray, K. (2003) A software filter to remove interference ions from drug metabolites in accurate mass liquid chromatography/mass spectrometric analyses. *Journal of Mass Spectrometry* **38**, 1110-1112
268. Halpert, J. R. (2001) A Truncation of 2B Subfamily Cytochromes P450 Yields Increased Expression Levels, Increased Solubility, and Decreased Aggregation While Retaining Function. *Archives of biochemistry and biophysics* **395**, 57-68
269. Treuheit, N. A., Redhair, M., Hyewon, K., McClary, W. D., Guttman, M., Sumida, J. P., and Atkins, W. M. (2016) Membrane interactions, ligand-dependent dynamics, and stability of cytochrome P4503A4 in lipid nanodiscs.(Report). **55**, 1058-1069
270. Bauer, S., and Shiloach, J. (1974) Maximal exponential growth rate and yield of E. coli obtainable in a bench-scale fermentor. *Biotechnology and Bioengineering* **16**, 933-941
271. Barr, I., and Guo, F. (2015) Pyridine Hemochromagen Assay for Determining the Concentration of Heme in Purified Protein Solutions. *Bio-protocol* **5**
272. Schenkman, J. B., and Jansson, I. (2006) Spectral analyses of cytochromes P450. *Methods in molecular biology (Clifton, N.J.)* **320**, 11-18
273. Kot, M., and Daniel, W. A. (2009) Effect of diethyldithiocarbamate (DDC) and ticlopidine on CYP1A2 activity and caffeine metabolism: an in vitro comparative study with human cDNA-expressed CYP1A2 and liver microsomes. *Pharmacol Rep* **61**, 1216-1220

274. De Montellano, P. R. O., and Kunze, K. L. (1981) Shift of the acetylenic hydrogen during chemical and enzymatic oxidation of the biphenylacetylene triple bond. *Archives of biochemistry and biophysics* **209**, 710-712
275. Ortiz de Montellano, P. R., Augusto, O., Viola, F., and Kunze, K. L. (1983) Carbon radicals in the metabolism of alkyl hydrazines. *The Journal of biological chemistry* **258**, 8623
276. Ortiz de Montellano, P. R., and Kunze, K. L. (1981) Formation of N-Phenylheme in the Hemolytic Reaction of Phenylhydrazine with Hemoglobin. *Journal of the American Chemical Society* **103**, 6534-6536
277. Mackman, R., Guo, Z., Guengerich, F. P., and Ortiz De Montellano, P. R. (1996) Active site topology of human cytochrome P450 2E1. *Chemical research in toxicology* **9**, 223-226
278. Evans, J. P., Niemevz, F., Buldain, G., and de Montellano, P. O. (2008) Isoporphyrin intermediate in heme oxygenase catalysis - Oxidation of alpha-meso-phenylheme. *J. Biol. Chem.* **283**, 19530-19539
279. Rivera, M., and Zeng, Y. (2005) Heme oxygenase, steering dioxygen activation toward heme hydroxylation. *Journal of Inorganic Biochemistry* **99**, 337-354
280. Wilks, A., and Heinzl, G. (2014) Heme oxygenation and the widening paradigm of heme degradation. *Archives of biochemistry and biophysics* **544**, 87-95
281. Guengerich, F. P. (1986) Covalent binding to apoproteins is a major fate of heme in a variety of reactions in which cytochrome P-450 is destroyed. *Biochem. Biophys. Res. Commun.* **138**
282. Schaefer, W. H., Harris, T. M., and Guengerich, F. P. (1985) Characterization of the Enzymatic and Nonenzymatic Peroxidative Degradation of Iron Porphyrins and Cytochrome P-450 Heme. *Biochemistry* **24**, 3254-3263
283. Kunze, K. L., and Ortiz de Montellano, P. R. (1983) Formation of a σ-Bonded Aryliron Complex in the Reaction of Arylhydrazines with Hemoglobin and Myoglobin. *Journal of the American Chemical Society* **105**, 1380-1381
284. Licad-Coles, E., He, K., Yin, H., and Correia, M. A. (1997) Cytochrome P450 2C11:Escherichia coliExpression, Purification, Functional Characterization, and Mechanism-Based Inactivation of the Enzyme. *Archives of biochemistry and biophysics* **338**, 35-42
285. Reinen, J., Smit, M., and Wenker, M. (2018) Evaluation of Strategies for the Assessment of Drug–Drug Interactions Involving Cytochrome P450 Enzymes. *European journal of drug metabolism and pharmacokinetics* **43**, 737-750
286. Stachulski, A. V., Baillie, T. A., Kevin Park, B., Scott Obach, R., Dalvie, D. K., Williams, D. P., Srivastava, A., Regan, S. L., Antoine, D. J., Goldring, C. E. P., Chia, A. J. L., Kitteringham, N. R., Randle, L. E., Callan, H., Castrejon, J. L., Farrell, J., Naisbitt, D. J., and Lennard, M. S. (2013) The Generation, Detection, and Effects of Reactive Drug Metabolites.
287. Perret, A., and Pompon, D. (1998) Electron shuttle between membrane-bound cytochrome P450 3A4 and b5 rules uncoupling mechanisms. *Biochemistry* **37**, 11412
288. Denisov, I., Baas, B., Grinkova, Y., and Sligar, S. G. (2007) Cooperativity in cytochrome P450 3A4 - Linkages in substrate binding, spin state, uncoupling, and product formation. *J. Biol. Chem.* **282**, 7066-7076
289. Locuson, C. W., Wienkers, L. C., Jones, J. P., and Tracy, T. S. (2007) CYP2C9 protein interactions with cytochrome b(5): effects on the coupling of catalysis. *Drug metabolism and disposition: the biological fate of chemicals* **35**, 1174
290. Serron, S. C., Dwivedi, N., and Backes, W. L. (2000) Ethylbenzene induces microsomal oxygen free radical generation: antibody-directed characterization of the responsible cytochrome P450 enzymes. *Toxicol Appl Pharmacol* **164**, 305-311

291. He, K., Woolf, T. F., Kindt, E. K., Fielder, A. E., and Talaat, R. E. (2001) Troglitazone quinone formation catalyzed by human and rat CYP3A: an atypical CYP oxidation reaction☆. *Biochemical pharmacology* **62**, 191-198
292. Sodhi, J. K., Delarosa, E. M., Halladay, J. S., Driscoll, J. P., Mulder, T., Dansette, P. M., and Khojasteh, S. C. (2017) Inhibitory Effects of Trapping Agents of Sulfur Drug Reactive Intermediates against Major Human Cytochrome P450 Isoforms. *International journal of molecular sciences* **18**
293. Vidova, V., and Spacil, Z. (2017) A review on mass spectrometry-based quantitative proteomics: Targeted and data independent acquisition. *Analytica Chimica Acta* **964**, 7-23
294. Treuheit, N. A., Redhair, M., Kwon, H., McClary, W. D., Guttman, M., Sumida, J. P., and Atkins, W. M. (2016) Membrane Interactions, Ligand-Dependent Dynamics, and Stability of Cytochrome P4503A4 in Lipid Nanodiscs. *Biochemistry* **55**, 1058
295. Raccor, B. S., Claessens, A. J., Dinh, J. C., Park, J. R., Hawkins, D. S., Thomas, S. S., Makar, K. W., McCune, J. S., and Totah, R. A. (2012) Potential contribution of cytochrome P450 2B6 to hepatic 4-hydroxycyclophosphamide formation in vitro and in vivo. *Drug metabolism and disposition: the biological fate of chemicals* **40**, 54
296. Shaw, P. M., Hosea, N. A., Thompson, D. V., Lenius, J. M., and Guengerich, F. P. (1997) Reconstitution Premixes for Assays Using Purified Recombinant Human Cytochrome P450, NADPH-Cytochrome P450 Reductase, and Cytochromeb5. *Archives of biochemistry and biophysics* **348**, 107-115
297. Ghisla, S., Massey, V., Lhoste, J. M., and Mayhew, S. G. (1974) Fluorescence and optical characteristics of reduced flavines and flavoproteins. *Biochemistry* **13**, 589
298. Macheroux, P. (1999) UV-visible spectroscopy as a tool to study flavoproteins. *Methods in molecular biology (Clifton, N.J.)* **131**, 1-7
299. Taguchi, M., Imaoka, S., Yoshii, K., Kobayashi, K., Hosokawa, M., Shimada, N., Funae, Y., and Chiba, K. (2001) Kinetics of testosterone 6beta-hydroxylation in the reconstituted system with similar ratios of purified CYP3A4, NADPH-cytochrome p450 oxidoreductase and cytochrome B5 to human liver microsomes. *Research communications in molecular pathology and pharmacology* **109**, 53
300. Stander-Grobler E., S. O., Strasser C.E., Albrecht M., Cronje S., Raubenheimer H.G. (2011) Normal and abnormal carbene complexes derived from thiazole: Preparation and a preliminary investigation of their relative catalytic performance. *Polyhedron* **30**, 7
301. Raner, G. M., Hatchell, A. J., Morton, P. E., Ballou, D. P., and Coon, M. J. (2000) Stopped-flow spectrophotometric analysis of intermediates in the peroxo-dependent inactivation of cytochrome P450 by aldehydes. *Journal of Inorganic Biochemistry* **81**, 153-160
302. Beer, S. M., Taylor, E. R., Brown, S. E., Dahm, C. C., Costa, N. J., Runswick, M. J., and Murphy, M. P. (2004) Glutaredoxin 2 catalyzes the reversible oxidation and glutathionylation of mitochondrial membrane thiol proteins: implications for mitochondrial redox regulation and antioxidant DEFENSE. *The Journal of biological chemistry* **279**, 47939
303. Hurd, T. R., Costa, N. J., Dahm, C. C., Beer, S. M., Brown, S. E., Filipovska, A., and Murphy, M. P. (2005) Glutathionylation of mitochondrial proteins. *Antioxidants & redox signaling* **7**, 999
304. Chen, Y., Chen, C., Pfeiffer, D., and Zweier, J. (2007) Mitochondrial complex II in the post-ischemic heart - Oxidative injury and the role of protein S-glutathionylation. *J. Biol. Chem.* **282**, 32640-32654
305. Hu, Y., Wang, T., Liao, X., Du, G., Chen, J., and Xu, J. (2010) Anti-oxidative stress and beyond: multiple functions of the protein glutathionylation. *Protein and peptide letters* **17**, 1234

306. Yang, X., Greenhaw, J., Ali, A., Shi, Q., Roberts, D. W., Hinson, J. A., Muskhelishvili, L., Beger, R., Pence, L. M., Ando, Y., Sun, J., Davis, K., and Salminen, W. F. (2012) Changes in mouse liver protein glutathionylation after acetaminophen exposure. *The Journal of pharmacology and experimental therapeutics* **340**, 360
307. Sun, C., Shi, Z.-Z., Zhou, X., Chen, L., and Zhao, X.-M. (2013) Prediction of S-Glutathionylation Sites Based on Protein Sequences.(Research Article). *PloS one* **8**, e55512
308. Harvison, P. J., Guengerich, F. P., Rashed, M. S., and Nelson, S. D. (1988) Cytochrome P-450 isozyme selectivity in the oxidation of acetaminophen. *Chemical research in toxicology* **1**, 47-52
309. Ghanizadeh, A. (2012) Acetaminophen may mediate oxidative stress and neurotoxicity in autism. *Medical hypotheses* **78**, 351
310. Hirano, T., Kaplowitz, N., Tsukamoto, H., Kamimura, S., and Fernandez-Checa, J. C. (1992) Hepatic mitochondrial glutathione depletion and progression of experimental alcoholic liver disease in rats. *Hepatology* **16**, 1423-1427
311. Lu, Y., Wu, D., Wang, X., Ward, S. C., and Cederbaum, A. I. (2010) Chronic alcohol-induced liver injury and oxidant stress are decreased in cytochrome P4502E1 knockout mice and restored in humanized cytochrome P4502E1 knock-in mice. *Free Radic Biol Med* **49**, 1406-1416
312. Cederbaum, A. I. (2012) CYP2E1 potentiates toxicity in obesity and after chronic ethanol treatment. *Drug Metabol Drug Interact* **27**, 125-144
313. Song, B. J., Akbar, M., Jo, I., Hardwick, J. P., and Abdelmegeed, M. A. (2015) Translational Implications of the Alcohol-Metabolizing Enzymes, Including Cytochrome P450-2E1, in Alcoholic and Nonalcoholic Liver Disease. *Adv Pharmacol* **74**, 303-372
314. Livero, F. A., and Acco, A. (2015) Molecular basis of alcoholic fatty liver disease: From incidence to treatment. *Hepatol Res*
315. Lisi, G. P., and Loria, J. P. (2016) Solution NMR Spectroscopy for the Study of Enzyme Allostery. *Chem. Rev.* **116**, 6323-6369
316. Cameron, M. D., Wen, B., Roberts, A. G., Atkins, W. M., Campbell, A. P., and Nelson, S. D. (2007) Cooperative binding of acetaminophen and caffeine within the P450 3A4 active site. *Chemical research in toxicology* **20**, 1434
317. Pearson, J. T., Isoherranen, N., Hill, J. J., Swank, J., Kunze, K. L., and Atkins, W. M. (2006) Surface plasmon resonance analysis of antifungal azoles binding to CYP3A4 with kinetic resolution of multiple binding orientations. *Biochemistry* **45**, 6341
318. Porubsky, P. R., Battaile, K. P., and Scott, E. E. (2010) Human cytochrome P450 2E1 structures with fatty acid analogs reveal a previously unobserved binding mode. *The Journal of biological chemistry* **285**, 22282-22290
319. Hsu, M.-H., Savas, U., and Johnson, E. F. (2018) The X-Ray Crystal Structure of the Human Mono-Oxygenase Cytochrome P450 3A5-Ritonavir Complex Reveals Active Site Differences between P450s 3A4 and 3A5. *Molecular pharmacology* **93**, 14
320. Shah, M. B., and Halpert, J. R. (2018) Crystal structure of CYP2B6 in complex with an efavirenz analog: From plasticity to PI interactions in CYP2B enzymes. *Drug Metabolism and Pharmacokinetics* **33**, S32-S33
321. Redhair, M., Clouser, A. F., and Atkins, W. M. (2019) Hydrogen-deuterium exchange mass spectrometry of membrane proteins in lipid nanodiscs. *Chemistry and Physics of Lipids* **220**, 14-22
322. Ye, Q., Lian, F., Chavez, P. R., Chung, J., Ling, W., Qin, H., Seitz, H. K., and Wang, X. D. (2012) Cytochrome P450 2E1 inhibition prevents hepatic carcinogenesis induced by diethylnitrosamine in alcohol-fed rats. *Hepatobiliary Surg Nutr* **1**, 5-18
323. Seitz, H. K., and Wang, X. D. (2013) The role of cytochrome P450 2E1 in ethanol-mediated carcinogenesis. *Sub-cellular biochemistry* **67**, 131-143

324. Lobo, I. A., and Harris, R. A. (2008) GABA(A) receptors and alcohol. *Pharmacol Biochem Behav* **90**, 90-94
325. Olsen, R. W. (2014) Analysis of gamma-aminobutyric acid (GABA) type A receptor subtypes using isosteric and allosteric ligands. *Neurochem Res* **39**, 1924-1941